# A Field Evaluation of the Perpetual Pavement Concept

Prepared by:
Issam Khoury
Eddie Chou (University of Toledo)
Mary Robbins
Roger Green
Mutaz Al Issa

Prepared for:
The Ohio Department of Transportation,
Office of Statewide Planning & Research

PID: 111438

October 2024

Final Report





OHIO UNIVERSITY

**Ohio Research Institute for Transportation and the Environment**

## Technical Report Documentation Page

| 1. Report No. | 2. Government Accession No. | 3. Recipient's Catalog No. |
|---|---|---|
| FHWA/OH-2025/12 | | |

| 4. Title and Subtitle | 5. Report Date (Month and Year) |
|---|---|
| **A Field Evaluation of the Perpetual Pavement Concept** | **October 2024** |
| | 6. Performing Organization Code |
| | |

| 7. Author(s) (include 16 digit ORCID ID) | 8. Performing Organization Report No. |
|---|---|
| **Issam Khoury (ORCID 0000-0003-4856-7535), Eddie Chou (ORCID: 0000-0003-4310-8567), Mary Robbins (ORCID 0000-0002-3394-8602), Roger Green (ORCID 0000-0003-2497-825X), and Mutaz Al Issa (0009-0001-0633-6950)** | |

| 9. Performing Organization Name and Address | 10. Work Unit No. (TRAIS) |
|---|---|
| **Ohio Research Institute for Transportation and the Environment Ohio University<br>Department of Civil Engineering<br>231 Stocker Center<br>Athens, OH 45701-2979** | |
| | 11. Contract or Grant No. |
| | **34883** |

| 12. Sponsoring Agency Name and Address | 13. Type of Report and Period Covered |
|---|---|
| **Ohio Department of Transportation<br>Research Section<br>1980 West Broad St., MS 3280<br>Columbus, OH 43223** | **Final Report** |
| | 14. Sponsoring Agency Code |
| | |

15. Supplementary Notes

**Prepared in cooperation with the Ohio Department of Transportation (ODOT) and the U.S. Department of Transportation, Federal Highway Administration.**

16. Abstract

**This report details the evaluation of a field study of the perpetual pavement concept. Seven test sections were instrumented on WAY 83 each with a specific build up to allow for a comprehensive examination of the effect of adding High Polymer to an asphalt mix. Sensors were installed in the test sections, including strain gages, temperature sensors and pressure cells. In addition a comprehensive laboratory testing protocol was completed to fully quantify the high polymer mixes.**

| 17. Key Words | 18. Distribution Statement |
|---|---|
| **Perpetual Pavement, High Polymer Modified asphalt concrete, endurance limit, Falling Weight Deflectometer (FWD), Dynamic Cone Penetrometer (DCP), Subgrade Stabilization, IDEAL-CT, Hamburg Wheel Track Tester, Cantabro Test, PerRoad** | **No Restrictions. This document is available to the public through the National Technical Information Service, Springfield, Virginia 22161** |

| 19. Security Classification (of this report) | 20. Security Classif. (of this page) | 21. No. of Pages | 22. Price |
|---|---|---|---|
| **Unclassified** | **Unclassified** | **220** | |

**Form DOT F 1700.7 (8-72)** **Reproduction of completed pages authorized**

# SI* (MODERN METRIC) CONVERSION FACTORS

## APPROXIMATE CONVERSIONS TO SI UNITS

| Symbol | When You Know | Multiply By | To Find | Symbol |
|---|---|---|---|---|
| **LENGTH** | | | | |
| in | inches | 25.4 | millimeters | mm |
| ft | feet | 0.305 | meters | m |
| yd | yards | 0.914 | meters | m |
| mi | miles | 1.61 | kilometers | km |
| **AREA** | | | | |
| $in^2$ | square inches | 645.2 | square millimeters | $mm^2$ |
| $ft^2$ | square feet | 0.093 | square meters | $m^2$ |
| $yd^2$ | square yards | 0.836 | square meters | $m^2$ |
| ac | acres | 0.405 | hectares | ha |
| $mi^2$ | square miles | 2.59 | square kilometers | $km^2$ |
| **VOLUME** | | | | |
| fl oz | fluid ounces | 29.57 | milliliters | mL |
| gal | gallons | 3.785 | liters | L |
| $ft^3$ | cubic feet | 0.028 | cubic meters | $m^3$ |
| $yd^3$ | cubic yards | 0.765 | cubic meters | $m^3$ |
| NOTE: Volumes greater than 1000 L shall be shown in $m^3$. | | | | |
| **MASS** | | | | |
| oz | ounces | 28.35 | grams | g |
| lb | pounds | 0.454 | kilograms | kg |
| T | short tons (2000 lb) | 0.907 | megagrams (or "metric ton") | Mg (or "t") |
| **TEMPERATURE (exact)** | | | | |
| °F | Fahrenheit temperature | 5(°F-32)/9 or (°F-32)/1.8 | Celsius temperature | °C |
| **ILLUMINATION** | | | | |
| fc | foot-candles | 10.76 | lux | lx |
| fl | foot-Lamberts | 3.426 | candela/$m^2$ | $cd/m^2$ |
| **FORCE and PRESSURE or STRESS** | | | | |
| lbf | poundforce | 4.45 | newtons | N |
| $lbf/in^2$ or psi | poundforce per square inch | 6.89 | kilopascals | kPa |

## APPROXIMATE CONVERSIONS FROM SI UNITS

| Symbol | When You Know | Multiply By | To Find | Symbol |
|---|---|---|---|---|
| **LENGTH** | | | | |
| mm | millimeters | 0.039 | inches | in |
| m | meters | 3.28 | feet | ft |
| m | meters | 1.09 | yards | yd |
| km | kilometers | 0.621 | miles | mi |
| **AREA** | | | | |
| $mm^2$ | square millimeters | 0.0016 | square inches | $in^2$ |
| $m^2$ | square meters | 10.764 | square feet | $ft^2$ |
| $m^2$ | square meters | 1.195 | square yards | $yd^2$ |
| ha | hectares | 2.47 | acres | ac |
| $km^2$ | square kilometers | 0.386 | square miles | $mi^2$ |
| **VOLUME** | | | | |
| mL | milliliters | 0.034 | fluid ounces | fl oz |
| L | liters | 0.264 | gallons | gal |
| $m^3$ | cubic meters | 35.71 | cubic feet | $ft^3$ |
| $m^3$ | cubic meters | 1.307 | cubic yards | $yd^3$ |
| **MASS** | | | | |
| g | grams | 0.035 | ounces | oz |
| kg | kilograms | 2.202 | pounds | lb |
| Mg (or "t") | megagrams (or "metric ton") | 1.103 | short tons (2000 lb) | T |
| **TEMPERATURE (exact)** | | | | |
| °C | Celsius temperature | 1.8°C + 32 | Fahrenheit temperature | °F |
| **ILLUMINATION** | | | | |
| lx | lux | 0.0929 | foot-candles | fc |
| $cd/m^2$ | candela/$m^2$ | 0.2919 | foot-Lamberts | fl |
| **FORCE and PRESSURE or STRESS** | | | | |
| N | newtons | 0.225 | poundforce | lbf |
| kPa | kilopascals | 0.145 | poundforce per square inch | $lbf/in^2$ or psi |

* SI is the symbol for the International Symbol of Units. Appropriate rounding should be made to comply with Section 4 of ASTM E380.

(Revised September 1993)

# A Field Evaluation of the Perpetual Pavement Concept

Prepared by

Issam Khoury, Roger Green, Mary Robbins, and Mutaz Al Issa

Ohio Research Institute for Transportation and the Environment
Russ College of Engineering and Technology
Ohio University
Athens, Ohio 45701-2979

Eddie Chou
Department of Civil Engineering
University of Toledo
Toledo, Ohio 43606

Prepared in cooperation with the
Ohio Department of Transportation



Final Report
October 2024

# Acknowledgements

The authors acknowledge the people who ensured the successful completion of this project starting with the project managers Jill Martindale and Jennifer Spriggs. Craig Landefeld, Patrick Bierl, Dave Miller, William Feehan Jr., Adam Au, and Andrew Clouse of ODOT Office of Pavement Engineering; Eric Biehl and Jacob Lautanen of ODOT Office of Materials Management; Julie Miller of ODOT Office of Construction Administration; Sandra Mapel of Technical Services; Scott Ockunzzi of District 3, and the staff and crew at the ODOT Wayne County garage who provided technical guidance and assistance in executing the project.

Josh Jordan contributed substantially to collecting the field data in this project. Graduate students working on this project included Hakeem Issa Mubarak Alshawabkeh and Mutaz Al Issa, Aashish Bhattarai, Austin Davenport, Abiskar Nepal.

We also acknowledge the contributions to this project by the design/build team of E.L. Robinson Engineering Company and Kokosing Construction Company.

# Contents

## List of Figures

## List of Tables

# PROBLEM STATEMENT

In early 2015 a Final Report Titled "*Implementation and Thickness Optimization of Perpetual Pavements in Ohio*" was delivered to the Ohio Department of Transportation's (ODOT) Office of Pavement Engineering (OPE). This report detailed the required thickness for a flexible perpetual pavement for Ohio soil conditions, traffic and weather. Additionally, this project investigated the properties of Highly Modified Asphalt (HiMA) and provided some insight as to the benefits of its use in the surface and intermediate courses of both standard AASHTO 93 designs as well as perpetual pavement designs. Considering the thicknesses described and the material properties of the HiMA as reported in the aforementioned project, it was desired to construct a perpetual pavement using a high polymer asphalt mix (HPM) and validate the perpetual pavement concept in real world conditions by instrumenting and collecting data on a roadway in Ohio. Additionally, ODOT is interested in the best way to utilize HPM (i.e., asphalt base only, surface and intermediate only, or full depth asphalt buildups). WAY-83-10.81 (PID 91095) was selected as the project site for the field evaluation. This project consists of reconstruction of 3.83 miles (6.16 km) of existing divided highway on SR83. Additional outcomes of this research are as follows:

- Incorporate the HPM material into the design and construction to evaluate its cost effectiveness and constructability.
- Investigate the perpetual pavement design software/concepts as it applies to the perpetual pavement design using the HPM material.

# RESEARCH BACKGROUND

Introduced in the United States in 2000 by the Asphalt Pavement Alliance (APA), the perpetual pavement design concept was meant to address the limitations of empirical design procedures of the American Association of State Highway and Transportation Officials (AASHTO) 1993 Guide for Design of Pavement Structures [Newcomb et al., 2010]. This design concept is rooted in mechanistic responses, in which pavement responses are kept below critical limiting stress, strain, or deflections in the cross-sections, no structural damage (bottom-up fatigue cracking or structural rutting) is incurred [Newcomb et el., 2010]. As a result, only functional distresses occur at the surface. Minimizing these critical pavement responses can be achieved through appropriate layer thickness and selection of pavement materials. As shown in Figure 1, to avoid bottom-up fatigue cracking the perpetual pavement design concept uses a fatigue resistant pavement material at the bottom of the asphalt build-up where tensile strains are the highest and a rut resistant surface layer where shear stresses are the highest [Newcomb et al., 2010].

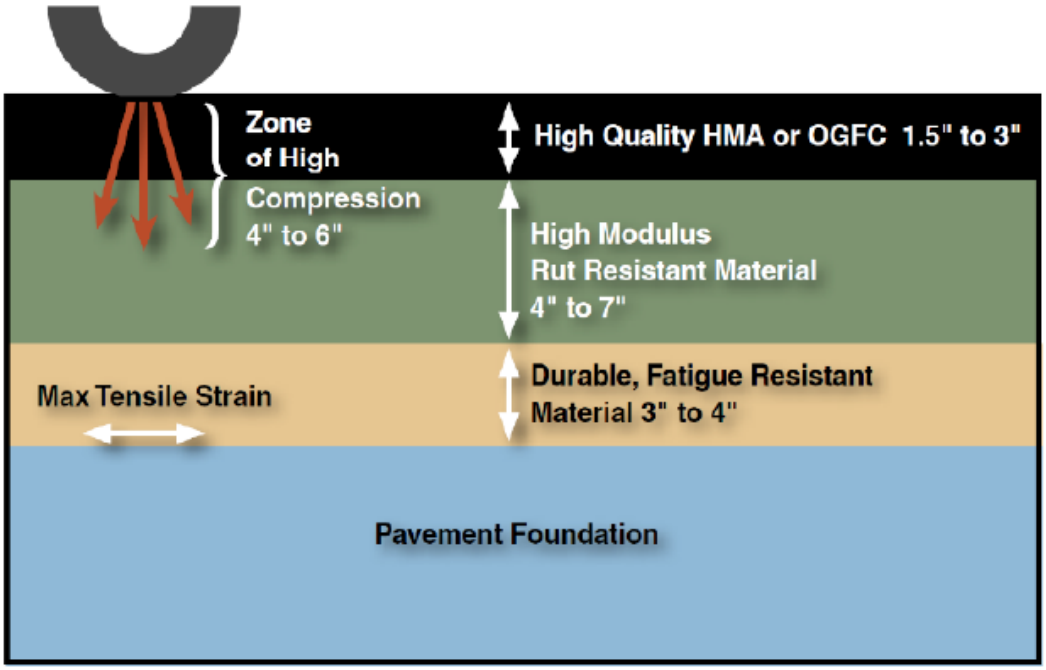


**Figure 1 Perpetual Pavement Concept [Newcomb et al., 2010]**

The Ohio Department of Transportation (ODOT) has a long history with perpetual pavements, with the first test sections designed as a perpetual pavement constructed in 2003 on I-77 in Stark and Summit counties in which 16.25" (413mm) of asphalt on 6" (150mm) of dense graded aggregate base was placed. The most recent study, published in 2015 [Sargand et al., 2015], was aimed at optimizing pavement thickness for perpetual pavement design in the state of Ohio. The study included the construction of instrumented test sections on the mainline and ramp of US 23 in Delaware county (DEL-23) in 2012. Sections were constructed with 6" (150 mm) of dense graded aggregate base (DGAB) and a 4" (100 mm) fatigue resistant layer with the total asphalt concrete (AC) thickness varied and stabilization of the subgrade varied. One section was constructed with 15" (380 mm) total AC thickness on unstabilized subgrade, another at 13" (330 mm) of AC on lime modified subgrade, and lastly one section at 11" (280 mm) of AC on lime modified subgrade. Tensile strains were measured at the bottom of the asphalt layer under controlled testing of an overloaded vehicle at a range of temperatures. The fatigue endurance limits of the fatigue resistant layer were determined at 40°F (4.4°C), 70°F (21°C), and 100°F (38°C) using the NCHRP 9-44 model based on dynamic modulus. It was found the thinnest section, 11" (280 mm) of AC on modified subgrade, significantly exceeded the fatigue endurance limited determined at 100°F (38°C). Sargand et al. [2015] concluded "the thickness of 13" (330 mm) or greater, constructed on a 6" (150 mm) aggregate base and stabilized subgrade met criteria for perpetual pavement, while the 11" (280 mm) section on the same base and subgrade did not. It was also determined a pavement thickness of 15" (380 mm) or greater, constructed on an aggregate base and compacted subgrade, also met perpetual pavement criteria."

As part of the same study [Sargand et al., 2015] test sections were constructed in 2014 in the Accelerated Pavement Load Facility (APLF) housed at Ohio University's Lancaster campus to evaluate cross-sections utilizing highly modified asphalt (HiMA) within the context of perpetual pavement design. HiMA, containing 7.5% styrene-butadiene-styrene (SBS), has improved fatigue and rutting resistance. Therefore, thinner cross-sections were evaluated

within the context of perpetual pavement design. Four instrumented test sections were constructed, three of which consisted of HiMA throughout (surface, intermediate, and base layers) and the fourth, which served as the control, included a conventional asphalt base layer and HiMA surface and intermediate layers. Unlike sections along DEL-23, these did not include a fatigue resistant layer. HiMA cross-sections included 8" (200 mm), 9" (225 mm), and 10" (250 mm) of total AC, while the control section was constructed with 11" (280 mm) of AC, and all four were placed on a 6" (150 mm) DGAB and cement stabilized subgrade. Sections were subjected to accelerated loading at pavement temperatures of 70°F (21°C), and 100°F (38°C). Measured strains were relatively low and generally fell below the fatigue endurance limits determined from the NCHRP 9-44 model at 70°F (21°C), and 100°F (38°C).

While HiMA sections performed well in the APLF, there was a need to further explore the use of High Polymer Modified (HPM) asphalt concrete on an in-service pavement to validate perpetual pavement design concept as it applies to HPM material. Furthermore, there was a need to determine the most appropriate use of HPM in a perpetual pavement. Due to the high SBS used in HPM, it is generally more costly than conventional asphalt. There was a need to determine where in the cross-section (throughout, base only, surface only, etc.) HPM can be used to achieve the most cost-effective perpetual pavement. Through this report HPM will refer to High Polymer Modified asphalt concrete with an ODOT specification of PG 88-22M.

At the NCAT Test Track Highly Modified Asphalt (HiMA) concrete mixes have shown to significantly improve a pavement's resistance to fatigue cracking and rutting [Timm et al., 2013]. In order to adequately reflect such benefits in the pavement design method currently used by Ohio DOT (the modified AASHTO 93 pavement design method), the structural layer coefficient of the HPM mixes needs to be determined. Research conducted for Florida DOT by University of Nevada [Habbouche et al., 2019] estimated fatigue-based structural coefficients range between 0.33 and 1.32 and indicated that through statistical analysis a structural layer coefficient of 0.54 may be used for HPM mixes. This research study will investigate under Ohio climatic conditions if this estimate (and perhaps others that may be found through literature review) is valid by: 1) using pavement deflections measured by Falling Weight Deflectometer (FWD) to back-calculate the modulus of the HPM layer, and 2) laboratory testing of HPM mixes to determine the dynamic modulus (|E*|). The back-calculated layer modulus and laboratory measured dynamic modulus would then be used to estimate the structural layer coefficient for HPM mixes.

According to the AASHTO 93 pavement design method, a higher structural layer coefficient would result in reduced layer thickness. Therefore, the benefits of using HPM mixes could be quantified. The mechanical properties of pavement layers and surface deflections of the perpetual pavement sections containing HPM were compared to those of the control sections. The design thickness of perpetual pavement sections using HPM binders (with various subgrades and traffic loadings) were compared with the thickness of perpetual pavement sections using conventional asphalt binders. This would enable assessment of the economic benefit of using HPM binders.

## Goals and Objectives

The primary goal of this research was to design, construct and instrument the first in-service perpetual pavement constructed with HPM. This research is expected to provide ODOT's Office of Pavement Engineering with a method for future perpetual pavement design. Specific objectives of this research were as follows:

- Conduct a literature review of current perpetual pavement design concepts, design tools, recommended fatigue endurance limits, field evaluations, and use of highly modified asphalt properties.
- Review and evaluate reports and data from existing perpetual pavement test sections in Ohio.
- Based on the above reviews, recommend the thickness design, instrumentation plan, and laboratory test plan for a field study of perpetual pavement containing HPM
- Monitor the construction of the test sections.
    - Collect and test pavement material samples.
    - Collect non-destructive tests during construction of test sections
    - Install instrumentation and conduct truck tests.
- Analyze data
- Develop structural layer coefficients for HPM
- Conduct benefit analysis of HPM material
- Provide a perpetual pavement design guide with recommended inputs and limitations.
- Provide training.

# RESEARCH APPROACH

## Literature Review

A literature review was conducted with focus on the following and is presented in its entirety in Appendix A:

- Perpetual pavement design concepts including fatigue endurance limit, strain distribution limit, fatigue ratio concept, and Miner's theory (damage, estimated by transfer functions, is kept very low (<0.1)).
- Perpetual pavement design tools such as PerRoad and AASHTOWare PavementME Design (PMED)
- Use of fatigue endurance limit in field evaluations of perpetual pavements
- High polymer modified (HPM) mixes
- Structural layer coefficient of HPM mixes

In following the perpetual pavement design concept, in which critical stresses and strains within the pavement build-up are kept below a limiting value, there are several design methods which can be used to achieve a perpetual pavement design.

Historically, a single strain threshold has been identified, in which the design results in predicted strains at or below the threshold to prevent damage. Thresholds for tensile strain at the bottom of the asphalt have ranged from 70 to 200 με [Tran et al., 2015]. Thresholds have been determined through fatigue endurance limit found in the laboratory, field measured strain, and predicted strain using backcalculated moduli [Tran et al., 2015]. Thresholds for preventing structural rutting have varied from controlling the vertical stress at the top of the subgrade using a subgrade stress ratio or limiting the vertical strain at the top of the subgrade to 200 με, as documented by Tran et al. [2015]. Recently Tran et al. [2015], proposed the $50^{th}$ percentile vertical strain at the top of the subgrade be 200 με or less.

Another method is to utilize Miner's theory, in which transfer functions are used to determine the number of loads to failure from predicted strain and taking the ratio of anticipated traffic loadings to number of loads to failure, the damage is calculated [Newcomb,

2010]. For standard designs a damage ratio of 1.0 is desired, however, for perpetual pavements, a ratio of 0.1 or less is targeted.

Recently, two other methods were introduced, the limiting strain distribution curve and the limiting fatigue ratio [Tran et al., 2015]. As opposed to a single strain threshold, a cumulative strain distribution serves as the strain thresholds. For these criteria, shown below in Table 1, to be effective, predicted strain must be less than the strain at all percentiles from the $50^{th}$ through the $99^{th}$. The limiting fatigue ratio is the ratio of the strain at the $n^{th}$ percentile to the laboratory determined fatigue threshold or endurance limit. In design, the user would divide predicted strain at each percentile by the fatigue endurance limit and compare it against the maximum fatigue ratio and revise the design until all ratios are less than the maximum fatigue ratios shown in Table 1 at each percentile.

**Table 1 Refined Limiting Distribution and Maximum Fatigue Ratios for Predicted Tensile Strain [Tran et al., 2015]**

| Percentile | Limiting Design Distribution for Predicted Strain | Maximum Fatigue Ratio for Predicted Strain |
|---|---|---|
| 1% | 29 | |
| 5% | 41 | |
| 10% | 48 | |
| 15% | 54 | |
| 20% | 60 | |
| 25% | 66 | |
| 30% | 71 | |
| 35% | 78 | |
| 40% | 84 | |
| 45% | 91 | |
| 50% | 100 | 0.68 |
| 55% | 110 | 0.74 |
| 60% | 120 | 0.81 |
| 65% | 131 | 0.88 |
| 70% | 143 | 0.96 |
| 75% | 158 | 1.06 |
| 80% | 175 | 1.18 |
| 85% | 194 | 1.31 |
| 90% | 221 | 1.49 |
| 95% | 257 | 1.73 |
| 99% | 326 | 2.19 |

While there are several methods, there are primarily two tools historically used to design perpetual pavements, the PerRoad software which is exclusively for perpetual pavement design and utilizes Monte Carlo simulations to account for variability in the cross-section, and the mechanistic-empirical pavement design software, AASHTO PMED software which is geared toward more traditional pavement designs. PerRoad has the capability of designing perpetual pavements by comparing predicted strain to strain thresholds. PerRoad also has default transfer functions to determine the damage ratio and years until failure is expected. Recently, Timm et al. [2017] incorporated the limiting strain distribution and fatigue ratio concepts into the software as well. AASHTO PMED does not have any specific method for designing perpetual pavement, however, in following the idea perpetual pavements should maintain structural integrity for 50 years, the Pavement ME software can be used to design pavements with a design life of 50 years or more. Additionally, the Pavement ME software now provides strain as an output. Strain can then be compared against a single threshold, or the limiting strain

distribution. It should be noted recent research [Islam et al., 2017] has shown strains resulting from the AASHTO PMED software are less than strains predicted in PerRoad.

As this research is focused on the use of Highly Polymer Modified (HPM) asphalt concrete to optimize perpetual pavement thickness. Literature relative to the contribution of HPM mixes to the pavement structure were also reviewed, as detailed in Appendix A. HPM asphalt mixes contain approximately 7.5% of styrene butadiene styrene (SBS) modifier. The first HPM mix, was developed by Kraton Corporation (Kraton™ D0243) and is referred to as highly modified asphalt (HiMA), other companies have since developed similar formulations with the same or similar dosage rates of SBS to achieve HPM binders. HPM mix costs more than conventional AC but has been shown to significantly improve resistance to rutting, fatigue cracking, and moisture damage, thus leading to better pavement performance and longer pavement life (Timm et al., 2013; Sargand, et al., 2015; Chen et al., 2018; Habbouche et al., 2019). In 2009, a full-scale experimental test section was funded by Kraton Performance Polymers, LLC and constructed at the National Center for Asphalt Technology (NCAT) Test Track to evaluate HiMA relative to a control section featuring conventional asphalt mixes. The NCAT Test Track HiMA asphalt concrete mixes have shown to significantly improve a pavement's resistance to fatigue cracking and rutting [Timm et al., 2013] based on laboratory data. Timm et al. reported that despite statistically higher strain value in the HiMA section, the HiMA section has improved fatigue characteristics which resulted in predicted fatigue life nearly 17 times greater than the control section. Research conducted for Florida DOT by University of Nevada [Habbouche et al., 2019] indicated a structural layer coefficient of 0.54 may be used for HPM mixes.

## Review of Existing Perpetual Pavement Test Sections in Ohio

Various perpetual pavement test sections have been constructed in Ohio, on in service roads in the northeast and central regions of Ohio, as well as the Accelerated Pavement Load Facility (APLF) housed at the Ohio University's Lancaster campus. These sections have been constructed over a 12 year time period:

- 2002: STA-77, 17.61 – 18.54; SUM-77, 0.00 – 1.44
- 2003: STA-77, 12.75 – 14.80
- 2005: WAY-30, 11.81 – 16.13
- 2006: APLF (WMA)
- 2012: DEL-23, 19.41 – 19.54 (Mainline); Northbound and Southbound Ramp
- 2014: APLF (HiMA)

A discussion of each test section, and measured pavement responses are provided in the following subsections.

### *Interstate 77, Stark County, Ohio*

The first pavement test section in Ohio designed using a perpetual concept was constructed in 2002 on a project encompassing STA-77-17.61 to 18.54 and SUM-77-0 to 1.44, near the Akron-Canton airport, however this section was not well documented. It is believed the cross-section was the same as the STA-77-12.75 to 14.80 project described below with a total of 16.25" (412.8 mm) of asphalt concrete (AC) atop 6" (150 mm) of dense graded aggregate base (DGAB) and unstabilized subgrade. Instrumentation was installed, however no data were collected.

A second test section was completed in December 2003 as part of a project on I-77 (straight-line mile: 12.75 to 14.80) in Stark County near Canton, Ohio (Sargand and Figueroa, 2010). The test section consists of 6" (150 mm) of dense graded aggregate base (DGAB) placed beneath a total of 16.25" (412.8 mm) of AC. The surface AC layer was 1.5 in. of ODOT 856 stone

mastic asphalt (SMA) wearing course with PG 76-22M polymer modified binder. The intermediate AC layer was 1.75 in. ODOT 442 Superpave, with PG 76-22M polymer modified binder. The AC base layer (also referred to as ATB in previous reports) was 9" (228.6 mm) of ODOT 302 large stone mix with PG 64 -22 asphalt binder. Lastly, a 4" (101.6 mm) modified ODOT 302 asphalt treated base (ATB) was used as a fatigue-resistant base layer (FRL). The AC sat atop 6" of DGAB on top of an unstabilized subgrade [Sargand and Figueroa, 2010]

Strain gages, pressure cells, and thermocouples were installed in the northbound driving lane near mile 13.7, Stark County, as shown in Figure 2. Controlled vehicle load testing (CVL) using an ODOT dump truck with a single rear axle loaded to 13.5 kip (60 kN) at speeds of 5 MPH (8 km/h), 30 MPH (48 km/h), 40 MPH (64 km/h), and 50 MPH (80 km/h) was performed on December 15, 2003, immediately after opening to traffic. Pavement temperature at the time of testing was 36°F (2.2°C). Maximum measured strain was 35.6 με [Sargand et al. 2015]. Due to the high traffic volume on this section of I-77, no further tests have been performed.

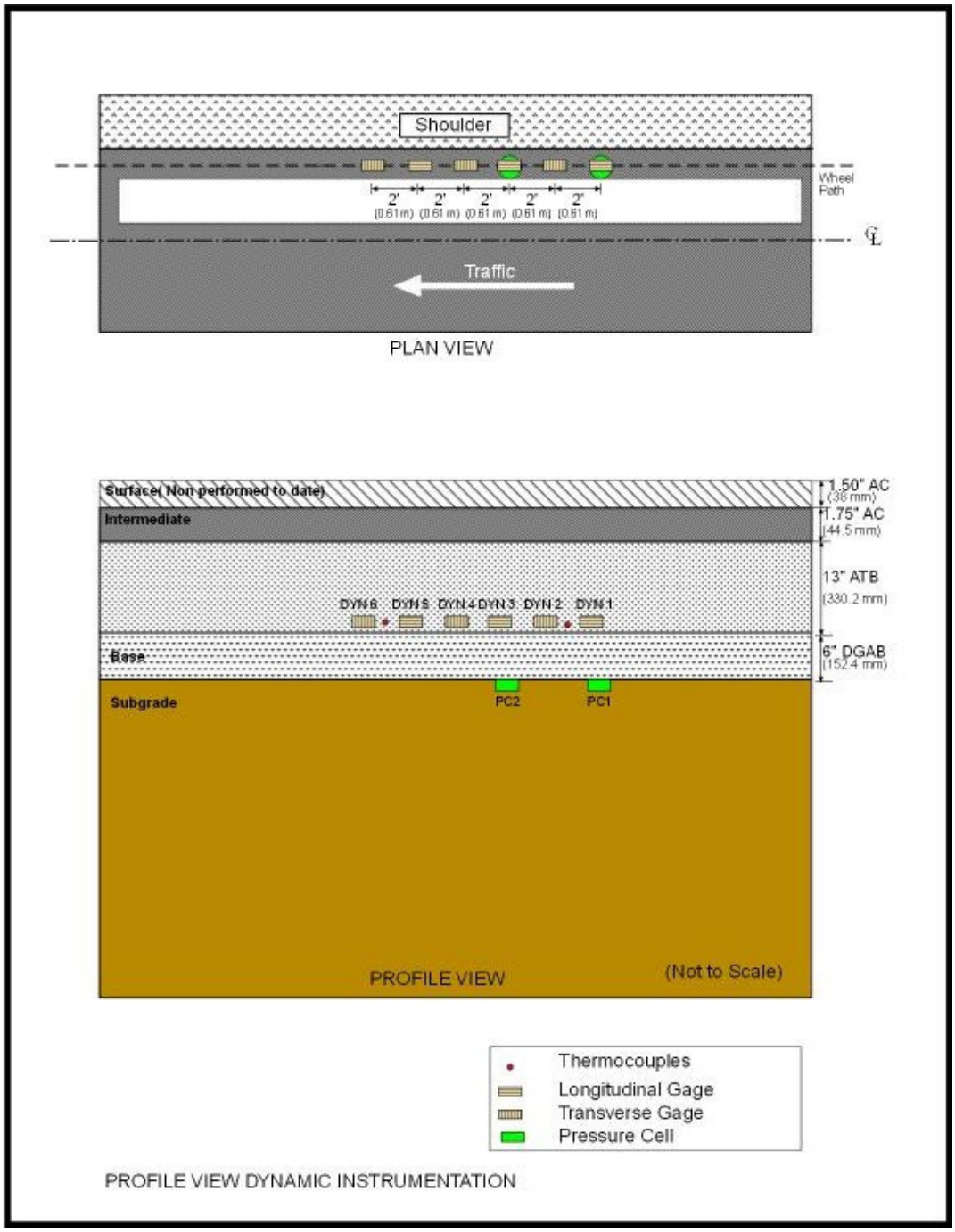


**Figure 2 Instrumentation Plan and Profile Views for STA-77**

ORITE researchers carried out a series of controlled vehicle load (CVL) tests in December, 2003, to measure pavement response from the installed instrumentation [Sargand et al., 2008]. At the time of testing, the surface course had not yet been constructed. The truck utilized was an ODOT single rear axle truck weighing 26 kips (116 kN) traveling at speeds ranging from 5 mph (8km/h) to 50 mph (80 km/h). Longitudinal strain at the bottom of the AC layer did not exceed 35 microstrains for any of the speeds tested, substantially lower than 70 microstrain, a conservative threshold used for perpetual pavement design. Testing was conducted at a pavement temperature of 36°F (2°C). Unfortunately, no further testing has been done due to

heavy traffic. Yet, these encouraging findings prompted ODOT and ORITE to carry out additional studies on perpetual pavements. [Sargand et al. 2008]

### *WAY-30, Wayne County, Ohio*

In response to the promotion of economic long-life pavements by both the asphalt and concrete industry, ODOT provided a 7.99 mi (12.86 km) long project for the evaluation of industry designed pavement sections. The asphalt industry proposed a perpetual pavement section and the concrete industry proposed a jointed concrete pavement with a widened lane on an asphalt base. The asphalt and concrete test sections are located adjacent to one another at Station 664+00 and Station 876+60 with the asphalt test sections located in the westbound direction and concrete sections in the eastbound direction.

A total of three test sections of flexible perpetual pavement were built with identical cross-sections: 876A-AC and 876B-AC were located 12 feet (3.7 m) apart at Station 876+00, the third section, Section 664-AC, was located near Station 664+00. Station locations are shown in Figure 3.


**Figure 3 Location of WAY-30 AC Perpetual Pavement Test Sections (Sargand et al., 2008)**

Both sections were designed by the respective industry. The asphalt industry formed a panel of ODOT and FHWA employees, industry representatives, and representatives from academia to develop specifications and a perpetual pavement design for typical Ohio materials. Various scenarios were considered, including elastic and viscoelastic analysis, legal and overloads, and summer vs. spring time loadings. The cross-section was designed using a layered elastic analysis with a limiting strain of 70 με, and using the material properties listed in Table 2 [Sargand et al., 2008]. The material properties were determined from previous projects in Ohio, primarily the SHRP Test Pavements on US 23, along with data from literature and laboratory testing of field cores. Loading configurations for the design consisted of 20-kip (89-kN) and 24-kip (107-kN) single axle truck and a 41-kip (182-kN) tandem axle truck. The design consisted of 16.25" (412.8 mm) of AC atop a dense graded aggregate base (DGAB) atop an unstabilized subgrade, with the following layers (from top to bottom) [Sargand et al., 2008]:

- 1.5" (38 mm) wearing layer, ODOT 12.5 mm stone mastic asphalt (SMA).

- 1.75” (44 mm) Superpave layer, ODOT 19 mm Superpave, Type A.
- 9” (221 mm) Asphalt Treated Base (ATB) layer, ODOT Item 302.
- 4” (102 mm) fatigue-resistant layer (FRL), ODOT Item 302.
- 6” (152 mm) highly crushed DGAB, ODOT Item 304.

**Table 2 WAY-30 AC Perpetual Pavement Design Properties (Sargand et al., 2008)**

| Layer | ODOT Item | Modulus of Elasticity (psi) | Modulus of Elasticity (MPa) | Poisons Ratio |
|---|---|---|---|---|
| Stone Mastic Asphalt (SMA) | 856 | 1,500,000 | 10,342 | 0.35 |
| 19 mm (0.75 in.) Superpave | 442 | 1,500,000 | 10,342 | 0.35 |
| Asphalt Treated Base (ATB) | 302 | 500,000 – 1,500,000 | 3,447 – 10,342 | 0.35 |
| Fatigue Resistant Layer (FRL) | Modified 302 | 500,000 – 1,500,000 | 3,447 – 10,342 | 0.35 |
| Dense Graded Aggregate Base (DGAB) | 304 | 10,000 | 69 | 0.40 |
| Subgrade | | 5,000 | 34.5 | 0.45 |

Strain gages, pressure cells, and thermocouples were installed in each test section, as shown in Figure 4 to Figure 6. A weather station and weigh-in-motion system were installed near the site at station 876+60. CVL testing using an ODOT dump truck was performed the winter of 2005-2006, prior to opening the road to traffic, and the summer of 2006, seven months after opening to traffic. Dump trucks with single rear axle and tandem rear axles were used.

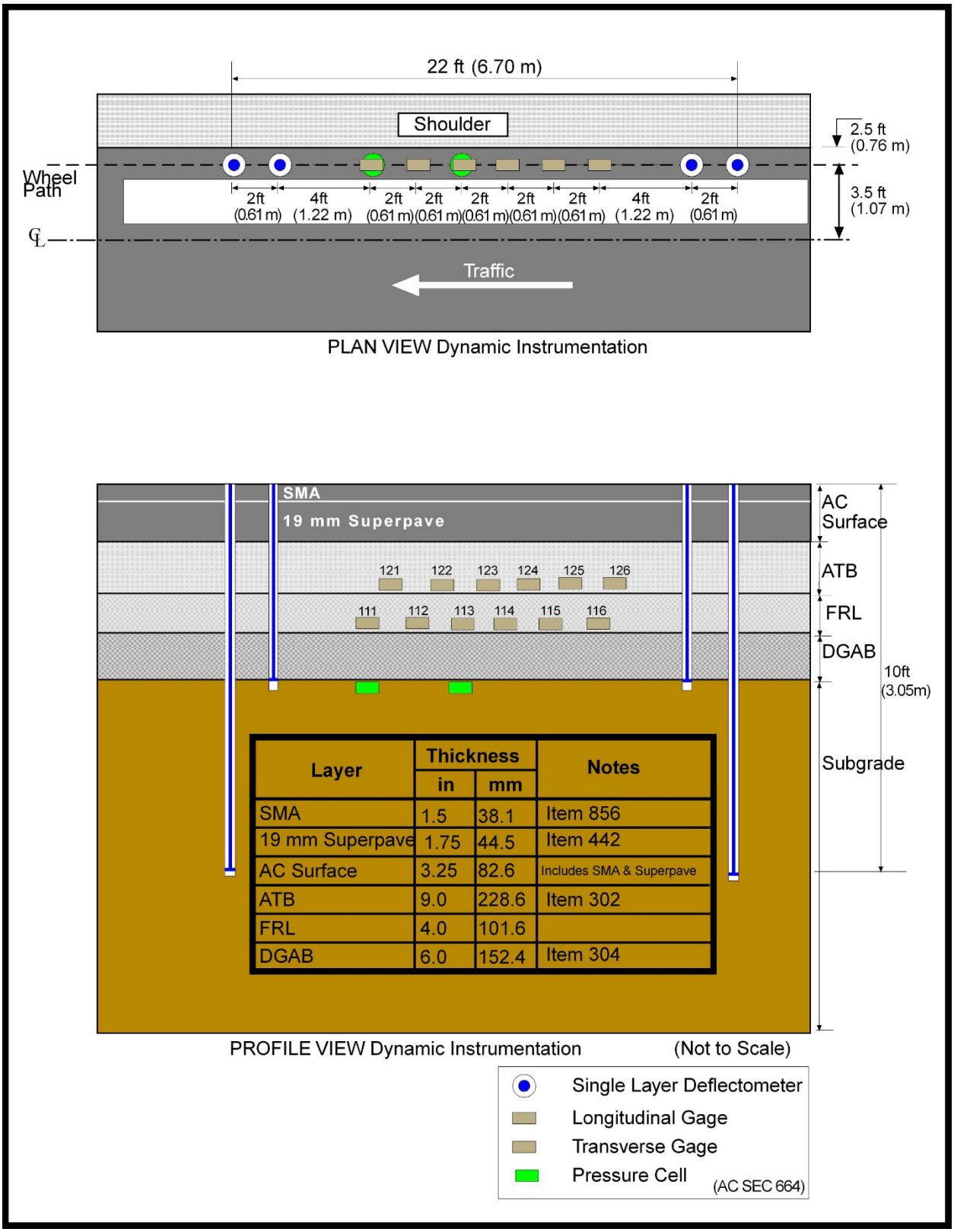


**Figure 4 Instrumentation Plan and Profile Views for AC Section 664 (Sargand et al. 2008).**

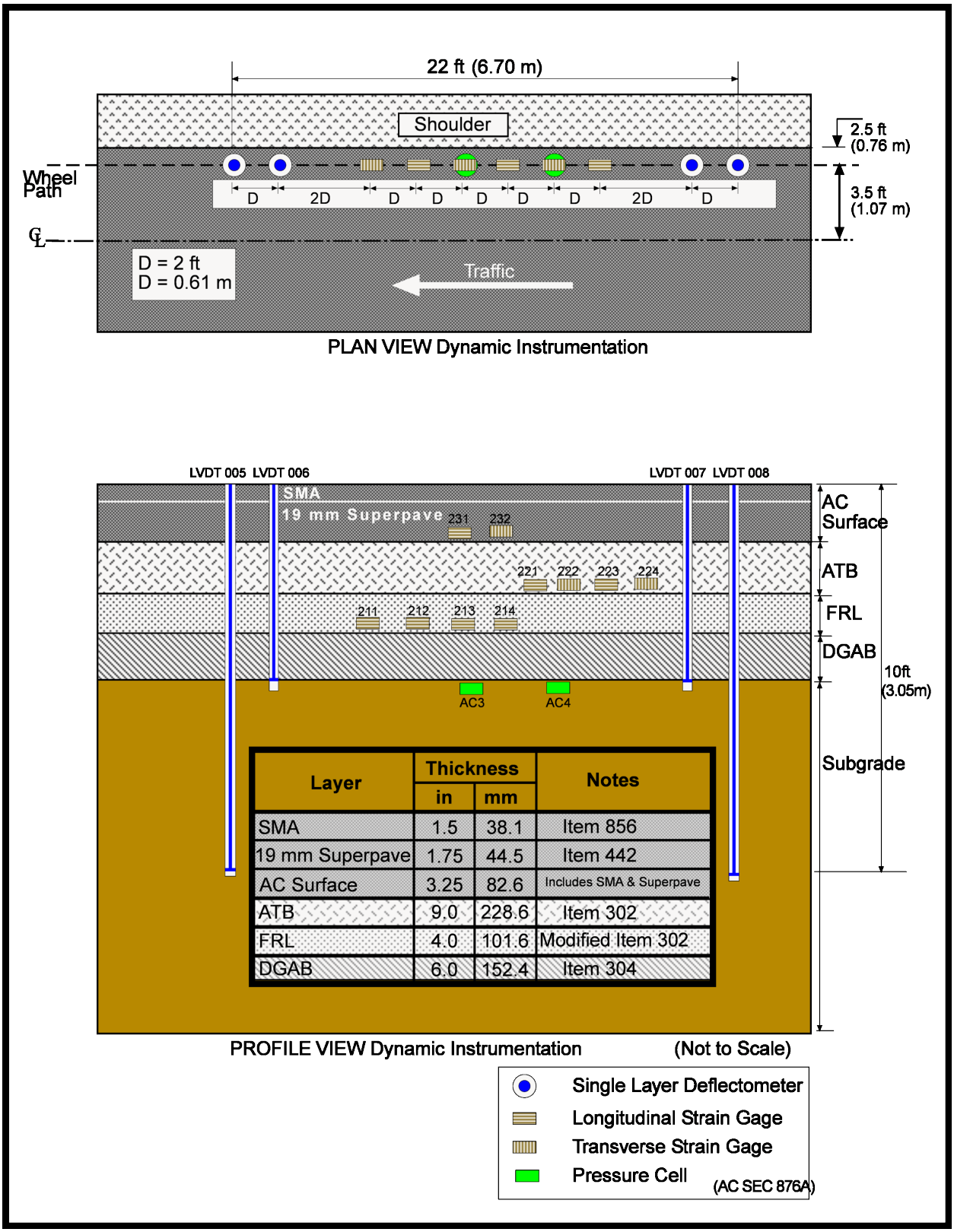


| Layer | Thickness | | Notes |
|---|---|---|---|
| | in | mm | |
| SMA | 1.5 | 38.1 | Item 856 |
| 19 mm Superpave | 1.75 | 44.5 | Item 442 |
| AC Surface | 3.25 | 82.6 | Includes SMA & Superpave |
| ATB | 9.0 | 228.6 | Item 302 |
| FRL | 4.0 | 101.6 | Modified Item 302 |
| DGAB | 6.0 | 152.4 | Item 304 |

**Figure 5 Instrumentation Plan and Profile Views for AC Section 876A (Sargand et al. 2008).**

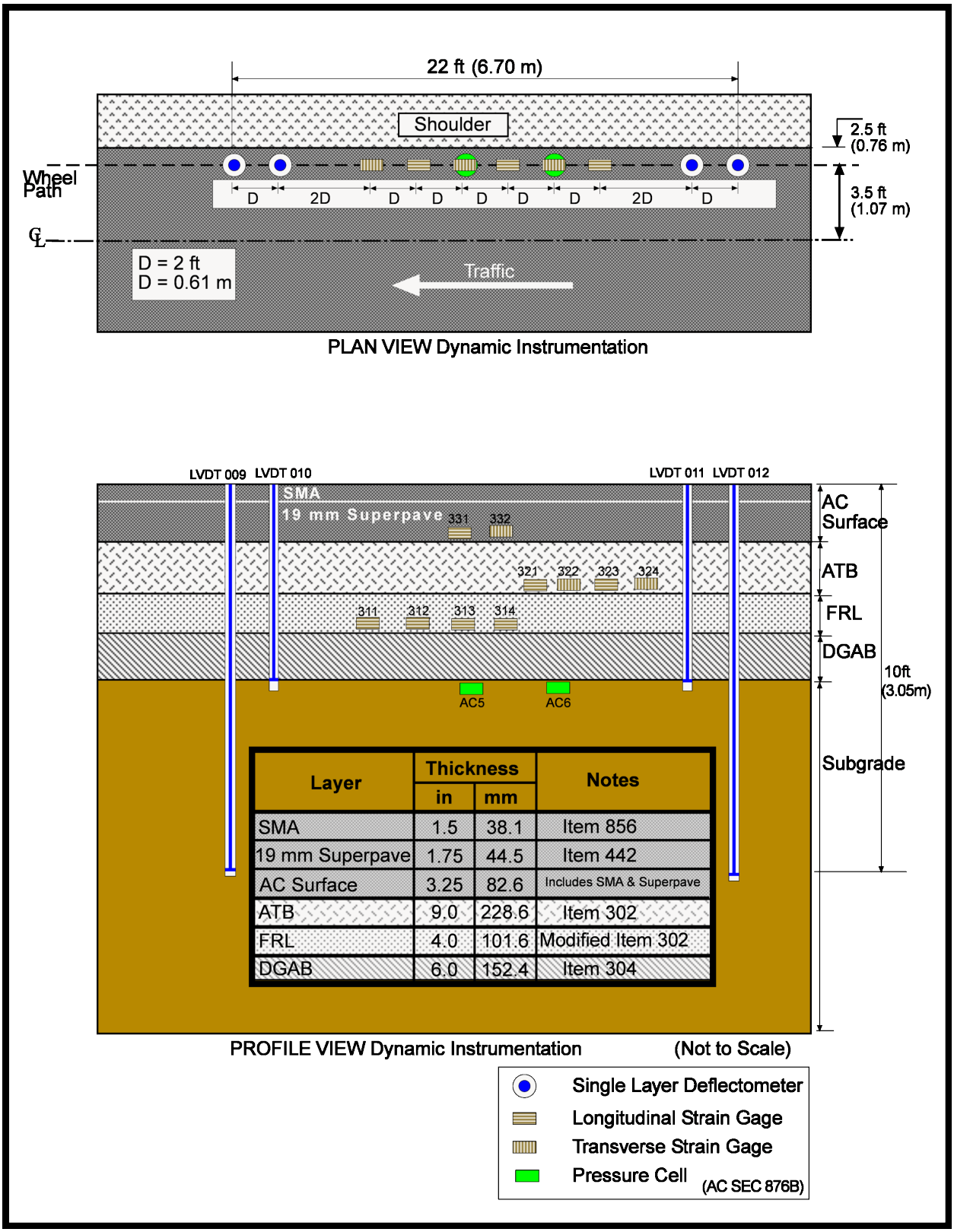


| Layer | Thickness | | Notes |
|---|---|---|---|
| | in | mm | |
| SMA | 1.5 | 38.1 | Item 856 |
| 19 mm Superpave | 1.75 | 44.5 | Item 442 |
| AC Surface | 3.25 | 82.6 | Includes SMA & Superpave |
| ATB | 9.0 | 228.6 | Item 302 |
| FRL | 4.0 | 101.6 | Modified Item 302 |
| DGAB | 6.0 | 152.4 | Item 304 |

**Figure 6 Instrumentation Plan and Profile Views for AC Section 876B (Sargand et al. 2008).**

CVL test was performed under different speeds ranging from 5 mph (8 km/h) to 55 mph (89 km/h) [Sargand and Figueroa, 2010]. CVL was conducted three times to capture the pavement response under a range of pavement temperatures [Sargand et al., 2015]:

- December 2005, where the pavement temperature ranged from 30°F (-1°C) to 35°F (2°C),
- July 2006, where the pavement temperature ranged from 95°F (35°C) to 126°F (52°C) and
- May 2008, where the pavement temperature ranged from 56°F (13°C) to 74°F (23°C).

Testing completed in December 2005 was conducted prior to opening the section to traffic. Both single and tandem axle trucks from ODOT were used for testing [Sargand et al., 2008]. The single axle loads ranged from 17.5 kips (78 kN) to 28.2 kips (125 kN) and the tandem axle loads ranged from 28.5 kips (127 kN) to 40.15 kips (179 kN). The maximum tensile strain, 128.7 με, was recorded under the most extreme conditions tested. This tensile strain was measured in July 2006 in the FRL under a 20.35-kip (78 kN) single axle load traveling at 5 mph (8 km/h) [Sargand et al., 2008]. Under speeds of 55 mph (89 km/h) which are typical for the roadway type, the maximum strain measured was 77.9 με, and was recorded during high pavement temperatures and under a heavy single axle load [Sargand et al., 2008]. It was concluded, based on the expected traffic speed at the site, strain would rarely reach strains of the magnitude associated with the slow speed tests.

### *Warm Mix Asphalt (WMA) Study at ORITE*

Since its construction in 1997, the Accelerated Pavement Loading Facility (APLF) at Ohio University has been used to carry out a broad variety of pavement studies; including two related to perpetual asphalt pavement research [Cichocki, 2015]. The APLF is a 45-foot-long (13.7 m), 38-foot-wide (11.6 m), and 8-foot (2.4 m) deep concrete-lined rectangular pit with the capability to conduct pavement testing at temperatures ranging from 10°F (-12°C) to 130°F (54°C). Wheel loads of up to 30 kips (133 kN) are applied via a dual or single wide-base tire on a track system, operating at speeds up to 5 mph (8 km/h). Loading can be applied with or without offset to simulate wheel wander.

The first research study on perpetual asphalt pavements conducted in the APLF investigated the pavement response and performance of perpetual pavements constructed with 3 different types of WMA additives relative to conventional asphalt [Sargand et al., 2009].

In this study, four lanes of perpetual pavement were constructed, each topped with a different surface mix. Three lanes featured a different WMA additive (Evotherm, Sasobit, and Aspha-Min), while the fourth lane utilized conventional HMA. Moreover, the lanes were divided into northern and southern halves, resulting in 8 test sections. The northern half had an asphalt pavement thickness similar to that on I-77 and WAY-30 perpetual pavement sections. In the other half the thickness decreased in one-inch increments by reducing the intermediate layer thickness, to balance the change in pavement thickness, the DGAB thickness was increased [Sargand et al., 2009]. Figure 7 illustrates the APLF profile view diagram for the pavement build-up.

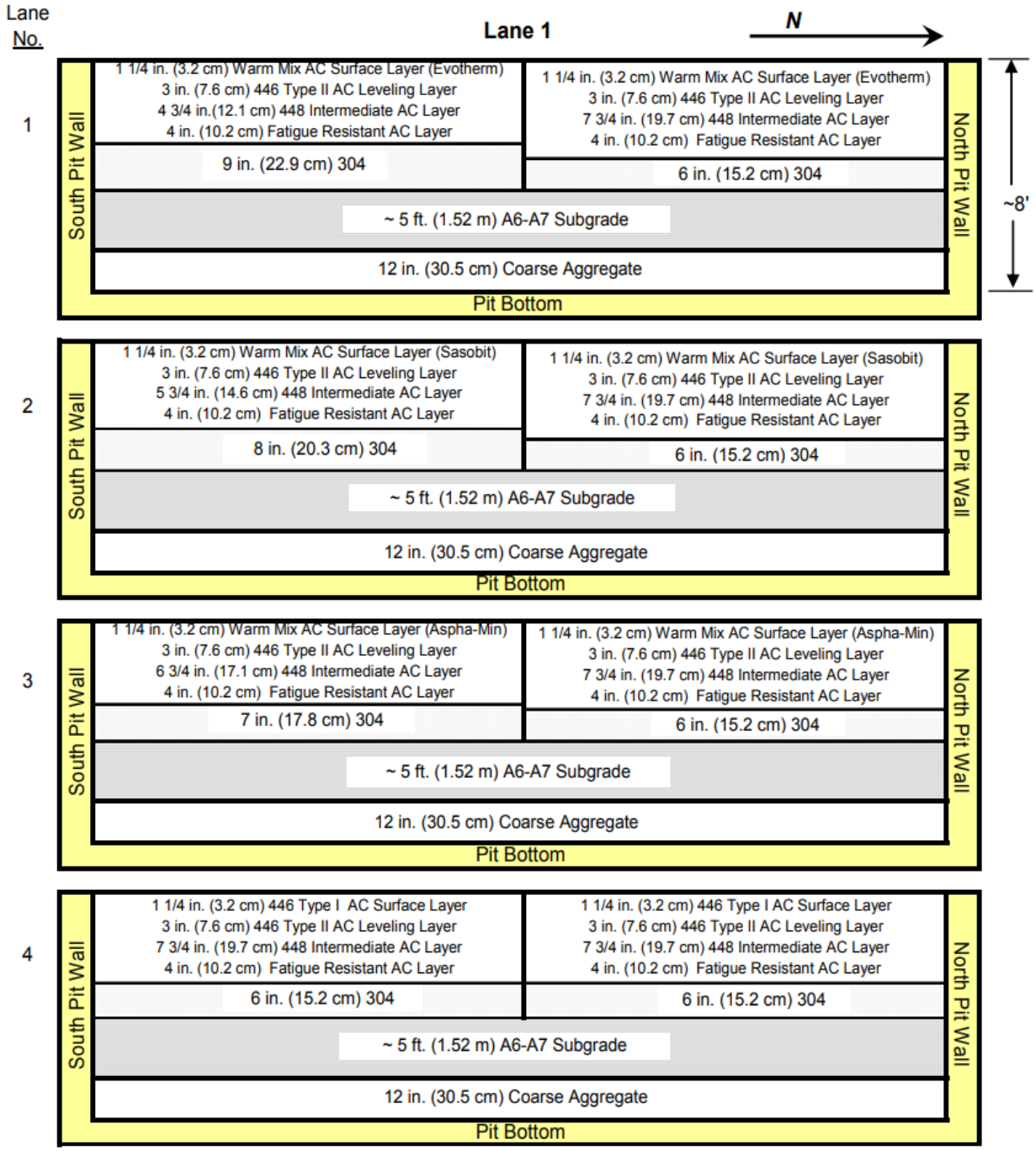


**Figure 7 APLF test section profile view diagram showing pavement build-up (Sargand et al. 2009)**

According to Sargand et al. [2009] instrumentation for capturing the temperature, subgrade pressure, and deflections relative to the top of the subgrade, and longitudinal and transverse strains at the base of the FRL were installed only in the southern half of each lane as shown in Figure 8.

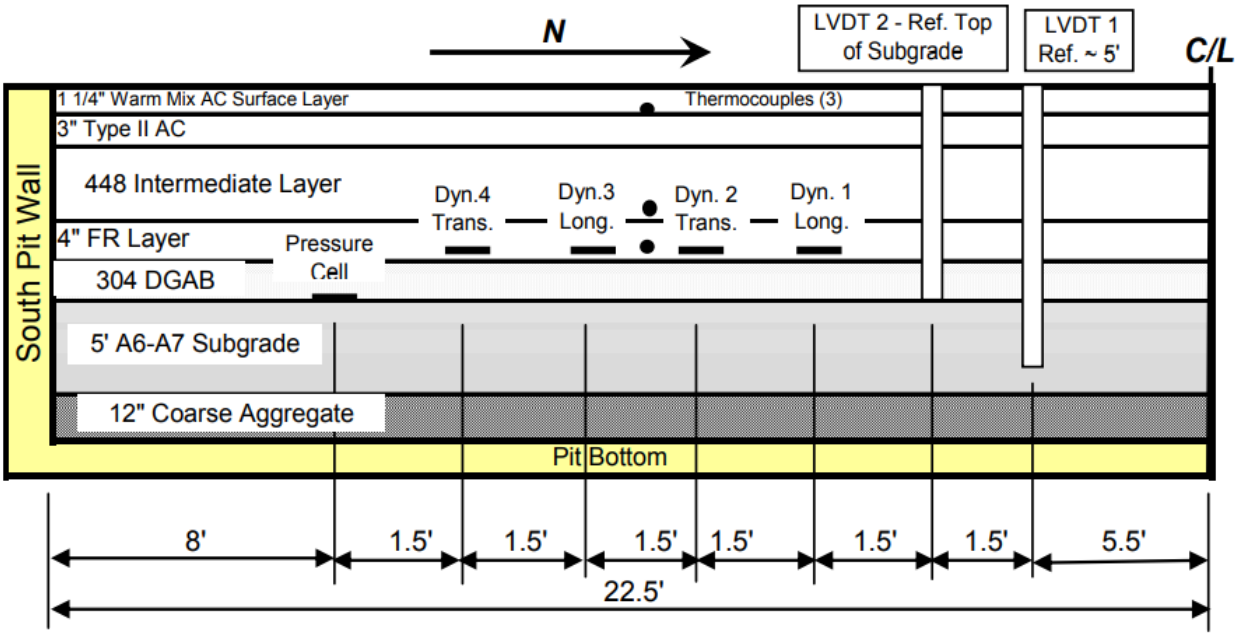


**Figure 8 Profile view showing sensor locations along southern section of each APLF lane (Sargand et al. 2009).**

In the APLF, the test sections were tested under wheel loads of 6, 9, and 12 kips (27, 40, and 53 kN) at three temperatures: 40˚F, 70˚F, and 104˚F (4˚C, 21˚C, and 40˚C) [Sargand et al., 2009]. A total of 10,000 passes of a 9kip axle with dual tires were conducted on each section at each temperature. Prior to and after completion of the 10,000 passes, wheel loads of 6, 9, and 12 kips (27, 40, and 53 kN) were applied at 4 offset locations to capture pavement responses. In this study, the measured transverse strains were greater than the longitudinal strains, therefore the transverse strains measured under the 9 kip load at the bottom of the FRL before and after the 10,000 passes at each temperature are presented in Figure 9 and Figure 10.

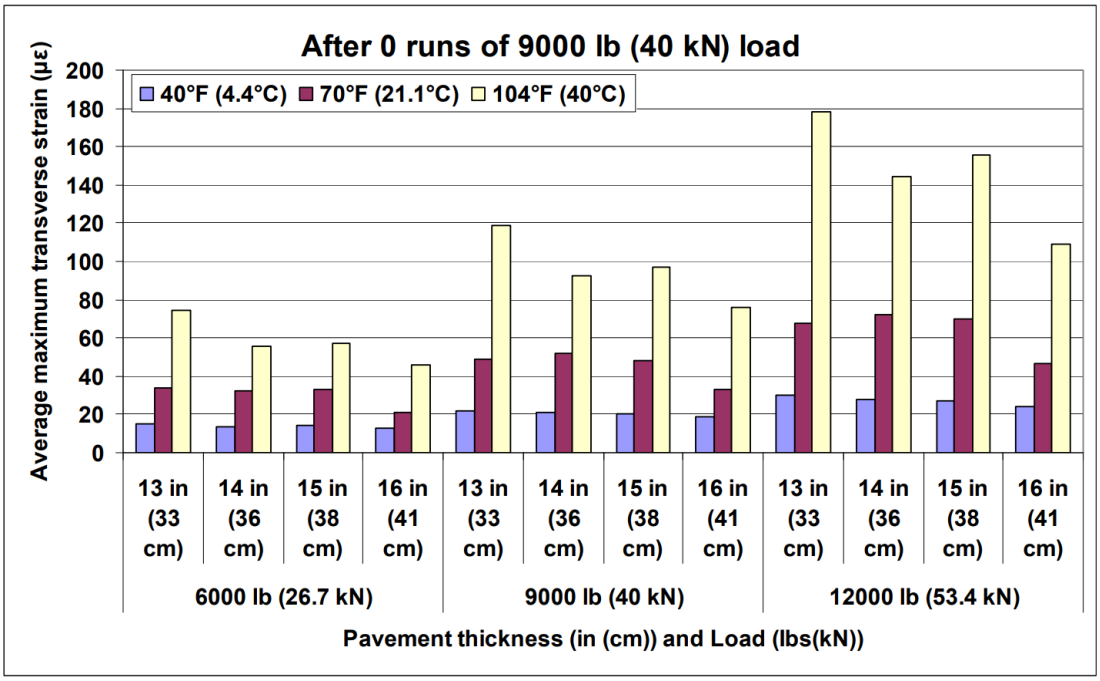


**Figure 9 Transverse Strain in FRL in APLF after 0 runs (Sargand et al., 2009).**

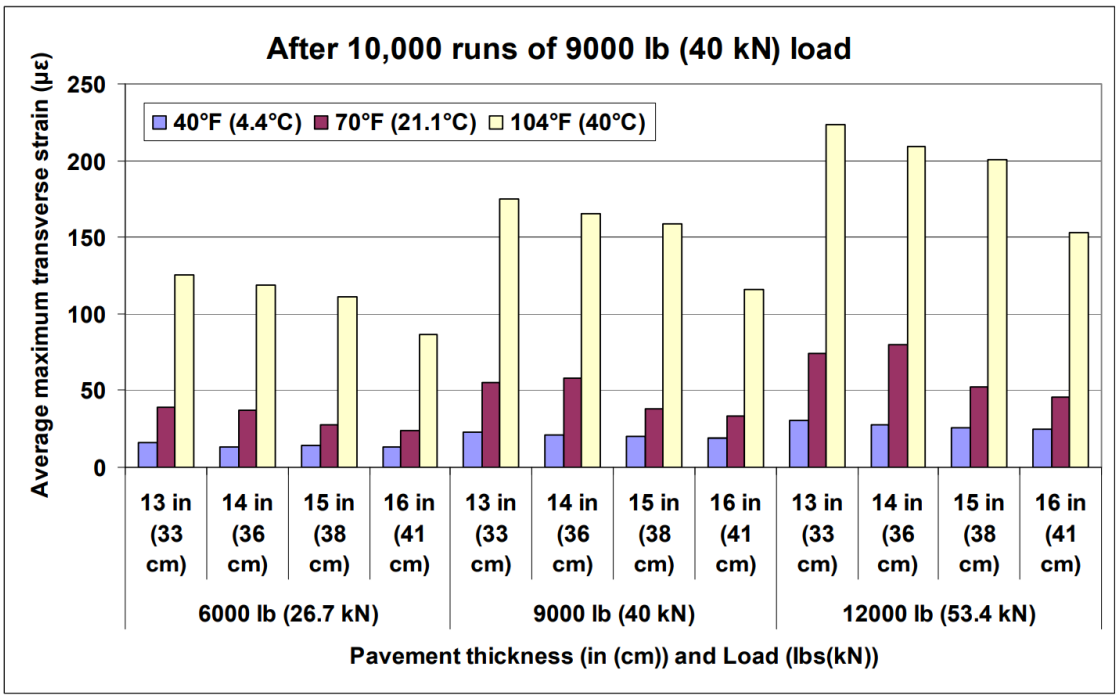


**Figure 10 Transverse Strain in FRL in APLF after 10,000 runs (Sargand et al., 2009).**

Strains in the longitudinal direction tended to fall below the limiting strain value of 70 microstrain, while strain in the transverse direction had a greater magnitude than in the longitudinal direction [Sargand et al., 2009]. The greatest transverse strains values, which far exceed 70 microstrain, were observed under a temperature of 104˚F (40˚C). According to Sargand et al. [2009], the temperature of the pavement is almost uniform throughout the AC layers due to the continuous applied heat in the APLF. However, a temperature gradient would

occur between the warmer pavement surface and the colder subgrade in real-world circumstances, thus reducing the strain at the bottom of the FRL. While differences in strain values are noted between the various pavement thicknesses, it was reported the differences were not significant. Sargand et al. [2009] concluded if the perpetual pavement thickness is reduced from 16" (406 mm) to 13" (330 mm) while increasing the thickness of the base structure, the pavement will be able to withstand loads just as effectively.

### *DEL-23*

ODOT and ORITE continued their research effort to develop optimized perpetual pavement design. When reconstructing test sections for the Strategic Highway Research Program (SHRP) Test Road on U.S. Route 23 in Delaware County, Ohio, four pavement test sections were constructed in 2012. These sections were built to verify prior findings from parts of WAY-30 and the APLF WMA/perpetual pavement project [Sargand et al., 2015]. Two sections were constructed on the mainline at DEL-23-19.41-19.54, located at the blue dot on the map below. Norton Waldo Road turns into US 23 Frontage road, which serves as an access road for the residents on Norton Waldo Road and US 23 and provides access to US 23. The sections constructed as part of this study were on Norton Waldo Road with the southern end of the sections located where one-way traffic begins and on the northern end the sections terminate at adjacent concrete test sections, shown by the green triangle on the map below.

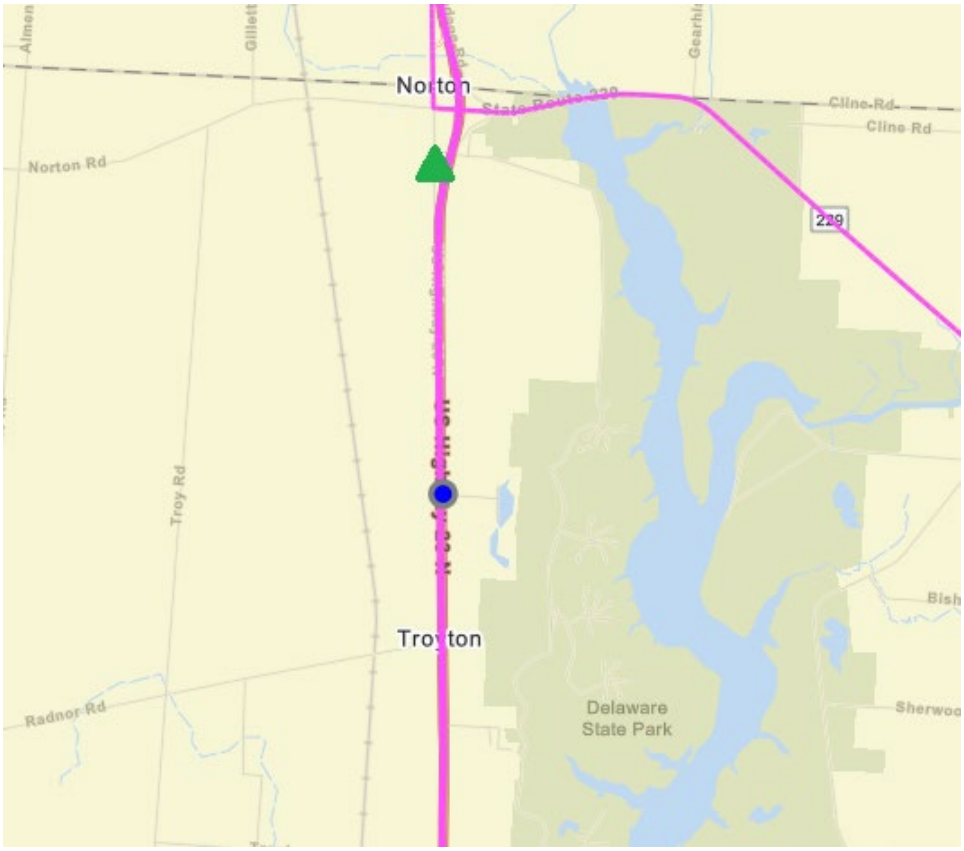


**Figure 11 Location of DEL-23 Test Sections on the Mainline (Blue Dot) and the Ramps (Green Triangle) (pathweb.pathwayservices.com/ohiopublic).**

According to Scheer [2013], four-layered sections of asphalt pavement with different thicknesses of 15” (381 mm), 13” (330 mm), 13” (330 mm), and 11” (279 mm) were constructed. Each test segment was constructed with a 6” (152 mm) DGAB and a 4” (102 mm) FRL. Table 3 summarizes the designed layer thicknesses. Both sections on the ramp, the 11” (279 mm) (Northbound) and 13” (330 mm) (Southbound) sections were constructed atop a lime-modified subgrade. The 13” (330 mm) and 15” (381 mm) sections on the mainline did not receive any subgrade stabilization or modification. A 3” (76 mm) increase in the mainline passing lane section (39P186) was discovered after the test section was built. It was therefore omitted from the investigation.

**Table 3 Specified layer thicknesses of DEL-23 pavement sections (Sargand et al., 2015).**

| Layer | 39D168 | | 39P186 | | 39BS803 | | 39BN803 | |
|---|---|---|---|---|---|---|---|---|
| | (in) | (cm) | (in) | (cm) | (in) | (cm) | (in) | (cm) |
| Surface Layer | 1 | 2.5 | 1 | 2.5 | 1 | 2.5 | 1 | 2.5 |
| Intermediate Layer | 2 | 5.1 | 2 | 5.1 | 2 | 5.1 | 2 | 5.1 |
| Base Layer | 8 | 20.3 | 6 | 15.2 | 6 | 15.2 | 4 | 10.2 |
| Fatigue Resistant Layer | 4 | 10.2 | 4 | 10.2 | 4 | 10.2 | 4 | 10.2 |
| Total Pavement Thickness | 15 | 38.1 | 13 | 33.0 | 13 | 33.0 | 11 | 27.9 |

Figure 12 shows the instrumentation installed in the wheel path of the lane to capture the pavement sections responses under the dynamic loading and the different environmental conditions, such as strain gages, pressure cells, LVDTs, and thermocouples.

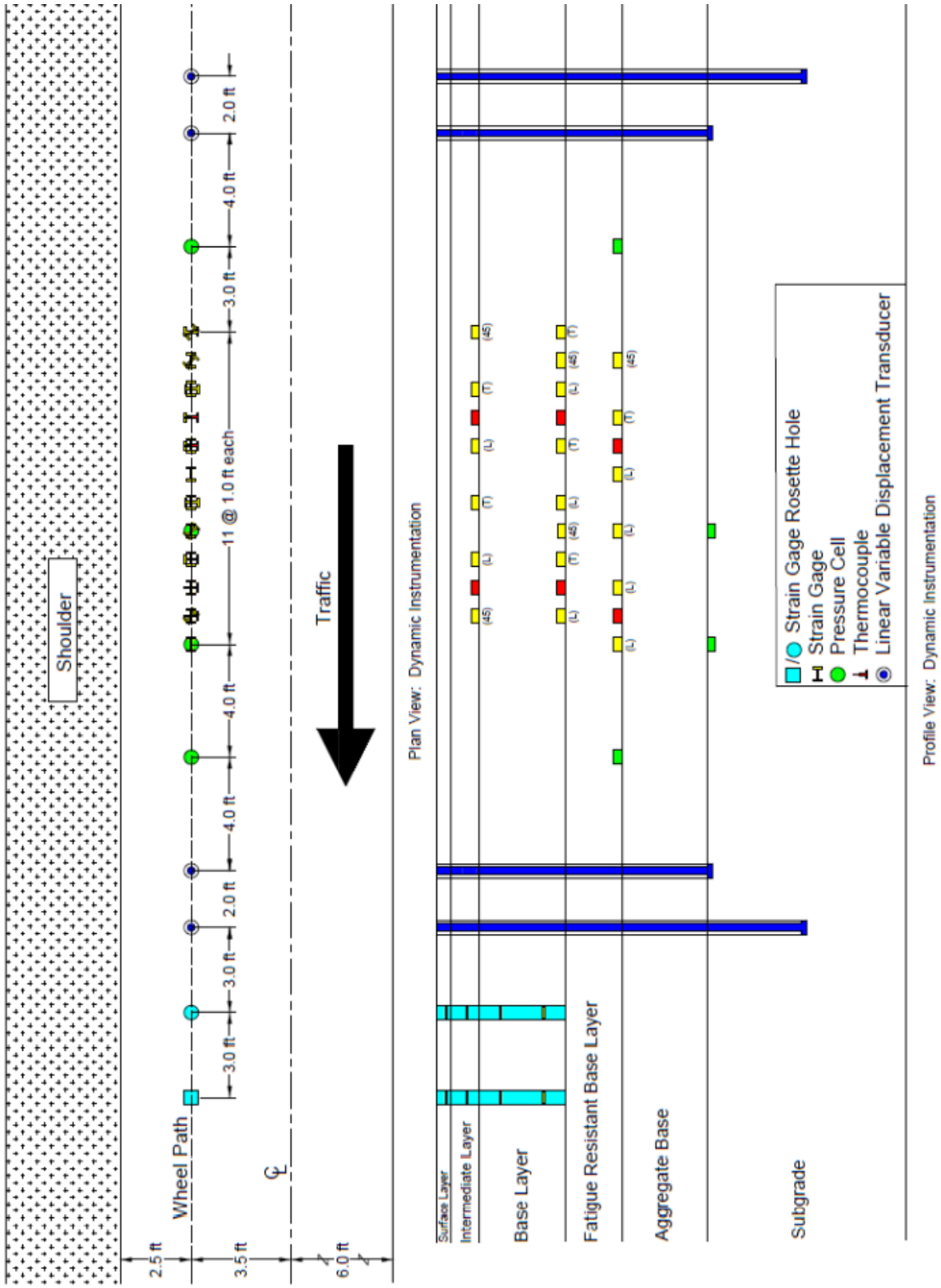


**Figure 12 Instrumentation Layout (Scheer, 2013)**

According to [Sargand et al., 2015], two CVL tests were performed with ODOT dump trucks. Winter conditions were measured for the first CVL tests in late November and December

2012. A summer-like environment was simulated for the second, which took place in July 2013. Similar axle configurations, weights, speeds, and tire pressure were used in both testing cycles. It was chosen to use two different axle configurations with the maximum possible carrying capacities for the trucks. When comparing the two trucks, the first had a tandem axle with a dual tire 37-kip (165 kN) axle load, while the second had a single axle with a wide-based tire and 29-kip (129 kN) axle load. Three tire pressures were evaluated 80 psi (552 kPa), 110 psi (758 kPa), and 125 psi (862 kPa), as well as three speeds, 5 mph (8 km/h), 30 mph (48 km/h), and 55 mph (89 km/h).

The average measured strain values at the bottom of the asphalt concrete layer (bottom of the FRL) were greatest in the longitudinal direction for each test section and are tabulated in Table 4. The temperature reported in Table 4 represents the average temperature measured in the FRL during the testing.

**Table 4 Average Measured Longitudinal Strain at Bottom of Asphalt Concrete, DEL-23 [*after* Sargand et al., 2015]**

| **Test Section:** | | **11 in (28 cm) (39BN803)** | | | **11 in (28 cm) (39BN803)** | | |
|---|---|---|---|---|---|---|---|
| Test Date and Temperature: | | December 18, 2012 43.9F (6.6C) | | | July 10, 2013 79.9F (26.6C) | | |
| Tire Pressure | | Speed | | | Speed | | |
| (psi) | (kPa) | 5 mph (8 km/h) | 30 mph (48 km/h) | 55 mph (89 km/h) | 5 mph (8 km/h) | 30 mph (48 km/h) | 55 mph (89 km/h) |
| 80 | 552 | 46.09 | 39.14 | 32.92 | **95.95** | **73.09** | **72.65** |
| 110 | 758 | 47.17 | 41.67 | 39.00 | **106.5** | **73.86** | 64.23 |
| 125 | 862 | 47.12 | 38.19 | 36.13 | **101.45** | **73.11** | 56.41 |
| **Test Section:** | | **13 in (33 cm) (39BS803)** | | | **13 in (33 cm) (39BS803)** | | |
| Test Date and Temperature: | | December 19, 2012 44.2F (6.8C) | | | July 11, 2013 81.5F (27.5C) | | |
| 80 | 552 | 31.10 | 26.37 | 22.054 | **75.04** | 44.20 | 39.88 |
| 110 | 758 | 31.07 | 25.61 | 25.45 | 68.51 | 45.59 | 37.62 |
| 125 | 862 | 31.88 | 25.57 | 23.54 | 66.00 | 40.13 | 35.98 |
| **Test Section:** | | **15 in (38 cm) (39D168)** | | | **15 in (38 cm) (39D168)** | | |
| Test Date and Temperature: | | November 29, 2012 41.4F (5.22C) | | | July 1, 2013 84.4F (29.1C) | | |
| 80 | 552 | 39.53 | 31.12 | 25.7 | **77.92** | 57.62 | 42.11 |
| 110 | 758 | 38.62 | 32.21 | 25.79 | **74.97** | 54.42 | 47.79 |
| 125 | 862 | 35.72 | 29.25 | 24.39 | **70.46** | 55.20 | 44.23 |

On the cold test dates, the measured strain values were low, with all maximum longitudinal strain measurements less than 50 microstrain at the bottom of the asphalt concrete layer. As expected, the highest strain values were recorded during the summer, with the highest strain values occurring in the 11" (280-mm) test section on lime-modified subgrade at the slowest test speed. In comparing the measured average strain values to a conservative, singular strain threshold of 70 microstrain, all sections had at least one measured strain value at the slowest speed that exceeded this threshold, as shown in bold in the table above. The 11" (280 mm) cross-section on lime-modified subgrade consistently exceeded a 70 microstrain threshold during the high temperature tests. The 13" (330 mm) cross-section on lime-modified subgrade only failed the threshold at the high temperature under 5 mph (8 km/h) and 80 psi (552 kPa) tire pressure, with a strain value slightly greater than the threshold. The 15" (381 mm) section

on un-modified subgrade exceeded 70 microstrain at the high temperature test for tire pressures at the slowest speed, but again, the amount by which the threshold was exceeded was not excessive.

The researchers (Sargand et al., 2015) further evaluated these cross-sections within the context of perpetual pavement design by applying the NCHRP 9-44A endurance limit model (Witczak et al., 2013) listed in equation 1, below to evaluate the susceptibility to bottom-up fatigue cracking. The researchers stated a SR greater than or equal to 1.0 indicates a cross-section is perpetual.

$$SR = 2.0844 - 0.1386\log(E_0) - 0.4846\log(\varepsilon_t) - 0.2012\log(N) + 1.4103\tanh(0.8471RP) + 0.0320\,(\log(E_0))\,(\log(\varepsilon_t) - 0.0954(\log(E_0))\,(\tanh(0.7154RP)) - 0.4746(\log(\varepsilon_t))(\tanh(0.6574RP)) + 0.0041\,(\log(N))(\log(E_0)) + 0.0557\,(\log(N))(\log(\varepsilon_t)) + 0.0689\,(\log(N))(\tanh(0.259RP)) \quad (1)$$

Where,

SR = Stiffness ratio (ratio of stiffness measured at any load cycle during beam fatigue testing to the initial stiffness of the specimen)
$E_0$ = Initial flexural stiffness (ksi)
$\varepsilon_t$ = Applied tensile strain (microstrain)
RP = Rest period
N = Number of load cycles

First, the researchers determined the SR for each test section by applying the average measured tensile strains at the slowest speed among the three tire pressures for each test date. The following assumptions were made:

- Initial flexural stiffness can be defined in two ways, both were evaluated:
  - Initial flexural stiffness is equivalent to dynamic modulus (E*): $E_0 = E^*$
  - Initial flexural stiffness is half the dynamic modulus: $E_0 = E^*/2$
  - E* was determined from a regression equation for the asphalt FRL mix generated from laboratory testing
  - E* was determined at a frequency of 10 Hz and the pavement test temperature
- RP = 5 seconds
- N = 200,000

Additionally, Sargand et al. (2015) determined the FEL in the field for each test date by setting the SR equal to one and solving for the tensile strain following the above assumptions. The results for SR and FEL are listed in Table 5 and Table 6 for the $E_0$ definitions listed above, respectively.

**Table 5 DEL-23 Results, SR and FEL calculated for $E_0$ = E* (*after* Sargand et al., 2015)**

| Test Date | Pavement Depth (in) | Pavement Depth (cm) | Avg. Temp (°F) | Avg. Temp (°C) | $E_0$ (ksi) | $E_0$ (GPa) | SR | Avg Strain (με) | FEL (με) |
|---|---|---|---|---|---|---|---|---|---|
| 12/18/2012 | 11 | 28 | 44 | 6.7 | 2364 | 16.3 | 1.1 | 47 | 71 |
| 12/19/2012 | 13 | 33 | 44 | 6.7 | 2352 | 16.22 | 1.2 | 31 | 71 |
| 11/29/2012 | 15 | 38 | 41 | 5.0 | 2460 | 16.96 | 1.15 | 38 | 70 |
| 7/10/2013 | 11 | 28 | 80 | 26.7 | 1192 | 8.22 | **0.96** | 101 | 85 |
| 7/11/2013 | 13 | 33 | 81 | 27.2 | 1151 | 7.94 | 1.05 | 70 | 86 |
| 7/1/2013 | 15 | 38 | 84 | 28.9 | 1075 | 7.41 | 1.04 | 74 | 88 |

**Table 6 DEL-23 Results, SR and FEL calculated for $E_0$ = E*/2 (*after* Sargand et al., 2015)**

| Test Date | Pavement Depth (in) | Pavement Depth (cm) | Avg. Temp (°F) | Avg. Temp (°C) | $E_0$ (ksi) | $E_0$ (GPa) | SR | Avg Strain (με) | FEL (με) |
|---|---|---|---|---|---|---|---|---|---|
| 12/18/2012 | 11 | 28 | 44 | 6.7 | 1182 | 8.15 | 1.15 | 47 | 86 |
| 12/19/2012 | 13 | 33 | 44 | 6.7 | 1176 | 8.11 | 1.25 | 31 | 86 |
| 11/29/2012 | 15 | 38 | 41 | 5.0 | 1230 | 8.48 | 1.20 | 38 | 85 |
| 7/10/2013 | 11 | 28 | 80 | 26.7 | 596 | 4.11 | 1.00 | 101 | 102 |
| 7/11/2013 | 13 | 33 | 81 | 27.2 | 575 | 3.96 | 1.10 | 70 | 103 |
| 7/1/2013 | 15 | 38 | 84 | 28.9 | 537 | 3.70 | 1.09 | 74 | 105 |

For $E_0$ = E*/2, the SR was greater than 1.0 for all sections and average pavement temperatures at which CVL testing was conducted. Results were similar for $E_0$ = E*, except for the hot temperature in the 11" (279 mm) cross-section on lime-modified subgrade which had a SR of 0.96 which would not be considered perpetual. Using the average measured tensile strain, the researchers use the NCHRP 9-44A model to estimate in-situ FEL, with results showing all sections had an FEL of 70 microstrain or greater, depending on the pavement temperature, and definition of $E_0$. Regardless of the definition of $E_0$, both the 13" (330 mm) and 15" (381 mm) cross-sections had average measured strain values less than the estimated in-situ FEL of the FRL layers. As noted above, the average measured tensile strain values shown in Tables 5 and 6 reflect the slowest speed applied (5 mph (8 km/h)), which is a conservative evaluation as it is expected most of the traffic would be traveling at a higher rate of speed and thus, inducing lower tensile strain values. The average measured tensile strain values in the 11-inch cross-section was substantially greater than the estimated FEL when $E_0$=E* and nearly equal to the estimated FEL when $E_0$ = E*/2.

Based on the results presented in Tables 4 – 6, the researchers concluded the 13" (330 mm) cross-section on lime-modified subgrade and the 15" (381 mm) cross-section on un-modified subgrade met the criteria for perpetual pavement. For both of these sections:

- The SR was greater than 1.0 for both definitions for $E_0$ at the intermediate and high temperature, and
- The average measured tensile strain was substantially less than the estimated FELs at each temperature and
- The average measured tensile strain only slightly exceeded 70 microstrain under the most extreme condition tested (5 mph (8 km/h) and high temperature) which was

expected to be outside of the normal conditions to which the pavement would be subjected.

### *Highly Modified Asphalt (HiMA) in the APLF*

Constructed in 2013, the second study conducted in the APLF related to perpetual pavements sought to evaluate thickness relative to the use of highly polymer modified asphalt throughout the cross-section [Sargand et al., 2015]. Lab testing at NCAT [Timm et al., 2013) found the highly polymer modified asphalt mix, with a 7.5% styrene-butadiene-styrene (SBS) polymer content, exhibited enhanced fatigue characteristics compared to the control section and high increased stiffness at high temperatures. ODOT, in cooperation with Kraton Corporation, funded the construction and testing of test sections in the APLF to evaluate highly polymer modified asphalt using Kraton polymers (referred to as HiMA). The HiMA sections were thinner than the sections constructed on US 23, having a total asphalt thickness of 8" (203 mm), 9 in (228 mm), 10" (254 mm) and 11" (279 mm). The three thinner sections were constructed with HiMA in all layers, while the 11" (279 mm) control section had HiMA in the surface and intermediate layer and a base layer of conventional asphalt. All sections were constructed on a 6" (150 mm) DGAB atop a cement-stabilized subgrade [Sargand et al., 2015]. Unlike the other perpetual pavements constructed prior, the HiMA sections did not have a fatigue resistant layer. Table 7 lists the APLF test section build-ups.

**Table 7 APLF test section build-ups [Sargand et al., 2015]**

| Layer | ODOT Item | Layer thickness for each section | | | | | | | |
|---|---|---|---|---|---|---|---|---|---|
| | | Lane A (HiMA) | | Lane B (HiMA) | | Lane C (HiMA) | | Lane D (Control) | |
| | | (in) | (cm) | (in) | (cm) | (in) | (cm) | (in) | (cm) |
| Surface | 424 | 1.50 | 3.81 | 1.50 | 3.81 | 1.50 | 3.81 | 1.50 | 3.81 |
| Intermediate | 442 | 1.75 | 4.45 | 1.75 | 4.45 | 1.75 | 4.45 | 1.75 | 4.45 |
| AC Base | 302 | 4.75 | 12.07 | 5.75 | 14.61 | 6.75 | 17.15 | 7.75 | 19.69 |
| **Total AC** | **-** | **8.00** | **20.33** | **9.00** | **22.87** | **10.00** | **25.41** | **11.00** | **27.95** |
| Aggregate Base | 304 | 6.00 | 15.24 | 6.00 | 15.24 | 6.00 | 15.24 | 6.00 | 15.24 |
| Cement stabilized subgrade | 206 | 18.00 | 45.72 | 18.00 | 45.72 | 18.00 | 45.72 | 18.00 | 45.72 |
| Subgrade (type) | - | A-6/A-7 | | A-6/A-7 | | A-6/A-7 | | A-6/A-7 | |

Based on the same instrumentation plan used in the APLF's previous study in 2009, strain gauges, thermocouples, and linear variable differential transformers (LVDTs) were installed for measuring the dynamic load responses of the 4 test sections [Cichocki, 2015]. Figure 13 shows the instrumentation plan for Lane A, which reflects the instrumentation plan of all four lanes.

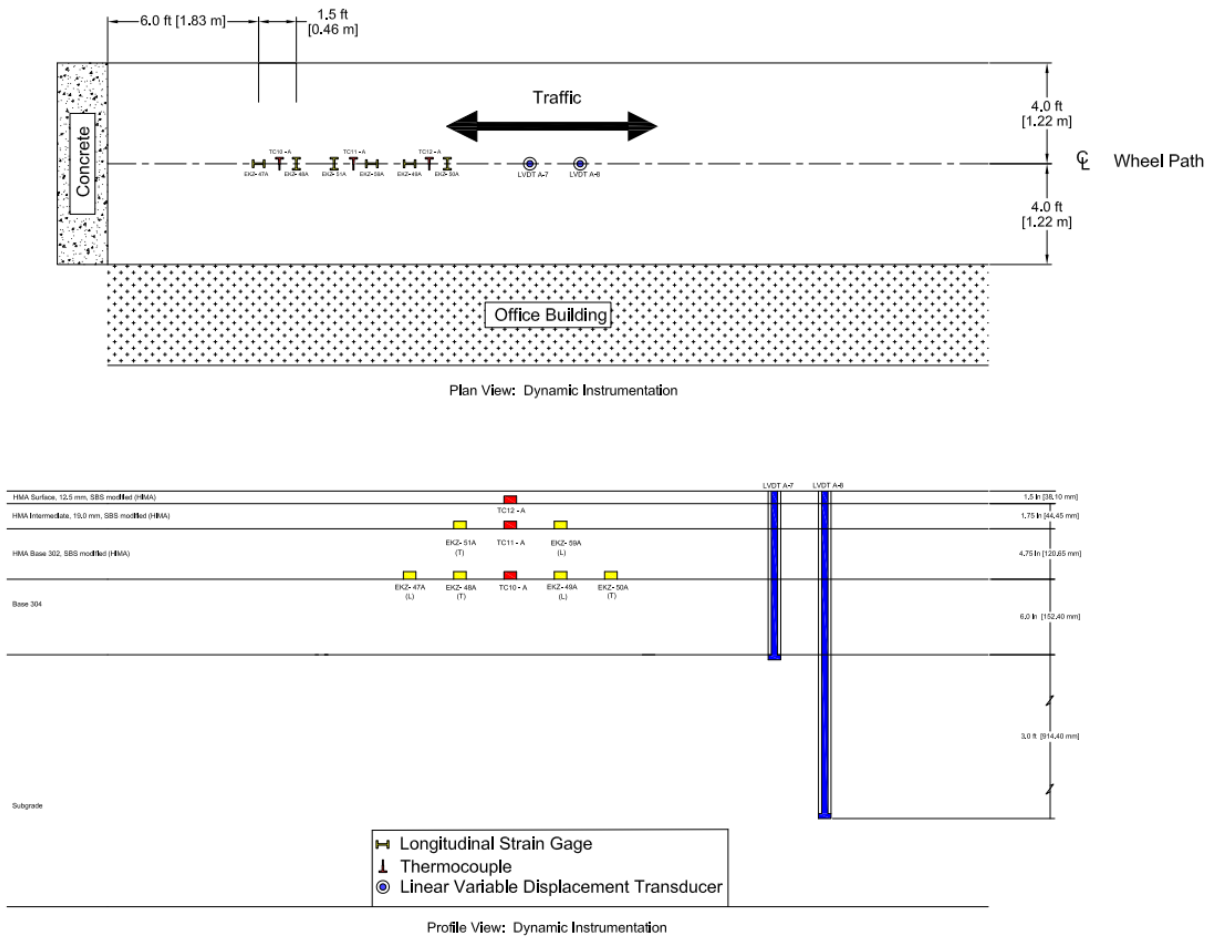


**Figure 13 Instrumentation plan for Lane A in the APLF (Cichocki, 2015)**

From May to September 2014, wheel load testing was conducted at 5 mph (8 km/h) in the APLF (Cichocki, 2015). Testing was conducted at 70F (21C) and 100F (38C), in which 10,000 passes of a single axle load of 9 kip (40 kN) were applied at each temperature for all test sections. Data from the embedded sensors were collected after 100, 300, 1000, 3000, and 10,000 passes. At each increment load levels of : 6 kip (27 kN), 9 kip (40 kN), and 12 kip (53 kN) were applied to collect strain responses at each load, then the load was returned to 9 kip (40 kN) and passes applied until the next data collection increment was hit. Strain at the bottom of the asphalt concrete layer was consistently greater in the longitudinal direction than the transverse. The average and maximum longitudinal strain measurements at 70° F (21° C) and 100° F (38° C), respectively are shown in Table 8. As expected, the highest strain values were measured in the thinnest section, Lane A, despite having HiMA in all asphalt layers. The lowest strain values were measured in Lane C, the 10" (254 mm) section featuring HiMA throughout the cross-section. Although Lane D was the thickest cross-section, it was the "control" section as a conventional asphalt base layer was used in place of the HiMA base layer that was used it the other three lanes. As a result, the maximum strain values in Lane D were comparable to those of Lane C at the high temperature, and greater than those in Lane C at the intermediate temperature. This illustrates the benefit of HiMA; by using HiMA in the all layers, as opposed to just the surface and intermediate layer, the total asphalt thickness required to produce comparable strain values to the control lane was reduced by 1" (25.4 mm). It is also known that HiMA is a strain tolerant material, as such, the higher strain values in Lane C at the high

temperature, may not indicate reduced performance. Sargand et al. (2015) reported minimal rutting in all lanes, with maximum rut depth in Lane C measured at 0.054" (1.38 mm) compared to 0.069" (1.74 mm) in Lane D after 10,000 passes at 100° F (37.8° C). No cracking was observed after 20,000 passes (10,000 each at test temperature), however the experiment was not designed to apply axle passes until pavement failure.

**Table 8 Average and Maximum Longitudinal Strain at the Bottom of the Asphalt Concrete Layer (Cichocki, 2015)**

| Lane | AC thickness | | Load (lb (kN)) | | | | | |
|---|---|---|---|---|---|---|---|---|
| | | | 6000 (27) | | 9000 (40) | | 12000 (53) | |
| | (in) | (cm) | Avg | Max | Avg | Max | Avg | Max |
| 70° F (21.1° C) | | | | | | | | |
| A | 8 | 20 | 35 | 43 | 54 | 61 | 70 | 79 |
| B | 9 | 23 | 31 | 36 | 48 | 54 | 62 | 69 |
| C | 10 | 25 | 21 | 24 | 35 | 46 | 46 | 51 |
| D | 11 | 28 | 27 | 43 | 40 | 52 | 52 | 67 |
| 100° F (37.8° C) | | | | | | | | |
| A | 8 | 20 | 62 | 66 | 89 | 93 | 106 | 113 |
| B | 9 | 23 | 41 | 46 | 63 | 73 | 79 | 83 |
| C | 10 | 25 | 34 | 44 | 50 | 56 | 61 | 67 |
| D | 11 | 28 | 27 | 34 | 43 | 56 | 56 | 73 |

From a perpetual pavement design concept, a single strain threshold of 70 microstrain, although conservative, has historically been used to assess the likelihood of perpetual pavement performance. The maximum strain values presented in Table 8 show Lanes A and B exceed 70 microstrain at the high temperature, whereas Lanes C and D do not. Loading is applied at approximately 5 mph (8km/h) and loading is not applied until the entire pavement cross-section maintains the target temperature, as such these conditions are extreme relative to conditions to which an in-service pavement are subjected.

The APLF sections were evaluated within the context of perpetual pavement design using the NCHRP Project 9-44A stiffness ratio (SR) and calculated FEL [Sargand et al., 2015], as was done for the DEL-23 project, described previously. The in-situ FEL was estimated by setting SR equal to one and solving for results of the analyses using the NCHRP 9-44A model are listed in Table 9 and Table 10.
The SR for each section at each temperature, also shown in Table 9 and Table 10, was estimated following Equation 1, in which

- Initial flexural stiffness can be defined in two ways, both were evaluated:
  - Initial flexural stiffness is equivalent to dynamic modulus (E*): $E_0 = E^*$
  - Initial flexural stiffness is half the dynamic modulus: $E_0 = E^*/2$
  - E* was determined from a regression equation for the asphalt base mix generated from laboratory testing
  - E* was determined at a frequency of 10 Hz and the pavement test temperature
- RP = 5 seconds
- N = 200,000
- Average tensile strain was the average strain measured under the 12,000 lb (53 kN) load level at 70° F (21° C) and 100°F (38° C)

**Table 9 HiMA APLF Results, SR and FEL calculated for $E_0$ = E* (after Sargand et al., 2015)**

| Lane | Mix | Pavement Depth (in) | Pavement Depth (cm) | Test Temp (°F) | Test Temp (°C) | $E_0$ (ksi) | $E_0$ (GPa) | SR | Avg Strain (με) | FEL (με) |
|---|---|---|---|---|---|---|---|---|---|---|
| A | HiMA Base | 8 | 20 | 70 | 21 | 1552 | 10.70 | 1.03 | 70 | 79 |
| | | | | 100 | 37 | 733 | 5.05 | **0.98** | 106 | 97 |
| B | HiMA Base | 9 | 23 | 70 | 21 | 1552 | 10.70 | 1.06 | 62 | 79 |
| | | | | 100 | 37 | 733 | 5.05 | 1.05 | 79 | 97 |
| C | HiMA Base | 10 | 25 | 70 | 21 | 1552 | 10.70 | 1.13 | 46 | 79 |
| | | | | 100 | 37 | 733 | 5.05 | 1.11 | 61 | 97 |
| D | Control Base | 11 | 28 | 70 | 21 | 1515 | 10.45 | 1.10 | 52 | 80 |
| | | | | 100 | 37 | 677 | 4.67 | 1.14 | 56 | 99 |

**Table 10 HiMA APLF Results, SR and FEL calculated for $E_0$ = E*/2 (after Sargand et al., 2015)**

| Lane | Mix | Pavement Depth (in) | Pavement Depth (cm) | Test Temp (°F) | Test Temp (°C) | $E_0$ (ksi) | $E_0$ (GPa) | SR | Avg Strain (με) | FEL (με) |
|---|---|---|---|---|---|---|---|---|---|---|
| A | HiMA Base | 8 | 20 | 70 | 21 | 776 | 5.35 | 1.03 | 70 | 95 |
| | | | | 100 | 37 | 367 | 2.53 | 1.02 | 106 | 116 |
| B | HiMA Base | 9 | 23 | 70 | 21 | 776 | 5.35 | 1.11 | 62 | 95 |
| | | | | 100 | 37 | 367 | 2.53 | 1.10 | 79 | 116 |
| C | HiMA Base | 10 | 25 | 70 | 21 | 776 | 5.35 | 1.18 | 46 | 95 |
| | | | | 100 | 37 | 367 | 2.53 | 1.16 | 61 | 116 |
| D | Control Base | 11 | 28 | 70 | 21 | 757 | 5.22 | 1.15 | 52 | 96 |
| | | | | 100 | 37 | 339 | 2.34 | 1.19 | 56 | 118 |

To be considered perpetual, the SR should be greater than or equal to one. In determining the SR, the initial flexural stiffness is assumed to be either 1) equivalent to the dynamic modulus, or 2) equivalent to one-half the dynamic modulus. Under the first assumption all lanes, except lane A (the 8" (203 mm) section), met the SR criterion to be perpetual. However, when the second assumption was applied, all lanes had SR greater than or equal to one [Sargand et al. 2015]. Similarly, Lane A was the only section with a measured tensile strain exceeding the estimated in-situ FEL (see Table 9) under the first definition of $E_0$. Sargand et al. [2015] recommended a field study be conducted to determine optimal thickness for perpetual pavement design and concluded the 9" (229 mm) HiMA cross-section built on top of a 6" (150 mm) dense graded aggregate base and chemically stabilized subgrade may be sufficient to provide perpetual pavement performance at 70° F (21° C) and 100° F (38° C).

### *Field Performance of Existing Perpetual Pavement Test Sections in Ohio*

A summary of the cross-sections that have been constructed to evaluate perpetual pavement design in Ohio is provided in Table 11. As described previously, CVL of the in-service test sections were conducted at various temperatures and speeds during the first year of service. Those test sections in the APLF were subjected to 10,000 passes of a 9-kip (40 kN) load at each test temperature. The strains measured in each test section are summarized in Table 12.

**Table 11 Summary of Designed Cross-sections of Instrumented Perpetual Pavement Test Sections in Ohio (1 inch = 2.54 cm)**

| Location | AC Layer 1 | | AC Layer 2 | | AC Layer 3 | | AC Layer 4 | | Total AC | DGAB | Subgrade |
|---|---|---|---|---|---|---|---|---|---|---|---|
| STA-77 | SMA | 1.50 in | 442 Type A | 1.75 in | 302 ATB | 9.0 in | FRL | 4.0 in | 16.25 in | 6.0 in | Unstabilized |
| WAY-30 | SMA | 1.50 in | 442 19 mm | 1.75 | 302 ATB | 9.0 in | FRL | 4.0 in | 16.75 in | 6.0 in | Unstabilized |
| APLF WMA 1S | WMA | 1.25 in | 446 Type 2 | 3.0 in | 448 Intermediate | 4.75 in | FRL | 4.0 in | 13.00 in | 9.0 in | Unstabilized |
| APLF WMA 2S | WMA | 1.25 in | 446 Type 2 | 3.0 in | 448 Intermediate | 5.75 in | FRL | 4.0 in | 14.00 in | 8.0 in | Unstabilized |
| APLF WMA 3S | WMA | 1.25 in | 446 Type 2 | 3.0 in | 448 Intermediate | 6.75 in | FRL | 4.0 in | 15.00 in | 7.0 in | Unstabilized |
| APLF WMA 4S | HMA | 1.25 in | 446 Type 2 | 3.0 in | 448 Intermediate | 7.75 in | FRL | 4.0 in | 16.00 in | 6.0 in | Unstabilized |
| DEL-23 Mainline | Fine Graded | 1.0 in | 19 mm Intermediate | 2.0 in | Asphalt Base | 8.0 in | FRL | 4.0 in | 15.00 in | 6.0 in | Unstabilized |
| DEL-23 SB Ramp | Fine Graded | 1.0 in | 19 mm Intermediate | 2.0 in | Asphalt Base | 6.0 in | FRL | 4.0 in | 13.00 in | 6.0 in | Lime-modified |
| DEL-23 NB Ramp | Fine Graded | 1.0 in | 19 mm Intermediate | 2.0 in | Asphalt Base | 4.0 in | FRL | 4.0 in | 11.00 in | 6.0 in | Lime-modified |
| APLF HiMA Lane A | HiMA Surface | 1.5 in | HiMA Intermediate | 1.75 in | HiMA Base | 4.75 in | | | 8.00 in | 6.0 in | Cement-stabilized |
| APLF HiMA Lane B | HiMA Surface | 1.5 in | HiMA Intermediate | 1.75 in | HiMA Base | 5.75 in | | | 9.00 in | 6.0 in | Cement-stabilized |
| APLF HiMA Lane C | HiMA Surface | 1.5 in | HiMA Intermediate | 1.75 in | HiMA Base | 6.75 in | | | 10.00 in | 6.0 in | Cement-stabilized |
| APLF HiMA Lane D | HiMA Surface | 1.5 in | HiMA Intermediate | 1.75 in | Conventional Base | 7.75 in | | | 11.00 in | 6.0 in | Cement-stabilized |

WMA: Warm-mix asphalt
HMA: Hot-mix asphalt

**Table 12 Summary of Measured Strain Values in Ohio Perpetual Pavement Test Sections (1 inch = 2.54 cm, 1 kip = 4.448 kN)**

| Location | CVL Load (kips) | CVL Speeds | Temperatures* | Measured Strain** |
|---|---|---|---|---|
| STA-77 (16.25 in) | Single axle: 26 | 5 – 50 mph (8 – 80 km/h) | 36F | < 35 με |
| WAY-30 (16.75 in) | Single axle: 17.5; 28.2; 20.35 Tandem axle: 28.5; 40.15; 34.55 | 5 – 55 mph (8 – 89 km/h) | 31F<br>97F | 19 - 33 με<br>71 - 129 με |
| APLF WMA 1S (13 in) | Single axle: 6.0; 9.0; 12.0 | 5 mph (8 km/h) | 40F<br>70F<br>104F | 16 – 30 με<br>39 - 74 με<br>125 – 221 με |
| APLF WMA 2S (14 in) | Single axle: 6.0; 9.0; 12.0 | 5 mph (8 km/h) | 40F<br>70F<br>104F | 13 – 29 με<br>37 – 78 με<br>120 - 208 με |
| APLF WMA 3S (15 in) | Single axle: 6.0; 9.0; 12.0 | 5 mph (8 km/h) | 40F<br>70F<br>104F | 14 – 26 με<br>28 – 53 με<br>118 - 205 με |
| APLF WMA 4S (16 in) | Single axle: 6.0; 9.0; 12.0 | 5 mph (8 km/h) | 40F<br>70F<br>104F | 13 – 25 με<br>23 – 46 με<br>87 – 150 με |
| DEL-23 Mainline (15 in) | Wide base tire: 29<br>Dual tire tandem: 37 | 5 – 55 mph (8 – 89 km/h) | 45F<br>83F | 29 – 43 με<br>51 – 102 με |
| DEL-23 SB Ramp (13 in) | Wide base tire: 29<br>Dual tire tandem: 37 | 5 – 55 mph (8 – 89 km/h) | 45F<br>83F | 27 – 35 με<br>42 - 85 με |
| **DEL-23 NB Ramp (11 in)** | **Wide base tire: 29<br>Dual tire tandem: 37** | **5 - 55 mph (8 - 89 km/h)** | **45F<br>83F** | **49 - 68 με<br>92 - 143 με** |
| **APLF HiMA Lane A (8 in)** | **Single axle: 6.0; 9.0; 12.0** | **5 mph (8 km/h)** | **70F<br>100F** | **43 - 79 με<br>66 - 113 με** |
| APLF HiMA Lane B (9 in) | Single axle: 6.0; 9.0; 12.0 | 5 mph (8 km/h) | 70F<br>100F | 36 – 69 με<br>46 - 83 με |
| APLF HiMA Lane C (10 in) | Single axle: 6.0; 9.0; 12.0 | 5 mph (8 km/h) | 70F<br>100F | 24 – 51 με<br>44 - 67 με |
| APLF HiMA Lane D (11 in) | Single axle: 6.0; 9.0; 12.0 | 5 mph (8 km/h) | 70F<br>100F | 43 – 67 με<br>34 - 73 με |

* Pavement temperatures reported, except for WAY-30
**APLF WMA sections: Transverse strain reported, all others are longitudinal strain

As expected the highest strain values were measured under the slowest speed (5 mph (8 km/h)) and high pavement temperatures. Measured strain values were compared to a conservative singular strain value of 70 microstrain as an initial assessment as to whether these cross-sections would likely perform perpetually. As was noted, measured strain exceeded this value in some cross-sections, however those sections constructed on in-service interstate or interstate look-a-likes, they would likely not be subjected to traffic at very slow speeds and high pavement temperatures. For the WMA sections in the APLF, the pavement temperature was for the entire cross-section, which is more extreme than would typically occur in the field.

Another approach to evaluate whether a pavement met perpetual pavement criteria was explored for DEL-23 and APLF HiMA sections in which the NCHRP 9-44A model was applied to determine the SR and the in-place FEL. Based on that evaluation it was concluded 2 sections, listed in bold in Table 12 were not likely to behave perpetually.

While the evaluation of measured strain is helpful in evaluating the likelihood a pavement will perform perpetually or not, field measured performance is the best method to confirm the results from the strain evaluations. Therefore, previously constructed test sections designed as perpetual pavements were reexamined to ensure field performance is in line with perpetual pavement requirements (no bottom-up fatigue cracking, only surface distresses). WAY-30 and STA-77 were revisited as part of the previous study [Sargand et al., 2015]. At that time, both sections showed good results in terms of structural integrity. The performance of the four in-service test pavements and were reviewed and documented herein. The APLF HiMA sections were removed shortly after this project began, but cores were taken to confirm the pavement cross-sections and FWD testing was conducted prior to its removal.

Although little data exists on the STA-77/SUM-77 project, pavement performance was reviewed for this study. In 2018 the Pathweb data (pathweb.pathwayservices.com/ohiopublic/) reported a pavement condition rating (PCR) value of 80. The following year, 17 years after construction, the project received its first resurfacing: a 0.5" (12.5 mm) mill, inlaid with 1.25" (31.7 mm) of Item 424. Based on a review of Google Maps, it was observed some patching was completed prior to resurfacing in 2016, approximately 14 years after construction. Google map images from 2018, 1 year prior to the resurfacing, and from 2022, 3 years after the resurfacing are presented below in Figure 14.

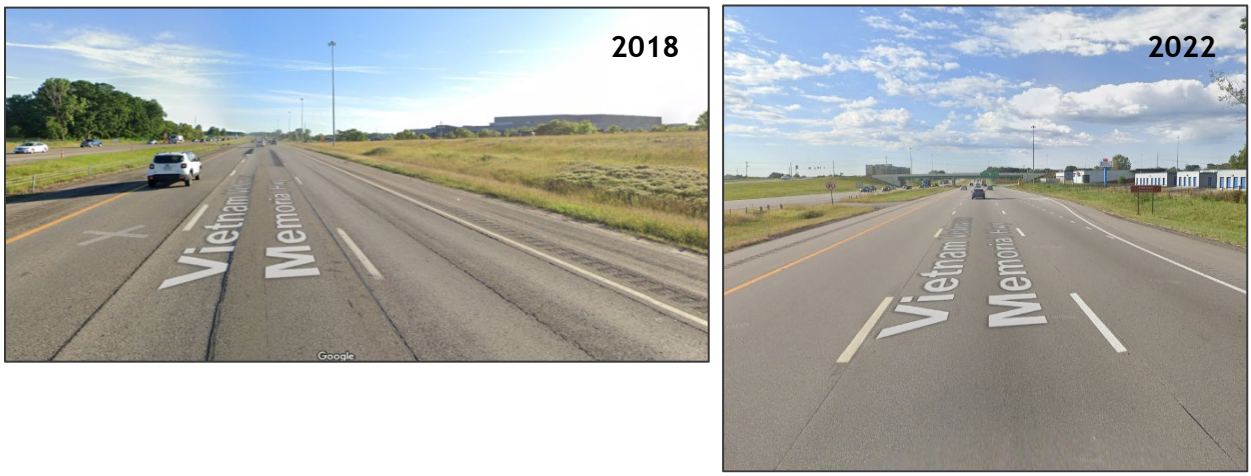


**Figure 14 STA/SUM-77-18.0 (approximately mile marker 113) in 2018 (left) and 2022 (right) (Google Maps).**

At that time, no surface distresses were found on STA-77, 12.75-14.80. Microsurfacing was applied in 2019. Figure 15 shows images of the pavement surface at approximately STA-77-13.26 from the 2011 visit and from Google Maps street view in 2018 just prior to the microsurfacing application, and in 2023, 4 years after the microsurfacing. Some longitudinal cracking was observed in 2018 in between the wheelpaths and near the longitudinal joint of the inside lane with the center lane. Overall the observed cracking in 2018 and 2023 is minor. The most recent Pathweb data (pathweb.pathwayservices.com/ohiopublic/) show a PCR for this segment of 90 in 2022; two years prior, in 2020, the PCR was listed as 97.


**Figure 15 STA-77-13.26 (approximately mile marker 108.5), from 2011 (left), 2018 (top-right) and 2023 (bottom-right) (Sargand et al., 2015; Google maps)**

WAY-30 was visited in July 2014, nine years after construction, at which time FWD testing was conducted and the section was found to have severe surface distress in the SMA, as shown in Figure 16. A 1.5" (38-mm) mill and fill of WAY-30 was conducted in 2015, 10 years after construction. Google map images from 2022 shown in Figure 17 show 7 years after resurfacing some longitudinal cracking has developed in the inside lane between wheelpaths and at the inside edge of the left wheelpath. However, as is the case with STA/SUM-77 and STA-77, there are no signs of structural distresses.

**Figure 16 Surface Distress in 2014 at WAY-30 STA 876 (left) and STA 664 (right) [Sargand et al., 2015]**


**Figure 17 WAY-30 Test Sections in 4 years and 7 years after resurfacing (2019 (left), and 2022 (right)) (Google Maps).**

Aside from a few thermal cracks noted and the longitudinal joint visible between lanes, the section at DEL-23-19.41-19.54 is performing well, 10 years after construction. To date, neither the mainline section nor the ramps have received any maintenance or rehabilitation treatments. The most recent PCR data (2023) shows the mainline section has a PCR of 84. Network level pavement condition data are not collected on the ramps. However, a visit in November, 2020 showed transverse cracks, at various locations, although primarily located at locations where cores had been extracted at the time of construction. Much of the transverse cracks were located on the 11" (279 mm) section on the northbound ramp, as shown in Figure 18, which based on early evaluation of measured strain data, researchers (Sargand et al., 2015) concluded was not likely to be a perpetual pavement.


**Figure 18 DEL-23 Test Sections on the Ramp, November, 2020; Top- and Bottom-Right are the NB Ramp**

Historical PCR data were requested for the test sections on STA/SUM-77, STA-77 and WAY-30, which are plotted in Figure 19. For reference, PCR curves for exceptional and average performance determined in a previous study are also plotted. The maintenance and rehabilitation treatments are evident in the figure by the jumps in PCR values. The structural deduct values for each test section were also reviewed and are provided in Figure 20. Structural deduct value is determined based on the severity and extent of certain types of cracking that are associated with structural distress. A value of 25 typically triggers major rehabilitation. As shown, in the figure all three sections had a structural deduct value below 10. All three test sections utilized an SMA surface, and after the SMA was removed or covered up as was the case for STA-77, the deduct values remain below 5. This helps to confirm the earlier observations from the previous study (Sargand et al., 2015) and those made in this study that the distress are functional distresses (raveling, de-lamination, increased texture) and can be associated with the surface layer. SMA surface is not a commonly placed surface mix in Ohio, as such, the performance could be related to mix design and/or construction of the SMA.

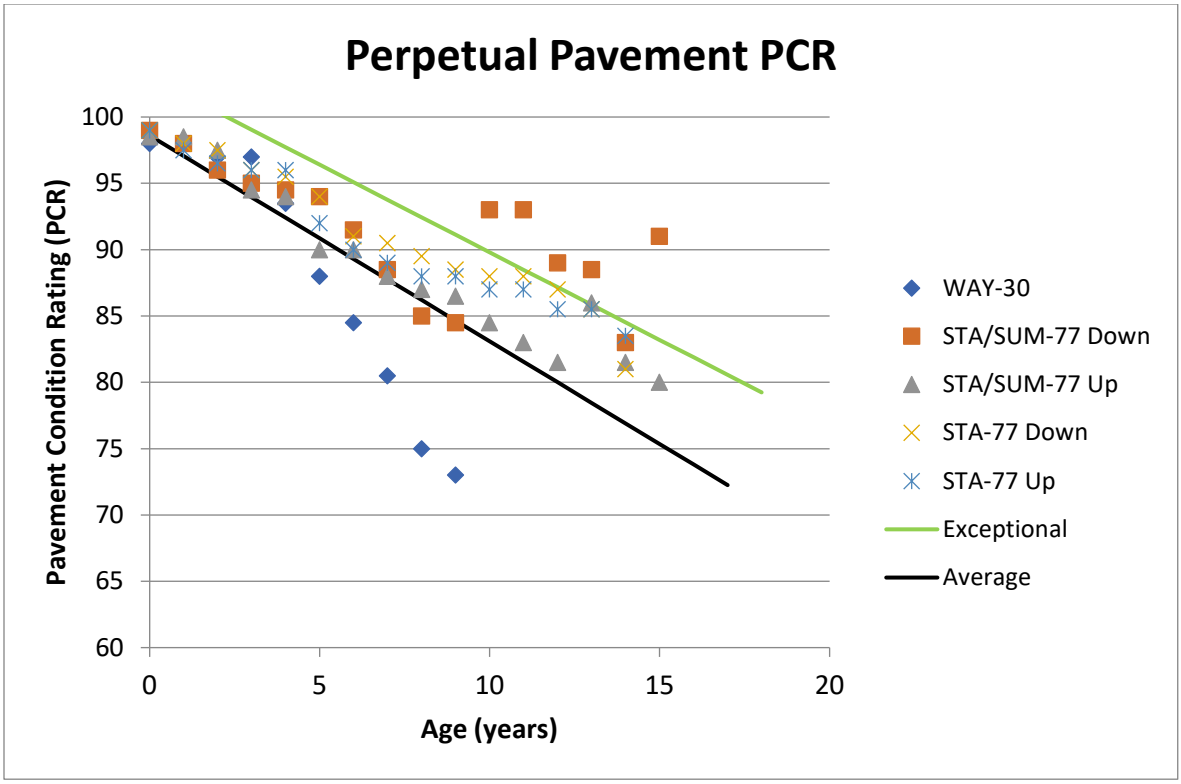


**Figure 19 Historical PCR Data.**

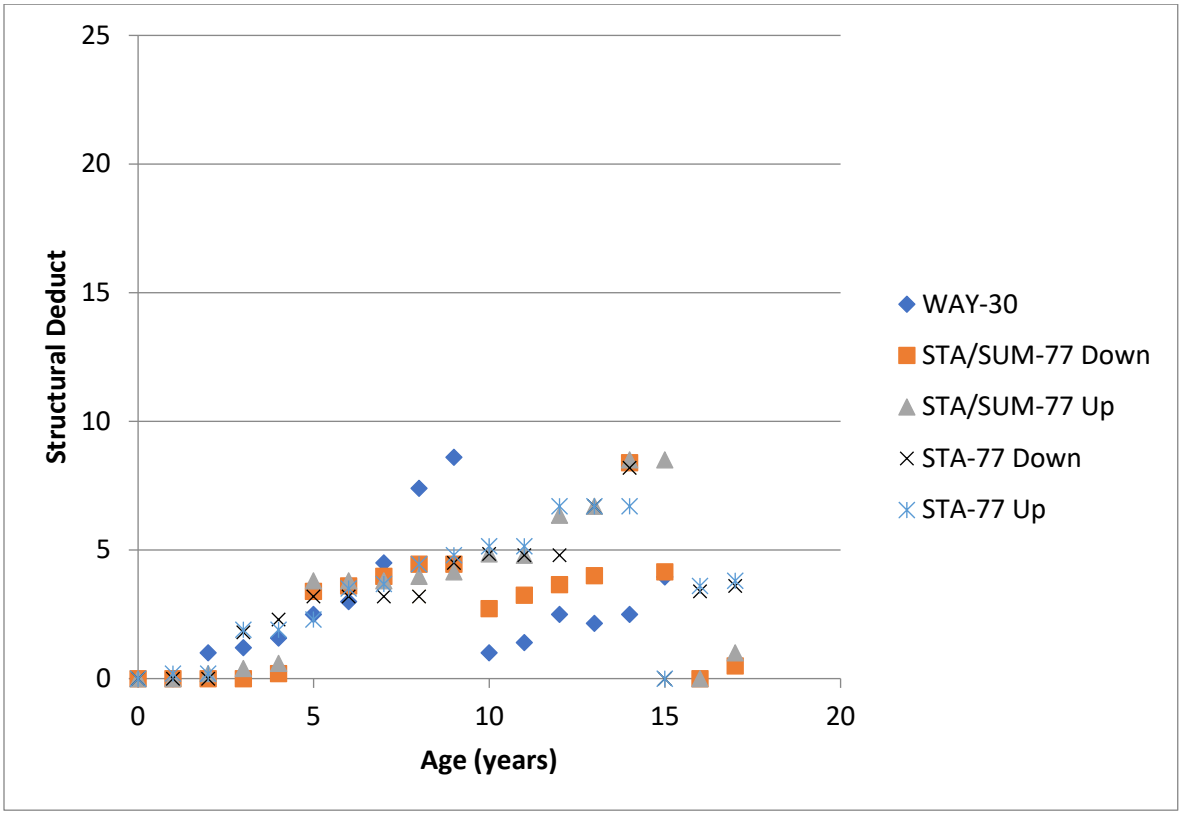


**Figure 20 Historical Structural Deduct Value.**

To further evaluate the structural condition of the in-service test sections FWD test results were reviewed. FWD testing was conducted on STA-77, 12.75 – 14.80 in 2011 (8 years after construction). Sargand et al. [2015] reported the spreadability and ratio of the deflection at sensor one to the deflection at sensor 7 (D1/D7) were similar to results for WAY-30, from which they concluded the results were reflective of the pavement age and the pavement was in structurally sound condition. FWD testing on WAY-30 in 2014 revealed a small reduction (4 to 8%) in average spreadability relative to that measured in October 2007. Sargand et al. [2015] reported spreadability is related to structural response of the entire cross-section, and the small reduction could be attributed to the surface condition and not necessarily the overall condition of the pavement.

In a previous study, Sargand and Figueroa [2010] evaluated the D1/D7 ratio for SHRP sections on DEL-23 and found performance levels in the field were distinguishable by the D1/D7 relationship. They found sections with poor performance failed within two years of service and had a ratio of 7.0 or greater, and sections with fair performance were close to failure after 6 years of service and had a ratio between 5.0 and 7.0. They further distinguished pavements with good performance as having a D1/D7 ratio between 2.5 and 5.0 and those with excellent performance has having a ratio less than 2.5. The D1/D7 ratios were determined from FWD results for the various perpetual pavement test sections and are presented in Figure 21. Ratios presented in the figure below are for the following test sections:

- WAY-30, measured in 2005
- STA-77 and STA/SUM-77 measured in 2011 and reported by Sargand et al. (2015) and
- HiMA APLF sections measured as part of this study.

Based on the plot in Figure 21, all sections fall into the good or better categories, except the HiMA 8-inch and 9-inch cross-sections which fell into the fair category. While the 10-inch HiMA section was in the good category, it is approaching the fair category.

In reviewing performance history (PCR and structural deduct), visual observations, and FWD data results of the existing perpetual pavement test sections it was concluded for the following test sections, there is no reason to believe their performance is not in-line with a perpetual pavement:

- STA/SUM-77
- STA-77
- WAY-30 876-A, 876-B, and 664
- DEL-23 mainline

The test sections on the DEL-23 ramps have very low traffic volume. The D1/D7 data are not in-line with conclusions drawn from the initial strain evaluations for the HiMA 9- and 10-inch test sections. Further evaluation of these test sections is warranted to determine optimal pavement thickness for perpetual pavement design.

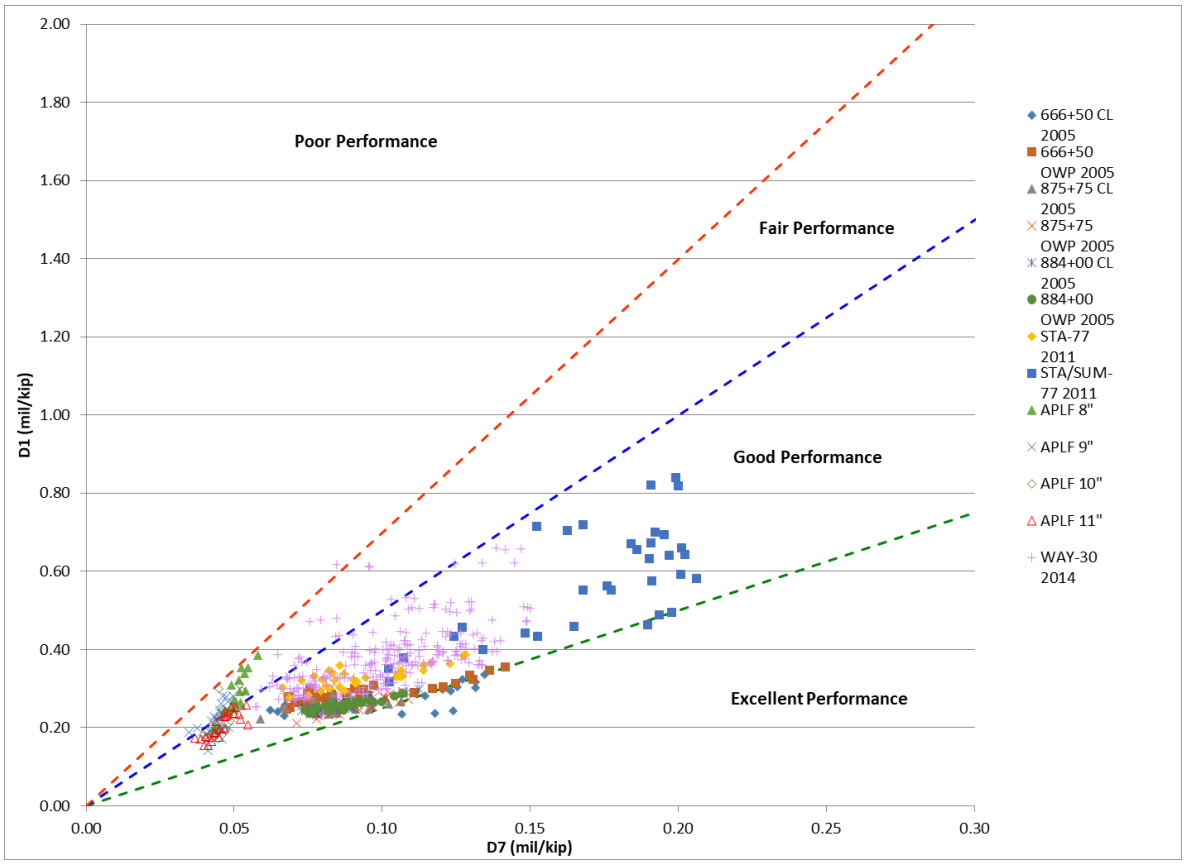


**Figure 21 D1/D7 Values for Perpetual Pavement Test Sections.**

### *Evaluate Existing Sections with various Perpetual Pavement Design Methods*

To help the research team select the most appropriate perpetual pavement design concept and tool for use in designing the field study select perpetual pavement test sections were further evaluated with perpetual pavement design methods. The following test sections were evaluated using PerRoad and AASHTOWare Pavement ME:

- DEL-23 Section 103, constructed 1996
- DEL-23-19.41 – 19.54 (Mainline), constructed 2012
- DEL-23 NB ramp and SB ramp, constructed 2012
- APLF HiMA Lanes A, B, C, and D, constructed 2013

DEL-23 Section 103 was part of the SHRP experiments and was the thickest cross-section that failed. The section was replaced in April, 2002 due to premature failure (Sargand et al., 2006). Although this section was constructed directly on top of the subgrade, it was included to provide a bookend in terms of predicted strains associated with a failed section or non-perpetual pavement. As shown in the table below, the cross-section was designed at 12” (305 mm) of AC on top of subgrade, with constructed AC thickness closely matching the design. Average actual layer thicknesses determined from field cores were used in PerRoad and Pavement ME analyses for all cross-sections and are also listed in Table 13. As shown below, actual constructed thickness tended to be slightly greater than designed thickness for the AC layers.

**Table 13 Constructed Layer Thicknesses**

| Layer | Avg Measured Thickness (in) | | | |
|---|---|---|---|---|
| | DEL-23-103 | DEL-23 Mainline | DEL-23 NB Ramp | DEL-23 SB Ramp |
| Asphalt Surface | 1.71 | 1.28 | 1.0 | 0.91 |
| Asphalt Intermediate | 2.16 | 2.13 | 1.94 | 2.62 |
| Asphalt Base | 8.04 | 8.25 | 4.31 | 5.81 |
| FRL | 0 | 4.0 | 4.0 | 3.69 |
| DGAB | 0 | 6.0 | 6.0 | 6.0 |
| Subgrade | Unstabilized | Unstabilized | Lime-modified | Lime-modified |
| (Total AC) | 11.91 | 15.66 | 11.25 | 13.03 |
| | APLF HiMA experiment | | | |
| | Lane A | Lane B | Lane C | Lane D |
| Asphalt Surface | 1.76 | 1.86 | 1.68 | 1.75 |
| Asphalt Intermediate | 1.45 | 1.66 | 1.82 | 2.58 |
| Asphalt Base | 4.81 | 5.94 | 6.76 | 7.20 |
| DGAB | 6 | 6 | 6 | 6 |
| Subgrade | Cement-stabilized | Cement-stabilized | Cement-stabilized | Cement-stabilized |
| (Total AC) | 8.02 | 9.46 | 10.26 | 11.53 |

**PerRoad Analyses**

For the PerRoad analyses, weather data from the John Glenn International Airport in Columbus, Ohio were used to determine the average daily air temperature. Data were sourced from Weather Underground's historical weather from 2019 to 2020. A cumulative distribution of the air temperature was broken into quintiles, to represent 5 seasons, from which the mid-point of each represented the mean seasonal air temperature (MMAT). Using the equation listed in PerRoad, the mean seasonal pavement temperature (MMPT) in degrees Fahrenheit for each season was calculated from the MMAT at the upper 1/3 of each AC layer using the total AC thicknesses listed in Table 13.

PerRoad is only capable of analyzing 5 pavement layers, therefore, where necessary, the surface and intermediate layers were combined. For the material properties of the AC layers, dynamic moduli (E*) determined in the laboratory as part of the previous study (Sargand et al., 2015) were used to determine the E* given at the MMPT, and a frequency of 12.57 Hz, which is approximately representative of 55 mph. Where layers were combined, the E* of each layer was first determined for each lift, then a weighted average of the E* data was completed to arrive at an E* representative of the combined layers. E* testing was not completed for DEL-23 Section 103, therefore the surface and intermediate layer were combined and the E* values from the DEL-23 Intermediate Superpave (Item 442) mix constructed in 2012 were used. Likewise, the E* for the AC base layer in the DEL-23 experiment (constructed in 2012) were used as the moduli for the DEL-23 Section 103 base layer. Although PerRoad can make seasonal adjustments based on the mean air temperature entered for each season, the seasonal moduli were manually entered as they were calculated from laboratory derived E* data, and it was assumed this would be more accurate.

For the DGAB layer, a modulus of 30,000 psi (207 MPa) was fixed for all seasons where the subgrade was unstabilized. Where stabilized subgrade was used, a value of 36,000 psi was used. For the subgrade, a fixed value of 12,000 psi (83 MPa) was used to model unstabilized subgrade, and a value of 16,320 psi was used to model stabilized subgrade (regardless of whether it was lime-modified or cement stabilized). These moduli values were determined

based on an assumed California Bearing Ratio (CBR) for the subgrade and the ODOT Pavement Design Manual.

PerRoad is a stochastic design tool and uses variability of the pavement layer thicknesses and moduli to predict strain under the various conditions the pavement may be subjected. For all sections except DEL-23 Section 103, the default was selected for the distribution type and coefficient of variation (CoV) for each layer thickness and layer modulus. For DEL-23 Section 103 numerous cores were taken as part of the experiment, therefore to characterize the AC layer thickness variability, the default distribution type was selected and a CoV of 6.7% was applied for the combined AC surface and intermediate layer, and a CoV of 4.2% was applied for the AC base layer. The default distribution type default CoV for the DGAB thickness was selected for DEL-23 Section 103. For the layer moduli variability on DEL-23 Section 103, all default values were selected.

A conservative approach was taken with the traffic inputs. Consistent with Tran et al. (2015) in their development of maximum pavement thicknesses, 100% of the traffic volume was a single axle load weighing 20-22 kips (89-98 kN). A cumulative distribution of the predicted tensile strains was developed for each section. That distribution was then compared with singular tensile strain values at the bottom of the AC layer that have been considered for use in perpetual pavement design to guard against bottom-up fatigue cracking, as shown in Table 14. Additionally, a cumulative distribution of the predicted vertical strains at the top of the subgrade were developed for comparison against a value of 200 microstrain. Tran et al. (2015) used a value of 200 microstrain at the 50$^{th}$ percentile at a limiting criterion for preventing structural rutting. All sections met the limiting criterion for rutting, therefore there no structural rutting is expected in any of these sections.

**Table 14 PerRoad Evaluation Results**

| | **Total AC thickness** | | **Bottom of AC Layers, % tensile strains** | | | **Top of Subgrade, % vertical strain** |
|---|---|---|---|---|---|---|
| **Section** | **in** | **cm** | **< 70 με** | **< 100 με** | **< 125 με** | **< 200 με** |
| **DEL-23 103** | 11.91 | 30.25 | 88.1 | 96.2 | 99 | 98.2 |
| DEL-23 PP Mainline | 15.66 | 37.78 | 100 | 100 | 100 | 100 |
| DEL-23 PP NB Ramp | 11.25 | 28.58 | 93 | 99.8 | 100 | 100 |
| DEL-23 PP SB Ramp | 13.03 | 33.10 | 100 | 100 | 100 | 100 |
| **APLF Lane A** | 8.02 | 20.37 | 55.4 | 83.3 | 95.2 | 100 |
| APLF Lane B | 9.46 | 24.03 | 75.7 | 95.7 | 99.3 | 100 |
| APLF Lane C | 10.26 | 26.06 | 84 | 98.2 | 99.8 | 100 |
| APLF Lane D | 11.53 | 29.29 | 92.2 | 99.5 | 99.9 | 100 |

Regarding the predicted tensile strains, two sections had 100% of the strains less than 70 microstrain, DEL-23 SB Ramp and DEL-23 Mainline, both of which were considered to be

perpetual based on the earlier evaluation by Sargand et al. (2015). However, consistent with the findings from Sargand et al. (2015) and Willis et al. (2009) which showed a singular strain value may not be appropriate, for the APLF test sections deemed perpetual (including the control in Lane D), predicted strains exceeded 70 microstrain.

The cumulative distributions of the predicted tensile strain values are presented in Figure 22 for the DEL-23 cross-sections evaluated. For reference, the limiting cumulative strain distribution developed at NCAT (Tran et al., 2015) is also plotted. However, as discussed in the literature review in Appendix A, the NCAT limiting cumulative strain distribution was developed using backcalculated moduli values from the NCAT Test Track. In this study, E* data were used to represent layer moduli. Generally, E* values are greater than backcalculated AC moduli and would therefore result in lower strain values. Therefore, despite section 103 on DEL-23 having premature failure, it passes the NCAT cumulative strain distribution. This implies the NCAT cumulative strain distribution cannot be applied to predicted strains based on E* data.

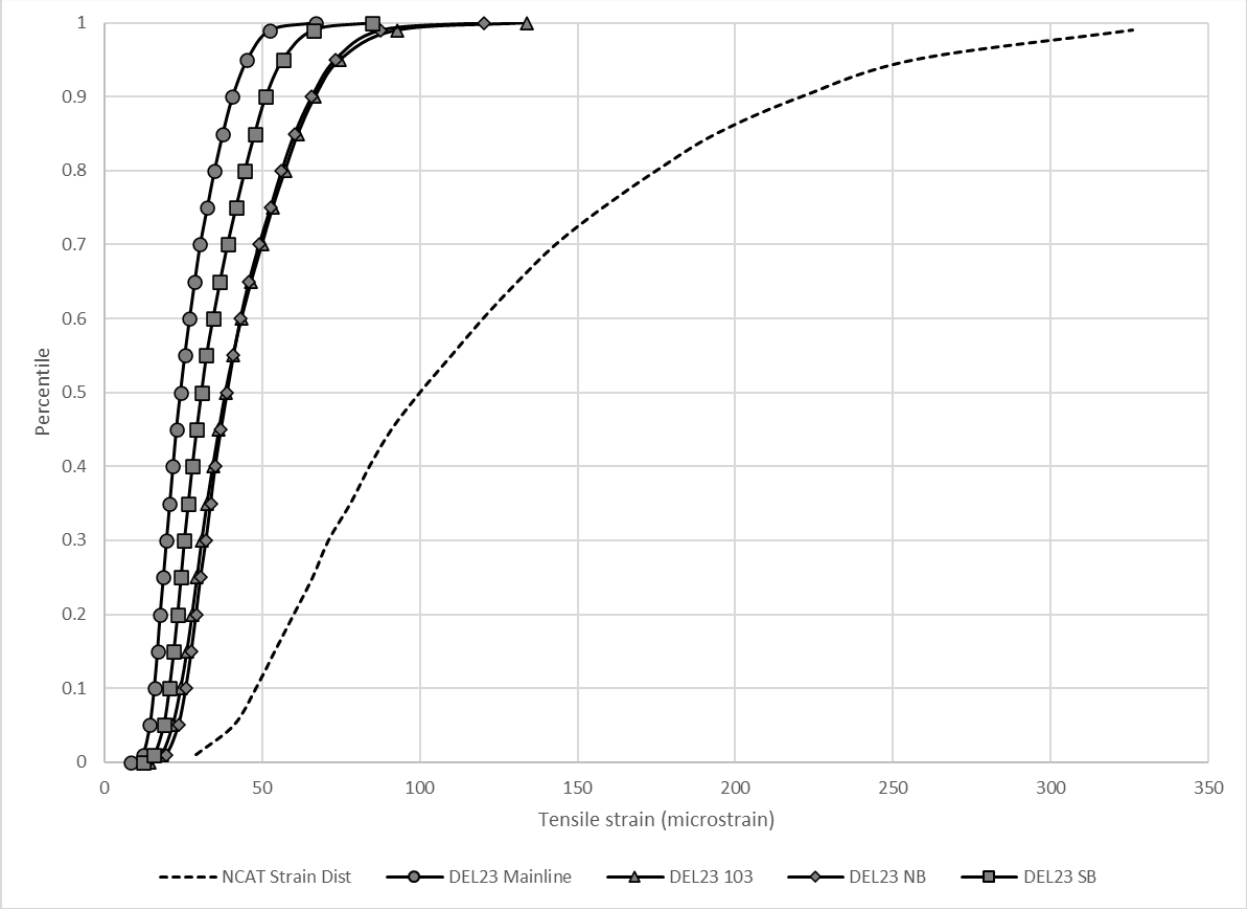


**Figure 22 Cumulative Predicted Strain Distribution from PerRoad, DEL-23 Sections**

Interestingly, the cumulative strain distributions for Section 103 and the NB ramp on DEL-23 lie on top of one another in the plot above; due to the early failure of Section 103 and the high strains and SR < 1.0 of the NB Ramp, neither section was considered perpetual. Cumulative strain distributions for the test sections believed to be perpetual, DEL-23 Mainline and DEL-23 SB Ramp sections, fall to the left of Sections 103 and the NB ramp and there is a sizeable gap between the thinnest perpetual section and the failed section, which is consistent with the

development of the NCAT cumulative strain distribution (Tran et al., 2015). The DEL-23 Mainline section was the thinnest cross-section with an unstabilized subgrade to be perpetual based on the historical review of perpetual pavement test sections in Ohio.

Cumulative strain distributions were developed from predicted tensile strains for each APLF test section as well, and were added to the plot of the DEL-23 test sections, shown in Figure 23 below. The APLF Lane A is far to the left of the NCAT cumulative strain distribution for perpetual pavements, indicating Lane A had lower strain values than NCAT strain distribution. This would imply Lane A is perpetual, however, Sargand et al. (2015) reported a SR < 1.0 and strains exceeding the calculated FEL from the NCHRP 09-44A model which suggests Lane A is not perpetual. This again indicates that when using E* data for the AC mix moduli the NCAT perpetual pavement cumulative strain distribution is not valid. It should also be noted that test sections in the APLF were constructed on aggregate base on cement stabilized subgrade. The NB and SB ramps on DEL-23 were constructed on aggregate base atop lime modified subgrade. The subgrade for the remaining DEL-23 test sections was not stabilized and DEL-23 Section 103 was placed directly on top of the unstablilized subgrade.

Interestingly, the cumulative strain distributions for APLF Lanes B and C fall to the right of the cumulative strain distributions of DEL-103 and DEL NB Ramp and Lane D lies on top of them. This means Lanes B and C had predicted strain higher than a section which failed prematurely (DEL-23 Section 103) and Lane D has predicted strain which is approximately equivalent to that same failed section. This would suggest either the APLF sections can withstand higher strains or they were not perpetual. Sargand et al. (2015) reported SR > 1.0 and measured strain values less than the FEL for each, Lanes B, C, and D, and based on the performance in the APLF, it was expected that Lanes C and D would be perpetual. Although the data and performance suggest Lane B may also behave perpetually, the plot of the D1/D7 deflection values in Figure 21, align with fair performance, therefore, in this analysis, Lane B was not considered to be perpetual. The cumulative strain distributions for the APLF Lanes C and D suggest higher strains can be tolerated when HPM AC mix is included in the entire cross-section as in Lane C, which is consistent with previous work at the NCAT Test Track (Timm et al., 2013). There is likely also a benefit, in terms of strain tolerance, for using a conventional base AC mix with HPM in the surface and intermediate AC mixes.

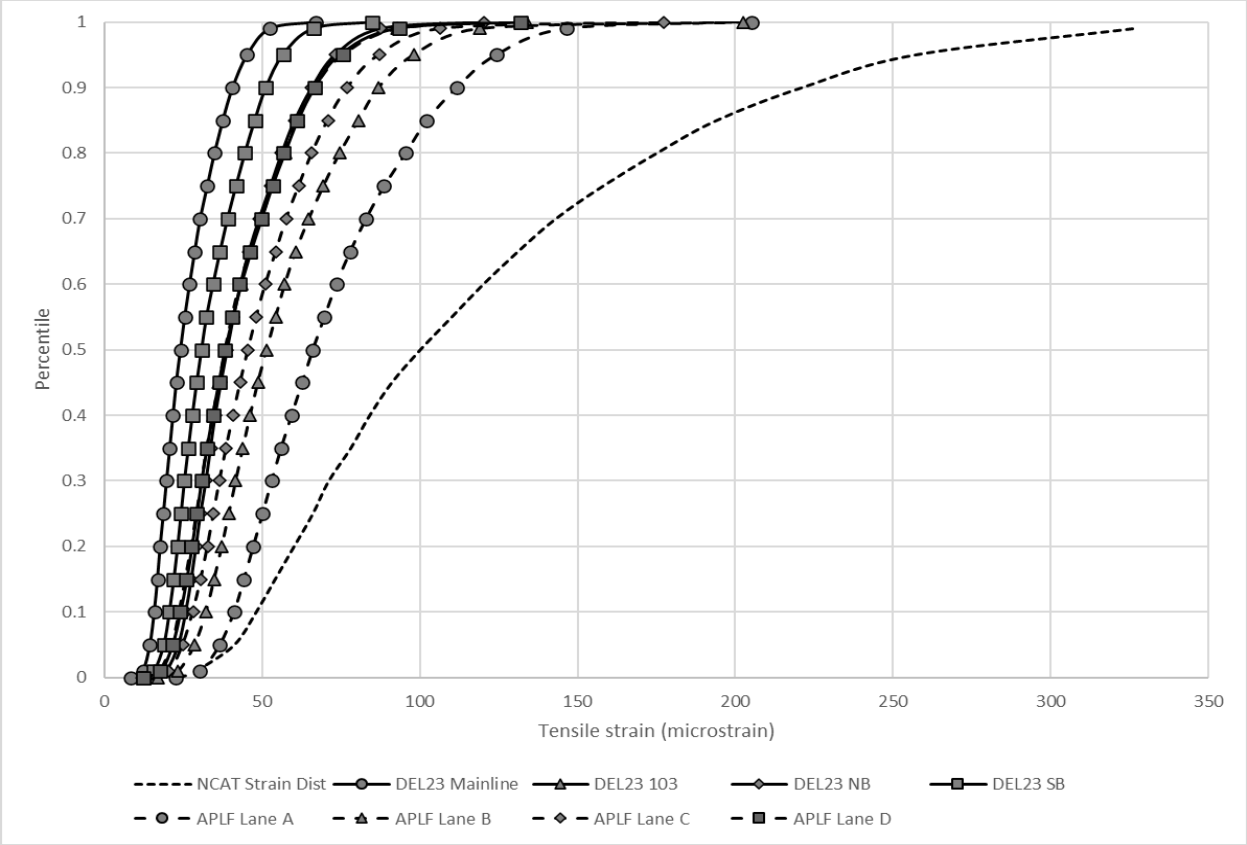


**Figure 23 Cumulative Predicted Strain Distribution from PerRoad Evaluations, DEL-23 and APLF Test Sections**

The above plot suggests differences exist in the cumulative strain distribution curves based on the use of stabilized subgrade, and the use of HPM AC mix in the asphalt base layer. As such three distributions are proposed for use in design for the following conditions:

- Conventional AC base with unstabilized subgrade (DEL-23 Mainline)
- Conventional AC base with stabilized subgrade (lime-modified) (DEL-23 SB ramp)
- HPM AC base with stabilized subgrade (APLF Lane C)

Listed in the following table are the proposed cumulative strain distributions for perpetual pavement design, calibrated to Ohio test sections.

**Table 15 Proposed Cumulative Strain Distributions Calibrated to Ohio Perpetual Pavement Test Sections**

| Percentile | Conventional AC base with unstabilized subgrade | Conventional AC base with stabilized subgrade | HPM AC base with stabilized subgrade |
|---|---|---|---|
| | Tensile Strain (με) | Tensile Strain (με) | Tensile Strain (με) |
| 0.5 | 24.03 | 30.70 | 45.52 |
| 0.55 | 25.38 | 32.25 | 48.15 |
| 0.6 | 26.93 | 34.35 | 51.02 |
| 0.65 | 28.55 | 36.56 | 54.40 |
| 0.7 | 30.27 | 38.93 | 57.64 |
| 0.75 | 32.54 | 41.64 | 61.62 |
| 0.8 | 34.78 | 44.47 | 65.77 |
| 0.85 | 37.42 | 47.59 | 70.77 |
| 0.9 | 40.55 | 51.15 | 76.98 |
| 0.95 | 45.15 | 56.53 | 87.01 |
| 0.99 | 52.39 | 66.16 | 106.30 |

**PavementME Analysis**

The same cross-sections were evaluated in AASHTOWare PMED. The same PerRoad inputs were utilized for PMED in terms of the structure and traffic loading and speed. The cross-sections modeled in PerRoad were reflected in PMED, such that where layers were combined in PerRoad, the same layers were combined when modeled in PMED. Where detailed information was not available default software values were used. To characterize the modulus of the AC layers, Level 3 E* inputs were used in which the performance grade (PG) of the binder were selected and the software calculates E* based the Witczak model. A climate station in north-central Ohio was selected. PMED does allow for the user to enter a FEL, however, it the user is warned the performance models have not been calibrated against a FEL. Rather, a design life of 50 years was selected, and the predicted strains values were extracted from the software. Cumulative strain distributions were then generated for the tensile strain at the bottom of the AC layer and the vertical strain at the top of the subgrade. The cumulative tensile strain distributions are plotted for the DEL-23 sections in Figure 24 and for the APLF sections in Figure 25. For comparison, the strain distributions determined from PerRoad for the same sections are also shown in each plot. While PMED ranks the sections in the same order in terms of cumulative tensile strain, the strain values are substantially smaller than those predicted by PerRoad. This finding is consistent with other studies (Islam et al., 2017; Castro et al., 2018).

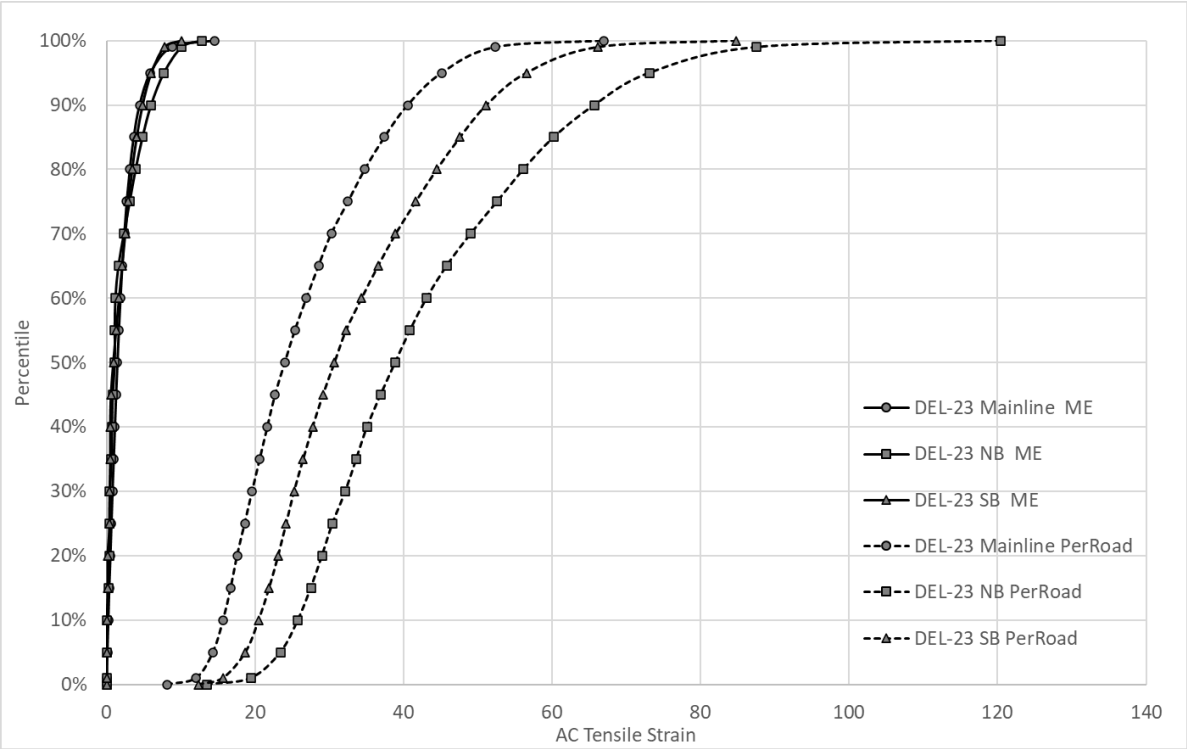


**Figure 24 DEL-23 Sections: Comparison of PerRoad and PMED Predicted Tensile Strain (Using Level 3 E* Inputs and Speed of 55 mph(88 km/hr))**

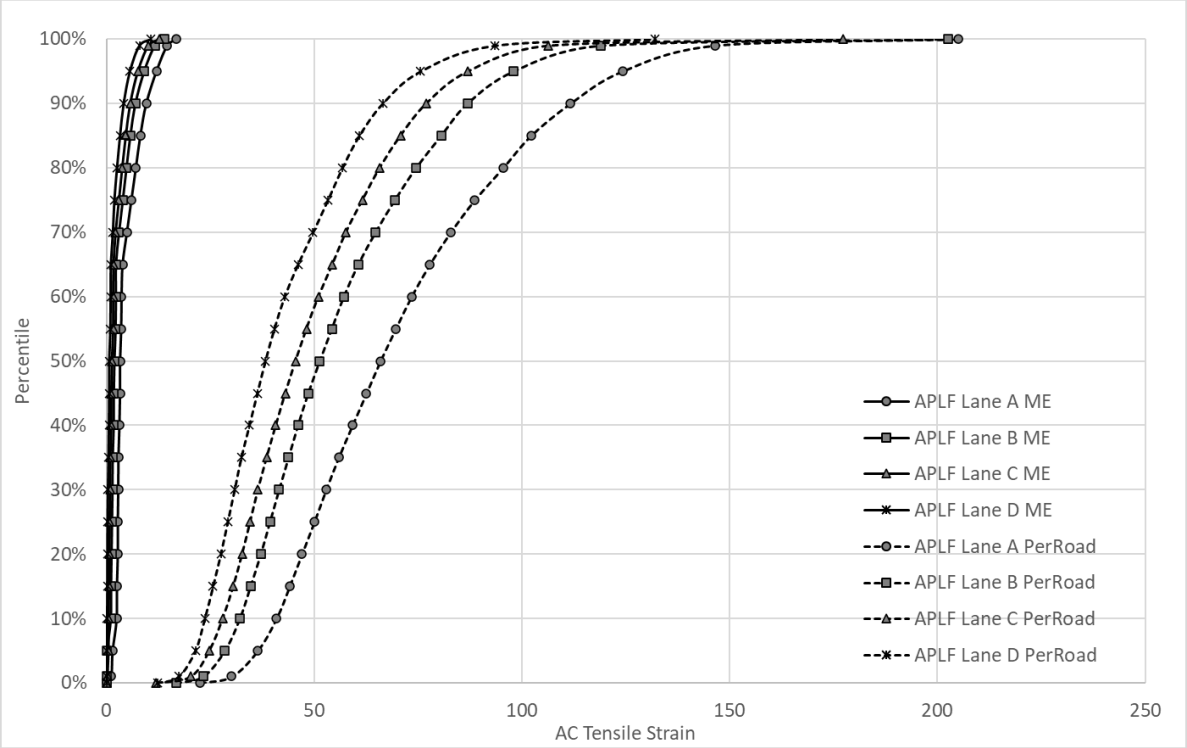


**Figure 25 HiMA APLF Sections: Comparison of PerRoad and PMED Predicted Tensile Strain (Using Level 3 E* Inputs and Speed of 55 mph (88 km/hr))**

Due to the small predicted strain values generated in PMED and the numerous inputs required for that software, the research team, in collaboration with ODOT, elected to utilize PerRoad to design the test sections on WAY-83.

## Study Design

### *Site selection*

The test site provided by ODOT was a reconstruction of SR 3 and SR 83 located in the northeast Ohio city of Wooster (see Figure 26).


**Figure 26 Location of Test Site in ODOT District 3, Wooster, OH (nationsonline.org/oneworld/map/USA/ohio_map.htm)**

The 3.8-mile (6.1 km) long project consisted of approximately 3.1 miles (5.0 km) of 4-lane with limited access right-of-way which transitioned to a multilane undivided pavement for approximately 0.7 miles (1.1 km) north of the SR 3 interchange (Figure 27)

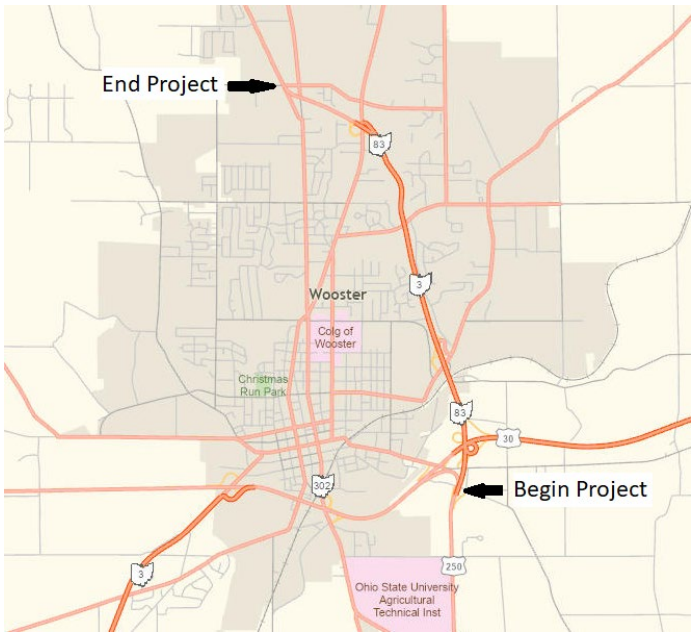


**Figure 27 Location of Test Site on SR-83 in ODOT District 3 (https://gis.dot.state.oh.us/tims/map)**

Seven test sections were proposed. The control would be conventional binder for the surface, intermediate, and base layers. To determine the effect of the HPM binder based on the location within the pavement thickness, three section were constructed; one with HPM binder in the base layer only, one with HPM binder in the base layer and intermediate layer, and one HPM binder in the intermediate and surface layer. Finally, three sections were constructed of various thickness using HPM binder in all three layers.

Test section locations were determined based on the following considerations:

- All sections would have homogeneous soil type, to the extent possible
- All sections would be constructed during the same season
- All sections would have homogeneous normalized (to 9 kip) FWD deflections 60" ($df_{60}$) from the load to the extent possible
- All sections would experience the same traffic
- Avoid areas which are not ideal for instrumentation or data collection equipment such as areas with steep side slopes, barriers, curves, entrance/exit ramps, etc.
- Avoid structures (bridges or culverts) which may affect response/performance

The undivided section on the north end of the project was not considered since controlled vehicle tests would be difficult and less safe with the type of traffic control procedures used for undivided roadways. The southern end of the project was not considered because of variation in traffic between interchanges and maintenance of traffic would be complicated and burdensome. Therefore, the search for test sites focused on the central portion of the project.

Soils borings were available for the original construction (1966) and the geotechnical investigation conducted by ODOT in 2018 for the current reconstruction. Pre-construction FWD data was collected in November of 2020.

Due to the variability of the subgrade soils and the number of ramps, curves, barriers and structures on the project, it was not possible to meet all the above criteria. The southbound section limits shown in Table 16 best met the criteria. The location of the test sections with respect to structures and soil type is shown in Figure 28.

**Table 16 Test Section Average FWD df60**

| Section | Begin Station | End Station | Length (ft) | FWD $df_{60}$ |
|---|---|---|---|---|
| 1 | 837+00 | 849+00 | 1200 | 0.31 |
| 2 | 849+00 | 861+00 | 1200 | 0.25 |
| 3 | 861+00 | 873+00 | 1200 | 0.17 |
| 4 | 873+00 | 885+00 | 1200 | 0.19 |
| 5 | 885+00 | 897+00 | 1200 | 0.22 |
| 6 | 897+00 | 909+00 | 1200 | 0.24 |
| 7 | 909+00 | 921+00 | 1200 | 0.25 |

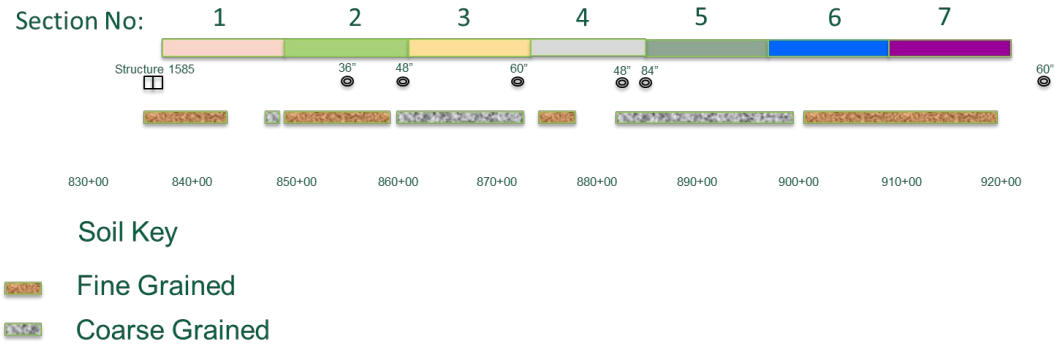


**Figure 28 Variability of Subgrade Along Test Site**

### *Cross-section Design of Test Sections*

Seven test sections, each 1200 feet (about 365.76 m) in length, were designed based on discussions with the Technical Advisory Committee (TAC). To support the effort to determine the structural layer coefficient of HPM asphalt mixes, a matrix was developed to include the following cross-sections. Based on the work by Sargand et al. [2015] in which it was concluded the "fatigue resistant layer could be replaced with an asphalt base course," a fatigue resistant layer was not included in the cross-sections.

- One cross-section composed entirely of conventional AC, referred to as the control section,
- One cross-section composed entirely of HPM asphalt mixes,

- One cross-section with HPM asphalt only in the surface only, and
- One cross-section with HPM asphalt only in the base layer.

While the researchers and ODOT felt most comfortable with basing designs on a proposed cumulative strain distribution, there was consensus that two additional cross-sections be constructed and instrument: one cross-section at 9" (228.6 mm) of HPM AC throughout, and another cross-section which reflects the mainline design (8.25" (209.6 mm) of HPM AC throughout). These additional cross-sections were expected to provide an opportunity to evaluate a minimum thickness to achieve a perpetual pavement. Analyses were conducted in PerRoad and based on those results, the additional HPM cross-sections had cumulative strain distributions which exceeded that of the HPM AC base with stabilized subgrade cumulative strain distributions listed in Table 15; as such it is not expected to have measured strain consistent with perpetual pavements.

For the five test sections that were designed to be perpetual, predicted strains from PerRoad and the following criteria were used:

- Predicted tensile strains must be less than the Ohio Calibrated Threshold presented in Table 15
- Predicted vertical strain at the top of the subgrade must have strain at the $50^{th}$ percentile less than 200 microstrain

All pavement cross-sections were designed using the HPM AC base with stabilized subgrade cumulative strain distribution listed in Table 15 which was the cumulative strain distribution from the APLF Lane C test section. After construction of the test sections, during the evaluation of measured strain data an error was found which resulted in the use of incorrect E* data for the evaluation of DEL-23 cross-sections. At the time of design it was anticipated only one strain distribution was needed for design and the difference between E* data for the conventional and HPM AC mixes would lead to thinner cross-sections where HPM AC mix was used. While this was the case, it was because incorrect E* data for conventional AC mix were used in the designs. After the discovery of the error, existing perpetual pavement cross-sections were re-analyzed in PerRoad and the three cumulative strain distributions listed in Table 15 were identified. As a result of the error, the test sections on WAY-83 which included conventional AC mix are slightly under designed. The following describes how the cross-sections were designed.

For the designs, the same procedure described under "Evaluate Existing Sections with various Perpetual Pavement Design Methods" was followed. To determine the MMPT, a cumulative distribution of air temperatures from the Akron-Canton Regional Airport from 2019-2020 sourced from Weather Underground was generated. The distribution was then divided into quintiles, with the mid-point of each representing the MMAT for that season. The MMPT and a fixed frequency of 12.57 Hz (to represent a design speed of 55 mph (89 km/hr)) was used with E* master curves to determine the seasonal moduli for each AC layer. For the conventional mixes E* data measured as part of the experiment on DEL-23 Mainline and Ramps and reported in Sargand et al., 2015 were used. Summarily, E* data determined in the laboratory for the HiMA APLF mixes were used for the HPM asphalt mixes. Traffic was modeled as 100% of the traffic volume being 20–22-kip (89-98 kN) single axle loads. Default values for the variability of the layer moduli and thicknesses were selected.

A CBR value of 10 was used for the subgrade based on the 20-year pavement designs completed by ODOT. Based on the reduced thickness on cement-stabilized subgrade in the HiMA

APLF study and on the DEL-23 ramps, a stabilized subgrade was recommended. Therefore, in following the ODOT PDM the design modulus of the DGAB which was set at 6", was 36,000 psi (248 MPa) and the design modulus of the stabilized subgrade was 16,320 psi (113 MPa).

While designing a cross-section to meet the identified criteria is an iterative process in which layer thickness are increased or decreased until the criteria are met, the layer thickness of the surface and intermediate layers were fixed as there a minimum requirement to achieve compaction based on the nominal maximum aggregate size of the mix. Therefore, as listed in Ta**ble 18**, the surface layer thickness was fixed at 1.5" (38 mm) and the intermediate layer was fixed at 1.75" (44 mm)", and only the AC base thickness was varied to achieve cumulative strain distributions less than the design cumulative strain distribution.

Cumulative strain distributions were generated from the predicted strains output by PerRoad. The tensile strain controlled the designs, as such only the cumulative tensile strain distributions are shown in Figure 29 for each cross-section, where "H" denotes HPM AC mix and "C" denotes conventional AC mix, listed in order of surface, intermediate, and base lifts. The goal for the five cross-sections intentionally designed to be perpetual was for the strain distributions to be to the left of the solid black line in Figure 29 which represents the HPM AC base with stabilized subgrade cumulative strain distribution. The 8.25" (209.6 mm) and 9" (228.6 mm) HPM asphalt sections fall to the right, indicating that they may not have performance consistent with a perpetual pavement.

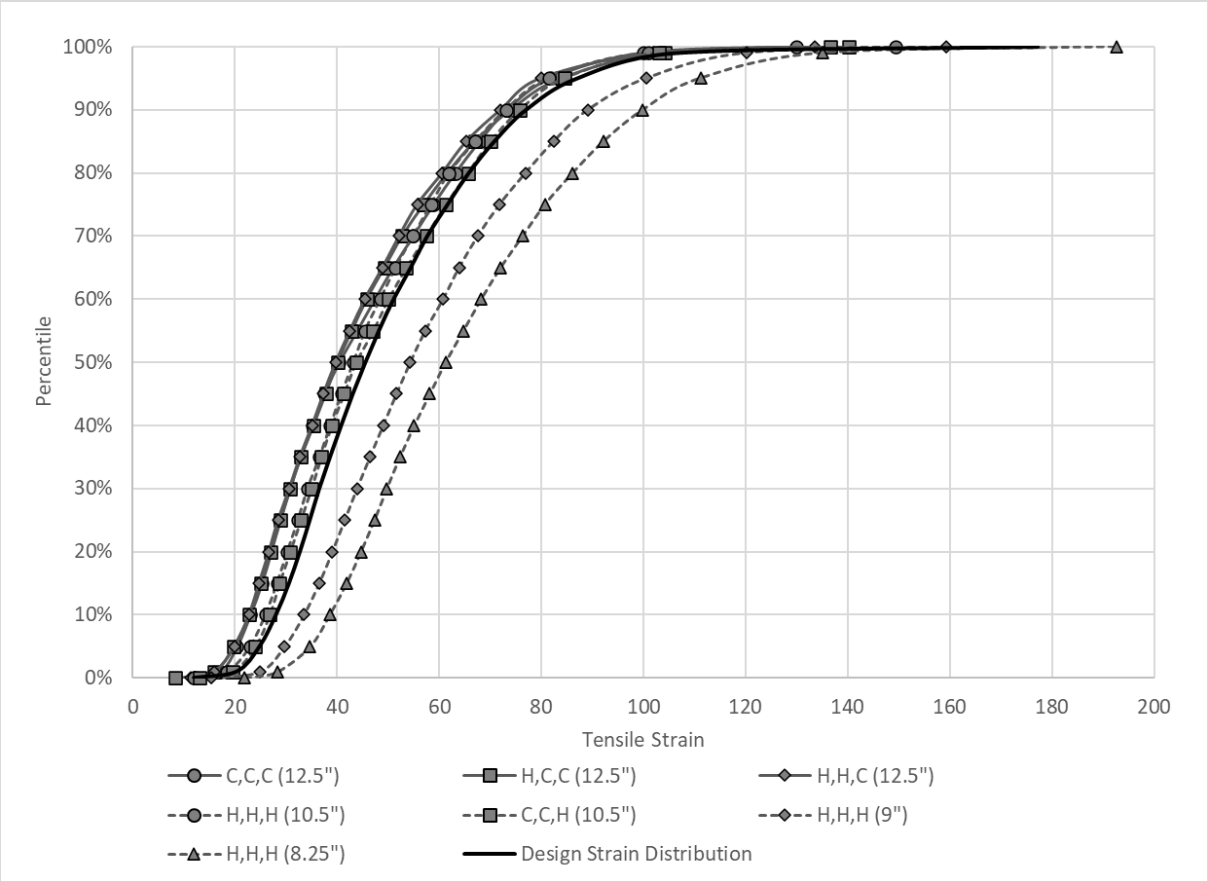


**Figure 29 Cumulative Tensile Strain Distributions for the WAY-83 Cross-Sections**

Once the base thicknesses were determined for each cross-section, the cross-sections were laid out along the section of the WAY-83 project selected for the test sections. Constructability of the cross-sections was considered when laying them out. The final cross-section, section location and location of the instrumentation within each test section are listed in Table 17. Table 18 lists the asphalt concrete (AC) mix type for each layer in each test section. All test sections were constructed on cement stabilized subgrade. Test sections, except for section 7 which is the same cross-section as mainline pavement, were designed utilizing a perpetual pavement design concept. Based on the work by Sargand et al. [2015] in which it was concluded the "fatigue resistant layer could be replaced with an asphalt base course," a fatigue resistant layer has been omitted from these cross-sections.

**Table 17 Test Section Pavements**

| Test Section Number | Station Begin | Station End | Monitoring Location | 304 Base Depth (in) | Base Depth (in) | Base Mix | Intermediate Layer Mix | Surface Layer Mix |
|---|---|---|---|---|---|---|---|---|
| **Mainline** | | | | 6 | 5 | 1 | 3 | 5 |
| **1** | 837+00 | 849+00 | 843+00 | 6 | 9.25 | 2 | 3 | 5 |
| **2** | 849+00 | 861+00 | 853+00 | 6 | 9.25 | 2 | 4 | 5 |
| **3** | 861+00 | 873+00 | 867+00 | 6 | 9.25 | 2 | 4 | 6 |
| **4** | 873+00 | 885+00 | 878+00 | 6 | 7.25 | 1 | 4 | 6 |
| **5** | 885+00 | 897+00 | 891+00 | 6 | 7.25 | 1 | 3 | 5 |
| **6** | 897+00 | 909+00 | 904+00 | 6 | 5.75 | 1 | 3 | 5 |
| **7** | 909+00 | 921+00 | 915+00 | 6 | 5 | 1 | 3 | 5 |
| **Mainline** | | | | 6 | 5 | 1 | 3 | 5 |

**Table 18 Test Section Pavement Mixes**

| Asphalt Concrete Mix Number | Pavement Depth (in) | Pavement Mix Description |
|---|---|---|
| **1** | See table | Item 302 Asphalt Concrete Base, PG 88-22M |
| **2** | See table | Item 302 Asphalt Concrete Base, PG 64-22 |
| **3** | 1.75 | Item SS861 Asphalt Concrete Intermediate Course 12.5 MM, Type A (446) As Per Plan, (PG 88-22M) |
| **4** | 1.75 | Item SS861 Asphalt Concrete Intermediate Course 12.5 MM, Type A (446) |
| **5** | 1.5 | Item 442 Asphalt Concrete Surface Course 12.5 MM, Type A (446) (PG 88-22M) As Per Plan |
| **6** | 1.5 | Item 442 Asphalt Concrete Surface Course 12.5 MM, Type A (446) |

Sections 1 – 5 were designed to meet a cumulative strain distribution which was calibrated to predicted strain for a pavement test section in Ohio which is expected to perform perpetually based on field- measured strain, laboratory testing and 9 years of field performance. Section 6 was designed to mimic pavement thickness of a full high polymer

asphalt pavement cross-section which performed perpetually based on laboratory testing and measured strain under loading in Ohio University's Accelerated Pavement Loading Facility (Sargand et al., 2015). Section 3 will serve as the control section in which all layers will be conventional AC mixes. Aside from AC base thickness, the remaining sections vary by the location of highly modified asphalt mix in the cross-section. A longitudinal cross section of the test site is shown in Figure 30.

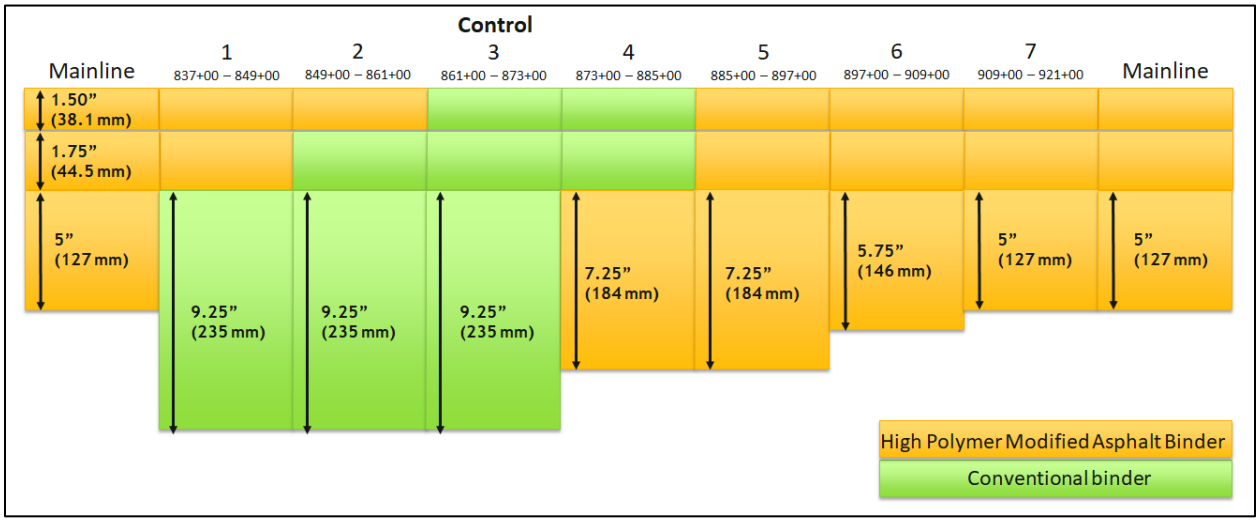


**Figure 30 Cross-Section of Design Test Sections for WAY-83**

### *Instrumentation Plan*

The instrumentation plan was developed to capture the tensile strain at the bottom of the asphalt concrete (AC) layer and stress at the top of the granular base and stabilized subgrade under controlled vehicle loading. The instrumentation plan incorporates redundancy in both the pressure plates and strain gauges. A total of 8 strain gauges were placed at the bottom of the asphalt concrete base layer, such that 4 were placed along the centerline of the outside wheel path, located 3.5 feet (1.1 m) from the centerline of the lane or 2.5 feet (0.8 m) from the outside lane line. Of these four strain gauges, two were oriented in the longitudinal direction and two were oriented in the transverse direction. An additional four strain gauges oriented in the same manner were placed downstream and offset one foot (0.3 m) to the right (toward the shoulder) of the first four strain gauges. These strain gauges captured any potential wheel wander during the controlled vehicle tests. Two pressure plates were installed at the top of the Item 304 aggregate base layer, 3.5 feet (1.1 m) to the right of the centerline of the lane. In a similar fashion, two pressure plates were installed at the top of the stabilized subgrade. Additionally, thermocouples were installed in the middle of the gauge array at 4 depths: bottom of the AC surface layer, bottom of the AC intermediate layer, bottom of the AC base layer, and mid-depth of the total AC thickness.

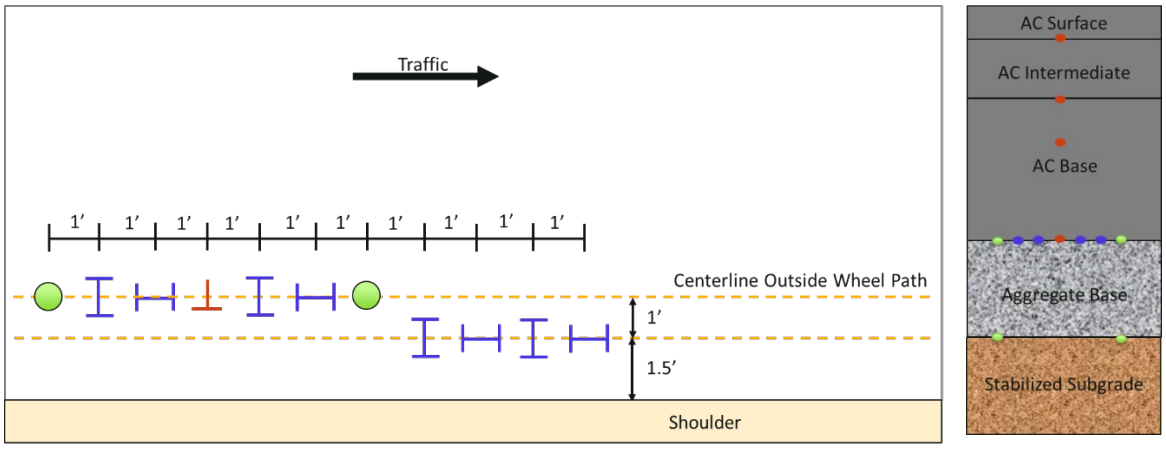


**Figure 31Instrumentation Plan**

Instrumentation was installed in all 7 test sections (listed in Table 19). Plan and profile views of the instrumentation arrays are provided in Figure 31. For the instrumentation array described above, the total number of gauges are listed in Table 19. Tensile strain at the bottom of the AC layer, stress at the top of the granular base and top of the subgrade, as well as temperatures throughout the pavement was collected during controlled vehicle loading.

| Instrumentation | Location (vertical) | Gauges Per section | Total Gauges |
|---|---|---|---|
| Longitudinal Strain gauge | 4 at the bottom of the AC base layer | 4 | 28 |
| Transverse Strain gauge | 4 at the bottom of the AC base layer | 4 | 28 |
| Thermocouples | 1 each at the bottom of AC surface layer, bottom of AC intermediate layer, bottom of AC base layer, and mid-depth of total AC thickness | 4 | 28 |
| Four pressure plates | 2 at the top of the stabilized subgrade and 2 at the top of the aggregate base | 4 | 28 |

**Table 19 Description of Instrumentation to be Installed**

### *Characterization of In-Situ Pavement Materials*

To capture in-situ material properties of the pavement layers, sampling and field-tests were conducted within a 1000’ (305 m) research area (see Figure 32). Field testing consisted of Falling Weight Deflectometer (FWD) and Dynamic Cone Penetrometer (DCP) testing. Layers tested and dates of testing are shown in Table 20.

FWD testing was conducted by ODOT in each test section on the stabilized subgrade, aggregate base, asphalt concrete (AC) base, and AC surface layers at the completion of each layer, prior to the placement of the next layer. FWD testing was conducted every 50 feet (15 m) along the outside wheel path. On the aggregate base and asphalt layers three drop heights were used to measure deflection at target loads of 6, 9 and 12 kips (26, 40, and 53 kN).

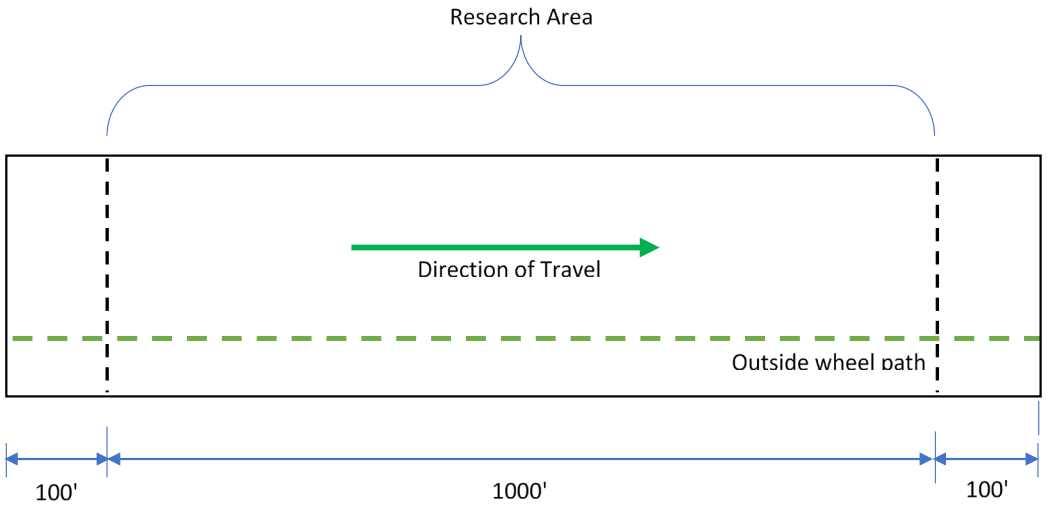


**Figure 32 Research Area**

**Table 20 FWD and DCP test dates**

| Field Test | Unstabilized Subgrade | Stabilized Subgrade | Aggregate Base | Asphalt Base | Asphalt Surface |
|---|---|---|---|---|---|
| **Falling Weight Deflectometer (FWD) (ODOT)** | | 9/26/2022 | 10/13/2022 | 10/28/2022 | 11/10/2022 |
| **Dynamic Cone Penetrometer (DCP)*** | 11/15/2022 | 11/15/2022 | 11/15/2022 | | |

*After completion of construction of all pavement layers

Full-depth cores with diameter of 4" (102 mm) were removed by the contractor at the completion of all pavement layers in the structure at 5 locations within each test section. Core and DCP test locations are shown in Table 21. Dynamic cone penetrometer (DCP) testing was conducted by the ORITE research team through full depth core holes. DCP testing provided the penetration rate (blows/depth) for the aggregate base, stabilized subgrade and unstabilized subgrade which was then correlated to California Bearing Ratio (CBR) and/or resilient modulus of the layers.

**Table 21 Full depth core and DCP test location**

| Core Number | Section 1 | Section 2 | Section 3 | Section 4 | Section 5 | Section 6 | Section 7 |
|---|---|---|---|---|---|---|---|
| 1 | 839+00 | 851+67 | 863+00 | - | 888+00 | 899+00 | 913+00 |
| 2 | 841+00 | 854+50 | 865+00 | 877+00 | 890+00 | 901+00 | 915+00 |
| 3 | 845+00 | 856+50 | 867+00 | 881+00 | 893+00 | 903+00 | 917+00 |
| 4 | 847+00 | 858+50 | 870+00 | 883+00 | 895+00 | 907+00 | 919+00 |
| 5 | 849+00 | 860+50 | 872+00 | 884+60 | 897+00 | 909+00 | 921+00 |

Upon completion of each AC layer, the contractor cut and extracted 6 cores within each pavement test section. Cores cut in the AC base layer were 6" (152 mm) in diameter, while cores in the AC intermediate and surface layers were 4" (102 mm) in diameter. These cores were used to quantify pavement thickness and measure the in-place density according to the bulk specific gravity determined by ORITE in the laboratory following AASHTO T 269. Average measured layer thickness determined from the cores are shown in Table 22.

**Table 22 Average layer thickness determined from cores. Shown in inches (mm)**

| Section No. | Asphalt Base | Intermediate | Surface | Total Core Thickness | Total Design Thickness |
|---|---|---|---|---|---|
| 1 | 9.0 (229) | 1.85 (47) | 1.5 (38) | 12.3 (312) | 12.5 (318) |
| 2 | 10.2 (259) | 1.75 (44) | 1.4 (36) | 13.3 (338) | 12.5 (318) |
| 3 | 9.4 (239) | 1.80 (46) | 1.4 (36) | 12.6 (320) | 12.5 (318) |
| 4 | 7.1 (180) | 1.83 (46) | 1.5 (38) | 10.4 (264) | 10.5 (267) |
| 5 | 7.2 (183) | 1.80 (46) | 1.4 (36) | 10.4 (264) | 10.5 (267) |
| 6 | 5.3 (135) | 1.96 (50) | 1.5 (38) | 8.8 (224) | 9.0 (229) |
| 7 | 5.0 (127) | 1.80 (46) | 1.5 (38) | 8.3 (211) | 8.25 (210) |

### *Laboratory Testing Plan*

Laboratory testing of plant-produced, lab-compacted specimens is being conducted to characterize the mixes in terms of performance and material properties needed for PerRoad and Pavement ME design. Table 23 provides information for the testing of the plant produced lab-compacted mix. Table 24 shows the matrix of laboratory testing for the various mixes as part of the study.

The contractor shipped plant-produced mix to the ORITE asphalt laboratory in Lancaster, Ohio. Mixes were re-heated, and specimens compacted based on the requirements of each test. The traditional 2-hour cure time was not utilized due to the reheating at low temperatures to split the sample into appropriate sample sizes and heating the mixture to compaction temperature.

**Table 23 Tests Conducted on Plant-Produced Lab-Compacted mix**

| Test | Spec. No. | Test Parameter | Notes |
|---|---|---|---|
| Dynamic Modulus | AASHTO T 342 or AASHTO T 378 | Dynamic modulus (\|E*\|) and phase angle | Measures modulus under varying temperature and frequency (speed). Input for Pavement ME design. |
| Creep Compliance and Indirect Tensile Strength | AASHTO T 322 | Creep Compliance and Indirect Tensile Strength at low temperature | Measure of creep compliance and susceptibility to low temperature cracking |
| Cantabro | AASHTO T 401 | Mass loss | Measure of durability |
| IDEAL CT | ASTM D8225-19 | Cracking index | Measure of cracking susceptibility at intermediate temperature |
| Hamburg Wheel Tracking Test | AASHTO T 324 | Rut depth and stripping inflection point | Measure of rutting susceptibility and stripping potential (moisture damage susceptibility) |
| Tensile Strength Ratio | AASHTO T 283 and ODOT S1051 | Indirect Tensile Strength and Tensile Strength Ratio (TSR) | Measure of moisture damage susceptibility |

**Table 24 Testing Matrix of Plant-Produced, Lab-Compacted Mix**

| Mix | Course | Cantabro Mass Loss | Dynamic Modulus | IDEAL CT | TSR | Hamburg Wheel Track | Creep Compliance (T = -4F, 14F, 32F) | Indirect Tensile Strength (T = 14F) |
|---|---|---|---|---|---|---|---|---|
| Control 302 | Base | X | X | X | X | | | |
| HPMA 302 | Base | X | X | X | X | | | |
| Control 442 Intermediate | Intermediate | X | X | X | X | X | | |
| HPM 442 Intermediate | Intermediate | X | X | X | X | X | | |
| Control 442 Surface | Surface | X | X | X | X | X | X | X |
| HPM 442 Surface | Surface | X | X | X | X | X | X | X |

HPM = High Polymer Modified Asphalt

In addition to testing plant-produced, lab-compacted mix, in-situ density was determined for extracted field cores (AASHTO T 166 with maximum specific gravity from QC samples) and layer thickness. Information such as gradation, asphalt content, volumetrics, and maximum specific gravity of the plant-produced mix obtained from the contractor's daily testing of mix in each test section will be utilized as needed for lab testing of plant-produced, lab-compacted mix.

Material properties determined from plant produced, lab compacted specimens and from extracted cores and QC/QA samples will be utilized for determination of input parameters for use in PerRoad and AASHTOWare PMED software. Material properties of the asphalt mix and asphalt binder required for PMED, based on the hierarchical level are shown in Table 25.

**Table 25 Material Properties Required for PavementME (after AASHTO, 2020 and Brink and Von Quintus, 2018)**

| Material | Property | Hierarchical level |
|---|---|---|
| Asphalt Concrete (AC) Mix | Dynamic Modulus (\|E*\|) and phase angle | Level 1: AASHTO T 342 or T378 and DSR Test Results for Asphalt Binder<br>Levels 2: Predicted via NCHRP 1-40D or NCHRP 1-37A model and DSR Test Results for Asphalt Binder<br>Level 3: Predicted via NCHRP 1-40D or NCHRP 1-37A model and Recommended values from A-VTS relationship (Viscosity/Penetration Grade or Superpave Performance Grade)<br>Software defaults to 1-37A model for Levels 2 and 3 |
| | Plastic Deformation Coefficients | Level 1: NCHRP Project 9-30A procedure |
| | Fatigue Strength Coefficients | Level 1: AASHTO T 321<br>Level 2: |
| | Indirect Tensile Strength | Level 1: AASHTO T 322, at 3 Temperatures, including T = 14F<br>Level 2: AASHTO T 322, at T = 14F<br>Level 3: Embedded regression equation (function of Va, VFA and binder viscosity) |
| | Creep Compliance | Level 1: AASHTO T 322, T = -4F, 14F and 32F<br>Level 2: AASHTO T 322, T = 14F, and used to extrapolate at -4F and 32F using power law<br>Level 3: Embedded regression equation (function of Va, VFA and binder viscosity) |
| | Poisson's Ratio | Constant, user-supplied value, or default Parameters A and B for predictive model (as a function of E*) |
| | Surface Shortwave Absorptivity | Default value = 0.85 |
| | Thermal Conductivity | Same for all Levels |
| | Heat capacity | Same for all Levels |
| | Coefficient of Thermal Contraction | Same for all Levels |

| Material | Property | Hierarchical level |
|---|---|---|
| | Effective Asphalt Content by Volume | Level 1: AASHTO T 308 |
| | Air Voids (as-built) | Level 1: AASHTO T 166 |
| | Aggregate Specific Gravity (as-built) | Level 1: AASHTO T 84 and T 85 |
| | Gradation (as-built) | Level 1: AASHTO T 27 |
| | Unit Weight (as-built) | Level 1: AASHTO T 166 |
| | Voids Filled with Asphalt (VFA) (as-built) | Level 1: AASHTO T 209 |
| Asphalt Binder | Asphalt Performance Grade *or* | Level 1: AASHTO T 315 |
| | Asphalt Binder Complex Shear Modulus (G*) and phase angle (d) *or* | Level 1: AASHTO T 49 |
| | Penetration *or* | Level 1: AASHTO T 53 |
| | Ring and Ball Softening Point<br>Absolute Viscosity<br>Kinematic Viscosity<br>Specific Gravity *or* | Level 1: AASHTO T 202<br>Level 1: AASHTO T 201<br>Level 1: AASHTO T 228 |
| | Brookfield Viscosity | Level 1: AASHTO T 316 |
| Unbound Layers: | Poisson's ratio | Same for all levels |
| | Coefficient of Lateral Earth Pressure | Same for all levels |
| | Resilient Modulus | Level 1: AASHTO T 307<br>Level 2: From correlations with other properties (DCP, CBR, R-value, volumetric properties)<br>Level 3: typical values based on material type (varied by month based on water content from climate model, or constant value for whole year) |
| | Gradation | |
| | Atterberg limits | |
| | Compaction | |
| | Maximum dry unit weight | |
| | Saturated Hydraulic Conductivity | |
| | Specific Gravity | |
| | Optimum gravimetric water content (%) | |
| | Soil water characteristics | |

The determination of the material properties required for use in the software is proposed as outlined in **Table 26** in conjunction with the default, national calibration models embedded in the software.

**Table 26 Proposed determination of HPM AC mix material properties for use in PavementME software.**

| Material | Property | Determination | Notes |
|---|---|---|---|
| AC – General | Endurance Limit | Varied | Endurance limit may be utilized based on preliminary evaluations of software |
| AC – General | Layer Interface | Full Friction Interface | |
| Volumetric AC Mix Properties | Unit weight (as-built) | Surface layer: 145.1 lb/ft$^3$<br>Intermediate layer: 144.5 lb/ft$^3$<br>Base layer: 150.3 lb/ft$^3$ | |
| | Effective binder content (as-built) | Surface layer $V_{be}$: 10.5 %<br>Intermediate layer $V_{be}$: 10.7%<br>Base layer $V_{be}$: 9.1 % | Vbe = VMA-Va<br>VMA = 100 – ($G_{mb}P_s/G_{sb}$) |
| | Air voids (as-built) | Surface layer: 6.7 %<br>Intermediate layer: 8.7%<br>Base layer: 5.2 % | |
| | Poisson's Ratio | Use default values for Parameters A and B, allow software to compute ratio from predictive model (including Parameters A and B) and E* | |
| Mechanical AC mix and asphalt binder properties | Dynamic Modulus (\|E*\|) | Level 1: AASHTO T 342 or T 378 for each mix<br><br>And/or Level 3: Viscosity based model<br><br>E* at reference temperature (70F) at 10 HZ<br><br>Surface layer: 742.22 ksi<br>Intermediate layer: 1097.00 ksi<br>Base layer: 1744.48 ksi | Must be paired with G* data (DSR test results of asphalt binder) at 10 rad/sec<br>Requires aggregate inputs (Percent passing 0.75 in, 0.375 in, No. 4 and No. 200 sieve) and Superpave performance grade or penetration/ viscosity grade of asphalt binder |
| | Aggregate inputs (required for E* predictive model) | Gradation of extracted aggregate from contractor's QC of each mix in each test section. Average values for each mix | |
| | Reference Temperature for E* master curve | Default value (70F) | |

| | | | |
|---|---|---|---|
| Mechanical AC mix and asphalt binder properties | Asphalt Binder (required for fitting parameters of E* master curve) | For E* Level 1: G* at 10 rad/sec (1.59 Hz) from ODOT<br><br>For PG 88-22<br>• DSR (virgin binder) at 88 C :<br>G* =1.35 Pa , δ= 52 degrees<br>• DSR (short term) at 88 C :<br>G* = 2.61 Pa, δ = 53.1 degrees<br>• DSR (long term) at 37 C :304 Pa<br>G*=304 Pa , δ = 42.5 degrees<br><br>For E* Level 3: Superpave performance grade of virgin binder | |
| | Indirect Tensile Strength | AASHTO T 322 at T = 14F<br>HPM: 591 psi<br>HMA: 532 psi | |
| | Creep Compliance | AASHTO T 322, T = -4F, 14F and 32F<br>HPM:<br>D(t) at -4F =3.89 E-08 psi<br>D(t) at 14F =6.07 E-08 psi<br>D(t) at 32F =8.66 E-08 psi<br>HMA:<br>D(t) at -4F =3.72 E-08 psi<br>D(t) at 14F =5.98 E-08 psi<br>D(t) at 32F =8.45 E-08 psi | Only needed for surface (wearing course)<br><br>Creep Compliance (Dt) (psi) at 50s (Avg) |

For PavementME analysis, properties of the unbound layers were assumed as outlined in Table 27.

**Table 27 Assumed Material Inputs for PavementME Analyses**

| Material | Property | Value/source of value | Notes |
|---|---|---|---|
| Unbound layer: Aggregate Base (General) | Unit weight | Default value | |
| | Poisson's ratio | Default value | |
| | Coefficient of lateral earth pressure | Default value | |
| Unbound Layer: Aggregate Base (Modulus) | Resilient modulus (psi) | Annual representative value = 30,000 psi (from ODOT PDM) | Values from FWD or DCP testing during construction may be used as an alternative |
| Unbound Layer: Aggregate Base (Sieve) | Gradation | Default for A-1-a | |
| | Atterberg limits | Default for A-1-a | |
| | Compaction | Yes, compacted layer | |
| | Maximum dry unit weight | Default for A-1-a | |
| | Saturated Hydraulic Conductivity | Default for A-1-a | |

| Material | Property | Value/source of value | Notes |
|---|---|---|---|
| | Specific Gravity | Default for A-1-a | |
| | Optimum gravimetric water content (%) | Default for A-1-a | |
| | Soil water characteristics | Default for A-1-a | |
| Unbound Layer: Stabilized subgrade (Modulus) | Resilient modulus (psi) | Based on ODOT PDM: 16,320 psi = 1.36*(1200*10) CBR of native soil on WAY-83 = 10 | Values from FWD or DCP testing during construction may be used as an alternative |
| Unbound Layer: Cement stabilized subgrade (Sieve) | Gradation | Default for selected AASHTO soil classification | Soil classification based on existing subgrade as listed in plans |
| | Atterberg limits | Default for selected AASHTO soil classification | |
| | Compaction | Default for selected AASHTO soil classification | |
| | Maximum dry unit weight | Default for selected AASHTO soil classification | |
| | Saturated Hydraulic Conductivity | Default for selected AASHTO soil classification | |
| | Specific Gravity | Default for selected AASHTO soil classification | |
| | Optimum gravimetric water content (%) | Default for selected AASHTO soil classification | |
| | Soil water characteristics | Default for selected AASHTO soil classification | |
| Unbound Layer: unstabilized subgrade (Modulus) | Resilient modulus (psi) | Based on ODOT PDM: Mr = 1200*CBR = 12,000 psi (CBR for WAY-83 = 10) | |
| Unbound Layer: unstabilized subgrade (Sieve) | Gradation | Default for selected AASHTO soil classification | Soil classification based on existing subgrade as listed in plans |
| | Atterberg limits | Default for selected AASHTO soil classification | |

| Material | Property | Value/source of value | Notes |
|---|---|---|---|
| | Compaction | Default for selected AASHTO soil classification | |
| | Maximum dry unit weight | Default for selected AASHTO soil classification | |
| | Saturated Hydraulic Conductivity | Default for selected AASHTO soil classification | |
| | Specific Gravity | Default for selected AASHTO soil classification | |
| | Optimum gravimetric water content (%) | Default for selected AASHTO soil classification | |
| | Soil water characteristics | Default for selected AASHTO soil classification | |

## Instrumentation Installation

The ORITE research team instrumented each test section during construction to gather pavement response data. This involved precisely embedding sensors within the pavement layers, collecting real-time response data under various load and environmental conditions. Instrumentation was installed as follows:

- Pressure Cells: To measure vertical stress, two pressure cells were installed atop the stabilized subgrade and two pressure cells were installed atop the granular base. Pressure gages were installed after construction of the granular base, as shown in Figure 33. After placement of the granular base, the base was excavated to the top of the stabilized subgrade, a bed of sand was placed to ensure uniform support of the pressure cells, then the granular base replaced and compacted. Pressure cells were then installed on the granular base.

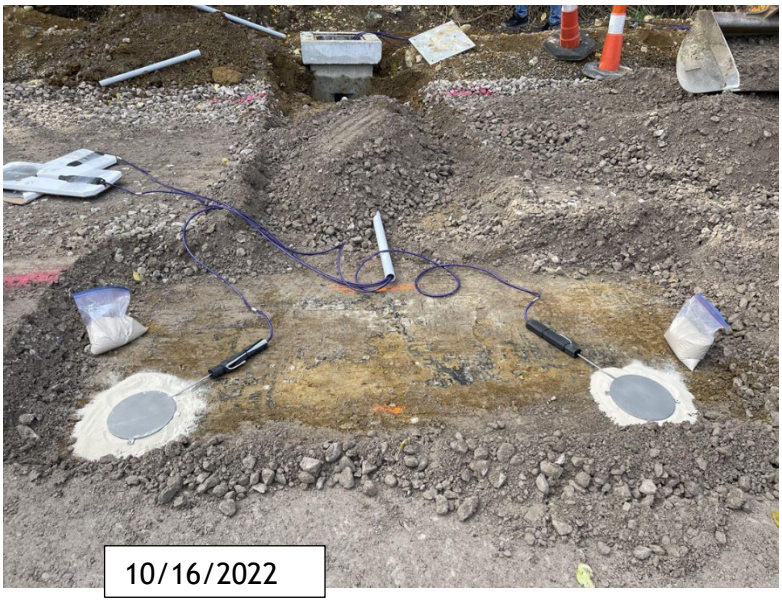


**Figure 33 Pressure Cell Installation**

- Thermocouples: To measure the temperature profile within the pavement during controlled vehicle tests, four thermocouples were installed; on top of the aggregate base, at the mid depth of the asphalt pavement thickness, on top of the asphalt base, and on top of the intermediate course (see Figure 34).

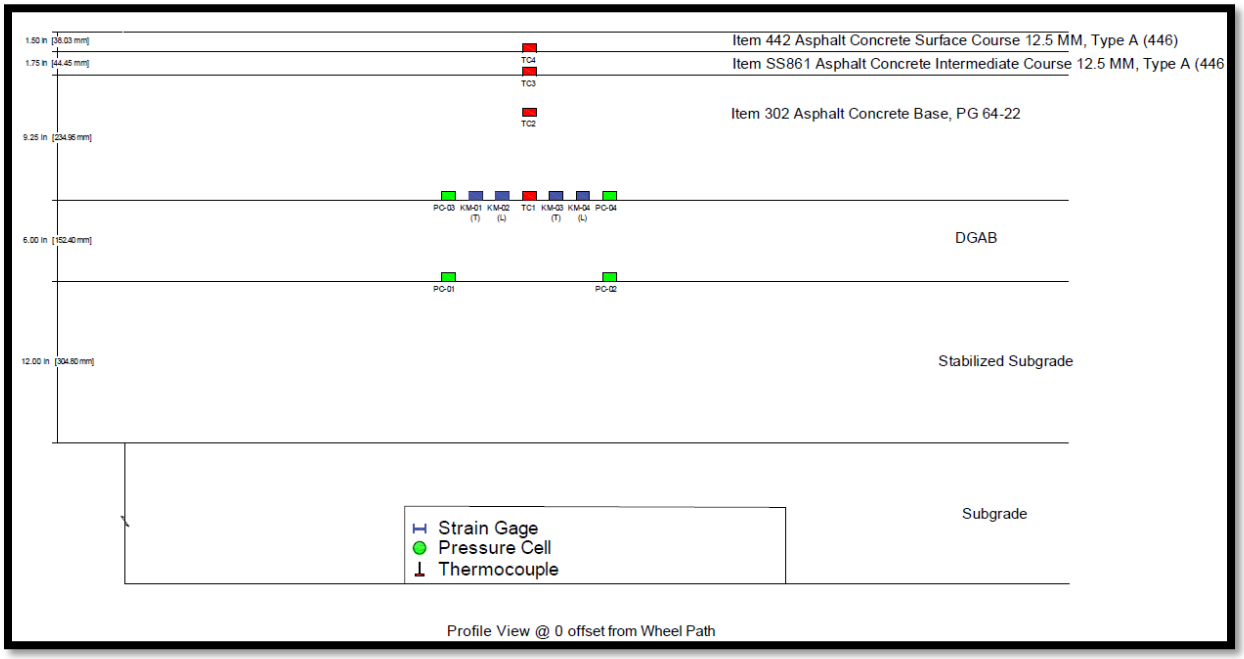


**Figure 34 Location of Instrumentation**

- Strain Gauges: Eight strain gauges were positioned at the bottom of the AC base layer. Four longitudinally in the traffic direction, while the other four were placed transversely, as shown in Figure 35 and Figure 36. These gauges would measure the strains experienced by the base layer under traffic loads.

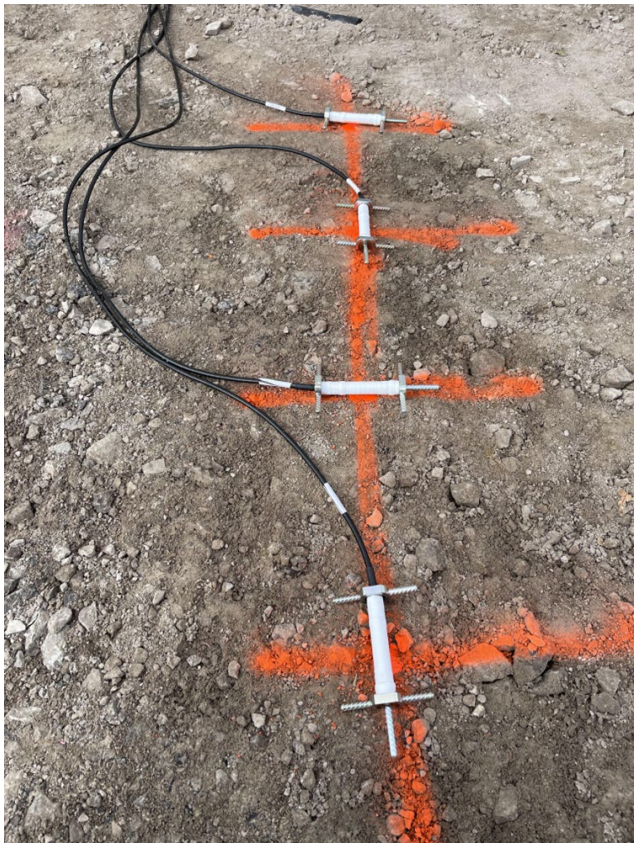

**Figure 35 Strain Gages Ready for Installation**

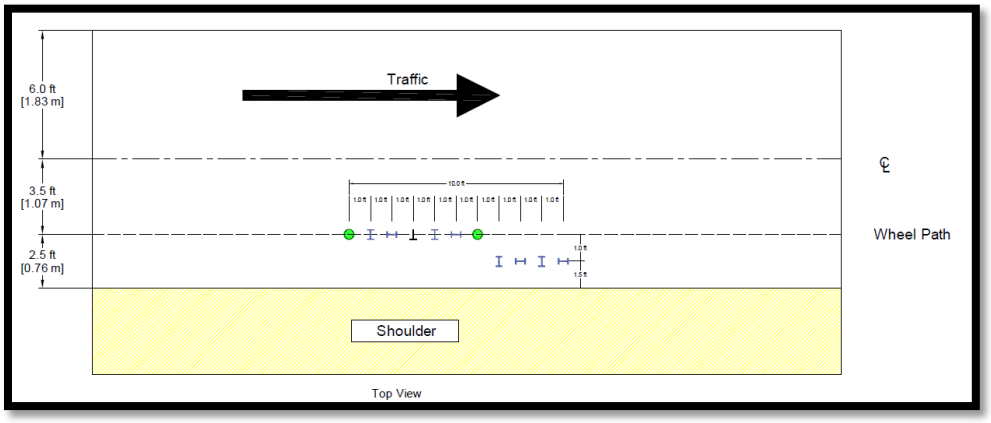


**Figure 36 Pressure Cell and Strain Gage Location**

To protect the gages during the paving process, the team covered the instrumentation with a thin layer of asphalt just prior to paving, as shown in Figure 37 an Figure 38, ensuring the sensors remained at their designated depths and orientations. This protection ensured the accuracy and reliability of the data to be collected.

**Figure 37 Protecting Strain Gages Prior to Paving**

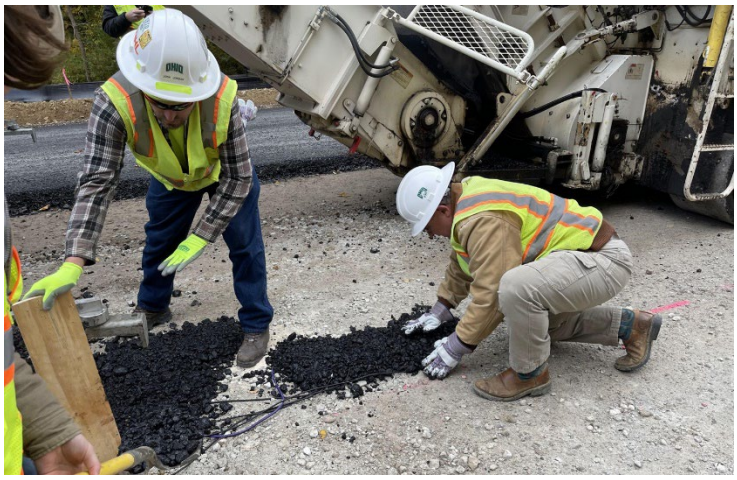

**Figure 38 Protecting Strain Gages Prior to Placement of Asphalt Base**

After the final layer was completed, three additional thermocouples were placed – two at the bottom of the surface layer and the intermediate layer, and one at the middle thickness of asphalt layers, and the pavement cuts sealed as shown in Figure 39.


**Figure 39 Installation of thermocouples**

## Controlled Vehicle Load (CVL) Tests

The pavement response data was collected to capture the variation in strain due to pavement thickness, high polymer modified binder in the mix, and the location of the high polymer modified mix within the pavement thickness, over a range of pavement temperatures. The first series of controlled vehicle load (CVL) tests were performed in May 2023, immediately after construction. The second set of CVL tests were performed in August 2023, during warm weather. The third and final sect of CVL tests were performed in November 2023, during cold weather. An additional test was performed in May 2024.

ODOT's Wayne County Garage provided a single axle, license plate number T 3 101, and tandem axle, license plate T 3 040, dump truck for the controlled vehicle load (CVL) testing. A photo of the single axle dump truck and dimensions are shown in Figure 40 and Figure 41, respectively. A photo of the tandem axle dump truck and dimensions are shown in Figure 42 and Figure 43, respectively.


**Figure 40 Single Axle Test Vehicle**

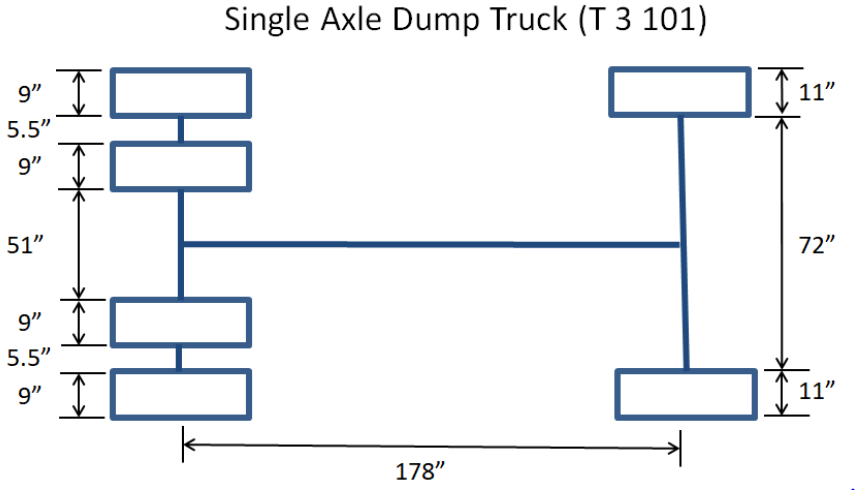


**Figure 41 Single Axle Test Vehicle Dimensions**

**Figure 42 Tandem Axle Test Vehicle**

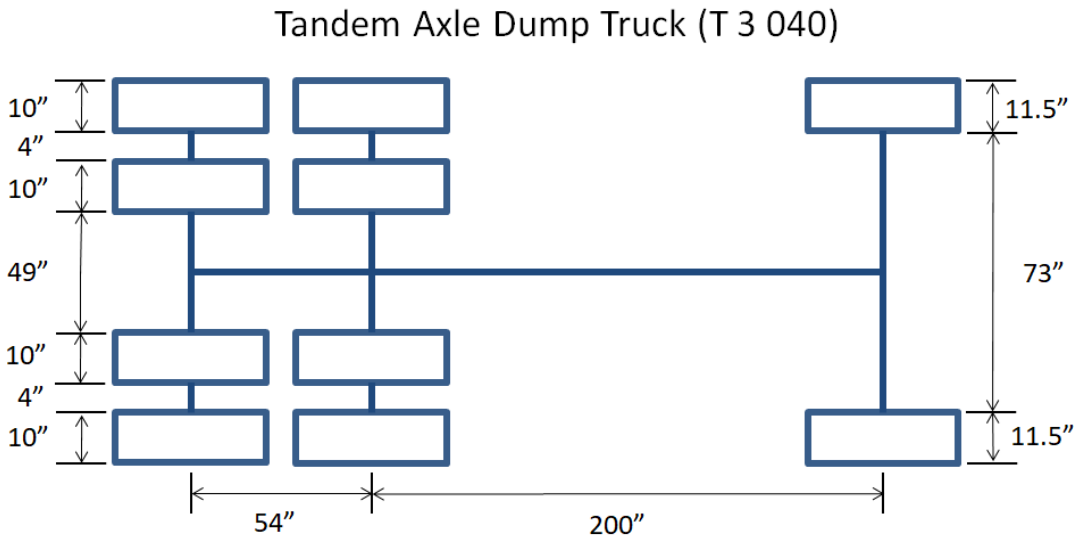


**Figure 43 Tandem Axle Test Vehicle Dimensions**

The trucks were loaded with aggregate the day prior to the first day of testing. ORITE measured tire loads using calibrated portable scales provided by ODOT and adjusted tire pressures. Measured tire loads and pressures are shown in Table 28 through Table 31.

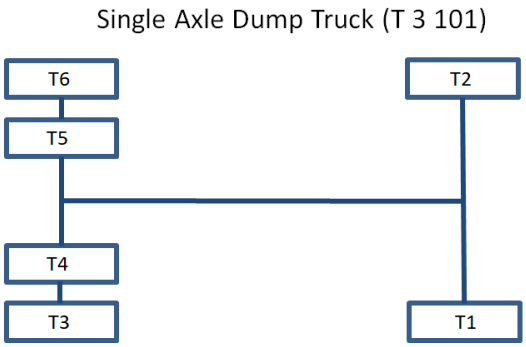


**Figure 44 Single Axle Test Vehicle Tire Number**

**Table 28 Single Axle Test Vehicle Wheel Weight (lbs.)**

| Test Date | T1 | T2 | T3 | T4 | T5 | T6 |
|---|---|---|---|---|---|---|
| 5/10/23 | 5300 | 6100 | 6750 | 7800 | 8200 | 7550 |
| 8/8/23 | 5500 | 5900 | 5980 | 7350 | 7100 | 6100 |
| 11/29/23 | 5950 | 6250 | 6600 | 7350 | 6750 | 6450 |
| 5/6/2024 | 6450 | 5950 | 7450 | 6350 | 6250 | 7300 |

**Table 29 Single Axle Test Vehicle Tire Pressure (psi)**

| Test Date | T1 | T2 | T3 | T4 | T5 | T6 |
|---|---|---|---|---|---|---|
| 5/10/23 | 113 | 114 | 100 | 110 | 107 | 102 |
| 8/8/23 | 112 | 112 | 100 | 104 | 104 | 100 |
| 11/29/23 | 106 | 106 | 100 | 103 | 100 | 102 |
| 5/6/2024 | 106 | 110 | 104 | 111 | 114 | 116 |

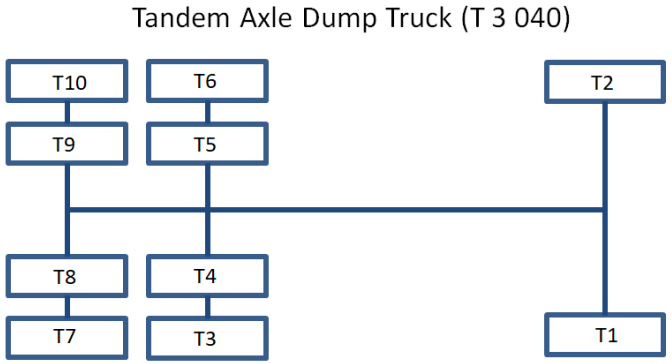


**Figure 45 Tandem Axle Test Vehicle Tire Number**

**Table 30 Tandem Axle Test Vehicle Wheel Weight (lbs.)**

| Test Date | T1 | T2 | T3 | T4 | T5 | T6 | T7 | T8 | T9 | T10 |
|---|---|---|---|---|---|---|---|---|---|---|
| 5/10/23 | 7900 | 8200 | 6100 | 6200 | 5950 | 5750 | 6100 | 5950 | 5650 | 5850 |
| 8/8/23 | 7700 | 8000 | 4795 | 5300 | 5150 | 4700 | 4900 | 5100 | 5350 | 4750 |
| 11/29/23 | 7150 | 6900 | 4300 | 5100 | 4900 | 5050 | 5150 | 5100 | 4900 | 4850 |
| 5/6/2024 | 7250 | 7500 | 5650 | 5200 | 4700 | 4900 | 5050 | 4800 | 4450 | 5000 |

**Table 31 Tandem Axle Test Vehicle Tire Pressure (psi)**

| Test Date | T1 | T2 | T3 | T4 | T5 | T6 | T7 | T8 | T9 | T10 |
|---|---|---|---|---|---|---|---|---|---|---|
| 5/10/23 | 112 | 110 | 102 | 104 | 103 | 100 | 100 | 102 | 103 | 102 |
| 8/8/23 | 112 | 110 | 100 | 102 | 100 | 100 | 100 | 100 | 100 | 100 |
| 11/29/23 | 110 | 110 | 104 | 104 | 104 | 100 | 102 | 104 | 110 | 104 |
| 5/6/2024 | 116 | 118 | 102 | 102 | 100 | 100 | 104 | 104 | 114 | 114 |

The May CVL test loads were 30.3 kips (135 kN) for the single axle and 47.6 kips (212 kN) for the tandem axle, which far exceed typical weights for these vehicle configurations. An effort was made to use more realistic axle weights for the remaining tests. The August test loads were 26.5 kips (118 kN) for the single axle and 40.0 kips (180 kN) for the tandem axle. The November test loads were 27.2 kips (121 kN) for the single axle and 39.4 kips (175 kN) for the tandem axle. An additional test was conducted in May 2024.

# FINDINGS

## Field Testing

### *Dynamic Cone Penetrometer (DCP)*

The DCP was used to determine the resilient modulus of the DGAB( ODOT 304 Base) , and Stabilized subgrade, The DCP was not able to penetrate any deeper than the stabilized subgrade. Table 32 shows a summary of these results.

**Table 32 Summary DCP Results**

| Section | No. of Tests | Average Mr (ksi) 304 (t=6”) | Average Mr(ksi) Stabilized Subgrade (t=12”) |
|---|---|---|---|
| 1 | 5 | 63 | 66 |
| 2 | 5 | 49 | 67 |
| 3 | 4 | 61 | 92 |
| 4 | 5 | 38 | 69 |
| 5 | 5 | 52 | 81 |
| 6 | 5 | 51 | 71 |
| 7 | 5 | 47 | 70 |

Average resilient modules values shown in Table 32 are similar to those reported to ODOT by Sargand et.al. and show that the addition of chemically stabilized base increases the modulus of both the subgrade and base as well.
These values were used for modeling of the base and subgrade.

### *Falling Weight Deflectometer (FWD)*

Falling weight deflectometer data was collected on the following dates: 11/2/20 during preconstruction , 5/8/23 prior to conducting the first CVL test, 8/7/23 prior to conducting the second CVL test, 11/26/23 prior to conducting the third CVL test, and 5/6/24 prior to conducting the fourth CVL test.

Preconstruction FWD data was collected on the existing composite pavement prior to reconstruction. Preconstruction tests were conducted every 250 +/- ft, after construction data was collected every 50 +/- ft along the right wheel path.

The FWD was performed as each pavement layer was constructed except the intermediate layer. Testing was performed every 50 +/- ft along the right wheel path. Three drop heights

were used to approximate loadings of 6000, 9000, and 12000 pounds (27, 40, and 53 kN). All measurements were normalized to 1000 lbs. (4 kN) to facilitate comparison between sections. Sensors were spaced at one-foot intervals with sensors at -12, 0, 12, 24, 36, 48 and 60 inches (-305, 0, 305, 610, 914, 1219, and 1524 mm), designated as D12, D0, D12, D24, D36, D48 and D60 respectively, from the center of the load plate.

Data from the FWD was used to back calculate the modulus for the various asphalt layers. BAKFAA software was used for this purpose.

The D60 sensor on the FWD would be a measure of the stiffness of the subgrade. Slight decrease for many of the sections but same general trend, middle sections stiffer than end sections. Difference may be due to difference in moisture, due to the location of the section within the project and the natural elevation changes

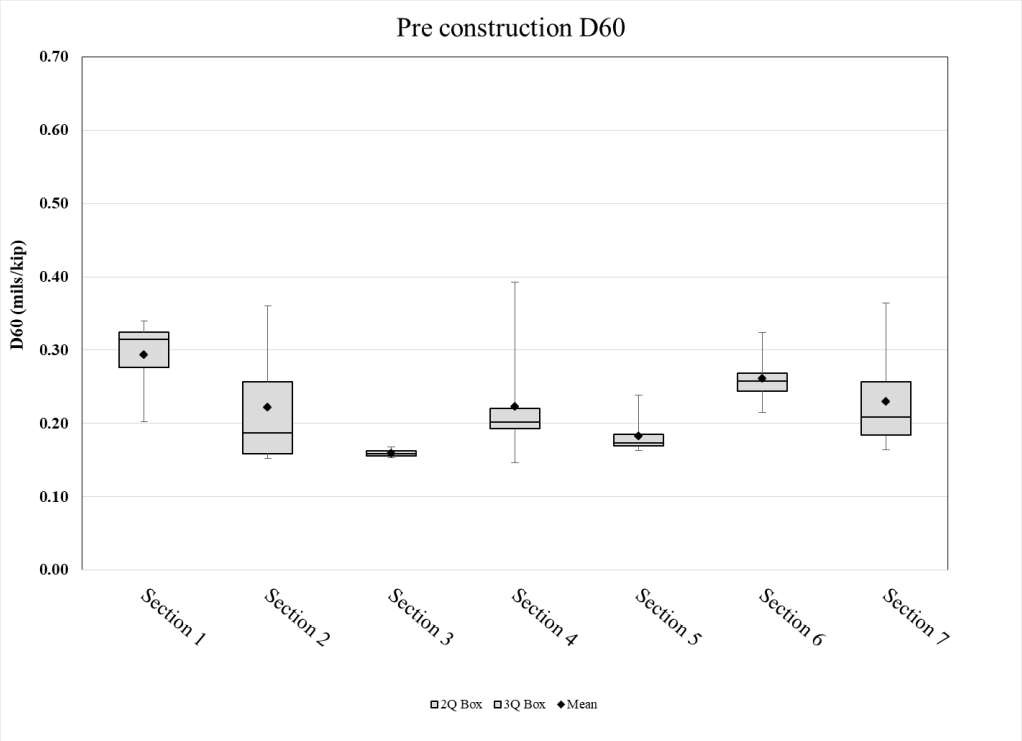


**Figure 46 D60 results from FWD tests during pre-construction of the test sections**

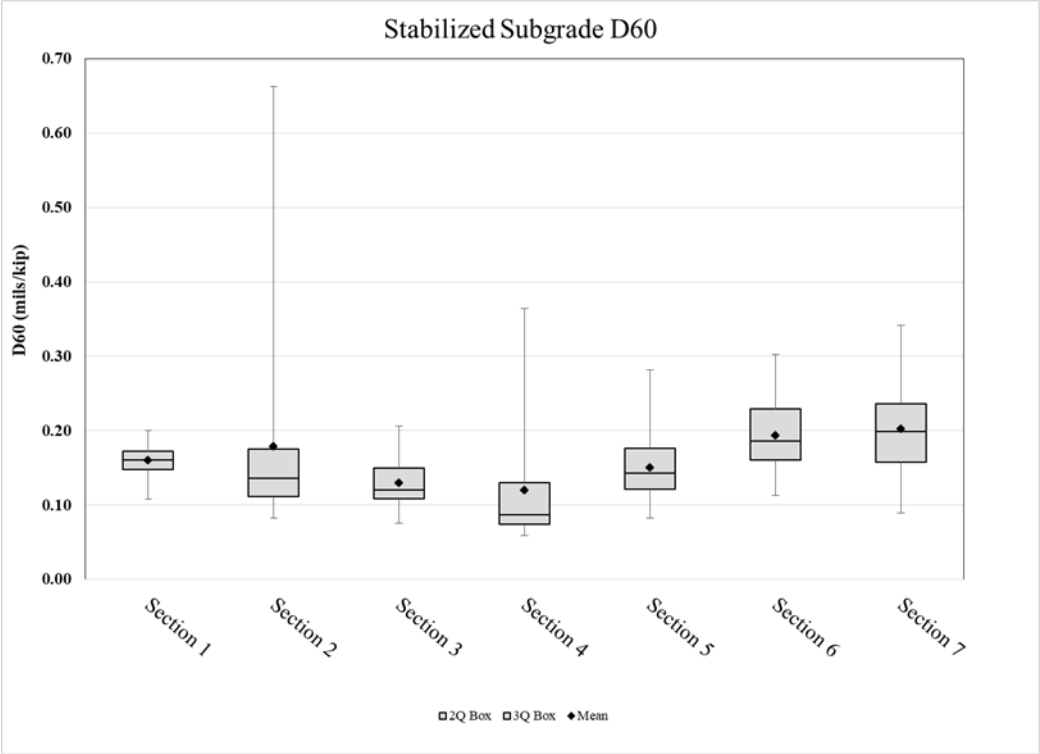


**Figure 47 D60 results from FWD data on the stabilized subgrade.**

D0 sensor on the FWD is a measure of the stiffness of the total pavement. After stabilization, D0 results are statistically the same except for section 5, which is stiffer and less variable. These results highlight some weak areas in Section 1, 4, 6 and 7.

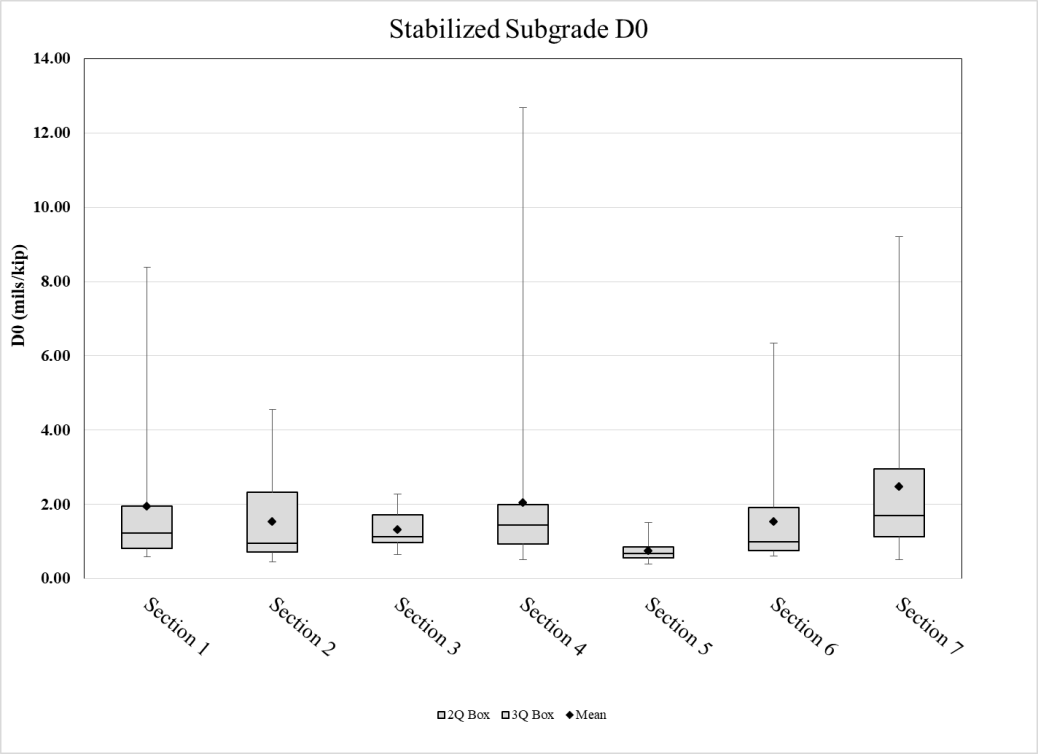


**Figure 48 D0 results for the stabilized subgrade**

Addition of granular base slightly decreased stiffness for most sections, and increased the variability of section 5 as shown in Figure 49.

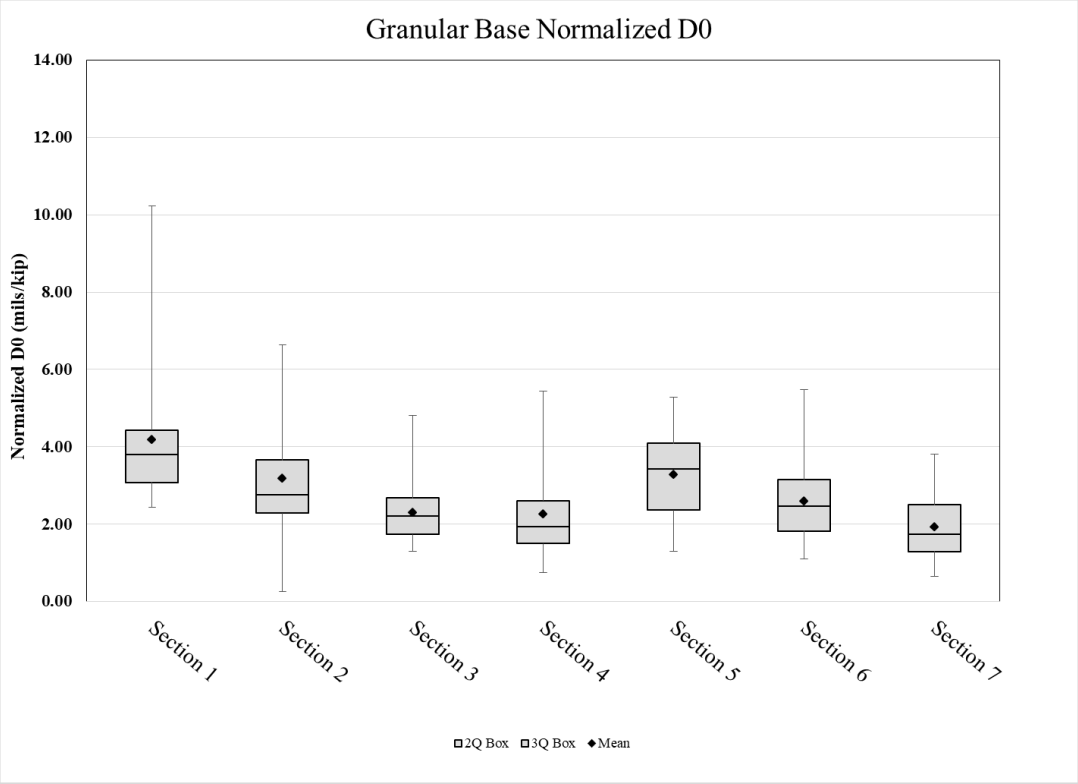


**Figure 49 D0 results from FWD data on the granular base.**

The addition of the asphalt base increased the pavement stiffness and greatly reduced variability. Horizontal axis C=control mix, H=highly polymer modified mix. Asphalt surface figure shows the mix type from top to bottom, i.e. HHC is high polymer modified surface, high polymer modified intermediate, and control mix asphalt base. The number following the letter is the design asphalt pavement thickness in inches.

Figure 52 shows the ratio of D0/D60 on the surface of the pavement for the FWD data conducted on November 2022 immediately after completion of construction. As previously mentioned, according to Sargand and Figueroa [2010] the D0/D60 ratio was found to be a predictor of future performance of the pavement. As can be seen, most of the sections thicker than 9.0 (229 mm) are within the good performance category.

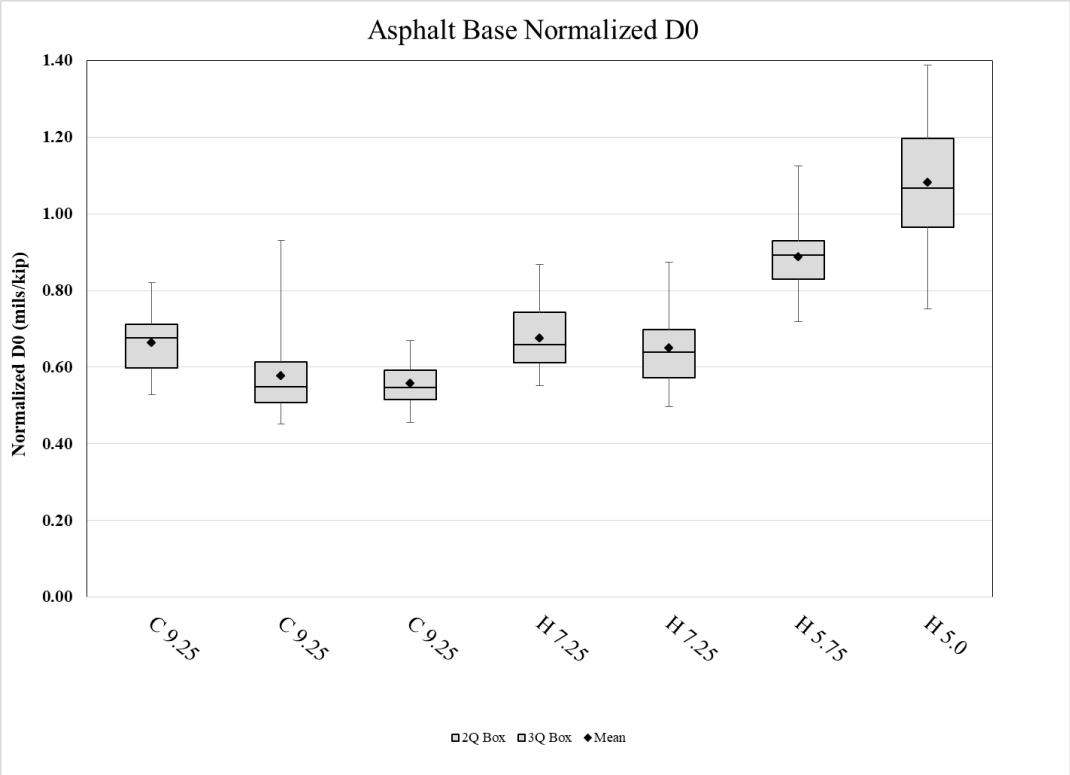


**Figure 50 Asphalt Base Normalized DO**

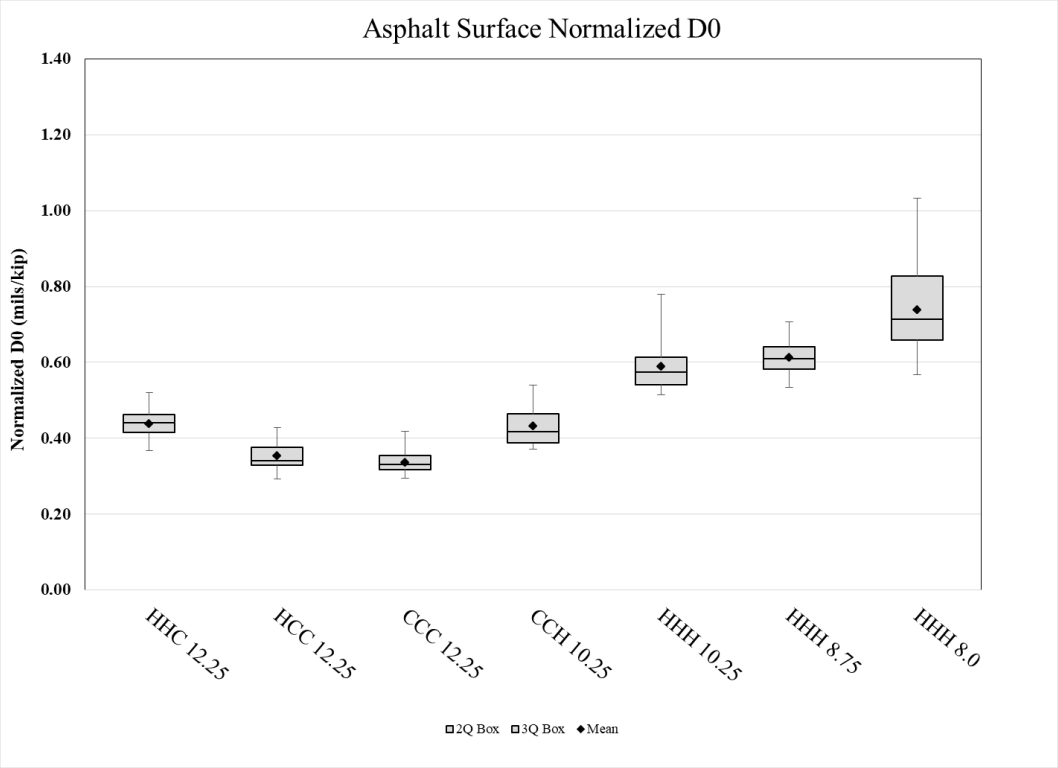


**Figure 51 Asphalt Surface Normalized D0**

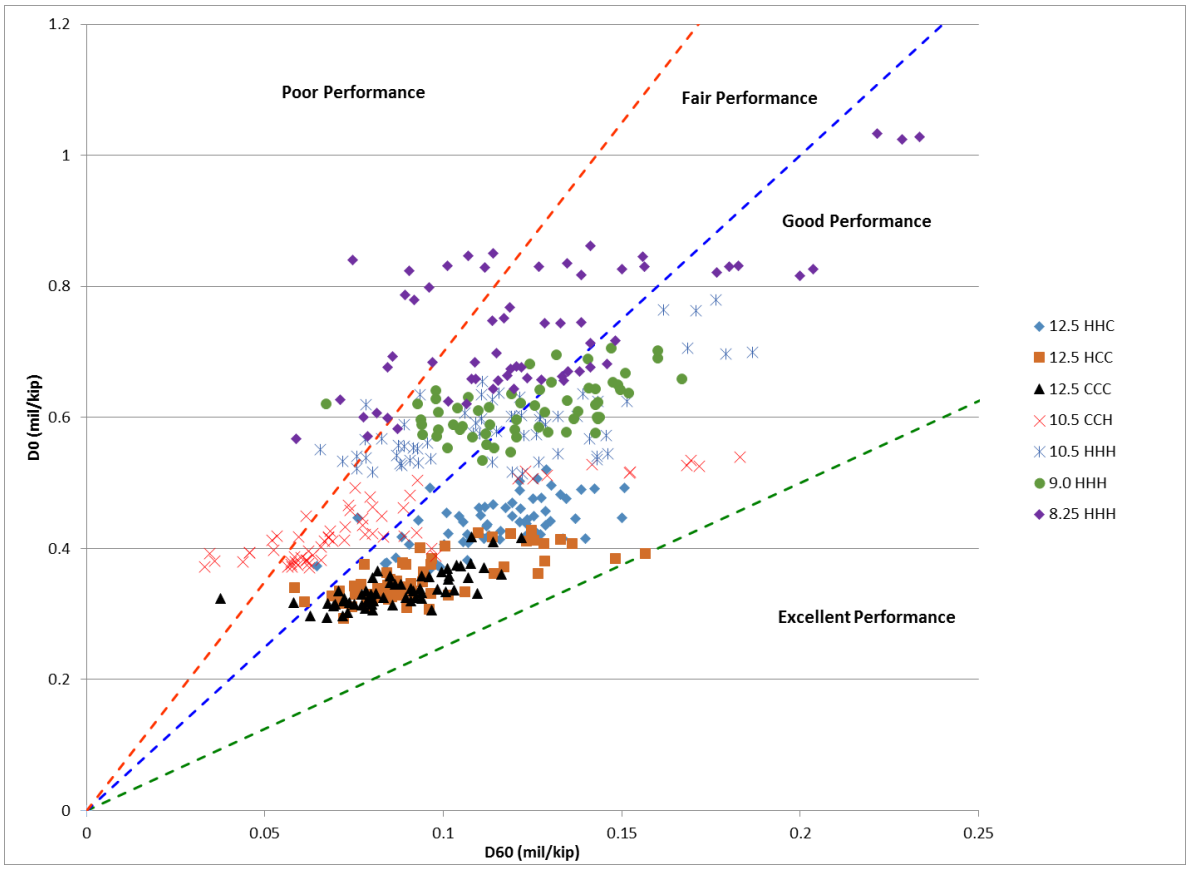


**Figure 52 D0_D60 on WAY-83 Surface, 11/10/22**

### *Controlled Vehicle Tests and Strain Results*

Controlled vehicle tests using ODOT Tandem and Single Axle Trucks as previously described were conducted on May 8th 2023, August 7th 2023 and November 26 2023. An Additional test was conducted on May 6th 2024. Table 33 shows the particulars of the truck tests. Data was collected during these tests from all sensors installed using a high speed data acquisition systems, at each of the test sections. Each test cycle consisted of controlled runs from a Tandem Axle and a Singel Axle truck. Each truck travelled over the sensors a minimum of three times at each of the three speeds 5 MPH, 35MPH and 45+MPH (8, 56, and 72+ km/h). For some of the sections it was not possible to reach a higher speed due to construction and MOT restrictions.

At each location sand patches were used to measure the truck tire offset from the pavement edge line to give an indication of the location of the rear axles and how closely it matched the line of the sensors. Figure 53 Example of sand patch used to measure truck tire offset. The distance between the edge of the tire print and the edge of the pavement edge marking was measured and noted. Since the sensors were installed at 2.5 feet (0.8 m) and 1.5 feet (0.5 m) respectively, we can then use the measured distance to calculate the tire offset.


**Figure 53 Example of sand patch used to measure truck tire offset.**

**Table 33 CVL Test date information**

| Test Start Date | Test End Date | Axle Configuration | Total Number of Passes |
|---|---|---|---|
| 5/8/23 | 5/10/23 | Single | 63 |
| | | Tandem | 63 |
| 8/7/23 | 8/9/23 | Single | 63 |
| | | Tandem | 63 |
| 11/27/23 | 11/29/23 | Single | 63 |
| | | Tandem | 63 |
| 5/6/24 | 5/8/24 | Single | 65 |
| | | Tandem | 65 |

Tire offset data was collected and tabulated to better understand the strain magnitudes as they are dependent on truck tire location. Table 34 and Table 35 show examples of the tire offset data. The complete set of tire offsets will be provided in an data addendum to this report.

**Table 34 Example tire offset table for single axle truck runs for section 1 August 2023 test**

| Speed (mph) | Run No. | Axle Load (lbs.) | Tire offset Approach (in) | Tire Offset Leave (in) | Average offset (in) | offset from the center of the tire to KM 1,2,3 and 4 | offset from the center of the tire to KM5,6,7 and 8 |
|---|---|---|---|---|---|---|---|
| 5 | 1 | 26530 | 13.5 | 11.75 | 12.6 | 4.4 | -7.6 |
| | 2 | 26530 | 16 | 13.5 | 14.8 | 2.3 | -9.8 |
| | 3 | 26530 | 11.25 | 9.75 | 10.5 | 6.5 | -5.5 |
| 35 | 7 | 26530 | 16 | 15 | 15.5 | 1.5 | -10.5 |
| | 9 | 26530 | 16 | 11 | 13.5 | 3.5 | -8.5 |
| | 11 | 26530 | 13.5 | 10.5 | 12 | 5 | -7 |
| 55 | 15 | 26530 | 14 | 13.5 | 13.8 | 3.3 | -8.8 |
| | 17 | 26530 | 12 | 9.5 | 10.8 | 6.3 | -5.8 |
| | 18 | 26530 | 15.5 | 15 | 15.3 | 1.8 | -10.3 |

**Table 35 Example tire offset table for tandem axle truck run, section 1 August 2023 test**

| Speed (mph) | Run No. | Axle Load (lbs.) | Tire offset Approach (in) | Tire Offset Leave (in) | Average offset (in) | offset from the center of the tire to KM 1,2,3 and 4 | offset from the center of the tire to KM5,6,7 and 8 |
|---|---|---|---|---|---|---|---|
| 5 | 4 | 40045 | 12 | 3.5 | 7.8 | 9.3 | -2.8 |
| | 5 | 40045 | 18 | 18.75 | 18.4 | -1.4 | -13.4 |
| | 6 | 40045 | 18.5 | 19.5 | 19 | -2 | -14 |
| 35 | 8 | 40045 | 10.5 | 9 | 9.8 | 7.3 | -4.8 |
| | 10 | 40045 | 6 | 3 | 4.5 | 12.5 | 0.5 |
| | 12 | 40045 | 2 | -4 | -1 | 18 | 6 |
| 55 | 13 | 40045 | 1 | 0 | 0.5 | 16.5 | 4.5 |
| | 14 | 40045 | 15 | 14 | 14.5 | 2.5 | -9.5 |
| | 16 | 40045 | 0 | -1 | -0.5 | 17.5 | 5.5 |

In addition to the data from the installed pavement sensors, data from the thermocouples installed was collected through the duration of testing. Figure 54, Figure 55, and Figure 56 show the temperature variation for the test sections during CVL tests. Temperature ranged from 30°F (-1°C) to 115°F (46°C) throughout the year. A complete set of temperature data will be provided in the addendum.

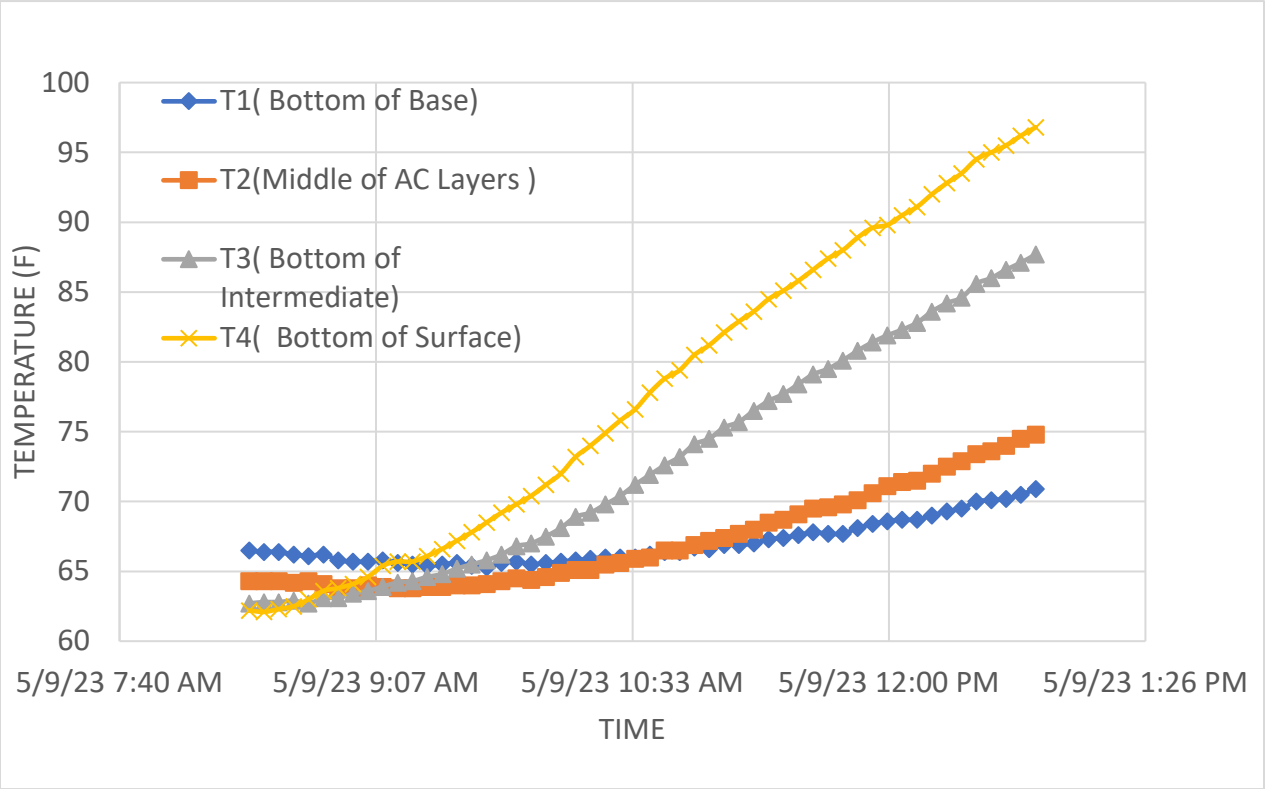


**Figure 54 Pavement temperature readings for May 2023 test**

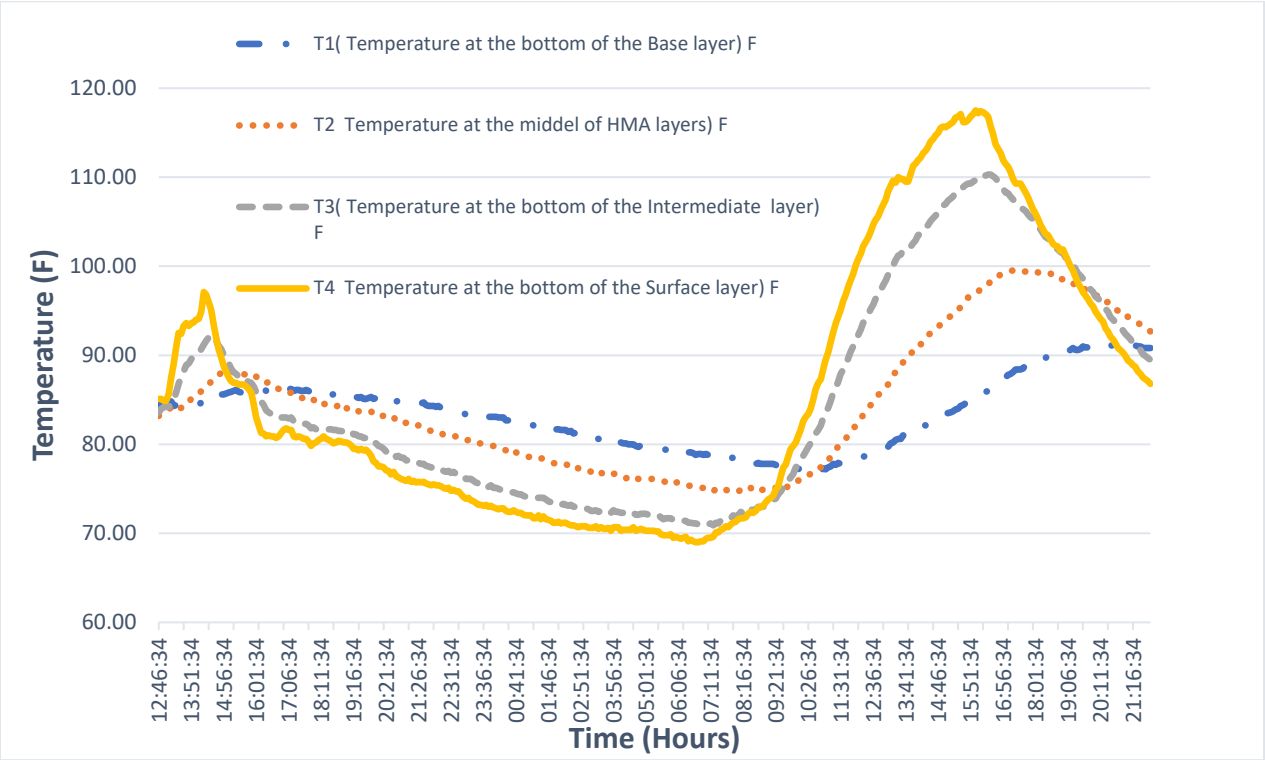


**Figure 55 Temperature variation for section 5, August 2023 test**

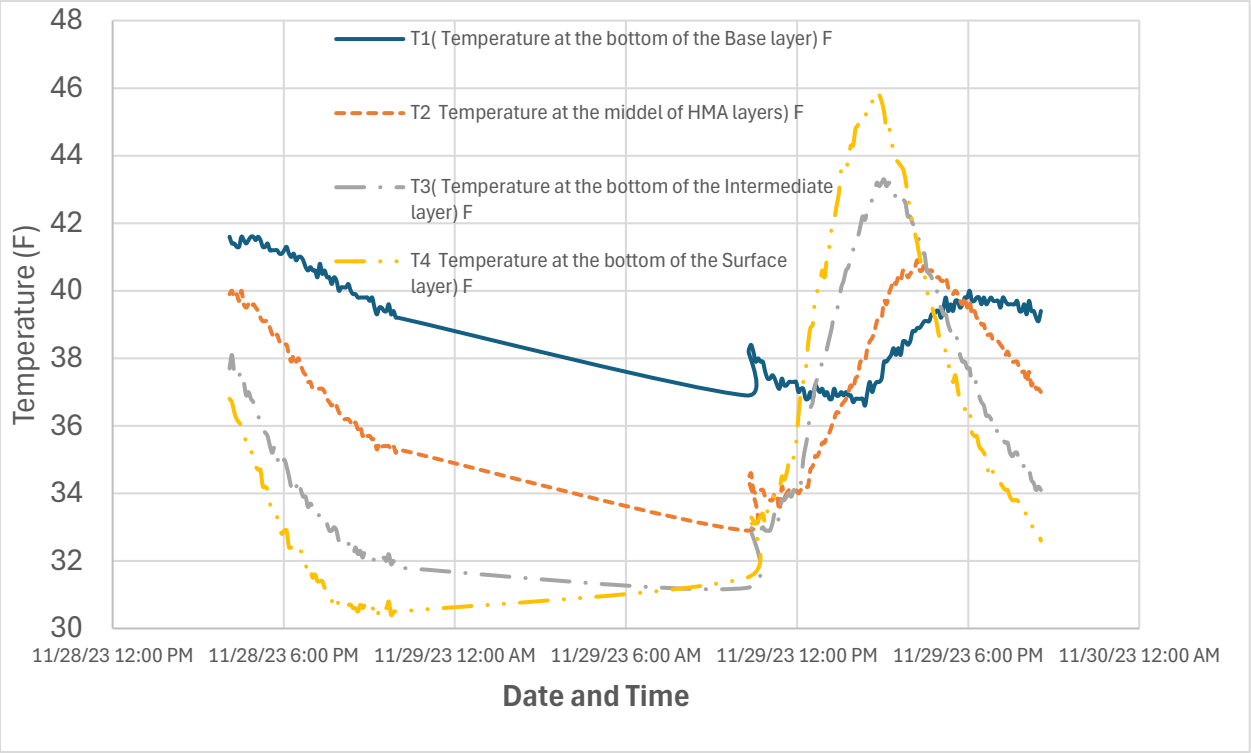


**Figure 56 Temperature variation for section 5, November 2023 tests**

Typical strain results from the CVL tests are shown in Figure 57 and Figure 58. The figures show the typical response of the strain gages installed in the asphalt base to the truck driving over the asphalt surface. The x-axis shows time in seconds and the y-axis shows the strain readings for the particular sensor. Data from all the sensors and test runs was compiled and aggregated in tables for analyses. For the analysis, the maximum strain values for each gage were extracted from the strain data.

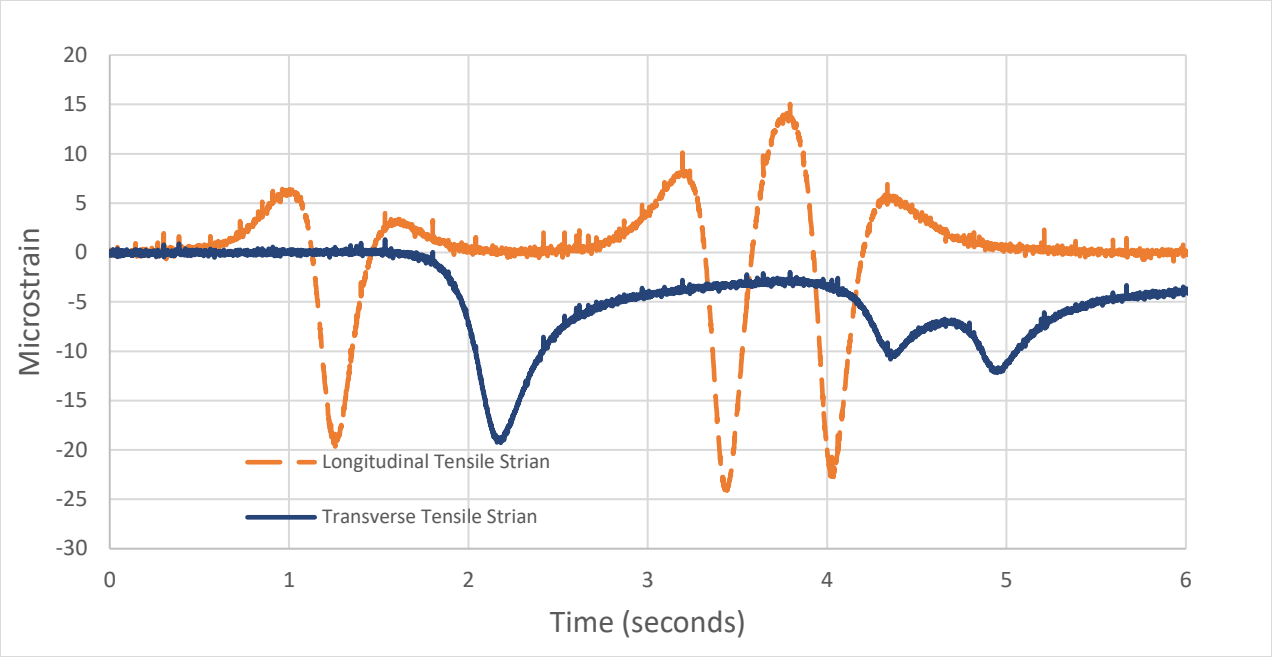


**Figure 57 Tandem axle truck response for section 3 at 5 mph (8 km/h)**

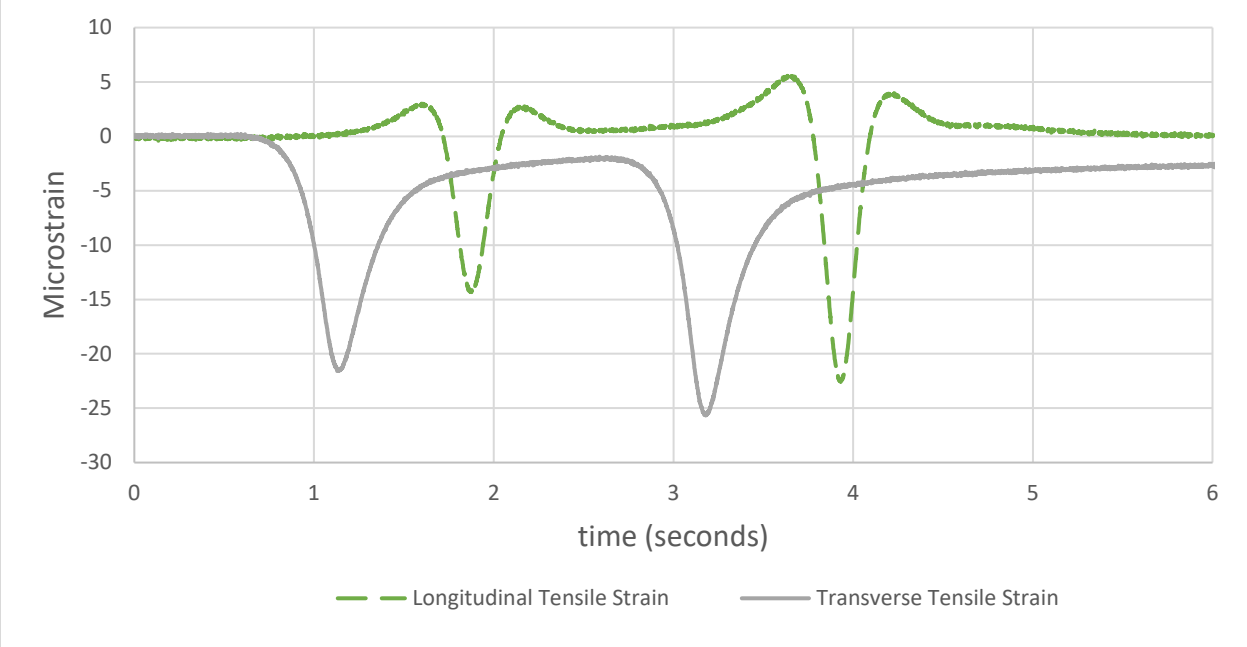


**Figure 58 Single axle truck response for section 5 at 5 mph (8 km/h)**

To recap from the earlier part of this report, the test section design as shown in Figure 30 incorporated two types of asphalt mixes, the conventional hot mix asphalt (HMA) and the high polymer asphalt mix (HPM) and designated by ODOT as PG88-22M. All sections have a 1.50" (38 mm) surface layer and 1.75" (44 mm) intermediate layer; in some sections one or both of these layers have HPM. Below that is a layer of asphalt treated base, which may be a 9.25"

(235 mm) layer using HMA base, or a thinner layer of HPM base, with depth varying by section as shown. Section 3 represented a traditional perpetual pavement design without any PG88-22M , serving as a control to the other sections. Sections 5, 6, and 7 had all layers with PG88-22M asphalt, with different thickness of the AC base; Section 7 being the thinnest design. All sections were placed on top of ODOT Item 304 dense graded aggregate base on top of chemically stabilized subgrade.

As indicated above, load tests were conducted on WAY-83 in May, August, and November 2023 and May 2024. Since truck loads varied slightly between tests, in order to compare the results, test results were normalized to 9 kip (40 kN) truck. In general, the 5 mph (8 km/h) truck runs provide the highest value for strain and thus the 5 mph (8 km/h) response will be emphasized in this analysis. The truck response due to 35 mph (56 km/r) and 45+mph (72+ km/h) is included in Appendix E.

Figure 59 shows the maximum transverse tensile strain normalized by load (9 kip (40 kN)) recorded for each section during load tests. Figure 60 shows the maximum longitudinal tensile strain normalized by load (9 kip (40 kN)) recorded for each section during load tests. In both figures C denotes conventional HMA mix, and H denotes HPM, PG88-22M mix.

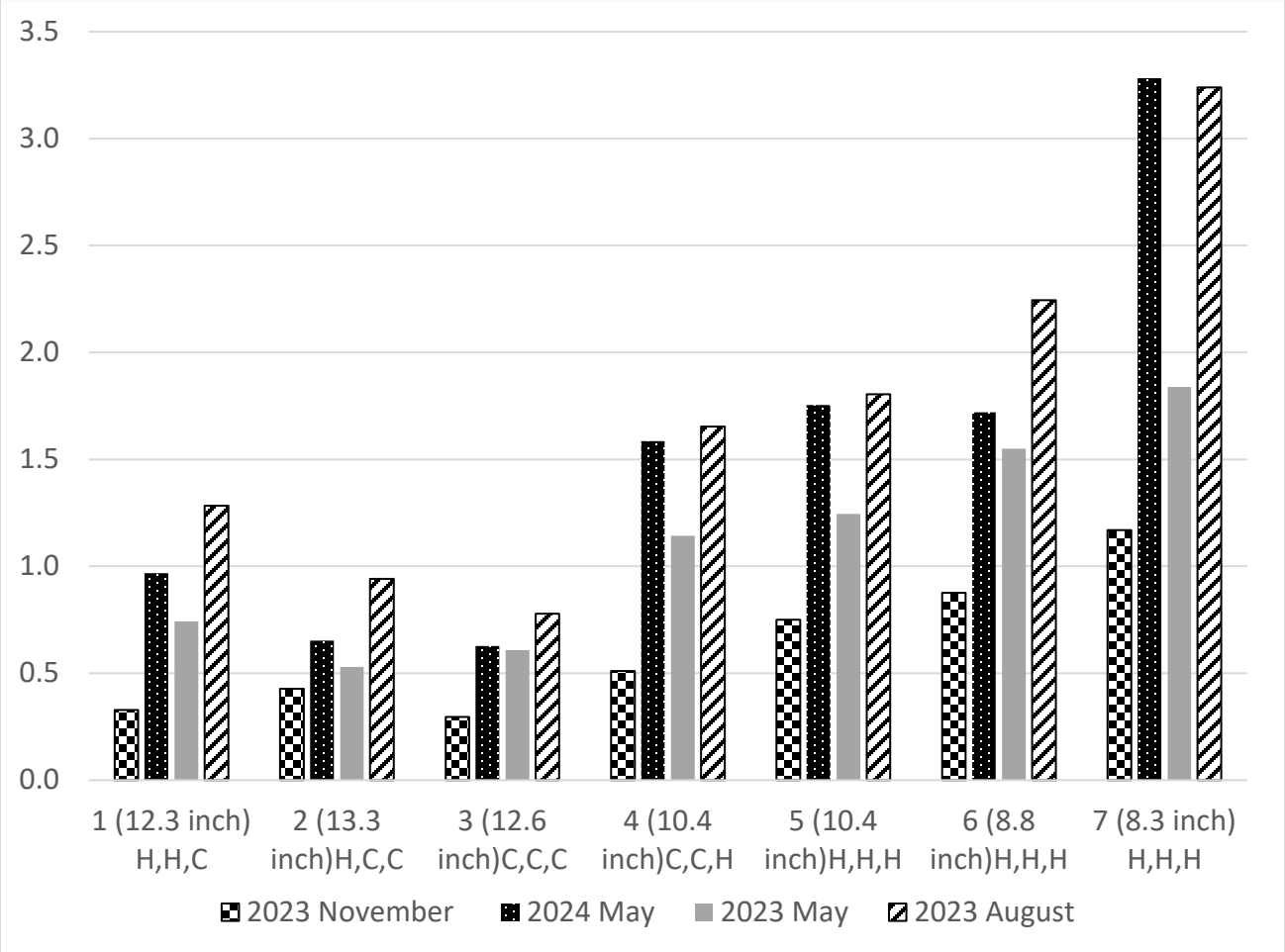


**Figure 59 Normalized transverse strain results for all test sections and CVL tests at 5 mph (8 km/h)**

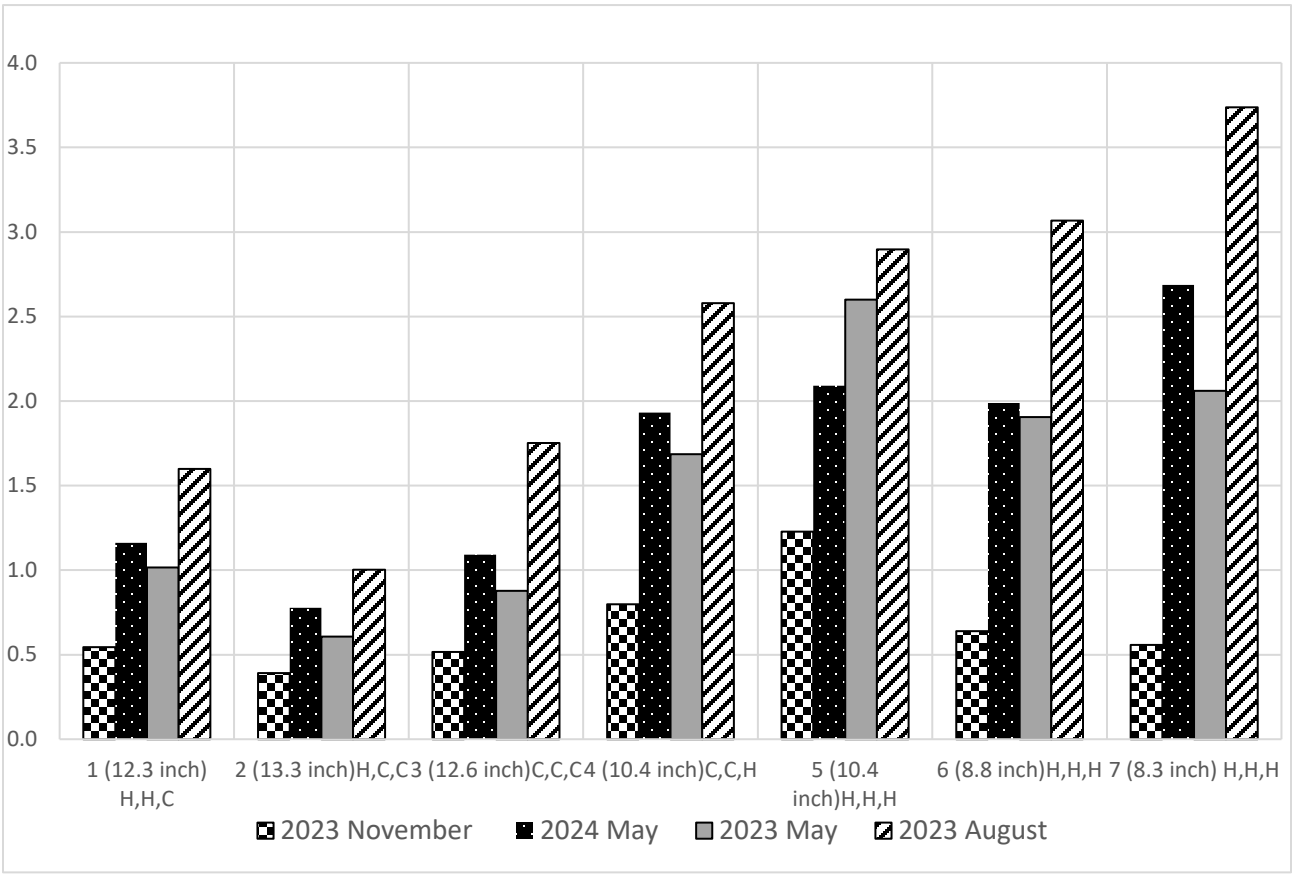


**Figure 60 Normalized longitudinal strain results for all test sections and CVL tests at 5 mph (8 km/h)**

Figure 61 shows the maximum transerve tensile strain per section for all CVL tests conducted at 5 mph (8 km/h), and Figure 62 shows the maximum transerve tensile strain per section for all CVL tests conducted at 5 mph (8 km/h) both figures normalized to 9 kip (40 kN) truck and per inch of pavement.

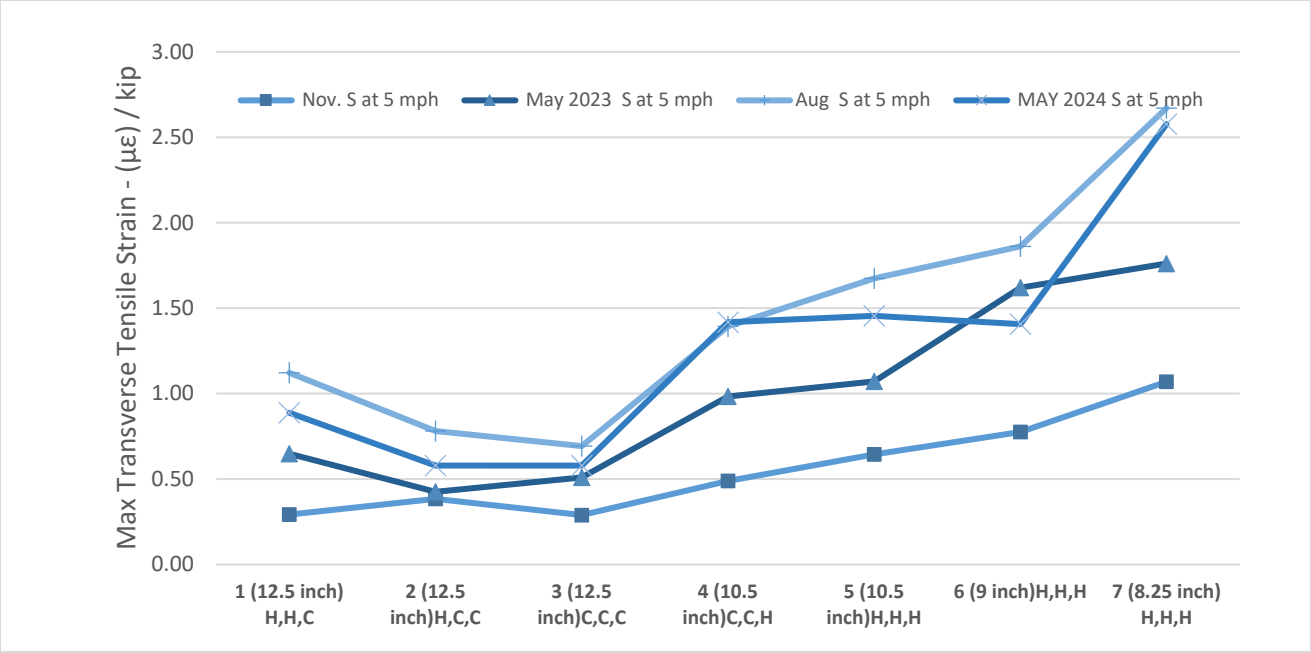


**Figure 61 Maximum transverse tensile strain for each section for 5 mph (8 km/h) CVL tests normalized per inch of pavement**

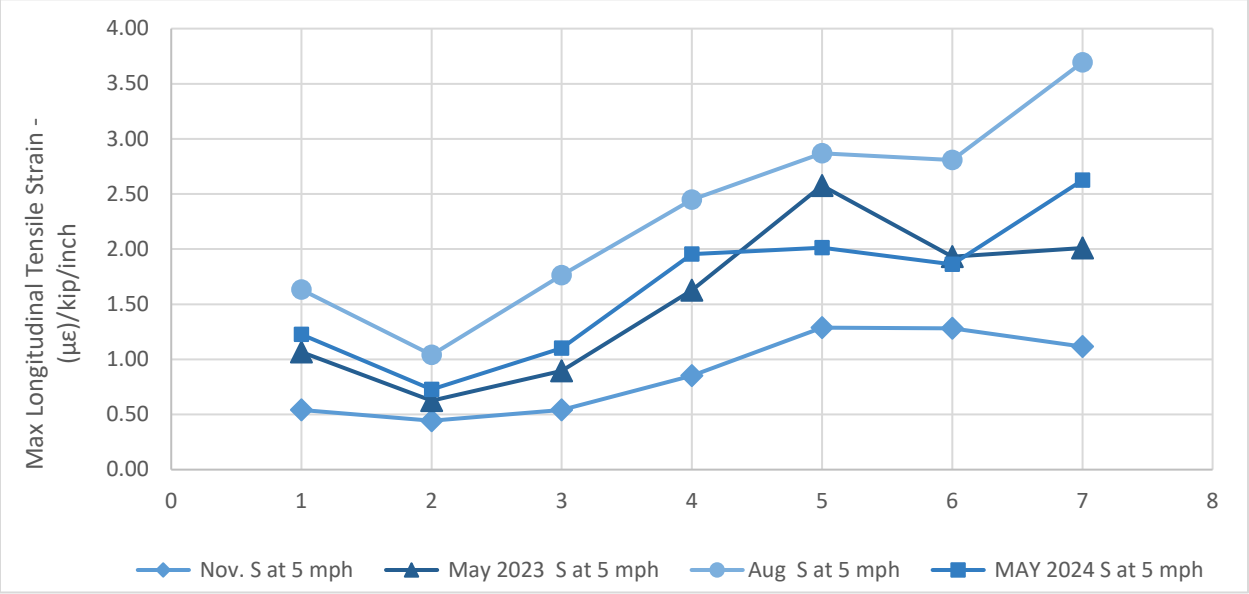


**Figure 62 Maximum longitudinal tensile strain for each section for 5 mph (8 km/h) CVL tests normalized per inch of pavement**

As expected, the longitudinal strain was greater than the transverse strain in most cases. The strain depends on several variables, including the depth beneath the surface, temperature of the pavement, speed of the truck, asphalt mix, and transverse position of the load relative to the strain gauge.

Overall the strain value are not high. In literature, as previously discussed when perpetual pavement was introduced, the strain limit criteria to qualify for perpetual pavement was set to 70 με. However, studies by Witczak (2013) showed that significantly higher values for strain endurance limit was a function of temperature and speed of vehicle. This would permit in practice strains exceeding 70 με in perpetual pavement. Here the field strain is generally significantly lower, so all sections of this pavement meet the perpetual criterion.

The highest strains were seen for the test runs conducted in August 2023, when the pavement temperature was highest, and when the test vehicle was driven the slowest, at 5 mph (8 km/h). In all cases, the normalized strains were below 4 με/kip, or 36 με, well below the original Witczak(2015) 70 με criterion.

Sections 1, 2, and 3 are the thickest layers, each having a nominal 9.25" (235 mm) thick HMA AC base layer. These sections had the lowest strains, consistent with the expectations that thicker pavement designs would have the least strain at the bottom.

Sections 4 and Section 5 have same thickness (10.4" (264 mm) overall), but higher polymer content in Section 5 means it has higher strains.

Section 6 and Section 7 show the effect of thickness for otherwise similar high polymer formulation, with the thinner Section 7 having higher strains.

Figure 63 compares Section 1 and Section 3 normalized transverse tensile strains as a function of pavement temperature as measured at the bottom of the base. Section 1 has HPM(PG88-22M) surface and intermediate layers, while the same layers in Section 3 are conventional HMA. The higher strains in Section 1 reflect the greater flexibility of the HPM (PG88-22M) material, particularly at higher temperatures.

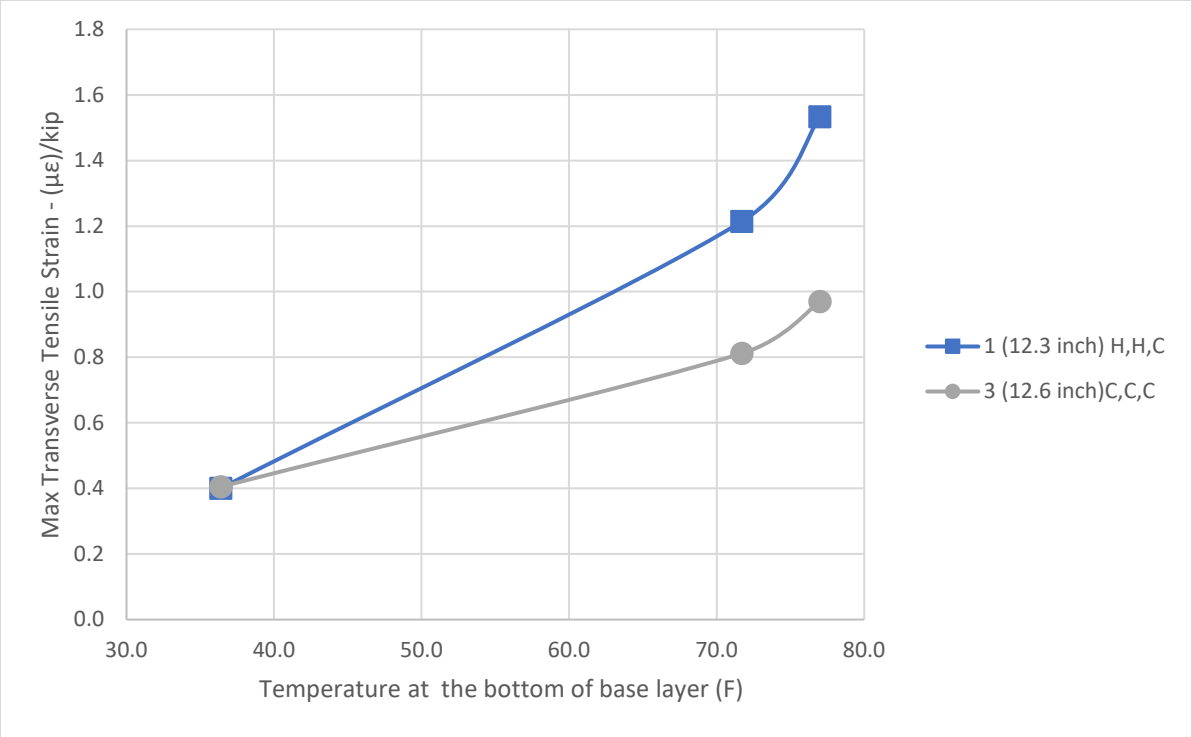


**Figure 63 Normalized transverse tensile strain as a function of pavement temperature**

Figure 64 shows the longitudinal strains versus temperature for all seven sections. Again, Sections 1, 2, and 3 have the lowest strains, while the thinnest section, Section 7, has the highest strain. All measured strains are well below the perpetual pavement endurance limit. These higher strains reflect the thinner construction and the more pliable nature of the HPM (PG88-22M) material used throughout.

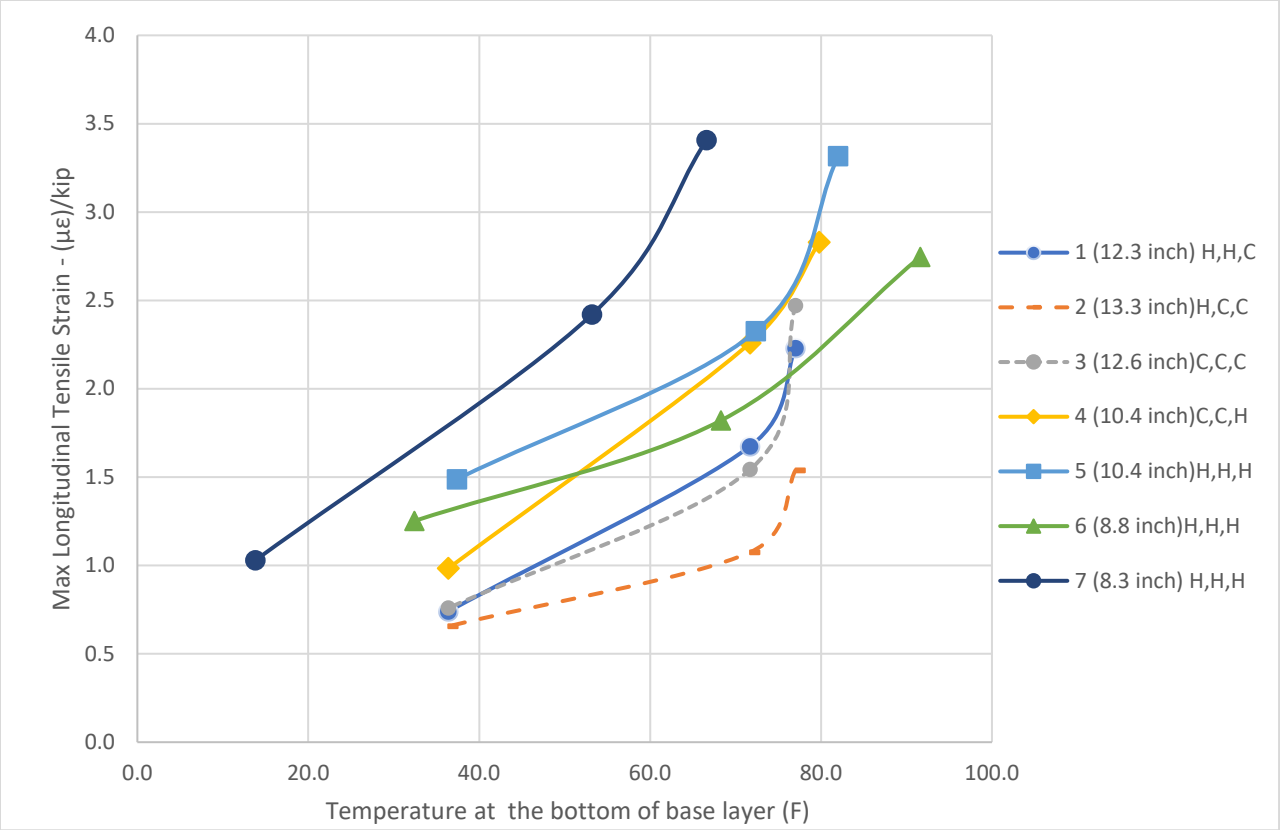


**Figure 64 Normalized longitudinal tensile strain as a function of pavement temperature**

It should be noted that all the HPM (PG88-22M) material incorporated RAP, which is known to make pavements stiffer. The high polymer binder increases the flexibility enough to overcome the increased stiffness of the RAP, making the resulting layers more flexible. It is possible that HPM mixes without RAP content may be even softer than those seen in this project.

## Lab Testing

Lab testing was conducted for all tests as described in Table 23 and Table 24 above. The sections below summarize the results of the tests. Lab results were used for the analysis in later sections of this report.

### *Creep Compliance and Indirect Tension*

Testing was performed in accordance with AASHTO T 322. Three specimens were compacted from plant mix to an air void content of 7 ± 0.5 percent in a gyratory compactor in accordance with AASHTO T 312. Specimens were tested at -20° C, -10° C and 0° C.
Figure 65 below shows the results of lab testing.

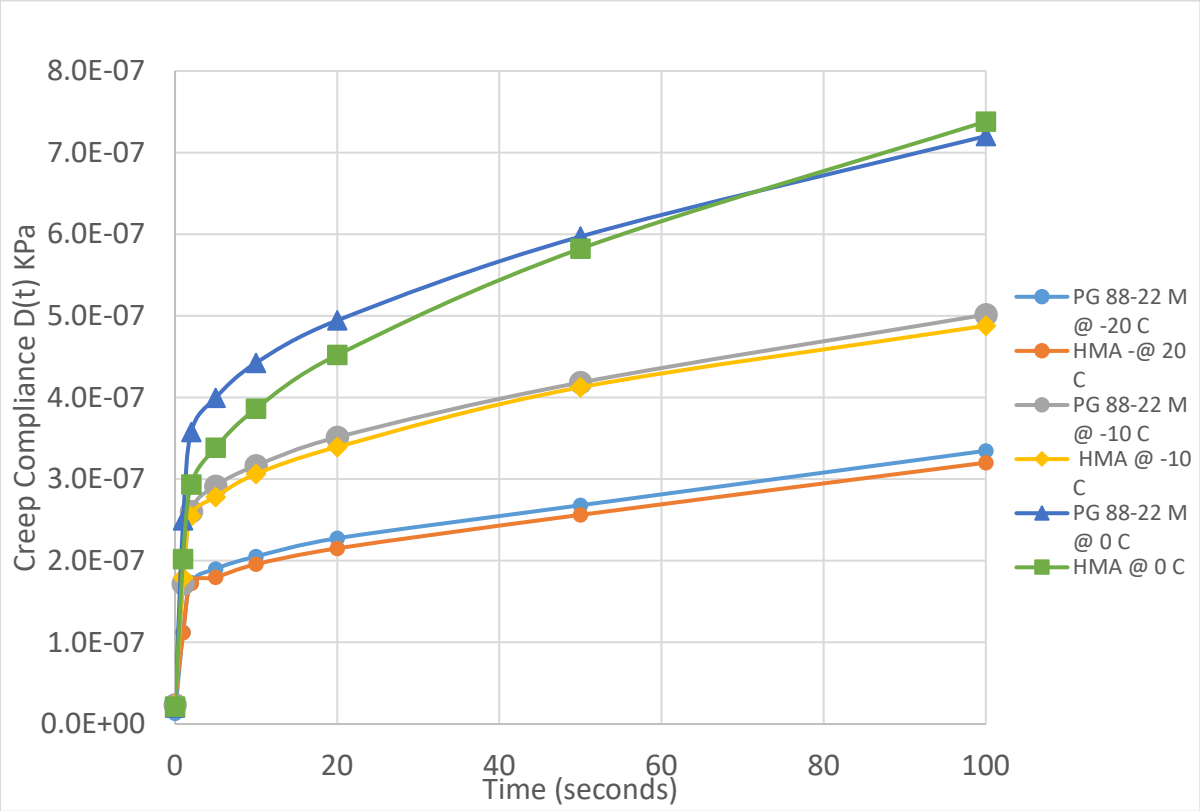


**Figure 65 Creep compliance lab test results**

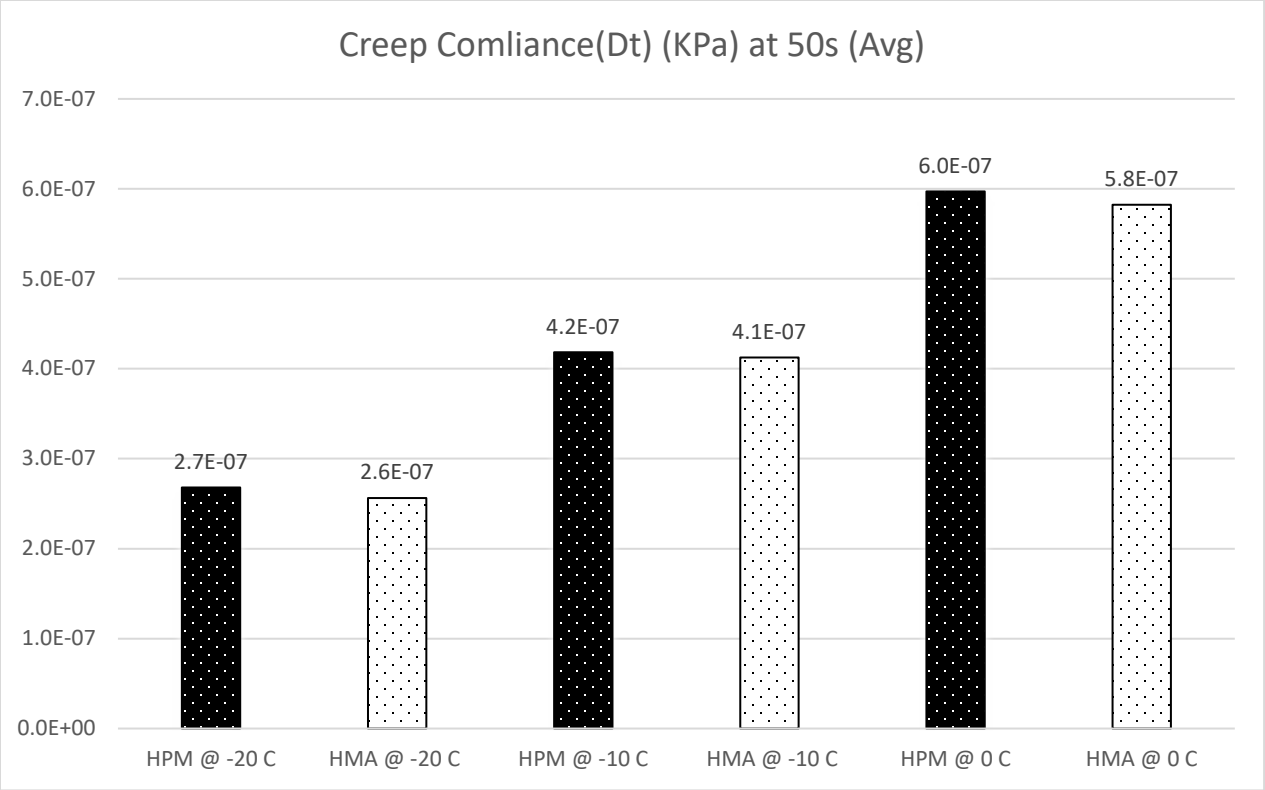


**Figure 66 Creep compliance results for each test at 50 seconds**

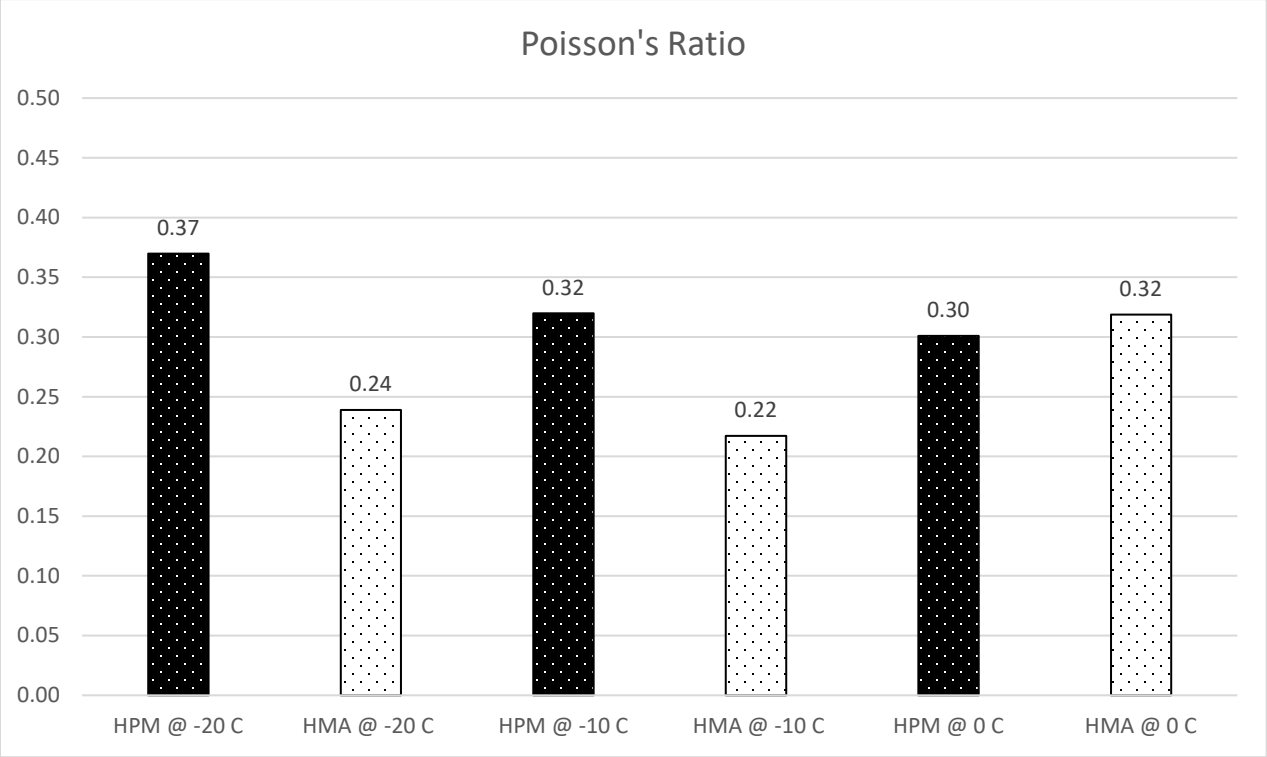


**Figure 67 Poisson's ratio calculations from creep compliance testing**

Upon completion of the creep compliance test, specimens were tested for indirect tension. The specimen was tested at a temperature of -10° C at a rate of 12.5 mm per minute. The tensile strength was calculated using Equation 2

$$\boldsymbol{S = (2 \times P)/(\pi \times t \times D)} \qquad \textbf{(2)}$$

Where:
S = tensile strength of specimen
P = maximum load
t = specimen thickness
D = specimen diameter

Results of the testing at -10°C is shown below in Figure 68. Figure shows that the high polymer mix has higher tensile strength than the control mixes at low temperature.

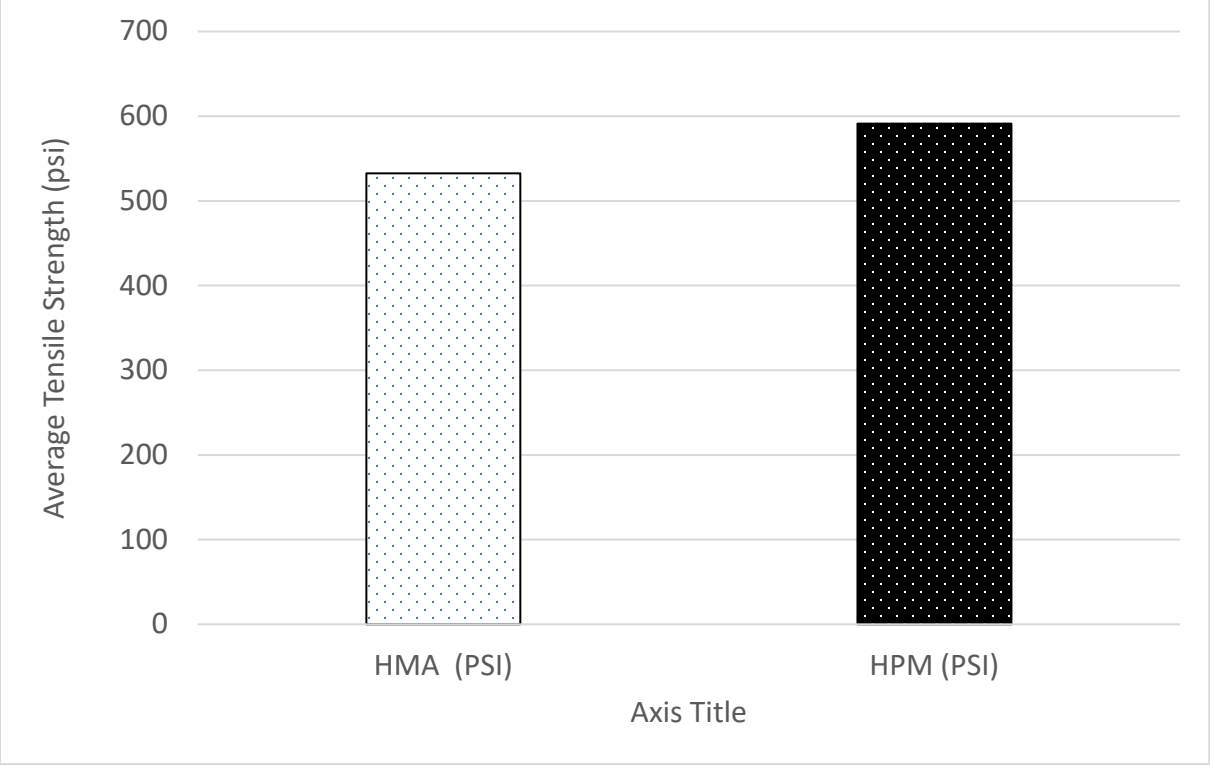


**Figure 68 Average tensile strength measured at -10°C (14°F)**

### *Dynamic Modulus*

Dynamic Complex modulus (|E*|) tests were performed in accordance with AASHTO T342 to get a linear viscoelastic properties for the HPM and control mixes. As specified in AASHTO T342, the test was conducted at loading frequencies of( 0.1, 0.5, 1, 5, 10, and 25 Hz) at different temperatures (10, 4, 21, 37 and 54 ◦C). Additionally,, three replicate samples from each mix were produced at a target air voids level of 7 ± 0.5% by cutting and coring Superpave gyratory compacted samples. The final |E*| test samples were cylindrical in shape, having a diameter of 100 mm and a height of 150 mm. Using a reference temperature of

21.1 ◦C (70 F).then to determine the master characteristics curve for each mix a sigmoidal model was fitted. In general, |E*| results at high frequencies provide an indication of the performance of mixture at low temperatures (cracking), while those at low frequencies indicates of the performance at high temperatures (rutting). to determine the frequency and temperature-dependent viscoelastic material properties of the asphalt concrete materials used in this project, using laboratory data master curves were computed.

The dynamic modulus can be determined by the following equation:

$$|E^*| = \sigma_0/\varepsilon_0 \qquad (3)$$

Where:

$|E^*|$ = Dynamic modulus
$\sigma_0$ = Average peak stress over the last five periods
$\varepsilon_0$ = Average peak strain over the last five periods

A shift factor must be determined in order to build a master curve. The shift factor *a(T)*, is calculated by finding the best-fit second-order polynomial when plotting the shift factor against the test temperature. The following equation describes this relationship:

$$\log a(T) = C1 + C2*T + C3*T2 \qquad (4)$$

Where:
$a(T)$ = Shift Factor
$T$ = Test Temperature
$Ci$ = regression coefficients

The dynamic modulus is determined at various temperatures and is plotted against frequency. The data is then shifted to a reference temperature (21.1°C (70°F)) to form the master curve for the mix. This parallel shift is performed by determining the reduced frequency for each test frequency and temperature based on the reference temperature. The following equation is used to determine the reduced frequency:

$$\log fr = \log f + \log a(T) \qquad (5)$$

Where:
$fr$ = Reduced Frequency at the Reference Temperature (Hz)
$f$ = Actual Test Frequency at the Test Temperature (Hz)

The AASHTO Mechanistic-Empirical Pavement Design Guide (MEPDG) uses the following sigmoidal model to estimate the dynamic modulus of an asphalt mix for curve-fitting purposes:

$$\log|E^*| = \delta + \frac{\alpha}{1+e^{\beta+\gamma(\log f_r)}} \qquad (6)$$

Where:
$|E^*|$ = Dynamic Modulus ($10^6$ psi)
$a$, $\beta$, $\gamma$, $\delta$ are fitting parameters:
$\delta$ is the minimum value of $E^*$ ($10^6$ psi);
$a + \delta$ = is the maximum value of $E^*$ ($10^6$ psi);
and $\beta$ and $\gamma$ are dimensionless parameters describing the shape of the sigmoidal function.
By using the Solver feature in Microsoft Excel, the laboratory-calculated dynamic modulus can be compared to the dynamic modulus estimated using the sigmoidal equation and minimizing the sum of the square of the Error, defined as follows:

$$Error^2 = \left[\frac{E^*_{Lab} - E^*_{Sigmoidal}}{E^*_{Lab}}\right]^2 \qquad (7)$$

The Error is calculated for each frequency and temperature and then summed for the entire data set ($\Sigma\ Error^2$). In Solver, the objective cell is the $\Sigma\ Error^2$; it is set to become as low as possible (min) by changing $\delta$, $a$, $\beta$, $\gamma$, $C1$, $C2$, and $C3$ using an iteration method. The following table ( Table 36) summarizes the curve fitting parameters and regression coefficients solved in Solver for each layer and site.

**Table 36 Curve fitting parameters and regression coefficient for each AC layer**

| Layer | δ | α | γ | β | c1 | c2 | c3 |
|---|---|---|---|---|---|---|---|
| **Surface HPM** | 0.956 | -10.658 | 0.204 | 1.975 | 5.067 | -0.089 | 0.00024 |
| **Surface HMA** | 0.518 | 0.518 | 0.518 | 0.518 | 0.518 | 0.518 | 0.51848 |
| **Intermediate HPM** | 0.680 | 0.680 | 0.680 | 0.680 | 0.680 | 0.680 | 0.68021 |
| **Intermediate HMA** | 0.655 | 0.655 | 0.655 | 0.655 | 0.655 | 0.655 | 0.65529 |
| **Base HPM** | 0.451 | 0.451 | 0.451 | 0.451 | 0.451 | 0.451 | 0.45061 |
| **Base HMA** | 0.518 | -2.176 | 0.649 | 1.277 | 10.968 | -0.218 | 0.00088 |

Figures 69, 70 and 71 show the master curves for the surface, intermediate and base mixes, respectively.

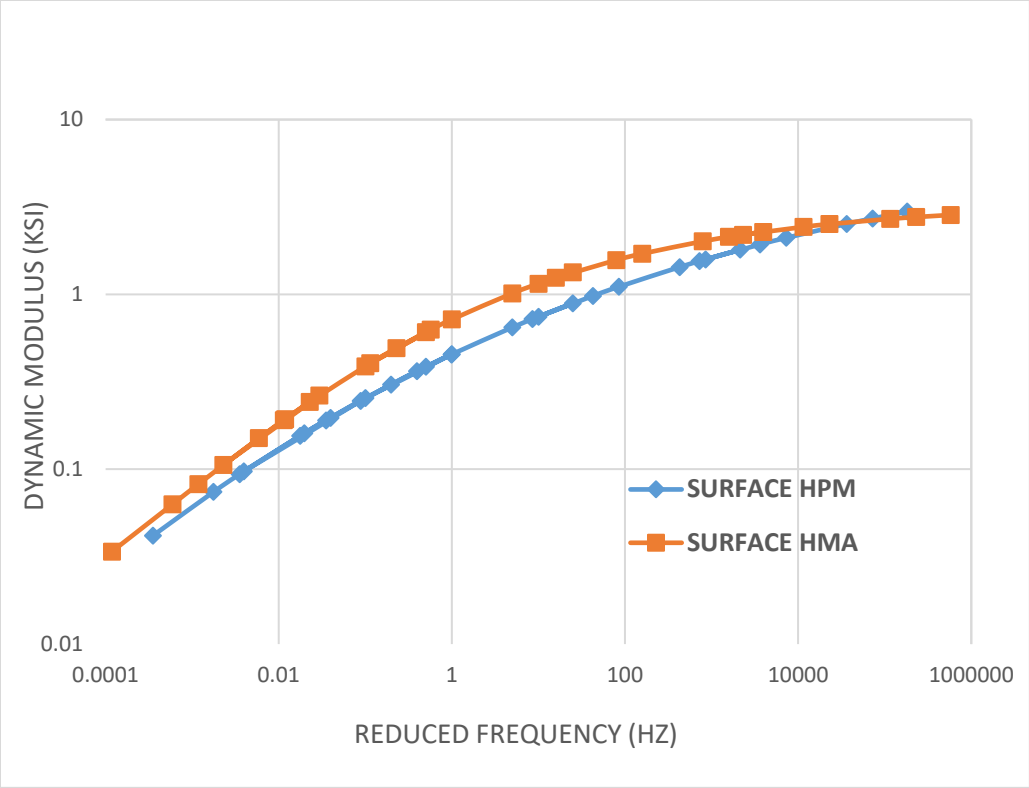


**Figure 69 Master Curve for the Surface Mix**

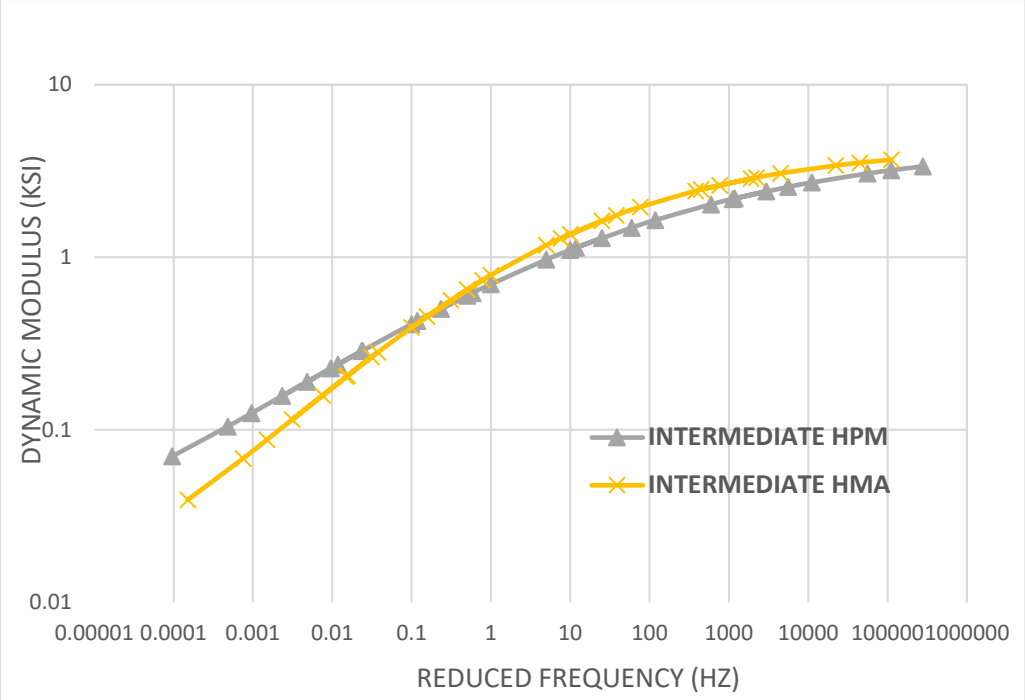


**Figure 70 Master Curve for the Intermediate Mix**

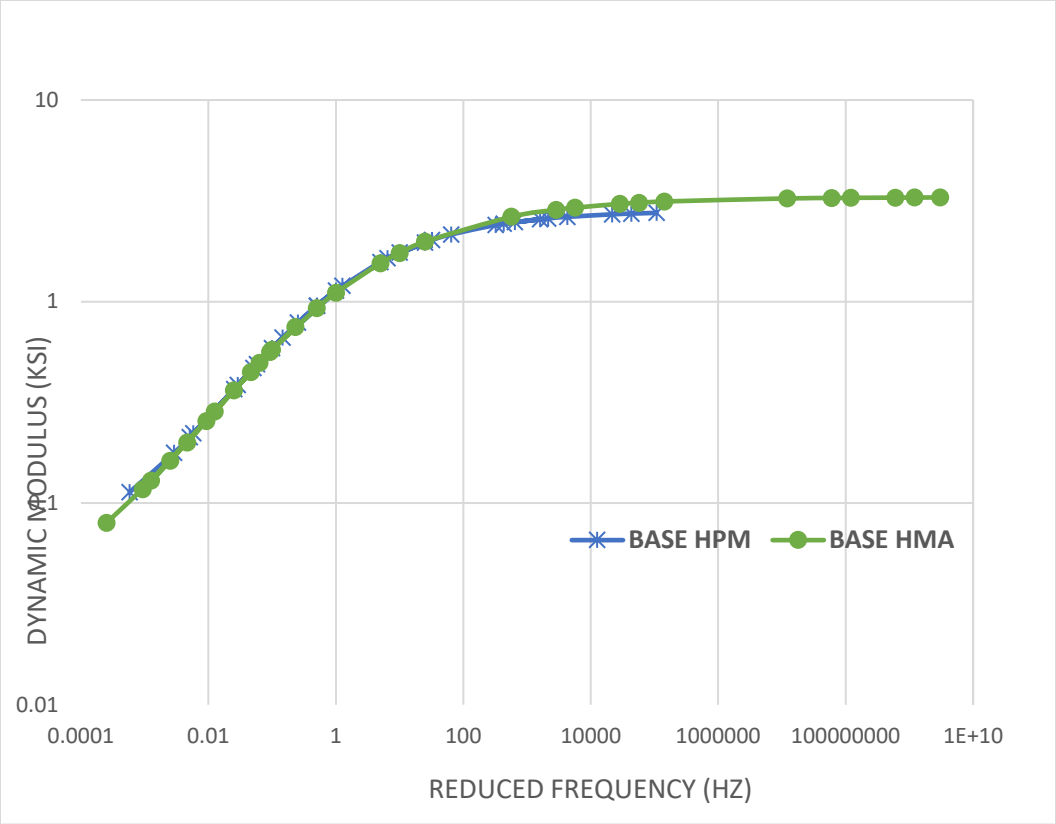


**Figure 71 Master Curve for the Base Mix**

### *Tensile Strength Ratio*

Testing was performed in accordance with AASHTO T 283 and ODOT Supplement 1051. For each mix, six specimens were compacted from plant mix to an air void content of 7 ± 0.5 percent in a gyratory compactor in accordance with AASHTO T 312. The specimens were then split into two groups such that the average air void content of one group would approximately equal to the average air void content of the second group. One group was conditioned in water by applying a vacuum until the degree of saturation was between 80% and 90%. The specimens were then wrapped in plastic, placed in a plastic bag with 10 mL of water, and placed in a freezer at -18° C for a minimum of 16 hours. The specimens were then placed in a water bath at 60° C for 24 ± 1 hour after which the specimen was placed in a water bath at 25° C for 2 hours ± 10 minutes before determining the indirect tension strength. The second group of specimens was wrapped in plastic, placed in a plastic bag, and conditioned in a water bath at 25° C for 2 hours ± 10 minutes before determining the indirect tension strength. The tensile strength ratio (TSR) was determined using Equation 8

$$\boldsymbol{TSR} = (\boldsymbol{average\ tensile\ strength\ of\ conditioned\ subset})/ (\boldsymbol{average\ tensile\ strength\ of\ dry\ subset}) \quad \textbf{(8)}$$

Figure 72 below shows the % TSR results from laboratory testing of the specimens. Results are shown for surface, intermediate and base each for the HMA and PG88-22M.

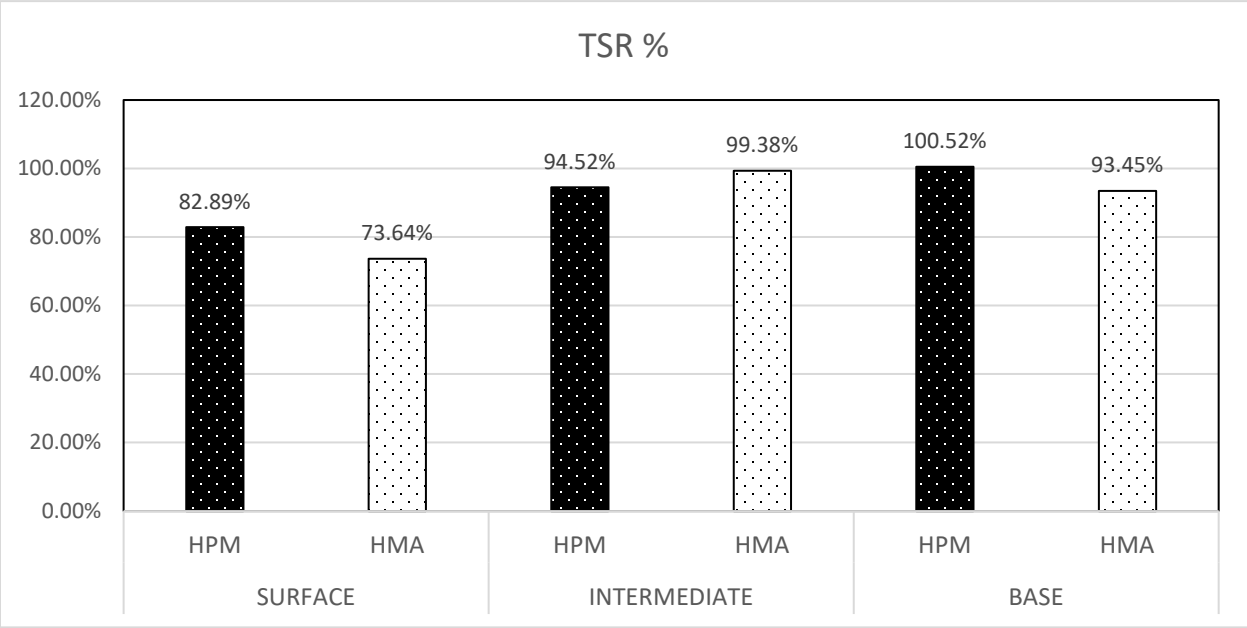


**Figure 72 Lab results of %TSR for each of the mixes tested.**

### *Hamburg Wheel Tracking Test (HWTT)*

Testing was performed in accordance with AASHTO T 324. For each mix, four specimens were compacted from plant mix to an air void content of 7 ± 0.5 percent in a gyratory compactor in accordance with AASHTO T 312. Samples were trimmed and two of the specimens placed cut end to cut end in a mold to form two samples for testing. Figure 73 shows the four specimens in the two molds mounted in the HWTT with the load wheels positioned above the samples. The HWTT is then filled with water heated to 50°C to a level approximately 1 inch (25 mm) above the top of the samples. The samples are allowed to condition in the heated water for 45 minutes before a load is applied through the wheel and the wheels cycle forward and backwards across the samples. The cyclic loading continues for 20000 cycles or until the rut depth exceeds 12.5 mm (1/2 inch). Figures 74 and 75 are typical plots of rutting versus cycles for the HPM and HMA surface mixtures, respectively. Figures 76 and 77 are charts showing the rut depth at 5000, 10000, 15000, and 20000 cycles for the intermediate and surface mixtures, respectively.

**Figure 73 Hamburg testing for WAY 83 samples**

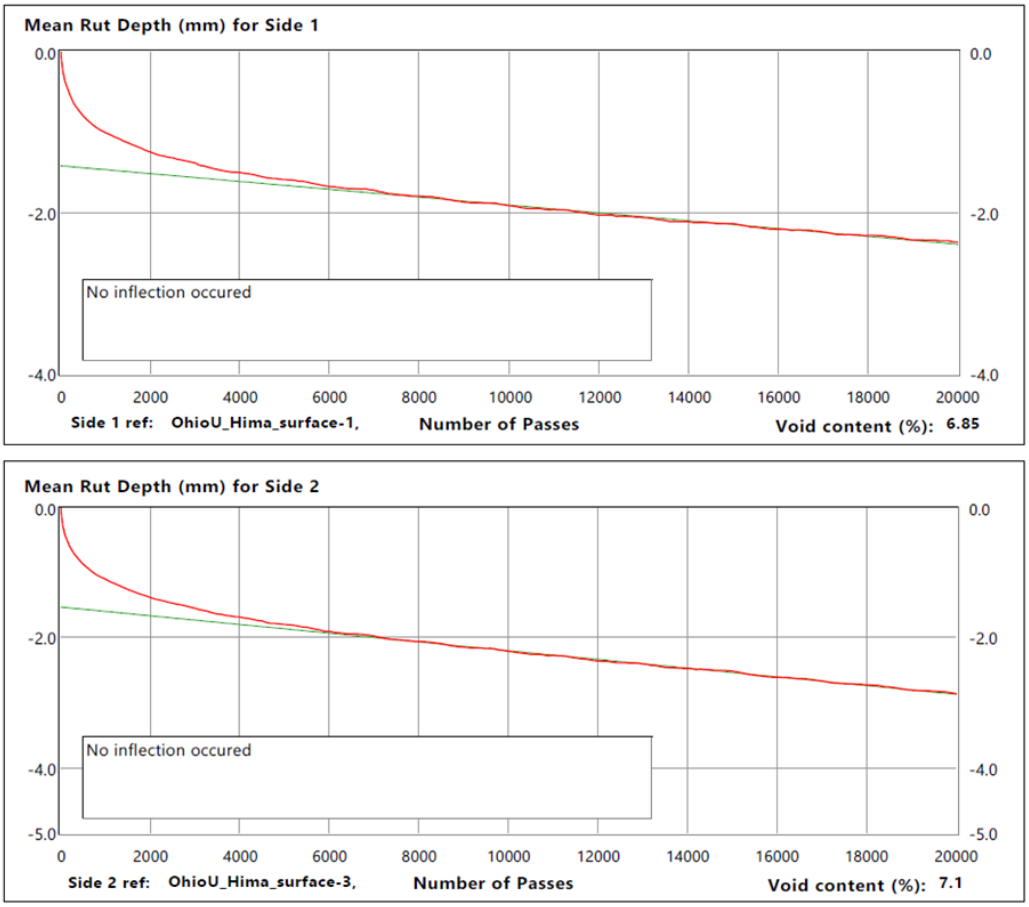


**Figure 74 Typical HWTT results for HPM (PG88-22M) surface mix**

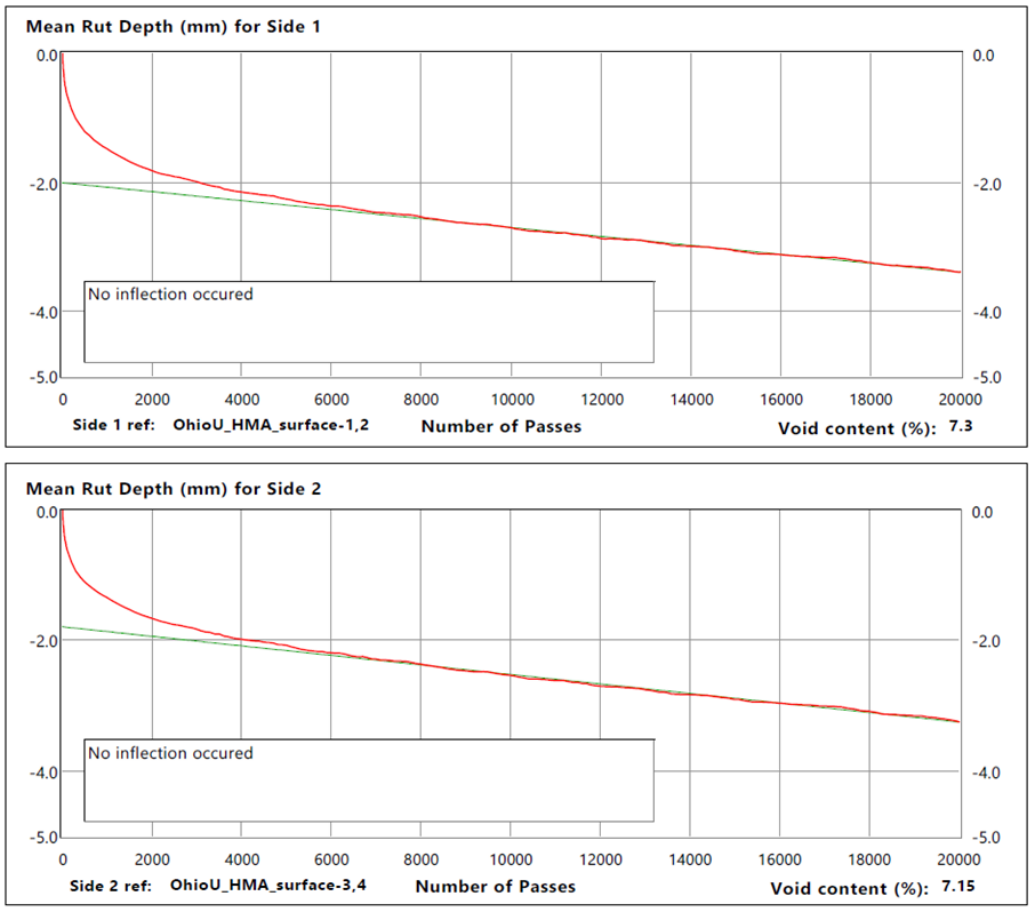


**Figure 75 Typical HWTT results for HMA surface mix**

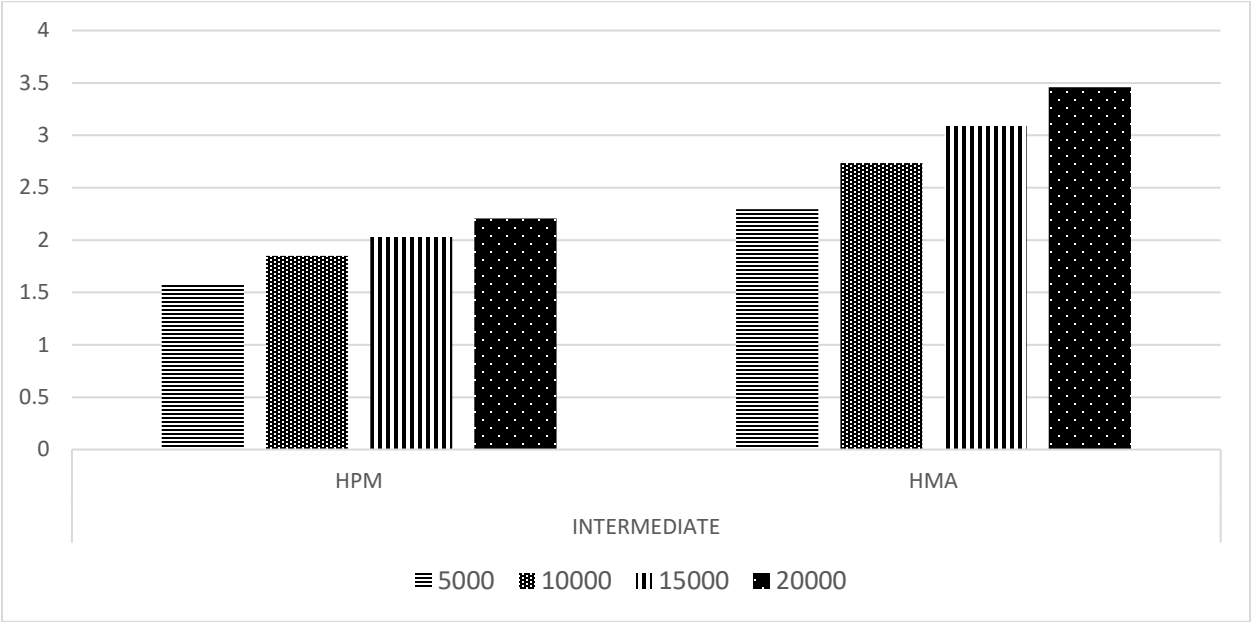


**Figure 76 HWTT results for intermediate layer**

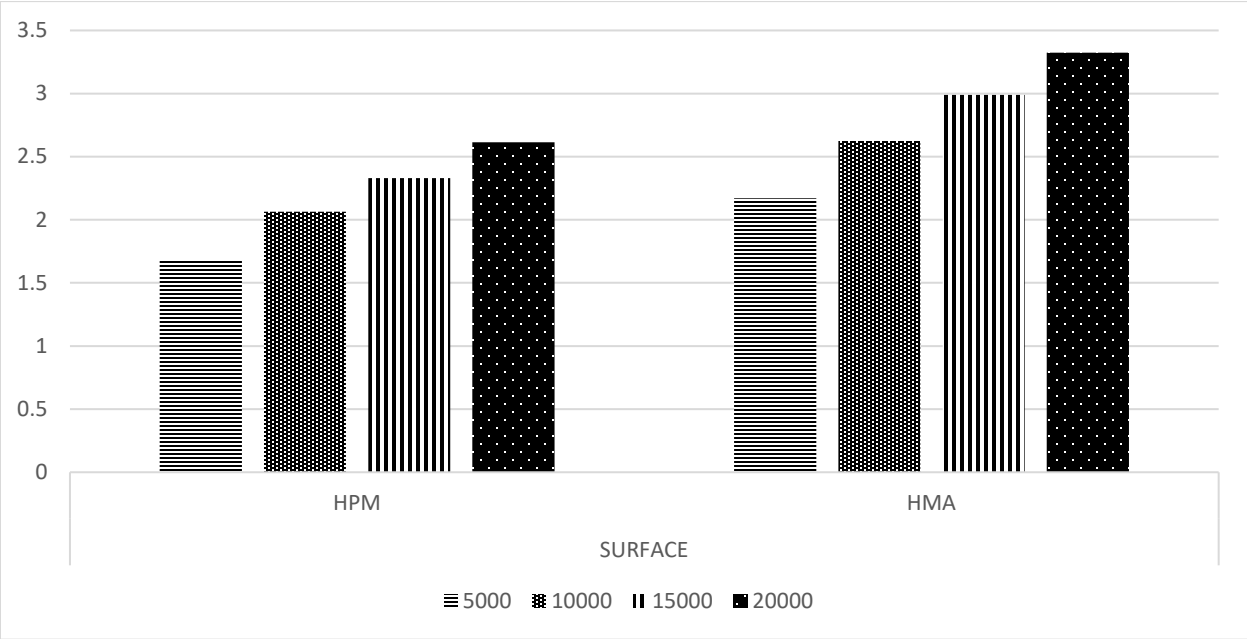


**Figure 77 HWTT results for surface layer**

### *IDEAL-CT*

Testing was performed in accordance with ASTM D8225 and ODOT Supplement 1033. Six specimens were compacted from plant mix to an air void content of 7 ± 0.5 percent in a gyratory compactor in accordance with AASHTO T 312. Figure 79 shows a picture of the cores used in this test. The samples were conditioned in an environmental chamber at 25°C for 2 hours ± 10 minutes. The specimen was then loaded at a rate of 50 mm/minute until the load drops below 100 N. The $CT_{index}$ is calculated from the post peak slope of the load deflections curve as shown in Figure 78 using equations 9 and 10. As specified in ODOT Supplement 1033, the results were checked for outliers as per ASTM E178. Non outlier values were averaged to determine the final $CT_{index}$.

$$[\![CT]\!]\_index = t/62 \times G\_f/|m\_75| \times l\_75/D \quad \textbf{(9)}$$

Where,
t = specimen thickness (mm)
D= sample diameter (mm)

$$m\_75 = (P\_85 - P\_65)/(l\_85 - l\_65) \quad \textbf{(10)}$$

Where,
$P_{85}$ = 85 percent of the peak load in the post-peak stage (kN)
$P_{65}$ = 65 percent of the peak load in the post-peak stage (kN)
$L_{85}$ = displacement corresponding to 85 percent of the peak load in the post-peak stage (mm)
$L_{65}$ = displacement corresponding to 65 percent of the peak load in the post-peak stage (mm)

Figure 78 shows an illustration of the calculations discussed above.

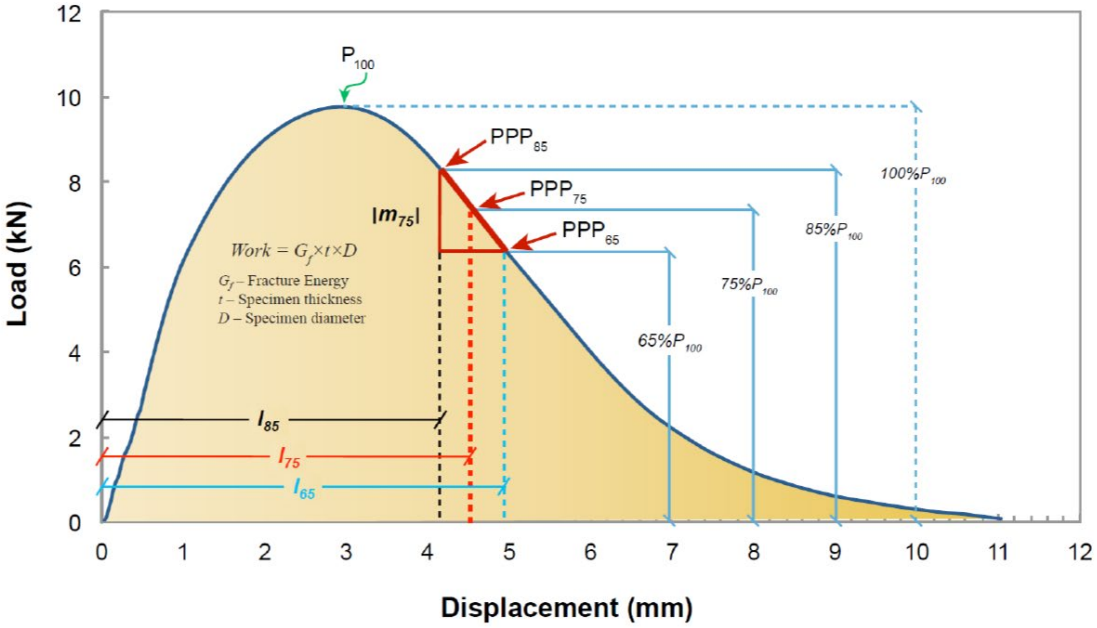


**Figure 78 Ideal CT calculation example. (Zhou 2019)**

The equations above can be combined to provide Equation 11 below.

$$CT_{index} = \frac{Thickness\ (t)}{62} * \frac{Deformation\ Tolerance\ (I75)}{Specimen\ Duameter(D)} * \frac{Fracture\ Energy\ (Gf)}{Post\ Peak\ Slope\ (m75)} \qquad (11)$$

The IDEAL CT test determines the cracking potential of asphalt mixtures with a fracture mechanics-based parameter: Cracking Tolerance Index, which is calculate by Equation 11. A larger CT Index value indicates better cracking resistance. Figure 80,Figure 81,and Figure 82 show the raw data from the Ideal CT test. The graphs were used to calculate the CT index. Figure 83 and Figure 84 show the CT index for both the HPM and HMA material for the WAY-83 project. The figures clearly show that the high polymer material has a significantly better cracking resistance than the control mixes.

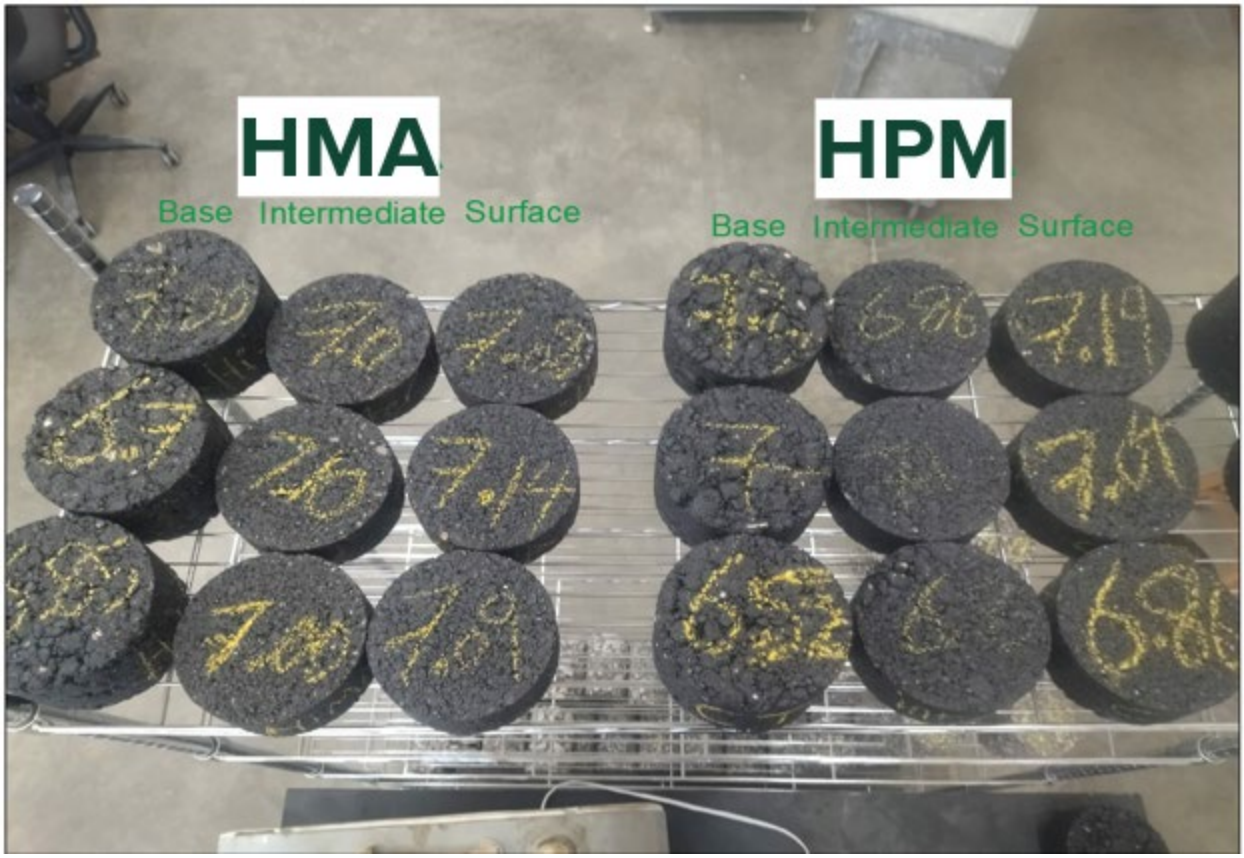


**Figure 79 Pictures of the cores used for the Ideal CT test**

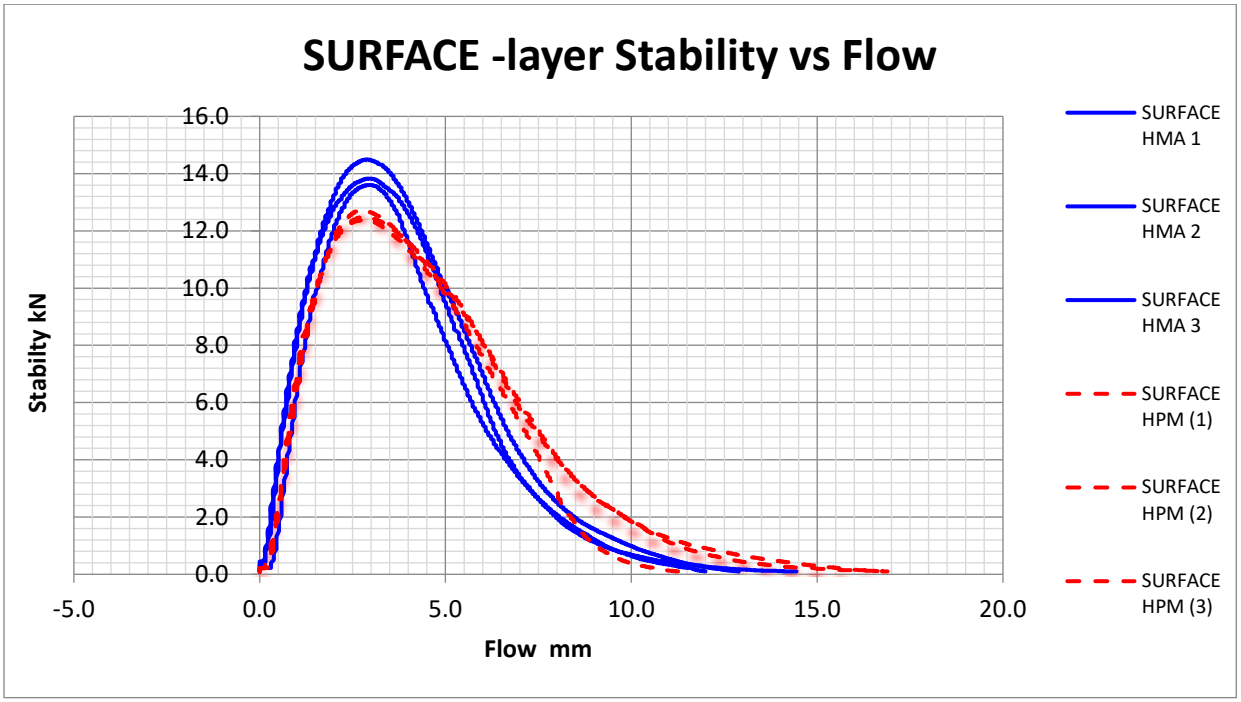


**Figure 80 Stability vs Flow for Surface layer, Ideal CT Results**

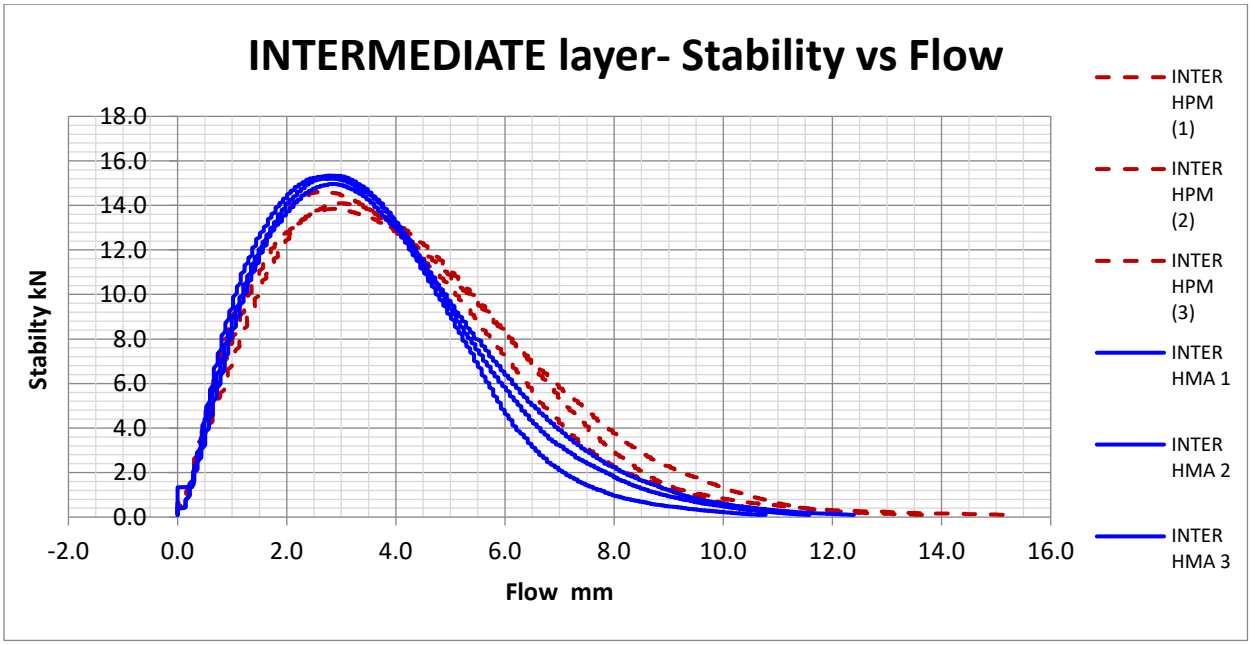


**Figure 81 Stability vs Flow for Intermediate layer, Ideal CT Results**

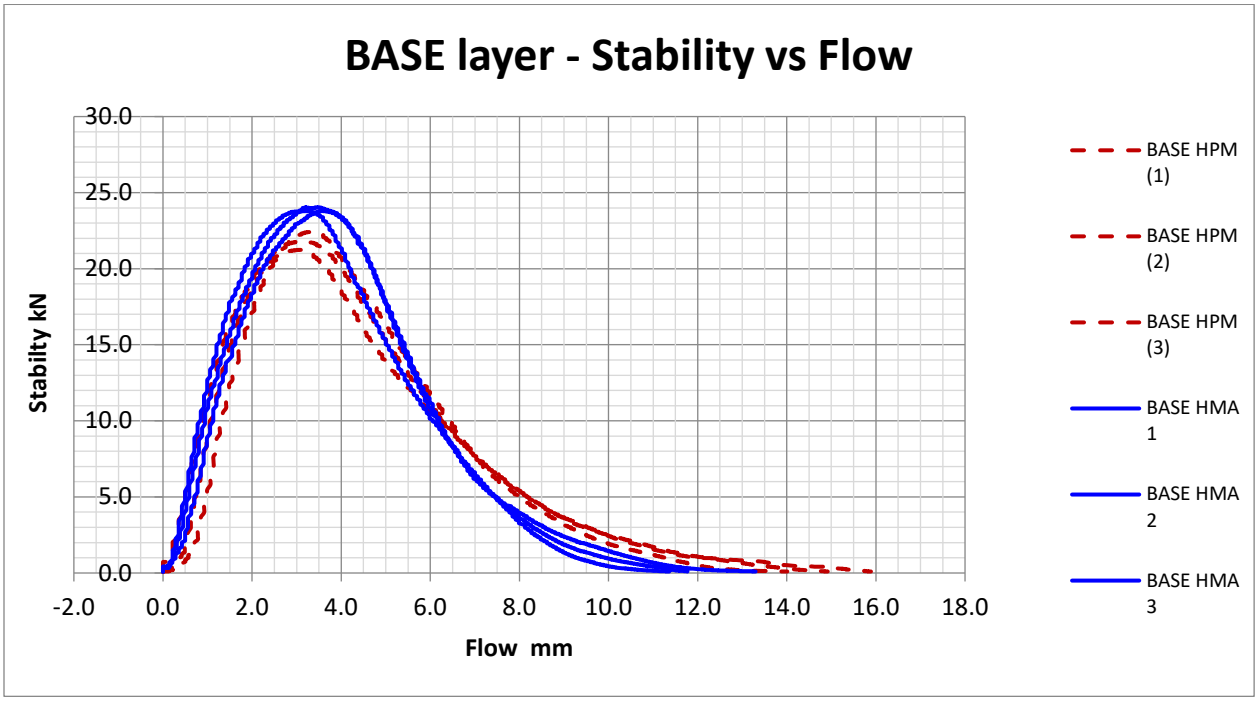


**Figure 82 Stability vs Flow for Base layer, Ideal CT Results**

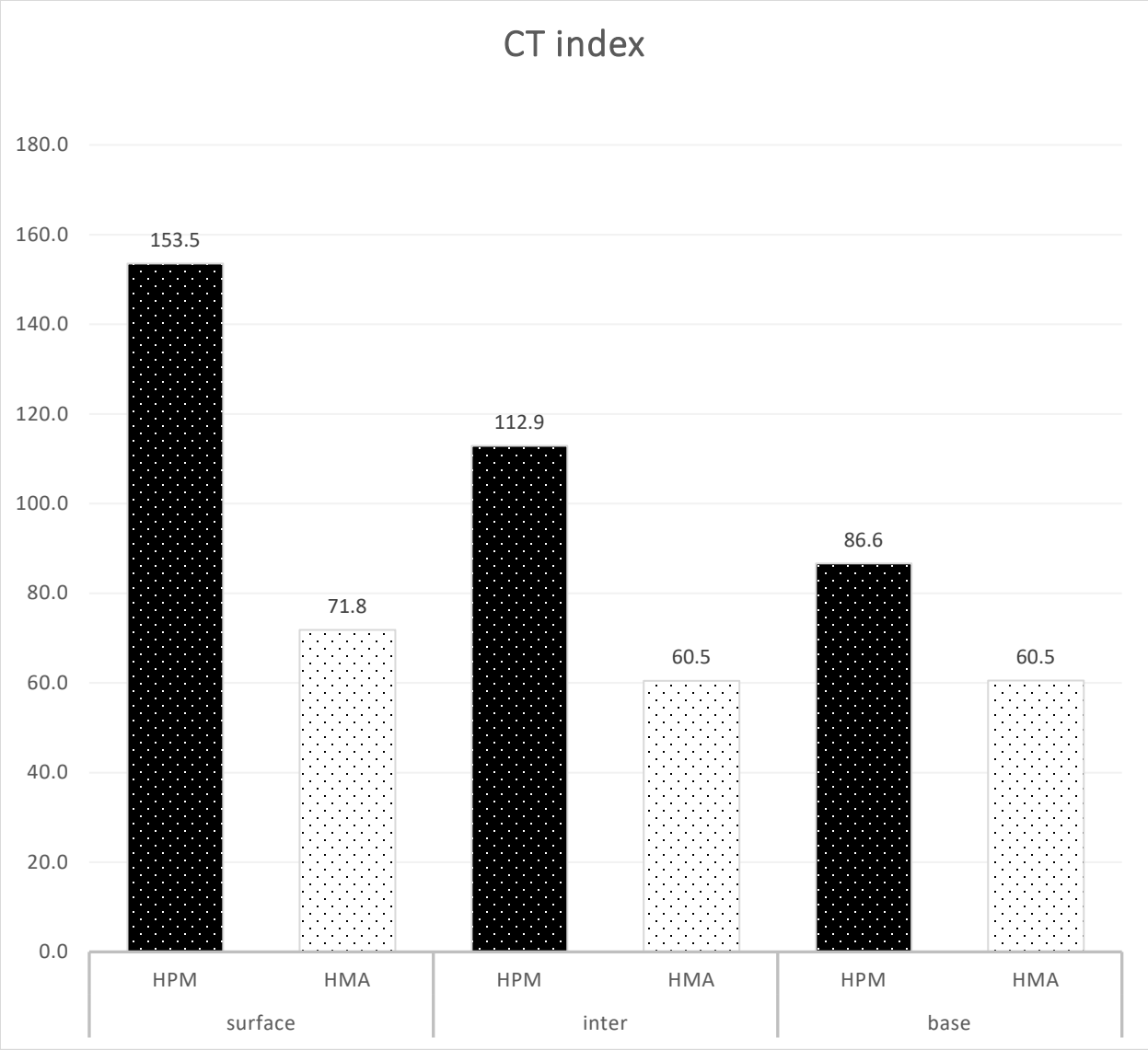


**Figure 83 CT Index results**

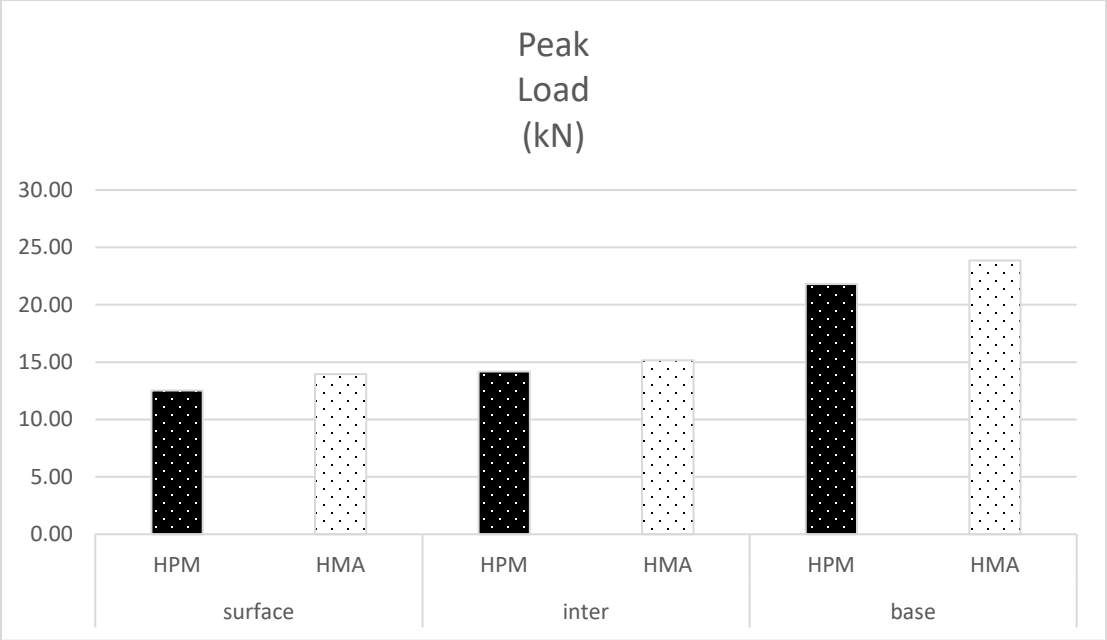


**Figure 84 Peak Load calculated from Ideal CT testing**

### *Cantabro Mass Loss (AASHTO TP 108-14 2020)*

The Cantabro test is a mixture toughness test that uses a Los Angeles Abrasion machine to estimate a mixture's durability. Figure 85 shows pictures of the cores used to run the Cantabro test. Table 37 shows the percent mass loss after 300 revolutions in the drum. Figure 86 shows a graphic representation of the results. The high polymer mixes (PG 88-22M) have significant less mass loss than control HMA mixes.

Overall, the laboratory test results confirm with previous research that HPM mixes have higher resistance to rutting and cracking than control mixes. The modulus and tensile strength of HPM mixes are lower than that of control AC mixes. This indicates that HPM mixes are not stiffer, but tougher than control mixes. The higher toughness of HPM enables it to withstand higher strain without fracturing compared with control AC.

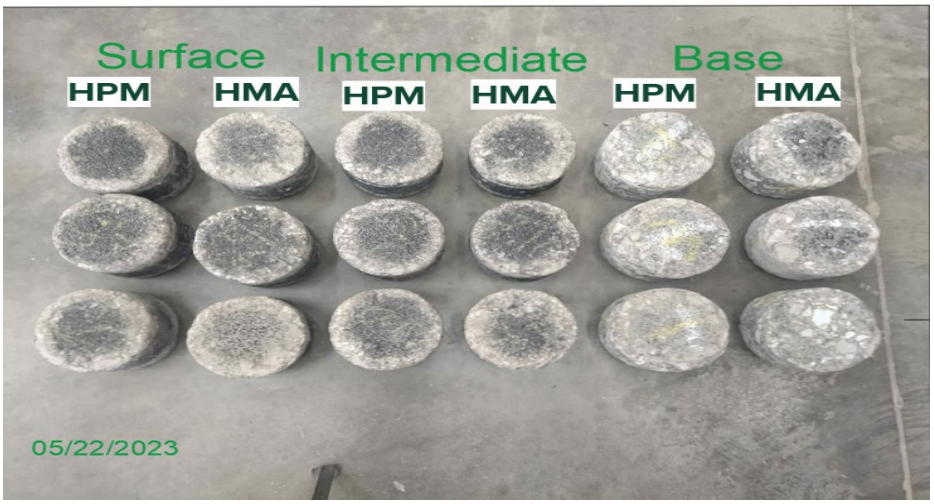


**Figure 85 Picture of cores used to conduct the Cantabro test**

**Table 37 Cantabro Test Results**

| Sample Number | Type | W1(g) | W2(g) | MASS LOSS % | AVG % |
|---|---|---|---|---|---|
| 1 | PG 88-22 M surface | 4475.0 | 4352.6 | 2.7% | 2.0% |
| 2 | | 4453.8 | 4383.1 | 1.6% | |
| 3 | | 4454.0 | 4379.9 | 1.7% | |
| 4 | HMA surface | 4489.0 | 4325.6 | 3.6% | 3.7% |
| 5 | | 4486.6 | 4350.6 | 3.0% | |
| 6 | | 4488.5 | 4294.4 | 4.3% | |
| 7 | PG 88-22M Inter. | 4550.4 | 4445.7 | 2.3% | 2.5% |
| 8 | | 4544.6 | 4432.7 | 2.5% | |
| 9 | | 4544.5 | 4422.0 | 2.7% | |
| 10 | HMA Inter. | 4564.0 | 4350.5 | 4.7% | 4.8% |
| 11 | | 4563.3 | 4365.5 | 4.3% | |
| 12 | | 4564.7 | 4315.7 | 5.5% | |
| 13 | PG 88-22 M base | 5268.6 | 4983.8 | 5.4% | 5.6% |
| 14 | | 5130.0 | 4797.9 | 6.5% | |
| 15 | | 5056.3 | 4800.4 | 5.1% | |
| 16 | HMA base | 5103.6 | 4828.9 | 5.4% | 7.0% |
| 17 | | 5122.7 | 4682.0 | 8.6% | |
| 18 | | 5179.3 | 4821.3 | 6.9% | |

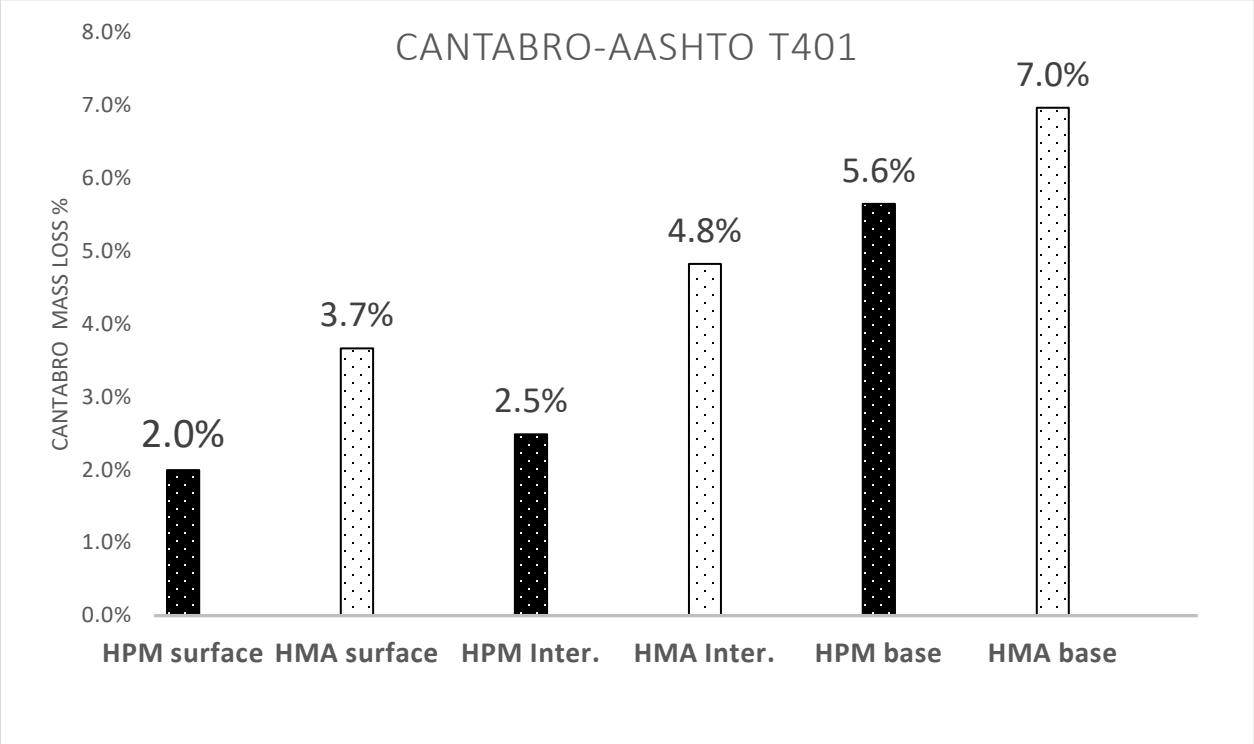


**Figure 86 Cantabro Test Results and % mass loss**

## Development of HPM(PG88-22M) Layer Structural Coefficient

HPM—high polymer asphalt concrete mixes (ODOT specification PG 88-22M) contain ~7.5% of styrene butadiene styrene (SBS) modifier. It is also referred to as highly modified asphalt or HiMA (Kraton™ D0243). HPM mixes have been shown to have increased binder softening point and reduced temperature susceptibility that led to improved rutting resistance and fatigue cracking resistance. Thus, pavements built with HPM are expected to have improved durability and longer service life.

HPM mix has been used in Ohio, mostly for pavements at high-stress locations subject to high traffic volumes, heavy loads, and/or high tire-pressure. Given its durability and potential to prolong pavement life, HPM could be used for most other highway pavements.

The objective of this task is to estimate the structural coefficient of HPM layers for ODOT's Office of Pavement Engineering to incorporate HPM in future pavement design. Table 38 shows that ODOT currently uses a layer structural coefficient of 0.43 for all asphalt surface and intermediate courses and 0.36 for asphalt bases.

**Table 38 Structural Coefficients Used by ODOT**

| Flexible Pavement Structural Coefficients | 401-1<br>January 2020<br>Reference Section<br>401 |
|---|---|

| ASPHALT CONCRETE STRUCTURAL COEFFICIENTS | | |
|---|---|---|
| **Material** | **English Coefficient** | **Metric Coefficient** |
| Items 424, 441, 442, 443, 823, 826, 859 AC Surface Courses | 0.43 | 0.0169 |
| Items 441, 442, 823, 826 AC Intermediate Courses | 0.43 | 0.0169 |
| Item 880 Warranty Asphalt - top 3" (75 mm) | 0.43 | 0.0169 |
| Items 301, 302 Asphalt Concrete Base Courses | 0.36 | 0.0142 |
| Item 880 Warranty Asphalt - below top 3" (75 mm) | 0.36 | 0.0142 |
| Item 321 Cracked & Seated Plain Concrete | 0.27 | 0.0106 |
| Existing Asphalt Concrete - old, oxidized, & weathered | 0.23 | 0.0092 |
| Item 304 Aggregate Base* | 0.14 | 0.0055 |
| Item 320 Rubblized Concrete | 0.14 | 0.0055 |
| Items 421 Microsurfacing | 0.0 | 0.0 |
| Item 803 Rubberized Open Graded Asphalt Friction Course | 0.0 | 0.0 |
| Items 822 Hot In Place Recycling | 0.0 | 0.0 |

* When the entire subgrade is chemically stabilized (global chemical stabilization), the coefficient for Item 304 Aggregate Base is increased to 0.17 (0.0067).

The structural coefficients used directly affects a pavement's thickness, since a pavement's Structural Number (SN) is a summed product of the layer structural coefficients and thicknesses:

$$SN = a_1D_1 + a_2D_2 + a_3D_3 \qquad (12)$$

SN represents the pavement's overall structural capacity necessary to withstand the design traffic loading (number of equivalent 18-kip axle load, $W_{18}$), for a given subgrade support ($M_R$). A higher layer structural coefficient ($a_i$) means a thinner layer thickness ($D_i$) would be required and vice versa.

Habbouche, et al (2019, 2020) found that HiMA and non-HiMA mixes have similar laboratory-measured dynamic modulus, but HiMA has significantly better rutting and cracking performance both in the laboratory and in the field. The researchers determined the structural coefficient for HP AC mixes based on the fatigue performance life of flexible pavements, by determining an equivalent HP AC layer thickness which resulted in similar fatigue life of a PMA pavement under static and dynamic loading. They indicated that multiple factors including applied traffic level, pavement structure, layers properties, and performance characteristics of the evaluated PMA and HP AC mixes resulted in different structural coefficients for HP AC mixes. From 72 different combinations of parameters, the reported fatigue-based structural coefficients ranged from 0.33 to 1.32. Through statistical analyses, they recommend a structural coefficient of 0.54 for HP AC mixes.

Timm, et al (2014) recommend $a_1$ = 0.54 for all AC in Alabama, while unpublished NCAT result suggested a structural coefficient ($a_1$) of 0.77 could be used for HiMA.

This task employed five approaches to estimate the structural coefficient of HPM: (1) Section 2.3.5 of the AASHTO Guide for Design of Pavement Structures, (2) Section 5.4.5 The AASHTO Guide, (3) laboratory testing, (4) field testing, and (5) in-service pavement performance.

***Approach 1: AASHTO 2.3.5 Method***

The first approach is to use the elastic modulus back calculated from the FWD deflections measured at the WAY US-30 test pavement sections or the dynamic modulus (E*) of HPM mixes compacted and measured in the laboratory to estimate the layer structural coefficient based on the method in Section 2.3.5 of the AASHTO Guide for the Design of Pavement Structures.

This method determines *a*1 from EAC through a correlation curve. The following formula was developed by fitting the curve to represent the same relationship and can be used to calculate the AC layer structural coefficient from its modulus, EAC.

$$a_1 = 0.404 \times \log_{10}(E_{AC}) - 1.8447 \qquad (13)$$

where $E_{AC}$ is the elastic (resilient) modulus (in psi) of the AC surface course (including the intermediate course) at 68 °F (20 °C).

The AASHTO Guide states that "*caution is recommended for modulus values above 450,000 psi (3.1 GPa). Although higher modulus asphalt concretes are stiffer and more resistant to bending, they are also more susceptible to thermal and fatigue cracking*". When $E_{AC}$ = 450,000 psi (3.1 GPa), Equation (13) produces $a_1$ = 0.44.

Improved mix design and compaction among many other improvements over the past six decades since the original AASHO Road Test in 1958-60 has enabled asphalt concrete mixes to routinely achieve $E_{AC}$ greater than 450,000 psi (3.1 GPa) at 68°F (20 °C). The modulus values back calculated from FWD deflections for this study, and the dynamic modulus measured in the lab show that both HPM and control mixes can be much greater than 450,000 psi (3.1 GPa) at 68° F (20 °C). The modulus of HPM mixes is often less than the modulus of control mixes.

Figure 87 and Figure 88 show the back calculated modulus values for HPM surface/intermediate courses and base course based on FWD deflection tests on 11/10/2022. FWD deflections measured at later dates (5/8/23, 8/8/23, 11/8/23, and 5/11/24) are smaller, so the back calculated modulus values are higher than shown in these figures.

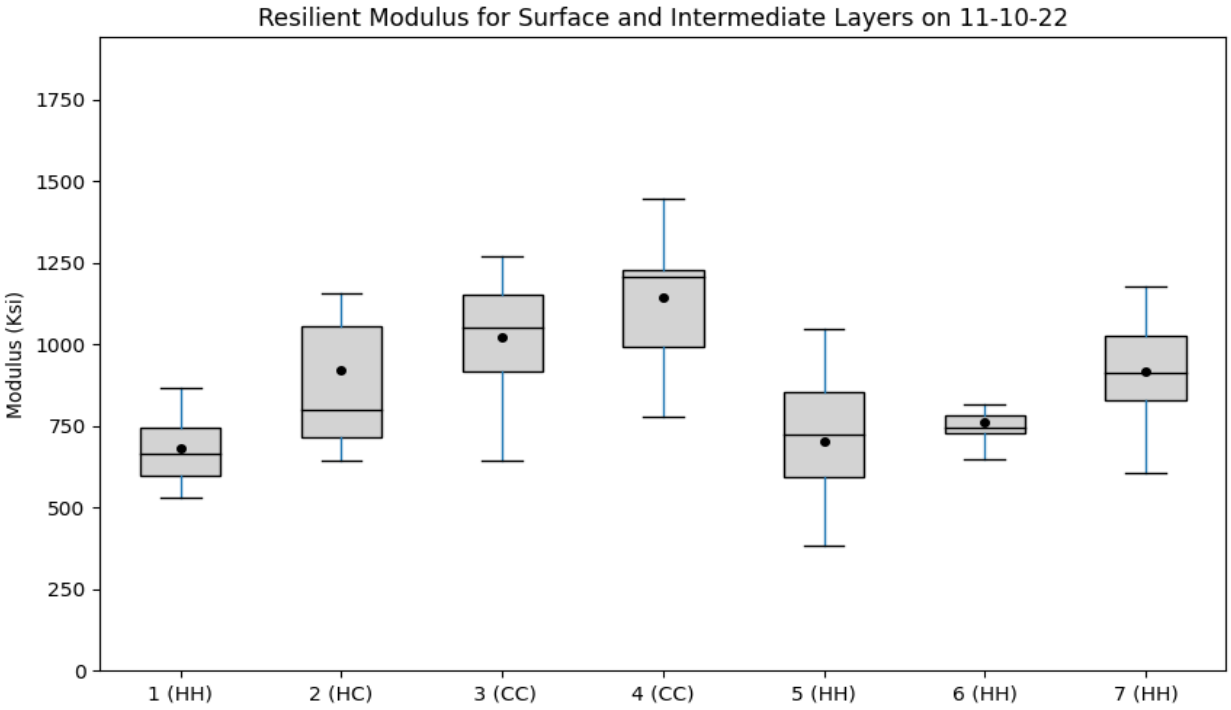


**Figure 87 Back Calculated Surface Layer Modulus from FWD Deflections**

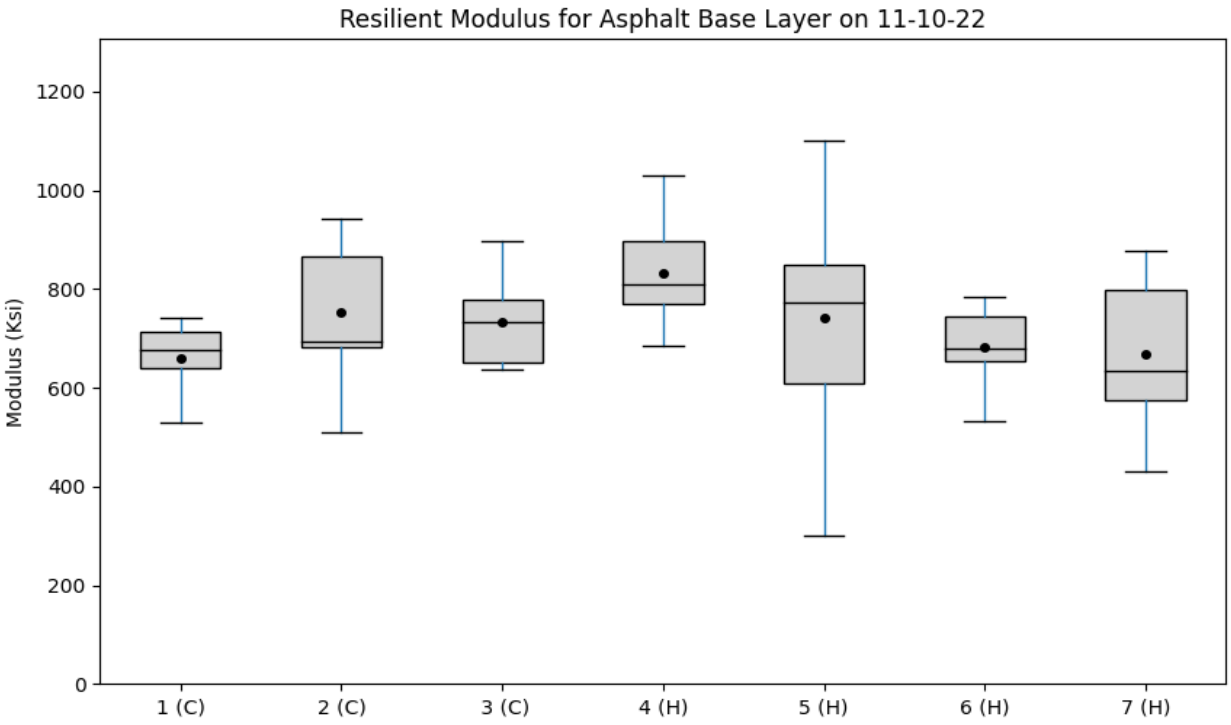


**Figure 88 Back Calculated Base Layer Modulus from FWD Deflections**

Table 39 shows that laboratory measured dynamic modulus E* of HPM is generally lower than the control mixes. At 70° F (21°C) and 10 Hz loading frequency (corresponding to vehicle traveling speed of ~40 mph (64 km/h)), the dynamic moduli of both mixes exceed 450,000 psi (3.1 GPa) by a wide margin.

**Table 39 Laboratory Measured Dynamic Modulus at 21°C**

| Frequency (Hz) | Surface PG88-22M | Surface Control | Inter. PG88-22M | Inter. Control | Base PG88-22M | Base Control |
|---|---|---|---|---|---|---|
| 25 | 938 | 1741 | 1368 | 1745 | 2318 | 2236 |
| **10** | **668** | **1380** | **1090** | **1362** | **1813** | **1692** |
| 5 | 559 | 1193 | 901 | 1149 | 1455 | 1512 |
| 1 | 395 | 864 | 665 | 751 | 1051 | 1018 |
| 0.5 | 345 | 727 | 569 | 626 | 928 | 959 |
| 0.1 | 244 | 461 | 393 | 392 | 708 | 659 |

Table 40 shows the impact of increasing E value on the structural coefficient and corresponding layer thickness. The last column shows potential thickness (i.e., cost) reduction.

**Table 40 Impact of Increased $E_{AC}$ and $a_1$ on Thickness $D_1$**

| $E_{AC}$ (psi) | $a_1$ | $D_1$ (in.) | $a_1 D_1$ | D1/3.25 |
|---|---|---|---|---|
| 425,000 | 0.43 | 3.25 | 1.40 | 1 |
| 450,000 | 0.44 | 3.18 | 1.40 | 0.98 |
| 500,000 | 0.46 | 3.04 | 1.40 | 0.94 |
| 550,000 | 0.47 | 3.00 | 1.40 | 0.92 |
| 600,000 | 0.49 | 2.86 | 1.40 | 0.88 |
| 650,000 | 0.50 | 2.80 | 1.40 | 0.86 |
| 700,000 | 0.52 | 2.69 | 1.40 | 0.83 |
| 750,000 | 0.53 | 2.64 | 1.40 | 0.81 |
| 800,000 | 0.54 | 2.59 | 1.40 | 0.80 |

The modulus values either back calculated from FWD deflection or measured in the laboratory show that the modulus HPM mixes are similar or smaller than control/conventional mixes. Therefore, based on this approach, it is not justified to increase the structure coefficient of HPM to be higher than that of control/regular AC.

### *Approach 2: AASHTO 5.4.5 Method*

The second approach uses the procedure in Section 5.4.5 of the AASHTO Guide for the Design of Pavement Structures to determine an effective layer coefficient. This procedure estimates the total Structural Number (SN) of the pavement structure layers from the FWD deflections. FWD measurements were taken on the surface of the stabilized subgrade, aggregate base, asphalt base, and asphalt surface when each layer was placed.

Using the FWD deflections on the surface of the stabilized subgrade and assuming a 2-layer system with the stabilized layer as the surface layer, the modulus of the un-stabilized subgrade was estimated from the deflection $d_{60}$. The $SN_{eff}$ contribution by the stabilized subgrade was determined. The contribution of each layer above the stabilized subgrade to the Structural Number was determined in the same way.

The steps are:

1. Estimate subgrade modulus from surface deflection: $M_R = \frac{0.33(0.24*P)}{d_r * r}$

2. Solve for effective modulus of all pavement layers, *Ep*, from the following equation:

$$d_0 = 1.5\,Pa\left\{\frac{1}{M_R\sqrt{1+\left(\frac{D}{a}*\sqrt[3]{\frac{E_p}{M_R}}\right)^2}}+\frac{\left[1-\frac{1}{\sqrt{1+\left(\frac{D}{a}\right)^2}}\right]}{E_p}\right\}$$

3. Determine effective Structural Number: $SN_{eff} = 0.0045 * D * \sqrt[3]{E_p}$

4. Determine Structural Coefficients from SN: $a_1$, $a_2$, $a_3$

$SN_1 = a_1D_1 + a_2D_2 + a_3D_3$
$SN_2 = a_1D_1 + a_2D_2 + a_3D_3$
$SN_3 = a_1D_1 + a_2D_2 + a_3D_3$

Figure 89 shows the structural coefficients determined using this approach. The surface and intermediate courses are combined as a single layer. In the figure, H represents HPM, and C represents control/regular AC. For surface layer, the average structural coefficient of HPM is 0.7, which is smaller than the 1.11 for control/regular AC. For base layer, it's 0.57 for HPM and 0.63 for control AC. These values are unrealistically high. This approach does not produce useful results, since it is based on pavement deflections, which are mainly a function of a pavement's overall structural thickness.

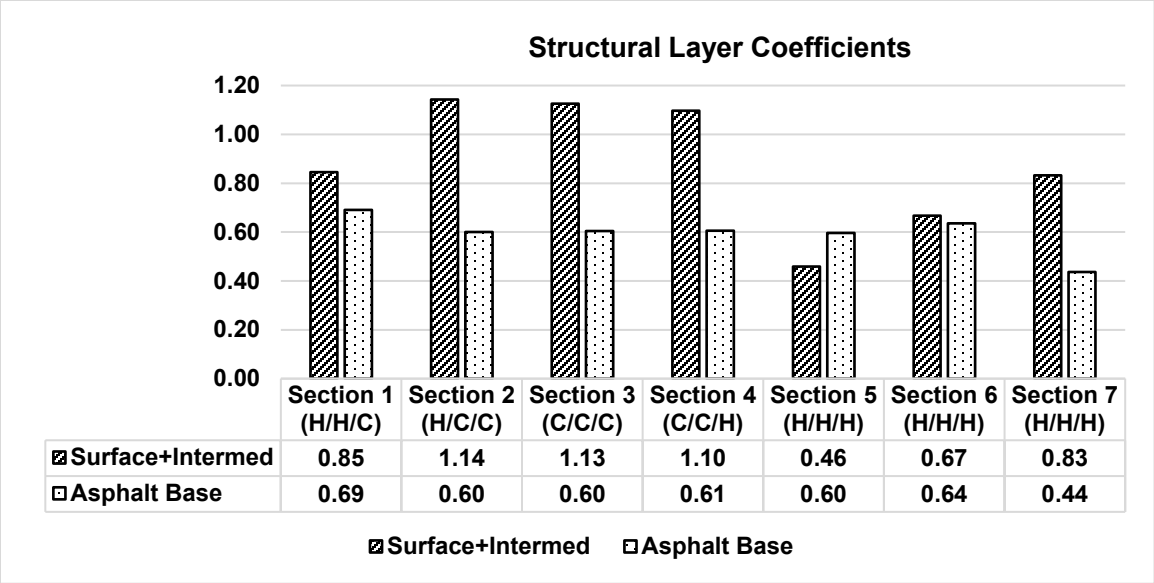


| | Section 1 (H/H/C) | Section 2 (H/C/C) | Section 3 (C/C/C) | Section 4 (C/C/H) | Section 5 (H/H/H) | Section 6 (H/H/H) | Section 7 (H/H/H) |
|---|---|---|---|---|---|---|---|
| Surface+Intermed | 0.85 | 1.14 | 1.13 | 1.10 | 0.46 | 0.67 | 0.83 |
| Asphalt Base | 0.69 | 0.60 | 0.60 | 0.61 | 0.60 | 0.64 | 0.44 |

**Figure 89 Average Structure Coefficients Determined by AASHTO 5.4.5 Approach**

### *Approach 3: Compare Laboratory Testing Results*

The third approach uses laboratory testing results to compare HPM versus regular HMA. As previously described above several lab tests were performed, the tests include:

(1) Hamburg Wheel Track test (for rutting performance)

Figure 90 shows the rut depths developed after 5,000, 10,000, 15,000, and 20,000 load repetitions by HPM and control AC specimens. HPM specimens show significant less rutting than control AC specimens at the same number of load repetition.

Figure 91 shows that the rut depth developed on HPM mix after 20,000 load repetitions is equivalent to the rut depth developed on control AC mix after about 6,700 load repetitions, indicating potentially a three-fold increase in rutting resistance.

Table 41 shows a summary of in-service HPM pavement sections in Ohio, including location, thickness of HPM, age and PCR data collected for this project. HPM pavements show minimum rutting distress in nearly all cases.

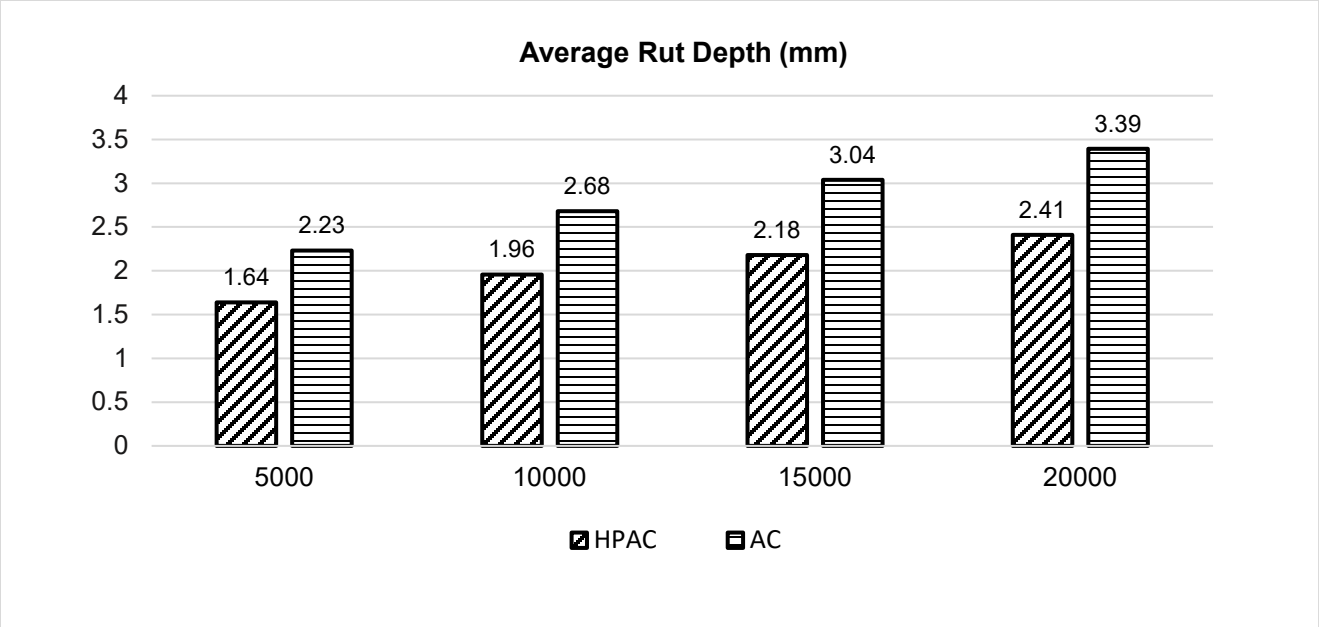


**Figure 90 Hamburg Wheel Track Test Results**

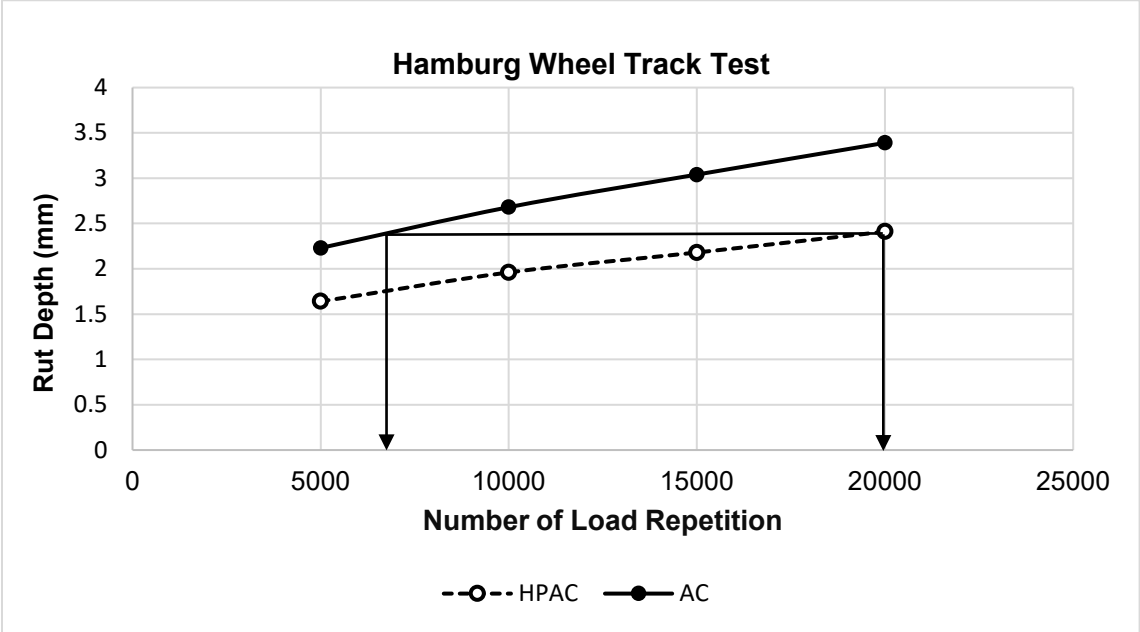


**Figure 91 Comparison of Rutting Resistance in Laboratory Testing**

**Table 41 ODOT In-Service HPM (PG88-22M) Pavements**

| Section | Project Number | HPM Thickness | Open to Traffic | Age @ 3/23 | PCR @ 3/23 | Rutting Deduct | Total Cracking Deduct | Age @ 2/24 | PCR @ 2/24 | Rutting Deduct (max=10) | Total Cracking Deduct (max=50) |
|---|---|---|---|---|---|---|---|---|---|---|---|
| WOO US23 12.00-12.09 | 13-0598 | 1.5+2.5 | 8/2014 | 8.6 | 86.9 | 0 | 7.6 | 9.52 | 82.55 | 1.8 | 10.15 |
| ASD US42 7.64-8.15* | 15-8008 | 1.5 | 12/2015 | 7.25 | 75.85 | 2.4 | 15.15 | 8.17 | 70.75 | 0 | 19.35 |
| ASD US250 16.09-16.64* | 15-8008 | 1.5 | 12/2015 | 7.25 | 78.76 | 2.4 | 10.84 | 8.17 | 73.68 | 2.4 | 12.12 |
| LUC US20 7.17-7.30 | 16-0366 | 1.5+1.75 | 11/2016 | 6.33 | 96 | 0 | 0 | 7.25 | 91.54 | 1.8 | 1.76 |
| LUC US20 7.50-8.166 | 16-0366 | 1.5+1.75 | 11/2016 | 6.33 | 94.2 | 1.8 | 0 | 7.25 | 91.54 | 1.8 | 1.76 |
| *FAI US 33 8.08-17.44* | *17-0206 PID 93009* | *1.5+1.75* | *11/2017* | *5.33* | *91-97**** | -- | -- | *6.25* | *85-97**** | --- | --- |
| FAI US 33 17.44-24.86 | PID 90315 | 1.5 | 11/2017 | 5.33 | 83-95*** | -- | -- | 6.25 | 75-90*** | --- | --- |
| ROS Ramp A/B 0.00-0.06** | 19-0168 | 1.5 or 1.5+1.5 | 6/2019 | 3.75 | 90.4 | 1.8 | 2 | 4.67 | 85.15 | 1.8 | 7.25 |
| ROS Ramp C/D 0.00-0.06** | 19-0168 | 1.5 or 1.5+1.5 | 6/2019 | 3.75 | 90.4 | 1.8 | 2 | 4.67 | 90.5 | 4.2 | 2 |
| ROS CR238 1.24-1.42** | 19-0168 | 1.5 or 1.5+1.5 | 6/2019 | 3.75 | 93.7 | 0 | 3.5 | 4.67 | 90.5 | 1.8 | 3.5 |
| FRA I-70 ramp to Wilson Rd. | 18-0597 | 1.5+1.75+ 11.75 | 6/2020 | 2.75 | 94.7 | 1.8 | 2 | 3.67 | 94.7 | 1.8 | 2 |
| HEN MR602 0.00-0.42 | 19-0629 | 1.25+1.75 | 6/2022 | 0.75 | 98.5 | 0 | 0 | 1.67 | 97.6 | 0 | 0 |
| HEN SR110 1.79-2.06 | 19-0629 | 1.25+1.75 | 6/2022 | 0.75 | 96.7 | 1.8 | 0 | 1.67 | 93.8 | 1.8 | 2 |
| HEN CR424 11.35-11.72 | 19-0629 | 1.25+1.75 | 6/2022 | 0.75 | 98.5 | 0 | 0 | 1.67 | 97.6 | 0 | 0 |

*Only 1.5” (38 mm) of HPM in surface course
**Part of the project has 3” (76 mm) of HPM in both surface and intermediate courses. The rest of the project has only 1.5” (38 mm) of HPM in surface course.
*** Multiple PCR sections within this project.

(2) Indirect Tensile Asphalt Cracking Test (IDEAL CT) Test

The IDEAL CT test determines the cracking potential of asphalt mixtures with a fracture mechanics-based parameter: Cracking Tolerance Index ($CT_{index}$). A larger CT Index value indicates better cracking resistance.
Figure 92 shows HPM mixes have significantly better cracking resistance than control mixes.

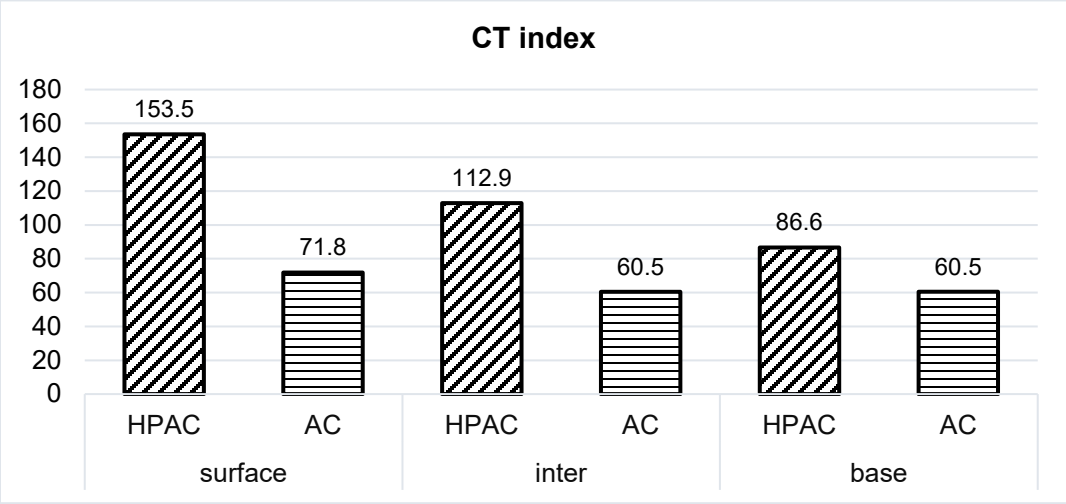


**Figure 92 IDEAL CT Test Results**

(3) Cold Temperature Tensile Strength

Figure 93 shows that the tensile strength of HPM mixes is higher than that of the control mixes at low temperature (-10°C or 14°F).

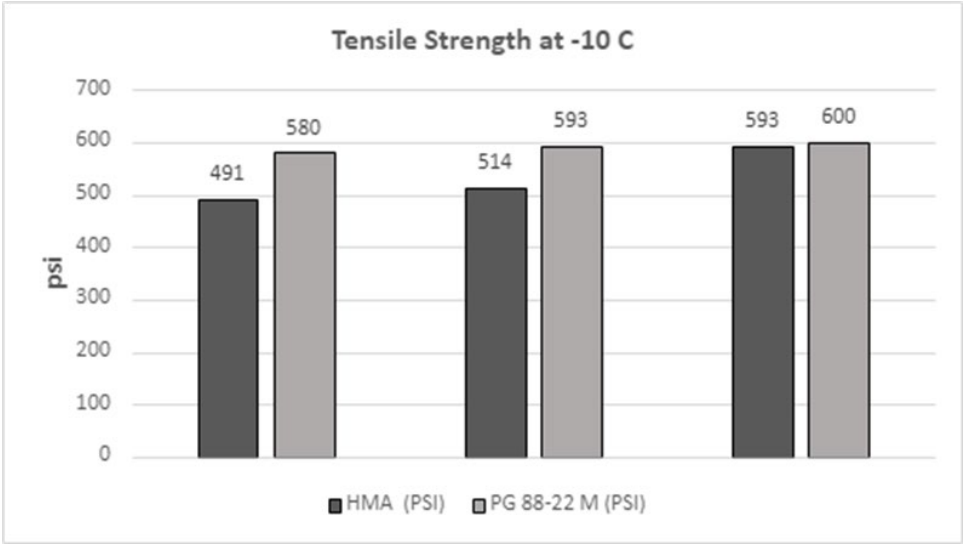


**Figure 93 Tensile Strength Measured at -10°C (14°F)**

(4) Tensile Strength Ratio (TSR)

Figure 94 shows the tensile strength of HPM mixes at room temperature are lower than the control AC mixes for the surface and intermediate courses, but slightly higher for the base course.

Tensile strength ratio measures an asphalt mix's resistance to moisture damage. It is the ratio of the tensile strength of conditioned specimen versus dry specimen. A specimen is conditioned by saturating it in water, then freeze it, and subsequently soak it in warm water. Figure 95 shows surface and base courses HPM have higher TSR% than control AC, whereas for the intermediate course, the HPM specimens has lower average TSR% than control AC.

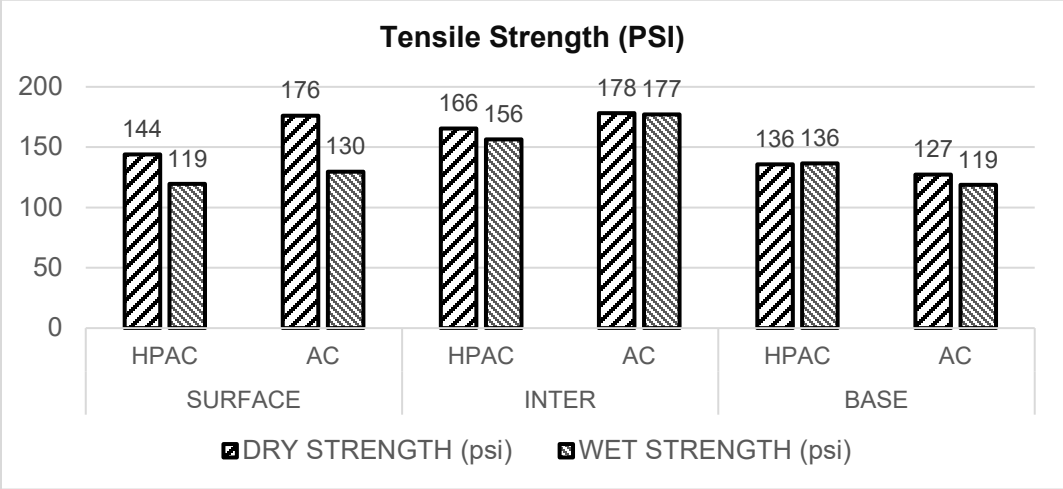


**Figure 94 Indirect Tensile Strength**

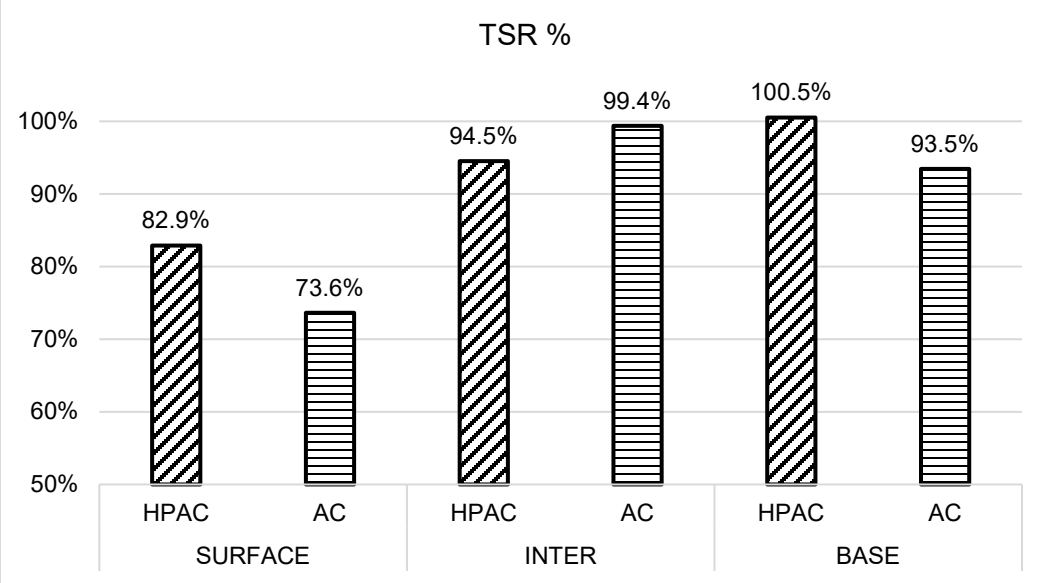


**Figure 95 Tensile Strength Ratio**

(5) Cantabro Test (AASHTO TP 108-14 (2020))

The Cantabro test is a mixture toughness test that uses a Los Angeles Abrasion machine to estimate a mixture's durability. Table 37 shows the percent mass loss after 300 revolutions in the drum. HPM (PG 88-22M) mixes have significant less mass loss than control HMA mixes.

Overall, the laboratory test results confirm with previous research that HPM mixes have higher resistance to rutting and cracking than control mixes. The modulus and tensile strength of HPM mixes are lower than that of control AC mixes. This indicates that HPM mixes are not stiffer, but tougher than control mixes. The higher toughness of HPM enables it to withstand higher strain without fracturing compared with control AC.

(6) Tensile Creep Compliance

Creep compliance, D(t), is the ratio of time-dependent strain, e(t), divided by a constant applied stress, s. Under a constant stress the creep compliance is the reciprocal of elastic modulus.

Higher creep compliance (lower E) is desirable at low temperatures to resist cracking, while lower creep compliance (higher E) is desirable at normal temperatures to resist rutting.

(7) Dynamic modulus (|E*|)

As shown previously in Table 39, the laboratory dynamic modulus test results show that dynamic modulus of HPM mixes are smaller than that of control mixes in almost all cases.

### *Approach 4: Compare Field Testing Results at WAY-83 Test Pavement*

The fourth approach compared the results of field testing, including the following tests:
(1) FWD deflections
(2) Strain measurements

Table 42 shows the as-built layer thicknesses of the seven test sections at the WAY-83 pavement project. The layer thickness is in inches. H means the layer is made of HPM and C means control AC. Figure 96 illustrates the seven pavement sections and their structure.

**Table 42 Pavement Layer Thicknesses at WAY-83 Test Sections**

| **Pavement Section** | **1** | **2** | **3** | **4** | **5** | **6** | **7** |
|---|---|---|---|---|---|---|---|
| **Surface course thickness (in.)** | 1.5 H | 1.4 H | 1.4 C | 1.5 C | 1.4 H | 1.5 H | 1.5 H |
| **Intermediate course** | 1.85 H | 1.75 C | 1.8 C | 1.83 C | 1.8 H | 1.96 H | 1.8 H |
| **Asphalt Base** | 9 C | 10.2 C | 9.4 C | 7.1 H | 7.2 H | 5.3 H | 5 H |
| **Aggregate Base** | 6 | 6 | 6 | 6 | 6 | 6 | 6 |
| **Stabilized subgrade** | 12 | 12 | 12 | 12 | 12 | 12 | 12 |
| **Total thickness above aggregate base** | 12.35 | 13.35 | 12.6 | 10.43 | 10.4 | 8.76 | 8.8 |

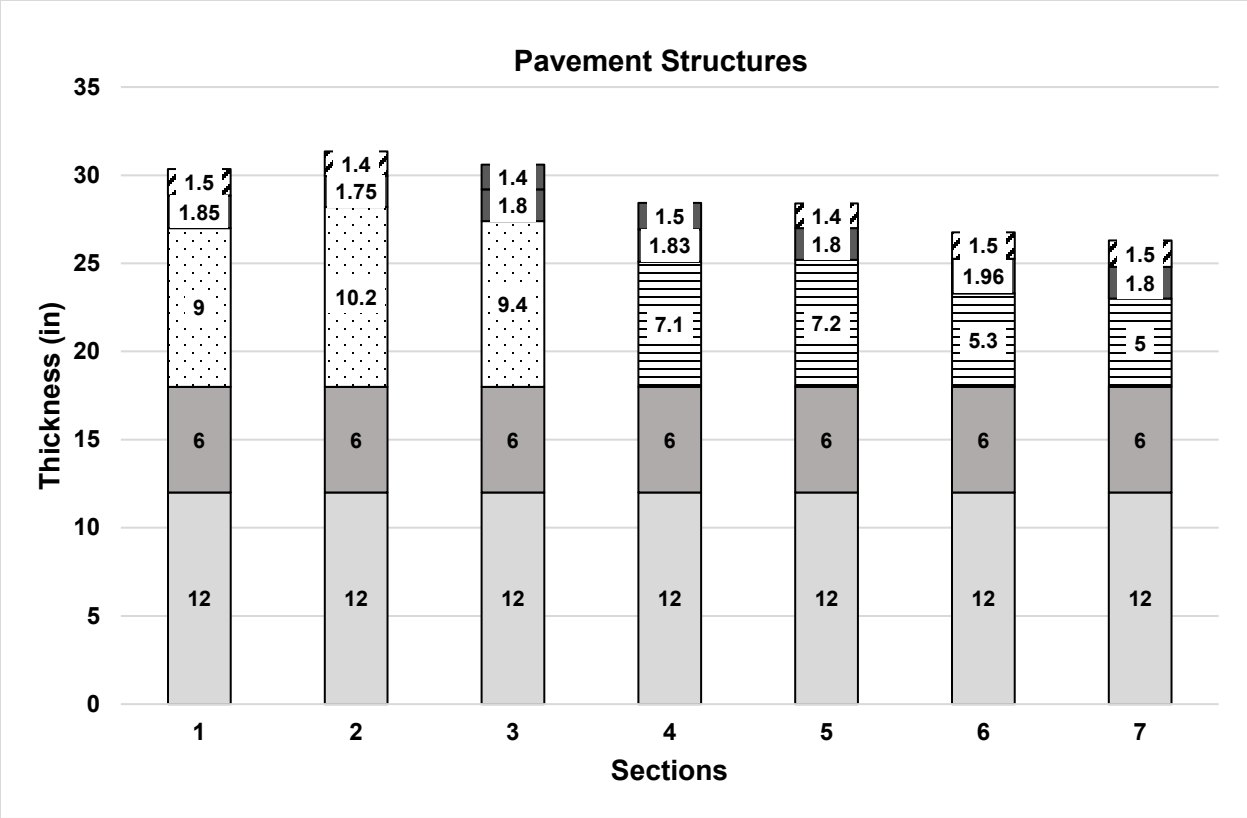


**Figure 96 Pavement Structures of WAY-83 Test Sections**

Figure 97 shows the FWD deflections measured at the WAY-83 pavement test sections. Larger deflections are generally found on thinner pavements, with one exception – average deflections are slightly higher on Section 1 than on Section 4.

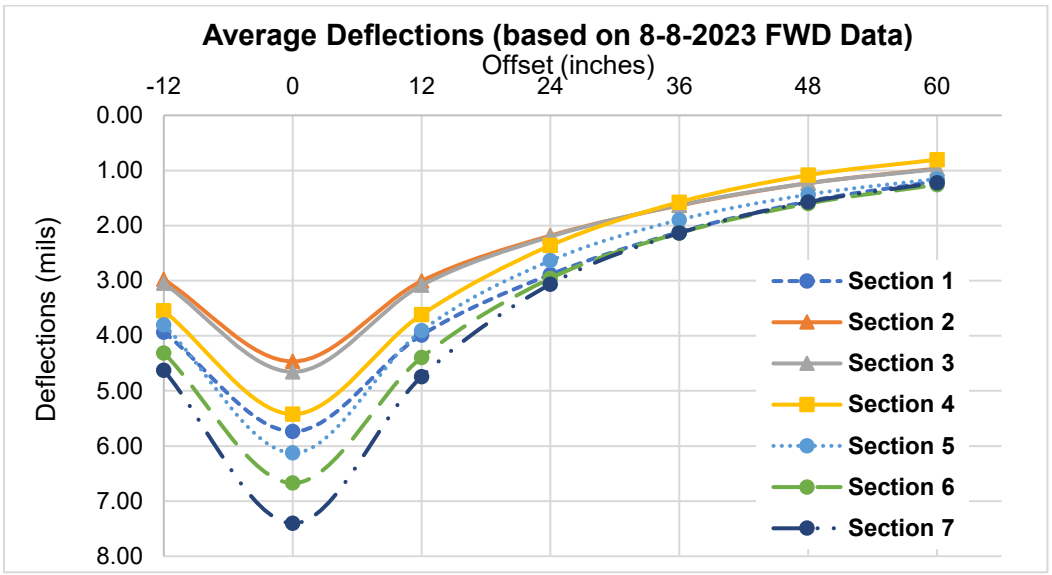


**Figure 97 Average Deflections at WAY SR-83 Pavement Test Sections**

The FWD deflection test conducted on the WAY-83 pavement test sections show that pavement deflection is primarily influenced by the total pavement structure thickness. Thicker pavement sections have smaller deflection. For pavement sections with similar total thickness, whether HPM or control AC was used does not have noticeable impact on deflections.

Strain measurements of HPM layers show higher strain than strain of control AC layers. As mentioned earlier, the higher toughness of HPM material enables it to withstand the higher strain.

### *Approach 5: Compare Pavement Performance*

The fifth approach is to use actual pavement performance to estimate the structure coefficient of HPM. This is the most preferred approach but requires long-term, continual monitoring of pavement condition (PCR distresses and pavement ride quality-IRI), accurate traffic loading ($W_{18}$ / ESAL) and seasonal variation of subgrade modulus $M_R$. A control section is necessary for comparison. Persistent monitoring of the test pavement sections constructed at WAY-83 is recommended to enable future calibration of HPM structural coefficient through this approach.

Figure 98 shows the performance of in-service HPM pavement sections based on limited PCR data. Most of the pavement sections are very short and have only two years of PCR data (3/2023 and 2/2024) specifically measured for this project. The only exception is FAI US-33, which has six years of PCR data since its last treatment. The average flexible pavement performance is also shown (blue curve).

Most of the HPM pavements have significant higher PCR values than average flexible pavement PCR value at the same age after minor rehabilitation. Two exceptions are ASD US-42 ASD US-250. These two pavement sections have only 1.5” (38 mm) of HPM in their surface course. ROS Ramp A/B, C/D, and ROS CR-238 also have some portions with only 1.5” (38 mm) of HPM (see Table 41 earlier).

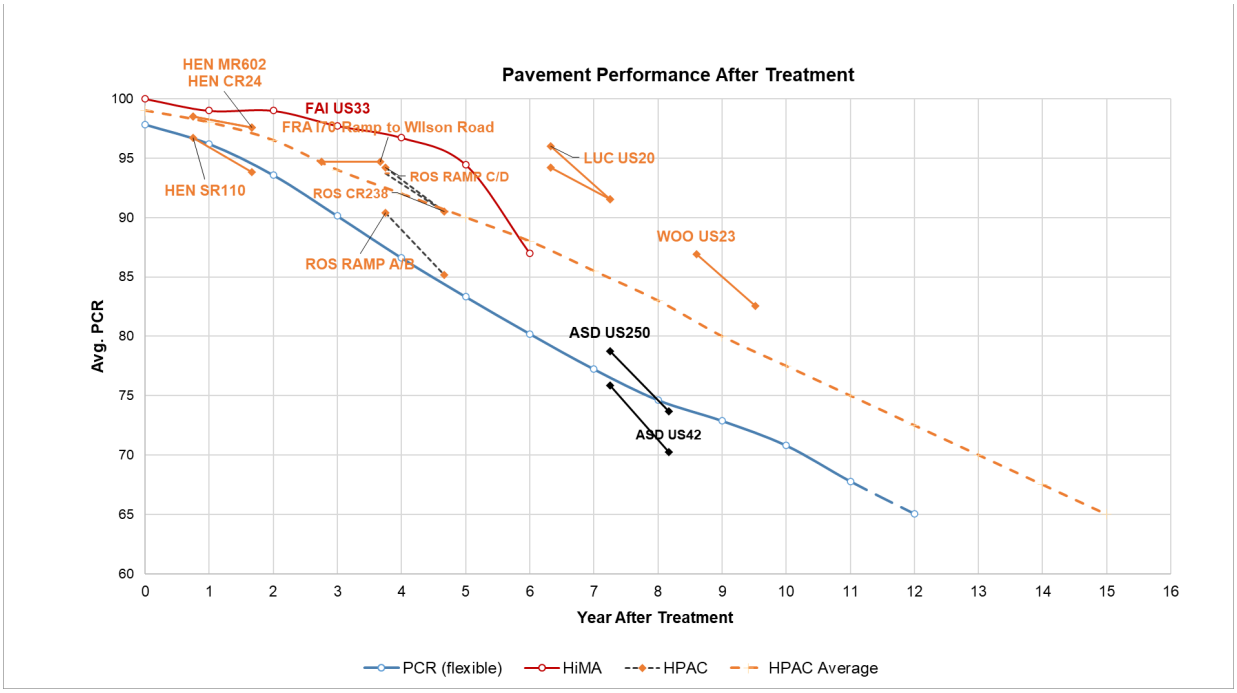


**Figure 98 PCR Deteriorations of HPM vs Average HMA Pavements**

Excluding the pavement sections with less than 3-in. of HPM (ASD US-250, ASD US-42, FAI US-33 (b), and ROS ramps A/B/C/D and ROS CR-238), it can be observed that pavement sections rehabilitated with HPM surface and intermediate courses could potentially extend the pavement service life by 3 years (about 25% of the normal service life of 12 years) or more. This is based on very limited data. Continued monitoring of these pavements and the HPM test pavements in WAY-83 would be necessary to confirm this projection.

If further monitoring does confirm that a significant number of HPM pavements can maintain better performance and achieve longer service life than regular asphalt pavements, that means HPM pavements will prolong the time interval between rehabilitation projects thus saving ODOT significant costs.

If after HPM pavements have consistently demonstrated much longer service life than conventional AC pavements and ODOT desires to assign a structural coefficient for HPM, the following method may be used to estimate the structural coefficient of HPM.

## *Summary*

This method is based on the empirical AASHTO Deign Equation below:

$$\log_{10} W_{18} = Z_R * S_0 + 9.86 \log_{10}(SN+1) - 0.20 + \frac{\log_{10}\frac{\Delta PSI}{4.2-1.5}}{0.4+\frac{1094}{(SN+1)^{5.19}}} + 2.32 \log_{10} M_R - 8.07 \quad (1)$$

where, $W_{18}$ = the number of 18-kip single-axle load applications

$Z_R$ = the normal deviate for a given reliability R

$S_o$ = the overall standard deviation.

SN = structural number of pavements.

Δ PSI = the reduction in serviceability

$M_{R_R}$ = the effective subgrade resilient modulus

Assuming everything else being equal (e.g., same subgrade, climate…), if a pavement constructed with HPM surface and intermediate courses can achieve *X*% longer service life (i.e., can carry *X*% more $W_{18}$) than a pavement with conventional AC surface and intermediate course (both have an $a_1$ of 0.43), the following equation can be derived:

$$\log_{10}\left(\frac{N}{N_c}\right) = 9.36 * \log_{10}\left(\frac{SN_2+1}{SN_1+1}\right) + \log_{10}\frac{\Delta PSI}{4.2-1.5} * \left(\frac{1}{0.4+\frac{1094}{(SN_2+1)^{5.19}}} - \frac{1}{0.4+\frac{1094}{(SN_1+1)^{5.19}}}\right) \quad (2)$$

where ($N/N_c$) = increase in the pavement life based on $W_{18}$

N = fatigue life of HPM layer

$N_c$ = fatigue life of control AC layer

$SN_1$ = Base SN of control AC layer

$SN_2$ = final SN based on the increase in pavement life due to HPM layer = $SN_1 + \Delta SN$

For a given $N/N_c$ (therefore X, X=($N/N_c$)-1), and assuming ΔPSI = 2.0, the change in the Structural Number (ΔSN) can be calculated from the difference between the new SN due to HPM and the existing SN due to control AC layer.

Considering the HPM layer as the sole contributor to the change in SN, ΔSN can be represented as:

$$\Delta SN = \Delta a_1 D_1 \quad (3)$$

The structural layer coefficient can be determined for any given thickness of the overlay. See Figures 99, 100 and 101 for D=3.25" (83 mm), D=2.5" (64 mm), and D=2" (51 mm), respectively.

As an example, if 25% longer service life has been achieved by pavement with 3.25" (83 mm) of HPM layer (surface + intermediate courses) and the entire pavement structure has a Structure Number, SN=6, then using Figure 99 the structural coefficient of HPM can be found as 0.48.

According to Table 40 shown previously, this means thickness D1 can be reduced to 2.9" (74 mm) from 3.25" (83 mm), representing a surface/intermediate layer material cost saving of over 10%. However, this is not worth it compared with the 25% longer service life that could be lost due to the thickness reduction.

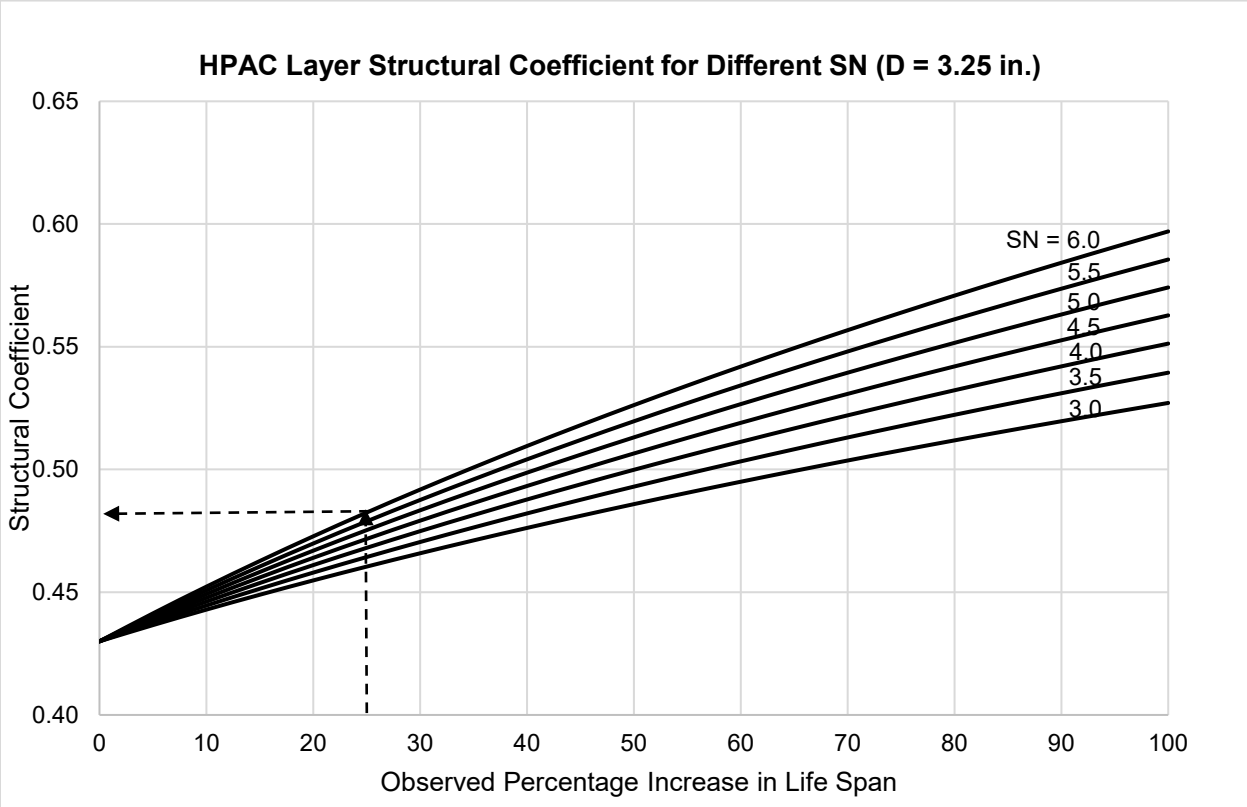


**Figure 99 Estimation of Surface/Intermediate Layer Structural Coefficient (D=3.25 in.)**

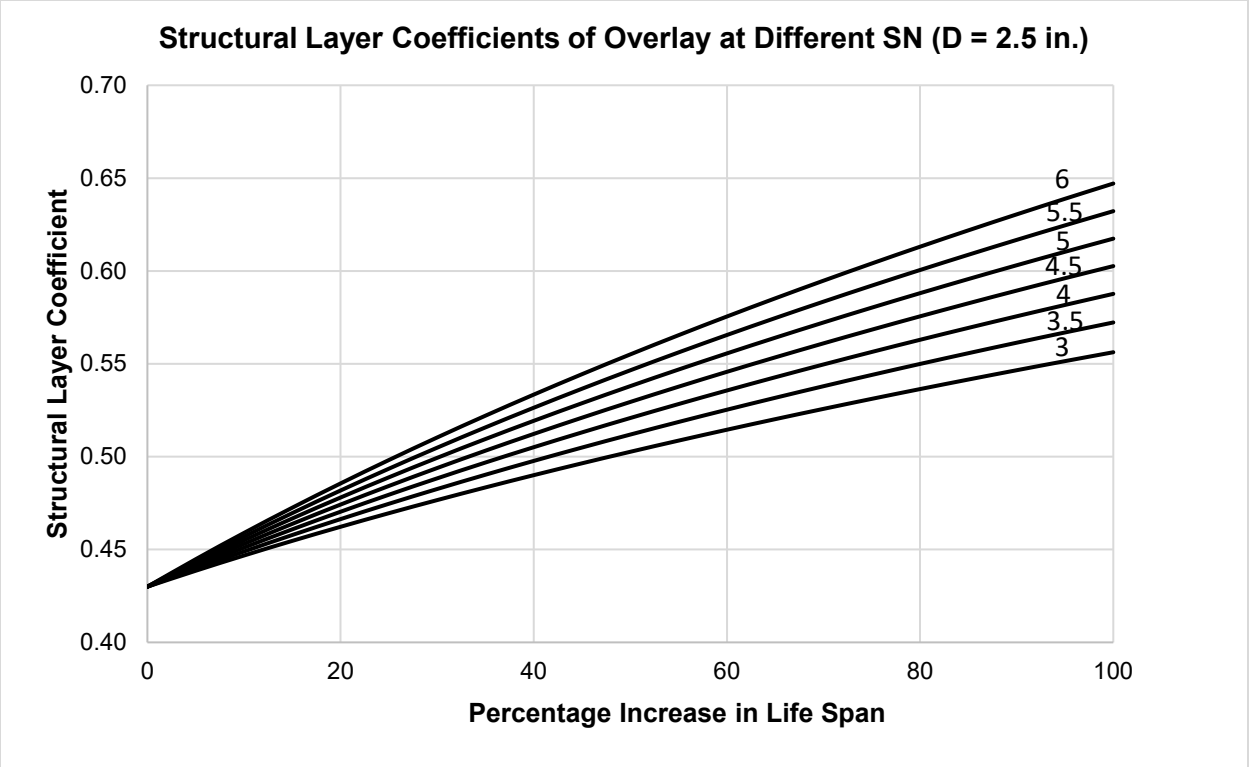


**Figure 100 Estimation of Surface/Intermediate Layer Structural Coefficient (D=2.5 in.)**

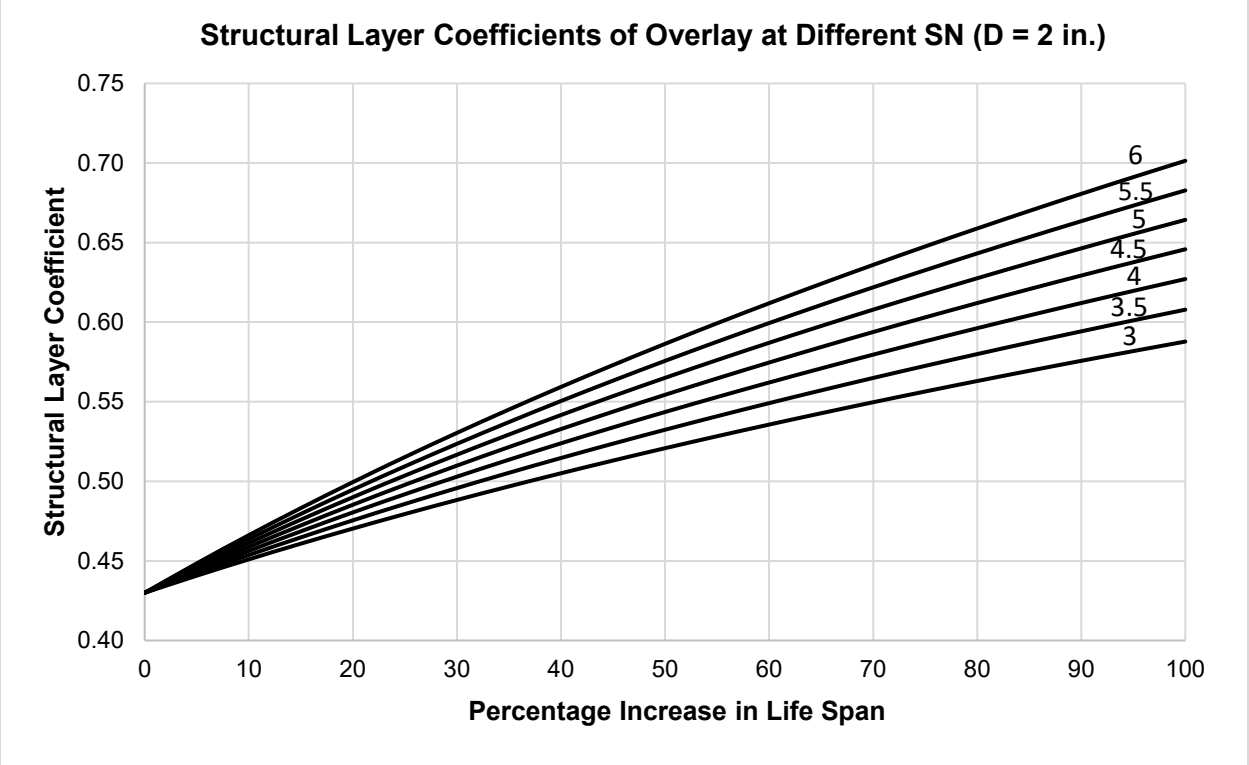


**Figure 101 Estimation of Surface/Intermediate Layer Structural Coefficient (D=2.0 in.)**

Based on the above figures, if continued performance monitoring show that pavement sections rehabilitated with HPM surface and intermediate courses consistently demonstrate a longer service, a higher structural coefficient may be used for HPM if a thinner pavement is desired such as under a bridge. For example, if service life of pavements rehabilitated with HPM is 25% longer on average compared with pavement sections rehabilitated with regular AC, a structural coefficient of 0.48 (up to 0.50) may be used for HPM. This compares to the currently used structural coefficient of 0.43 for regular AC.

Since the current ODOT Pavement Design Procedure (which follows the AASHTO 1993 Pavement Design Guide) is an empirical design procedure, the structural coefficient used for design would be best estimated through empirical field performance monitoring. Only very limited HPM pavement field performance data are available for this study. Therefore, further monitoring of long-term performance of existing and additional HPM pavement sections is necessary to confirm the long-term potential of HPM in extending pavement service life. Increasing the structural coefficient of HPM mix to reduce pavement thickness is not recommended, as the benefits of longer pavement service life likely out weights the cost savings of building thinner pavement by a wide margin.

## Benefit Cost Analysis of HPM

High polymer asphalt concrete (HPM, i.e., PG88-22M) mixes typically exhibit higher resistance to rutting and cracking than conventional asphalt concrete (Habbouche et al., 2020). Timm & Tran (2014) found that perpetual pavements built with high polymer modified (HPM) asphalt had a 26% cost savings compared to a conventional pavement. Their research also concluded that HPM mixes have a significantly longer life, higher temperature resistance, more moisture resistance and significantly lower rutting. Thus, pavements that use HPM mixes as a structural component, either for surface, intermediate, or base courses, can be expected to have a longer service life with less rehabilitation cost. The same research studies also show that the structural layer coefficients of HPM would be higher than that of conventional asphalt concrete; thus, pavements constructed with HPM could have thinner thickness for the same level of performance.

The objective of this task is to perform a benefit cost analysis to determine whether using HPM is cost-effective by quantifying the performance benefit of HPM and compare it with the higher costs of HPM mixes.

### *Cost of HPM*

HPM typically cost more than normal HMA, so generally it has been used mostly for short stretches of pavement where heavy traffic loadings are expected, such as truck lanes, bus stops or intersections. The quantity of HPM in each project is typically quite small, so the cost data are limited. There are only two large quantity HPM projects in Ohio (PN# 17-0206 and PN# 17-0385), both located on US-33 in Fairfield County.

Based on data summarized from the ODOT Historical Bid Data Item Search Spreadsheet, ODOT has estimated that on average, cost of HPM surface course is 10%-20% higher than regular HMA, and HPM intermediate course is 10-15% higher. This estimate is based on very limited data.

### *Benefits of HPM*

Results of the laboratory testing performed for this study confirm with previous studies that HPM significantly improves resistance to rutting and cracking.

The results of the Hamburg Wheel Track Testing show that HPM mixes exhibit significantly less rutting than regular AC mixes at the same number of loading cycles. Figure 91 shows that the HPM specimen can withstand 20,000 load repetitions before reaching a rut depth of ~2.41 mm, while the regular AC specimen reached the same rut depth in only about 6,600 load repetitions. This means that, at least in the laboratory, HPM mixes can achieve a three-fold increase in life against rutting distress.

The results of the IDEAL-CT test show that the Cracking Tolerance Index is 114% higher for HPM surface, 87% higher for intermediate course, and 43% higher for based course, compared with regular AC courses, respectively.

Tensile strength and dynamic modulus measured in the lab and resilient modulus back calculated from FWD deflections are lower than regular AC. This indicates that HPM is not stronger nor stiffer, but tougher compared with regular AC.

This study further quantifies the benefit of HPM in terms of the increase in performance of ODOT in-service HPM pavements in comparison with the average performance of ODOT HMA pavements.

Table 41 ODOT In-Service HPM (PG88-22M) Pavements shows a list of ODOT in-service HPM pavements. Nearly all the HPM pavement sections are very short, with the only exception being FAI-33, which was consist of two projects (PID 93009 and PID 93015). PID 93009 has a 1.5-in. of HPM surface course and a 1.75-in. of HPM intermediate course. PID 93015 has only a 1.5-in. surface course. There are multiple PCR sections within each project.

Figure 98 shows a plot of the available Pavement Condition Rating (PCR) scores versus pavement age since resurfacing. The only pavement for which complete PCR data are available since resurfacing is FAI-33. PID 93009 is labeled FAI as US-33(a) and PID 93015 is labeled as FAI US-33(b) in the plot. All other HPM projects have only two years of PCR data collected in March 2023 and February 2024, specifically for this study.

The PCR curve shown for FAI US-33(a) and FAI US-33(b), respectively is the average PCR of all PCR sections within each project. PID 93009 (FAI US-33(a)) outperforms PID 93015 (FAI US-33(b)) likely due to having thicker HPM. However, FAI US-33(a) has poor subgrade underneath and the base course has started to fail, as a result, despite good performance during the first few years, its average PCR score began to drop after the fifth year, but still above FAI US-33(b).

The average PCR deterioration curve of all flexible pavements after rehabilitation (Activities 50 and 60) is also shown in Figure 98. This represents the average performance of flexible pavements built with conventional AC), which last about 12 years before PCR score decreases to 65.

As shown in Table 41, ASD US-42 and ASD US-250 have only 1.5" (38 mm) of HPM in the surface layer. ROS Ramps B/A and C/D and ROS CR-238 also partly have only 1.5" (38 mm) of HPM for surface layer, so their performance is not comparable with other HPM pavements. The other HPM pavements included 3 (76 mm) or 3.25 inches (83 mm) of combined HPM in surface and intermediate courses. WOO US-23 has 4 inches (102 mm) total of HPM.

As can be observed in Figure 98, when only PCRs of pavement sections with 3 (76 mm) or 3.25 inches (83 mm) of HPM are considered and excluding the last year PCR drop of FAI US-33(a), the average lifespan of a HPM pavement after rehabilitation till reaching a PCR score of 65 may be extrapolated to be approximately ~15-16 years. This is based on very limited data and continued monitoring of the condition of WAY83 HPM test pavement sections would help to assess the performance and lifespan of HPM pavements more accurately.

### *Summary*

It can be concluded that since the cost of HPM mixes is 10-20% higher for surface course and 10-15% higher for intermediate course, while a pavement with HPM surface and intermediate courses could achieve a useable lifespan of 15 years — a 3-year or 25% increase from the average lifespan of 12 years for conventional AC pavements, using HPM would be cost-effective. Note a pavement project's cost is more than just the material cost, so a 3-year increase in lifespan is very significant.

# CONCLUSIONS AND RECOMMENDATIONS

## Summary

After reviewing previous studies on perpetual pavement including several test sections in Ohio, ODOT initiated this study to incorporated the impact of High Polymer on standard ODOT design. To that end, an experiment on WAY-83 was designed to study the effect of thickness variation and the addition of high polymer AC binder on the field performance of AC pavement. Seven test sections were instrumented and monitored on WAY 83 for a period of year and a half. The seven sections consisted of one control section made with conventional ODOT HMA binder mix for the surface, intermediate and base layers, three test sections with various thickness using High Polymer Modified Binder (PG88-22M) for the surface, intermediate and base layers, and three sections with combination of conventional and high polymer mixes. Sensors, including strain gages, pressure cells and thermocouples were installed at the bottom of the asphalt base to collect data on the strain at each section and study the in-situ behavior of these test sections. Samples were collected and laboratory tests conducted to get the mechanical properties of the mixes used. Falling weight deflectometer, and DCP data was collected throughout the project to characterize the in-situ pavement properties, and controlled truck tests were conducted during 4 test periods to collect strain data from the pavement sections.

## Conclusions

The test sections were constructed in the fall of 2022, and were in service shortly thereafter. Controlled truck testing and FWD data collection was first conducted in May 2023, and last conducted in May 2024.

As of the time of the last field visit in May 2024, all test sections were in excellent condition, with no distresses at any of the sections. Due to the low strain values collected at the site, all sensors were still functioning and able to collect data. It should also be noted that six of the seven sections have significant tree cover, allowing the pavement sections to remain at more-or-less constant temperature as opposed to sections that are fully exposed to the sun, thus keeping the base temperature low and further contributing to the low strain values.

Strain data collected from all the test sections were well below the endurance limit set in the literature. However, it should be noted the field measured tensile strain values are somewhat limited in terms of pavement conditions, as data were only collected on four test dates. The temperatures for a given date varied from section to section, with large differences noted on the hottest test date (8/8/2023). To provide a more fair comparison between test sections, regression equations were used to estimate field measured strain at the same conditions as for which strain measurements were made on the DEL-23 SB ramp and the APLF HiMA experiments to compare against previous test sections which are believed to be perpetual pavements. As a reminder, the DEL-23 SB ramp which consisted of conventional AC throughout the structure, and was constructed on an aggregate base and lime-modified subgrade had a stiffness ratio > 1.0, and measured strain values less than the calculated FEL as reported by Sargand et al. (2015). Similarly, APLF HiMA Lane C which had HiMA in all AC layers and was constructed on an aggregate base and stabilized subgrade met the stiffness ratio (> 1.0) and had low measured strain values, as reported earlier in this report and Sargand et al. (2015).

Test sections 1 through 4 on WAY-83 consisted of conventional AC in the base. Comparisons with of estimated strain at the same conditions (T = 81.5F, 5 mph, 10.5 kip load) at which some of the highest strain was measured on DEL-23 SB ramp provides a good check as to whether these sections can be expected perform as well or better than the DEL-23 SB ramp section. All four test sections had estimated strain well below the 77 microstrain measured on DEL-23 SB ramp. The highest estimated strain was 23 microstrain, which represents a 62% reduction relative to the strain measured on DEL-23 SB ramp. Based on this check, it is expected that Test Sections 1 through 4 will perform as well or better than the DEL-23 SB ramp.

WAY-83 test sections with HPM AC in the base which are expected to perform perpetually should have measured strain at the same extreme conditions (T = 100F, 5 mph speed, 12 kip load) under which the maximum strain was measured in the APLF Lane C. This holds true for Sections 4 – 6, in which estimated strain at those conditions was less than 67 microstrain. Sections 6 and 7 were not expected to perform perpetually. Section 7 has estimated strain at the extreme conditions to be greater than 67 με, thus, it is not expected to perform perpetually. Section 6, however, had an estimated strain of only 35 με which is nearly half of the maximum strain (67 με) in Lane C of the APLF. Just like section 7, section 6 was also constructed with HPM mixes throughout, albeit ½" (13 mm) thicker than section 7. The DCP moduli and backcalculated moduli for the aggregate base and stabilized subgrade in section 6 are in-line with section 7. The small increase in AC thickness for section 6 is unlikely to result in the large decrease in strain relative to section 7. Therefore, section 6 should be closely monitored moving forward.

Due to the unexpectedly low measured strain values, it was postulated the moduli of the underlying layers on WAY-83 were much greater than typical pavements with stabilized subgrade. In Appendix C, DCP and backcalculated moduli for stabilized subgrades reported in previous literature were reviewed and compared to the corresponding moduli on WAY-83. While it was observed that in most cases the DCP derived modulus and backcaclulated modulus of the stabilized subgrade do not agree, no conclusion could be drawn about the relative differences. Furthermore, no conclusion could be drawn as to whether the stabilized subgrade moduli determined for test sections on WAY-83 represented typical values for pavements with stabilized subgrade. Therefore, it is recommended future evaluations be conducted across the state to determine expected in-situ moduli of stabilized subgrade and the overlying aggregate base for initial construction values.

Three cumulative strain distributions were developed (Table 15), based on whether HPM or conventional AC mix is used in the AC base layer and whether the subgrade is stabilized or not. However, only the cumulative strain distributions for HPM AC in the base layer and constructed with a stabilized subgrade and for conventional AC in the base layer and constructed with a stabilized subgrade were evaluated in this study. It is recommended that these two cumulative strain distributions be used in conjunction with the ODOT PDM inputs for the aggregate base and stabilized subgrade (based on CBR of the project site) to design perpetual pavement cross-sections using PerRoad.

Another notable observation: adding polymer to the asphalt binder makes the asphalt layers proportionately more flexible, reducing stiffness, and makes the strains greater, even with the presence of RAP content.

A comprehensive laboratory testing protocol was conducted for this project, lab testing of field collected materials, included creep compliance and indirect tension, dynamic modulus testing, tensile strength ratio, Hamburg wheel tracking test, Ideal CT and Cantabro tests each were conducted in accordance with AASHTO and ODOT specifications.

The laboratory data confirmed the polymer additive increases the flexibility of the asphalt and lowers its modulus. The addition of polymer will improve the resistance to cracking and rutting. Increasing the polymer content increases strain, but also increases resistance to rutting, increases resistance to cracking and durability of the pavement. High polymer modified asphalt binders allowed the use of RAP content without compromising the quality of the mix.

A method was developed to estimate the structural coefficient of HPM based on comparing the potentially longer service life of HPM pavements compared with regular pavements. For example, if continued monitoring confirms that pavements rehabilitated with HPM surface and intermediate courses can achieve a 25% increase in service life compared with pavement rehabilitated with regular AC, then a structural coefficient of 0.48 to 0.50 may be used for HPM. The structural coefficient is not a material constant and is dependent on several factors including design traffic loading, $\Delta$PSI, pavement structure number (SN), design traffic, and subgrade modulus.

Nevertheless, if after high polymer pavements have consistently demonstrated much longer service life than conventional AC pavements, ODOT may assign a structural coefficient for HPM. It can be concluded that since the cost of HPM mixes is 10-20% higher for surface course and 10-15% higher for intermediate course, while a pavement with HPM surface and intermediate courses could achieve a useable lifespan of 15 years — a 3-year or 25% increase from the average lifespan of 12 years for conventional AC pavements, using HPM would be cost-effective. Note a pavement project's cost is more than just the material cost, so a 3-year increase in lifespan is very significant.

## Recommendation

Based on the finding of this study, it is recommended PerRoad be utilized for future perpetual pavement designs with the following criteria:

- Predicted tensile strain at the bottom of the AC layers are less than the cumulative strain distribution curves listed in Table 15 for pavements with stabilized subgrade
- Vertical strain at the top of the stabilized subgrade does not exceed 200 $\mu\varepsilon$ at the $50^{th}$ percentile of the cumulative vertical strain distribution

As part of the perpetual pavement design procedure, it is recommended laboratory measured E* data or the recommended E* values listed in Appendix D are used for characterizing the AC layer moduli in PerRoad. Regarding the underlying layers, it is recommended the ODOT PDM equations be utilized to characterize the aggregate base modulus over a stabilized subgrade and the modulus of the stabilized subgrade. While three cumulative strain distribution were developed in this study, only the tensile strain criteria for pavements constructed on stabilized subgrade were verified in the field, therefore caution should be used when applying the cumulative strain distribution for conventional AC base and non-stabilized subgrade. To support

these recommendations, a design guide has been developed, presented in Appendix D, to be used with the provided Excel Spreadsheets and the free PerRoad software.

A significant amount of data has been obtained in the short term on load response of these test sections Continued performance monitoring of these test sections and monitoring of HPM sections constructed in the future is still needed since the sample size of the performance of in-service pavements used for this analysis is rather small to confidently suggest the benefit of service life extension is accurate. More pavements consisting of HPM should be studied for a longer period until they reach a threshold PCR value of 65 to confirm the lifespan of HPM pavements. The cost data for the HPM are also very limited. Only a handful of projects were included in the average cost and only a single project has cost data for HPM base course. It should also be noted that only the US33 project in Fairfield County has significant quantity of HPM in the pavements, however the design of that project is outside of the ODOT standard practice. Other projects included only a short stretch of HPM pavement so the quantity of HPM used is small. This could also distort the cost data for HPM.

It is recommended an examination for the potential of crack initiation at the interface between the intermediate and asphalt base when high polymer is used in the asphalt base due to the variation of stiffness between the various layers used.

Based on this study, the effect of adding high RAP content may be potentially softened by the use of High Polymer, this also warrants further investigation.

Increasing the structural coefficient of HPM mix to reduce pavement thickness is not recommended currently, as the benefits of longer pavement service life likely out-weights the cost savings of building thinner pavement by a wide margin. Nevertheless, certain situations such as under a bridge may warrant a thinner pavement structure, a structural coefficient of 0.48 to 0.50 may be used for HPM.

# REFERENCES


Chou, Y. J., Randolph, B., Heydinger, A., 1999. *Rational Determination of Pavement Layer Structural Coefficients*. Ohio Department of Transportation Report No. FHWA/OH-99/006. The University of Toledo, Toledo, Ohio.

Habbouche, J., Hajj, E. Y., Sebaaly, 2019. *Structural Coefficient for High Polymer Modified Asphalt Mixes*, Final Report, Florida Department of Transportation, June 2019.

Habbouche, J., Hajj, E. Y., Sebaaly, P. E., & Piratheepan, M. (2018). A critical review of high polymer-modified asphalt binders and mixtures. *International Journal of Pavement Engineering*, *21*(6), 686–702. https://doi.org/10.1080/10298436.2018.1503273

Islam, S., Sufian, A., Hossain, M., Miller, R., and Leibrock, C. (2017). *Perpetual Pavement Design Analysis*, Presented at the 96th Annual Meeting of the Transportation Research Board, National Research Council, January 8-12, 2017, Washington D.C.

Benjamin B. Jordan and Shad Sargand, 2014, "Asphalt Perpetual Pavement Design: Utilizing Existing Pavement Systems In Ohio", paper presented at the International Conference on Perpetual Pavement 2014, Columbus, Ohio, USA, October 30-31, 2014.

Issam Khoury, Shad Sargand, Roger Green, Benjamin Jordan, and Paul Cichocki, 2016a, "Rutting Resistance of Asphalt Mixes Containing Highly Modified Asphalt (HiMA) Binders at the Accelerated Pavement Load Facility in Ohio", paper presented to 5th International Conference on Accelerated Pavement Testing, San Jose, Costa Rica, September 19-21, 2016, DOI: 10.1007/978-3-319-42797-3_28, in José P. Aguiar-Moya, Adriana Vargas-Nordcbeck, Fabricio Leiva-Villacorta, Luis G. Loría-Salazar, eds, *The Roles of Accelerated Pavement Testing in Pavement Sustainability: Engineering, Environment, and Economics*, Berlin: Springer, September 16, 2016, p. 429-439.

Issam Khoury, Shad Sargand, Benjamin Jordan, Paul Cichocki, and Matthew Sheer, 2016b, "Structural Study of Perpetual Pavement Performance in Ohio", paper presented to 5th International Conference on Accelerated Pavement Testing, San Jose, Costa Rica, September 19-21, 2016, DOI: 10.1007/978-3-319-42797-3_29, in José P. Aguiar-Moya, Adriana Vargas-Nordcbeck, Fabricio Leiva-Villacorta, Luis G. Loría-Salazar, eds, *The Roles of Accelerated Pavement Testing in Pavement Sustainability: Engineering, Environment, and Economics*, Berlin: Springer, September 16, 2016, p. 441-459.

John Liao and Shad Sargand, 2009, "Controlled Load Vehicle Testing and Numerical Modeling of US30 Perpetual Pavement AC Test Section 664", International Conference on Perpetual Pavement 2009, September 30-October 2, Columbus, Ohio.

John Liao and Shad M. Sargand, 2010, "Viscoelastic FE Modeling and Verification of a U.S. 30 Perpetual Pavement Test Section", *Road Materials and Pavement Design: An International Journal*, Vol. 11, No. 4, p. 993-1008, December 2010. DOI: 10.366/rmpd.11.993-1008.

Newcomb, D., R. Willis, and D. Timm. 2010. *Perpetual Asphalt Pavements: A Synthesis*. Asphalt Pavement Alliance, Lanham, MS, 2010.

Perpetual Pavement Committee. 2002. *Perpetual Pavement Minutes 4-10-02*. Columbus, OH. Ohio Department of Transportation, April 10, 2002.

Jianfeng Qin and Shad Sargand, 2014, "Determining Optimum Thickness of Perpetual Pavement", paper presented at the International Conference on Perpetual Pavement 2014, Columbus, Ohio, USA, October 30-31, 2014.

Sargand, S., Figueroa, J.L., and Romanello, M. 2008. *Instrumentation of the Way-30 Test Pavements*, Technical Report No. FHWA/OH-2008/7 for the Ohio Department of Transportation, State Job No. 14815, June 2008.

Sargand, S., Edwards, W.F., and Bendaña, L.J. 2008. "Testing of Perpetual Pavement with Warm Asphalt Concrete Surface Mixes in the Ohio APLF", Paper No. 82, Third International Conference on Accelerated Pavement Testing, October 1-3, 2008 Madrid, Spain.

Sargand, S., Masada, T., Hernandez, J., and Kim, S.-S. 2010. *Determination of Mechanical Properties of Materials Used in Way-30 Test Pavements*, Technical Report No. FHWA/OH-2010/9 for the Ohio Department of Transportation, State Job No. 437046, May 2010.

Sargand, S. and Figueroa, J.L. 2010. *Monitoring and Modeling of Pavement Response and Performance Task A: Ohio*, Technical Report No. FHWA/OH-2010/03A for the Ohio Department of Transportation, Pooled Fund Project TPF-5(121), State Job No. 134287, June 2010.

Sargand, S., Khoury, I., and Morrison, J. 2012. *Monitoring and Modeling of Pavement Response and Performance Task B: New York: Volume 1: I490, RT9A, and I86 Perpetual Pavement*, Technical Report No. FHWA/OH-2012/08A for the Ohio Department of Transportation, State Job No. 134287, May 2012.

Sargand, S., Edwards, W., and Khoury, I., 2012, "Assessment of response and performance of perpetual pavements with warm mix asphalt surfaces at the Accelerated Pavement Load Facility", in David Jones, Ed., *Advances in Pavement Design through Full-Scale Accelerated pavement Testing*, Proceedings of the 4th International Conference on Accelerated Pavement Testing, September 19-21, 2012, Davis, CA, p. 175-185.

Sargand, S., Khoury, I., Gray, J., Al-Jhayyish A., "Incorporating Chemical Stabilization of the Subgrade in Pavement Design and Construction Practices", Technical Report No. ODOT/FHWA-2014/12, for the Ohio Department of Transportation, State Job 134659, October 2014.

Sargand, S., Figueroa, Romanello, M. 2008. *Instrumentation of the WAY-30 Test Pavements*. Ohio Department of Transportation Report No. FHWA/OH-2008/7. Ohio Research Institute for Transportation and the Environment (ORITE), Athens, OH

Sargand, S., Figueroa, J.L., Edwards, W., Al-Rawashdeh, A. 2009. *Performance Assessment of Warm Mix Asphalt (WMA) Pavements*. Ohio Department of Transportation Report No. FHWA/OH-2009/08. Ohio Research Institute for Transportation and the Environment (ORITE), Athens, OH

Sargand, S., Vega-Posada, C., and Arboleda-Monsalve, L. G. 2013. "Long-Term Performance of Existing Asphalt Concrete Pavement Sections", *Rev. Fac. Ing. Univ. Antioquia*, No. 66, March 2013, p. 45-56.

Sargand, S., Khoury, I., Jordan, B., Scheer, M., and Cichocki, P. 2015. *Implementation and Thickness Optimization of Perpetual Pavements in Ohio*. Ohio Department of Transportation Report No. FHWA/OH-2015/17. Ohio Research Institute for Transportation and the Environment, Athens, Ohio.

Sargand, S., Green, R., Burhani, A., Alghamdi, H., Jordan, B. 2016. *Investigation of In-Situ Strength of Various Construction/Widening Methods Utilized on Local Roads*. Ohio Department of Transportation Report No. FHWA/OH-2016/02. Ohio Research Institute for Transportation and the Environment, Athens, Ohio.

Shad Sargand, Issam Khoury, and Matthew Scheer, 2017, "Instrumentation of a perpetual test pavement in Ohio", 4th conference of transportation research group of India (CTRG), Mumbai, India, December 17-20, 2017.

Timm, D., Robbins, M., Willis, J., Tran, N., and Taylor, A. 2013. *Field and Laboratory Study of High-Polymer Mixtures at the NCAT Test Track: Final Report*, NCAT Report 13-03, National Center for Asphalt Technology at Auburn University, Auburn, AL, 2013.

Tran, N., Robbins, M., Timm, D., Willis, J., and Rodezno, C. 2015. *Refined Limiting Strain Criteria and Approximate Ranges of Maximum Thicknesses for Designing Long-Life Asphalt Pavements*, NCAT Report 15-05R, National Center for Asphalt Technology at Auburn University, Auburn, AL, 2015.

Timm, D., Tran, N., and Rodezno, C. 2017. *Redesign and Updates of the Perpetual Pavement Design Software: PerRoad Version 4.3*, Research Synopsis 17-06, National Center for Asphalt Technology at Auburn University, Auburn, AL, 2017.

American Association of State and Highway and Transportation Officials (AASHTO) (2020). *Mechanistic-Empirical Pavement Design Guide: A Manual of Practice*. 3rd Edition, AASHTO, Washington, D.C., 2020.

Brink, W. and H. Von Quintus (2018). FY 2018 Enhancements Released with Version 2.5. *Webinar*, AASHTOWare Pavement ME Design, (https://me-design.com/MEDesign/Webinars.html) accessed September 22, 2021.

Sargand, S., Khoury, I., Jordan, B., Scheer, M., and Cichocki, P. 2015. *Implementation and Thickness Optimization of Perpetual Pavements in Ohio*. Ohio Department of Transportation Report No. FHWA/OH-2015/17. Ohio Research Institute for Transportation and the Environment, Athens, Ohio.

Witczak, M., Mamlouk, M, Souliman, M., and Zeiada, W., 2013, *Laboratory Validation of an Endurance Limit for Asphalt Pavements*. NCHRP Report 762. Transportation Research Board. Washington, D.C.

Zhou, F. 2019, Development of an IDEAL Cracking Test for Asphalt Mix Design, Quality Control and Quality Assurance. Final Report for NCHRP IDEA Project 195, January 2019.

# APPENDIX A: LITERATURE REVIEW

## Critical Vertical Strain at the top of the subgrade layer

Walubita et al. (2008) referred to perpetual pavements as structurally sufficient in resisting rutting by controlling the vertical response on the top of the subgrade layer to less than or equal to 200 με. Tran et al. (2015) suggested using a cumulative strain distribution, in which the threshold to resist rutting was a $50^{th}$ percentile vertical strain at the top of the subgrade less than 200 με.

## Fatigue Endurance Limit

Providing a fatigue endurance limit for perpetual pavements has been the subject of much discussion and investigation since the perpetual pavements concept was first introduced. A fatigue endurance limit for a flexible pavement has been defined as "the horizontal asymptote of the relationship between the applied stress or strain and the number of load repetitions, such that a lower stress or strain will result in an infinite number of load repetitions" (Von Quintus, 2001).

Fatigue endurance limit (FEL) is a critical strain value that mainly targets the lowest part of the bottom layer of the asphalt concrete (AC). The part subject to this study sits directly on top of the aggregate base layer. Recent studies show that maintaining an FEL value under a certain threshold could reduce fatigue damage that typically starts at the bottom layers and propagates up towards the upper layers. Ultimately, causing damage known as bottom-up fatigue cracking failure that significantly decreases the pavement's structural capacity. [Zeiada et al. 2017].

Monismith and McLean [1972] postulated the fatigue endurance limit concept in 1970 and found a proposed level of 70 micro strains (με) resulted in extraordinarily long fatigue life. At that time, there was a lack of enough test data to support their conclusion. Considering such value, ambiguity around maximum pavement thickness was reduced, as additional thickness would not increase the structural resistance to fatigue damage and, therefore, reduced unnecessary expenses.

Carpenter et al. [2003] defined the endurance limit for Extended Life Hot Mix Asphalt Pavements (ELHMAP), or perpetual pavements (PP) as the strain at which fatigue damage does not develop or is very minimal. Data were analyzed for surface and binder mixtures where specimens were loaded in the lab under varying load repetitions and evaluated for fatigue using the dissipated energy approach. A fatigue endurance limit was determined in hot-mix asphalt concrete specimens, corresponding to 70 to 90 microstrain under 10 Hz loading frequency at 20 °C. As long as the fatigue life of the hot mix asphalt concrete mixtures is maintained below the thresholds, its lifespan would extend for the entire design period.

According to previous fatigue endurance limit research [Thompson and Carpenter 2006], a 70 microstrain level is a conservative number that ensures a structural design will operate in the region of prolonged fatigue life and "no damage" performance. Under the most severe situations, a design that incorporates this 70 microstrain threshold can be called a perpetual pavement. There is no buildup of HMA fatigue damage if the strain maintains at 70–100 microstrain throughout the pavement life.

Prowell et al. [2010] described the FEL as the stress or strain level below which neither fatigue damage occurs and arising from the bottom of the pavement structure or causing a beam fatigue specimen to fail at precisely 50 million loading cycles in the laboratory testing.

Using a shift factor of 10 recommended by SHRP to relate the laboratory performance to the field performance, such loading simulates approximately 500 million load cycles in the field or the maximum probable loading over 40 years life span of the pavement. Applying this methodology in testing specimens, predicted strain levels ranged from 75 to 200 microstrain.

Nishizawa et al. [1996] conducted fatigue analysis for existing thick pavements in Japan and concluded fatigue cracking does not happen due to the healing effect in the asphalt layers if the tensile strain level is kept less than 200 microstrain. Likewise, strain levels of between 96 and 158 microstrain were determined at the bottom of the asphalt layer for a long-life pavement in Kansas using back-calculated stiffness data from the falling-weight deflectometer [Wu et al. 2004].

Two out of eight perpetual pavement sections in Texas were modeled and designed using the Flexible Pavement System Software, denoted as FW 01-Superpave and FW 02-Conventional. Designers typically attempted to retain two limiting criteria responses for the perpetual pavement design; (1) the horizontal tensile strain below 70 με at the base of asphalt layers to prevent fatigue failure from happening and protect the flexible perpetual pavement against fatigue cracking; and (2) the vertical compressive strain less than 200 με at the top of the subgrade layer to prevent the rutting failure to occur. For both sections, the in-situ FWD back-calculated material characteristics and actual field thicknesses were used. Both sections fulfilled the PP mechanistic response criteria, with strain level much below the commonly accepted limits of 70 με and 200 με, respectively. [Walubita et al., 2008].

In NCHRP 9-44 (Witczak et. al., 2013), the endurance limit of hot mix asphalt has been described as the point of balance between damage and healing during the load pulse in the field or the load cycle in the laboratory test. The damage happens when the healing potential in the pavement is less than the strain level at that moment. On the other hand, the damage will be short and completely repaired thru the healing process if the strain level is less than the FEL. As part of the NCHRP 9-44 study, the AASHTO T3 21-03 test protocol was used to conduct laboratory displacement-controlled flexure fatigue testing. Testing was performed under different conditions such as binder contents, binder types, air void percentage, strain levels, test temperatures, and rest times between loading cycles. As a result of these tests, there was no single value for the fatigue endurance limit at these different conditions, and the range of endurance limit was found to be from 22 microstrain up to 264 microstrain.

Timm et al. [2012] conducted studies on the effect of HPM on pavement performance, two test sections, N7 (Kraton) and S9 (Control), have been constructed as part of the 2009 Test Track. N7 section featured HPM produced using Kraton polymer-modified asphalt binder with a Performance Grade (PG) of 88-22. HPM asphalt binder was used in all asphalt layers with a total asphalt thickness of 5.75” (146 mm). The control section was built with three asphalt layers with an approximate total thickness of 7” (178 mm). The PG grade of the binder in the surface and intermediate layer was 76-22, and for the base layer, the PG grade was 67-22. This research included two design gradations. The surface layers had a nominal maximum aggregate size (NMAS) of 9.5 mm, while the intermediate and base mixes had an NMAS of 19 mm.

Although the N7 test section was not intended to be perpetual, the bending beam fatigue test was completed on the HPM asphalt base mix as well as the control asphalt base mix to determine the fatigue endurance limit of each. Using the recommended procedure developed by NCHRP 9-38, the fatigue endurance limit was estimated using Equation 1. Based on a 95 percent one-sided lower predictions of the endurance limit and depending on the cycles to failure, the predicted fatigue endurance limit for the control base mixture was 77 microstrain. In comparison, the expected fatigue endurance limit for the Kraton base mixture was 231

microstrain. In other words, the fatigue endurance limit was three times higher in the HPM base mixture than in the control mixtures.

$$\text{Endurance Limit} = \hat{y}_0 - t_\alpha s\sqrt{1+\frac{1}{n}+\frac{(x_0-\bar{x})^2}{S_{xx}}} \qquad \text{Equation 1}$$

where:

$\hat{y}_o$ = log of the predicted strain level (microstrain)

$t_\alpha$ = value of $t$ distribution for n-2 degrees of freedom = 2.131847 for n = 6 with $\alpha = 0.05$

$s$ = standard error from the regression analysis

$n$ = number of samples = 9

$S_{xx}$ = $\sum_{i=1}^{n}(x_i-\bar{x})^2$ (Note: log of fatigue lives)

$x_o$ = log (50,000,000) = 7.69897

$\bar{x}$ = log of average of the fatigue life results

## Strain distribution curve limit and Fatigue ratio limit

The fatigue endurance limit concept has been successfully used to design long-lasting pavements. There is considerable controversy regarding how high the fatigue endurance limit can be to maintain the perpetual pavement before failure can occur and whether one limiting strain value can prevent fatigue cracking from happening. Willis et al. [2011] hypothesized a large percentage of strain occurrences remaining below the laboratory fatigue endurance can extend the pavement's life, but no significant correlation was detected, in terms of the percent needed to be below a certain value.

In the 2003 NCAT pavement test track experiment, eight sections shown in Figure 1 were designed and constructed to study performance responses in pavements within Mechanistic-Empirical pavement design [Willis et al., 2009].Section N8 was found to behave poorly compared to the other section's performance.

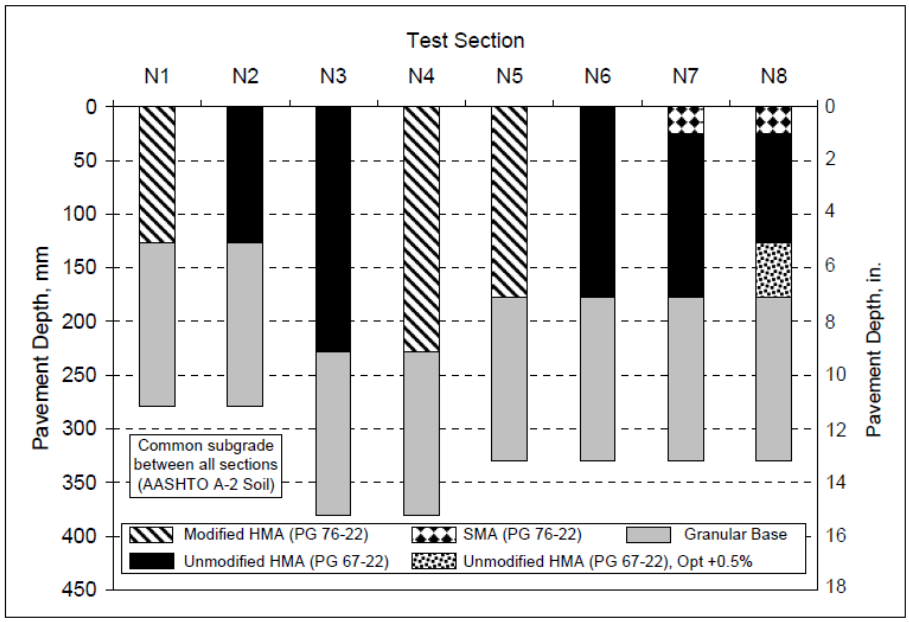


**Figure 1 Structural sections at the 2003 NCAT Test Track**

A cumulative strain distribution was created using the cumulative distribution function based on the strain captured from the field over the entire performance period of the pavement. Once the cumulative distributions were determined for each structural section, the 1st, 99th, and every 5th percentile were identified to develop cumulative distribution plots as shown in Figure 2 [Willis et al., 2009].

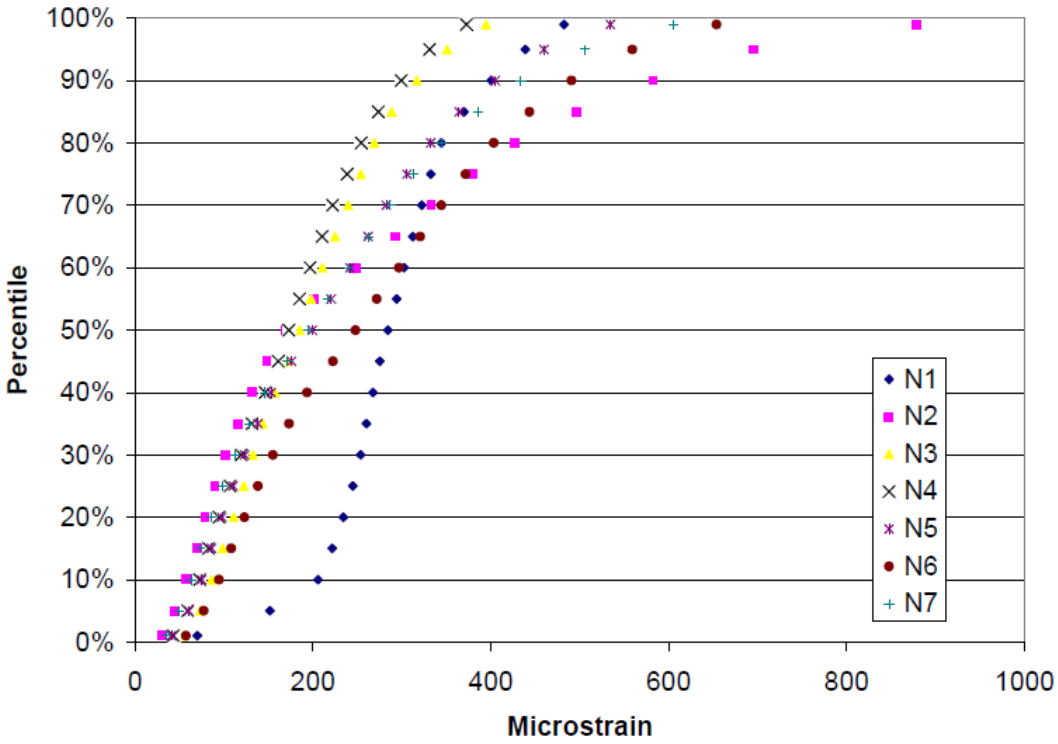


**Figure 2 Cumulative distribution plots for 2003 test sections**

According to Willis et al. [2009], fatigue cracking was seen in five of the seven sections investigated in the NCAT 2003 Test Track experiment: N1, N2, N5, N6, and N7. There was no evidence of fatigue cracking in N3 or N4 sections. The cumulative strain distribution for sections N3 and N4 were compared to the commonly used laboratory fatigue criterion of 70 με or 100 με. It was reported that only around 10% of the strain values for both sections were lower than 70 με. Fewer than 15% of the strain values in section N3 were below 100 με, whereas 25% of the strain values in N4 were less than 100 με. Based on the previous definitions of FEL, it was expected that for a pavement to perform perpetually, 100% of the strain values should be less than the defined FEL. As a result, the authors concluded that measured strains in the field might exceed traditional fatigue thresholds without experiencing fatigue damage on the pavement and thus behaving perpetually. Willis et al. (2009) expanded on the cumulative strain distributions for the 2003 Test Track cycle by evaluating measured strains from the 2006 Test Track cycle. In plotting the cumulative field measured strain distributions, Willis et al. (2009) found that test sections that suffered bottom-up fatigue cracking differentiated from those of test sections that did not crack. A clear breakpoint between the cracked and uncracked section (the hatched area), which starts at around the 45th percentile, can be seen in Figure 3. The sections which exhibited bottom-up fatigue cracking fall to the right; the uncracked sections grouped to the left. Based on this observation, a limiting cumulative strain distribution based on field-measured strains was identified to control bottom-up fatigue cracking.

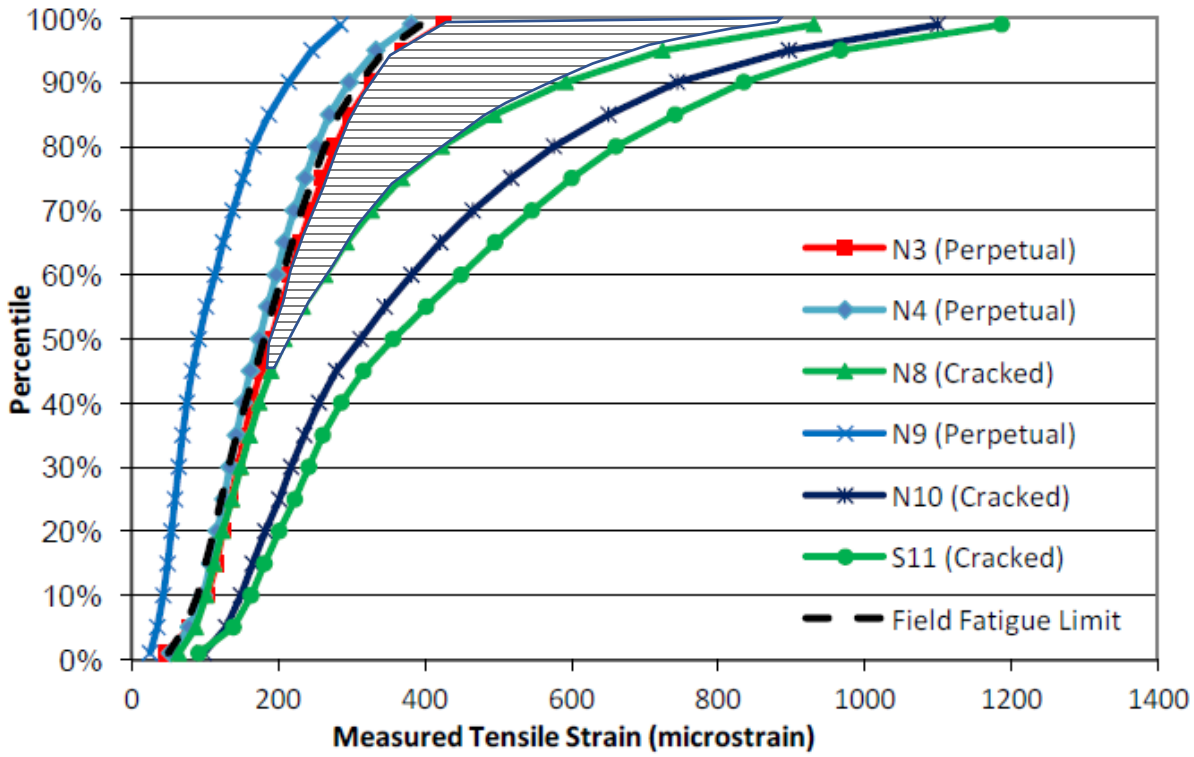


**Figure 3 Cumulative Distributions of Measured Strains, Sections Placed in 2003 and 2006 Willis et al. [2009].**

Making connections between laboratory and field data has been challenging. Therefore, another objective of Willis et al.'s (2009) work was to develop a relationship between laboratory fatigue thresholds found under NCHRP 9-38 and field measured strain. A three-phase analysis was conducted to find the relationship between the laboratory and field fatigue endurance limit values. In the first two phases, the techniques were confined to either the cumulative strain distribution or the strain-temperature correction curves, which found no link between field and laboratory fatigue data. The third phase of comparisons involved using a fatigue ratio to evaluate each section's whole cumulative strain distribution to the fatigue threshold. In order to minimize fatigue cracking during PP design, control points may be set along strain distributions curves based on the fatigue ratio. Table (4), these control points were based on the undamaged sections that produced the greatest fatigue ratio during the 2003 and 2006 Test Track assessments. The fatigue ratio measures how far over the fatigue threshold the strain distribution extends (Willis et al., 2011).

Willis et al.'s (2011) work showed that the concept of fatigue ratio is the most effective way to connect field strains, laboratory fatigue endurance limit, and pavement performance. As shown in Equation 2, the ratio is found by dividing the $n^{th}$ percentile of the cumulative strain distribution by the laboratory determined fatigue threshold, taken as the lower limit of the 95th percentile confidence interval.

$$Rn = \frac{\varepsilon_n}{\varepsilon_f} \qquad \text{Equation 2}$$

where,

Rn = fatigue ratio at the $n^{th}$ percentile

εn = field determined strain at the nth percentile, microstrain

εf = laboratory determined fatigue threshold, microstrain

According to Willis et al. (2009), fatigue ratios determined for NCAT Test Track Sections from 2003 and 2006 showed a clear difference between the fatigue ratios of the sections that failed and those that did not. At the 99th percentile, all fatigue cracked sections had ratios of more than 3.2, while all uncracked sections had less than 2.85.

Willis et al. [2009] proposed maximum control points for the cumulative strain distribution for field-measured strains and the fatigue ratio, based on the test sections that did not experience bottom-up fatigue cracking. The resulting control points for preventing fatigue cracking to achieve PPs are shown in Table 1.

**Table 1 Field-based Fatigue Control Points for Fatigue Crack Prevention [Willis et al., 2009]**

| Percentile | Maximum Fatigue Ratio | Upper Bound Fatigue Limit |
|---|---|---|
| 99% | 2.83 | 394 |
| 95% | 2.45 | 346 |
| 90% | 2.18 | 310 |
| 85% | 1.98 | 282 |
| 80% | 1.85 | 263 |
| 75% | 1.74 | 247 |
| 70% | 1.63 | 232 |
| 65% | 1.53 | 218 |
| 60% | 1.44 | 205 |
| 55% | 1.35 | 193 |
| 50% | 1.27 | 181 |
| 45% | [redacted] | 168 |
| 40% | | 155 |
| 35% | | 143 |
| 30% | | 132 |
| 25% | | 122 |
| 20% | | 112 |

| Percentile | Maximum Fatigue Ratio | Upper Bound Fatigue Limit |
|---|---|---|
| 15% | | 101 |
| 10% | | 90 |
| 5% | | 72 |
| 1% | | 49 |

Willis et al. (2009) provided essential findings in understanding how FEL typically used to design PPs relate to field measured strain and how laboratory-derived FEL can be used in conjunction with field measured strain to minimize fatigue cracking. However, the limiting cumulative strain distribution and fatigue ratios proposed by Willis et al. (2009) were based on strain observed in the field and instrumenting all PPs is not practical. Furthermore, field-measured strains at the bottom of the AC layer differed significantly from tensile strains anticipated by a structural pavement design tool like PerRoad (Tran et al., 2015). As a result, the limiting strain distribution and fatigue ratios based on field-measured strains were updated by Tran et al. (2015) to consider such variations. Willis et al.'s (2009) work utilized strain measured in the field at the bottom of the asphalt pavement layer using embedded strain gauges. As such, there was a need to develop a thresholds that could be used in design. Therefore, Tran et al. (2015) had to then model those same cross-sections in a perpetual pavement design tool to develop a cumulative strain distribution and fatigue ratios using predicted tensile strains. Therefore, there is a need to have a brief discussion on the material inputs which Tran et al. used in PerRoad. Tran et al. (2015) utilized construction survey data to characterize the thickness and associated variability of the total asphalt layer, and aggregate base layer. For each test section, moduli and associated variability of the aggregate base and subgrade were determined from the backcalculation of falling weight deflectometer (FWD) testing, and were modeled as fixed values for all seasons. In PerRoad, the asphalt layers were modeled as one layer using backcalculated modulus. To determine the seasonal moduli, a modulus-temperature relationship was developed for each test section using the mid-depth pavement temperature at the time of FWD testing (note FWD testing was conducted at the track on a monthly basis). Once developed, the relationship was then applied to the average mid-depth hourly pavement temperature recorded throughout the two-year trafficking period. A cumulative distribution of the back-calculated moduli were developed for each test section, and the mid-point of each quintile was used for the seasonal modulus in PerRoad. The coefficient of variation was determined by temperature correcting the moduli to 68° F (20° C), as described by Tran et al. (2015). The load spectra for the trucks at the NCAT Test Track were used for the traffic inputs.

As was the case with the field measured strain distribution presented previously, the predicted cumulative strain distributions clearly distinguish between uncracked (N3 and N4) and cracked sections. There is a gap between the cumulative strain distributions for predicted strain, as shown in Figure 4 where those sections with bottom-up fatigue cracking fall to the right, and the uncracked sections fall to the left of the gap. Sections N3 and N4 were used to define the fatigue limit using predicted strain values, illustrated in the Figure by the solid black line.

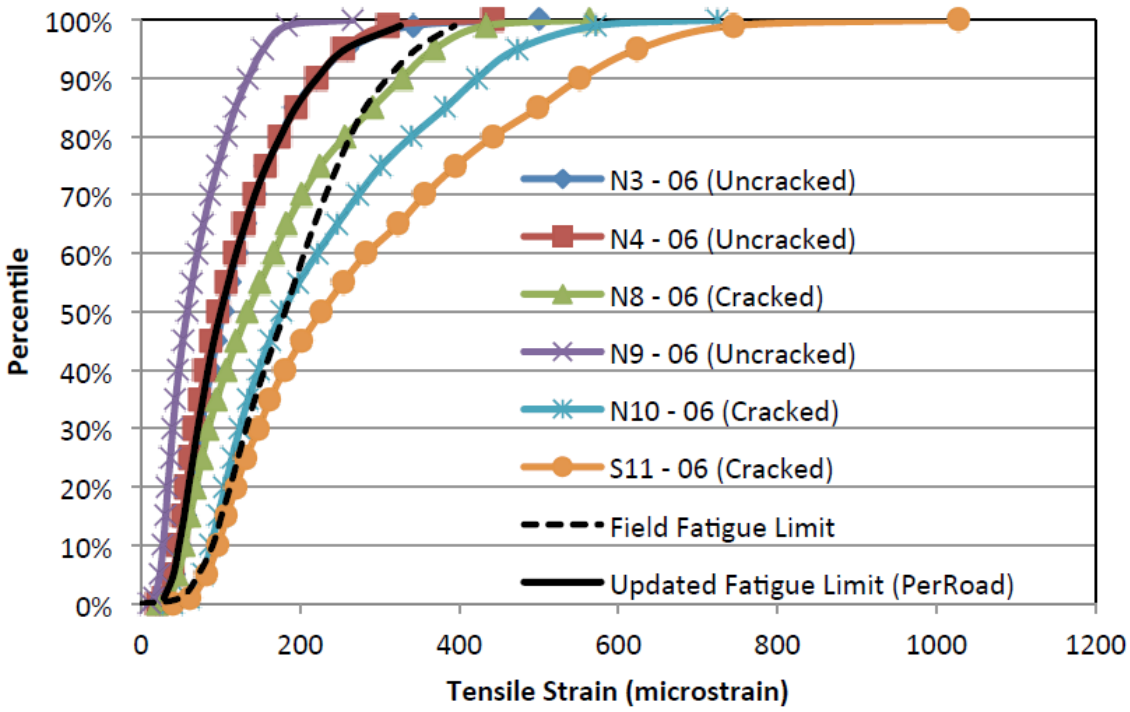


**Figure 4 Cumulative Distributions of predicted tensile strain 2006 sections Tran et al. (2015)**

As a result of the work by Willis et al. (2009) and the refined cumulative strain distribution, Tran et al. (2015) recommended a modified limiting cumulative strain distribution or the modified fatigue ratios, shown in Table 2 to control bottom-up fatigue cracking. The authors recommended that the modified limiting cumulative strain distribution or fatigue ratios be used instead of a single FEL in PP design.

**Table 2 Refined limiting distribution and maximum fatigue ratios for predicted tensile strain [Tran et al., 2015]**

| Percentile | Limiting Design Distribution for Predicted Strain | Maximum Fatigue Ratio for Predicted Strain |
|---|---|---|
| 1% | 29 | |
| 5% | 41 | |
| 10% | 48 | |
| 15% | 54 | |
| 20% | 60 | |
| 25% | 66 | |
| 30% | 71 | |
| 35% | 78 | |
| 40% | 84 | |
| 45% | 91 | |
| 50% | 100 | 0.68 |
| 55% | 110 | 0.74 |
| 60% | 120 | 0.81 |
| 65% | 131 | 0.88 |
| 70% | 143 | 0.96 |

| | | |
|---|---|---|
| 75% | 158 | 1.06 |
| 80% | 175 | 1.18 |
| 85% | 194 | 1.31 |
| 90% | 221 | 1.49 |
| 95% | 257 | 1.73 |
| 99% | 326 | 2.19 |

## Miner's theory

Newcomb (2010) stated that the mechanistic-empirical criteria are the best criteria for designing PPs because it uses a rational engineering analysis of the pavement's response in terms of stresses, strains, and displacements within the pavement's lifetime. For a given loading and material properties, a mechanistic-empirical approach uses mechanical properties to predict pavement response to loading. It applies empirical relationships to relate pavement response to damage or distress. These relationships are referred to as transfer functions, and the outcome of such functions is typically the number of loads to failure (Nf). The degree of damage is defined by dividing the actual traffic load (n) by Nf. Failure is typically described as the point when the damage equals one. The term degree of damage was coined by Miner (1959) to describe metal fatigue.

According to (Ali et al.,1998), Miner's theory is a mathematical formula proposed by Miner as a way to describe metal fatigue; it can be used for combining various levels of damage caused by a combination of traffic loads and environmental factors. According to Miner's theory, structural fatigue damage accumulates over time, and a structure's fatigue life, defined by the maximum load that can be applied before it fails, is finite. Ali et al. (1998) note that it is critical to remember that each load application consumes a small amount of fatigue life. If the number of applied loads is equal to the number permitted, fatigue damage is 1.0, or 100 percent; cumulative values equal to or greater than 1.0 indicate pavement failure McDonald et al., (2012). Miner's hypothesis is described by the following Equation 3 (Miner, 1959):

$$Fatigue\ Damage, D_f = \sum \frac{n_i}{N_i} \quad (3)$$

where

$D_f$ = Cumulative fatigue damage.
$n_i$ = Actual number of load applications for a given set of conditions i.
$N_i$ = Allowable number of load applications to failure for a given set of conditions i.

According to Priest and Timm (2006), creating transfer functions, or performance equation, that connects the calculated pavement response to performance is the most complex component of the design process. The following functions are the typical fatigue and rutting cracking transfer functions for fatigue and rutting:

$$N_f = k_1 \left(\frac{1}{\varepsilon_t}\right)^{k_2} \quad (43)$$

$$N_r = k_3 \left(\frac{1}{\varepsilon_v}\right)^{k_4} \quad (5)$$

Where,

$N_f$ = Number of load cycles until fatigue failure.
$N_r$ = Number of cycles until rutting failure
$\varepsilon_t$ = Horizontal tensile strain at the bottom of the HMA layer
$\varepsilon_v$ = Vertical compressive strain at the top of the subgrade layer
$k_1$, $k_2$, $k_3$, $k_4$ = Empirical constants.

Pavement damage is expressed as a ratio of the actual load to the number of loads allowed to be applied for a given load combination; this is known as the damage ratio, Df. In order to accumulate the damages caused by different equivalent single axle loads (ESALs), Miner's cumulative damage hypothesis is used (Elnashar et al., 2019). In terms of design, the pavement thickness is determined through an iterative process to achieve the number of expected loads (in terms of ESALs) in the design period, equal to or slightly less than the number of loads to failure. For PPs, the goal is to achieve a damage ratio of 0.1 or less, rather than 1.0 for standard pavements (Newcomb, 2010).

## Perpetual Pavement Design Tools

Several tools exist to design PPs. The first tool is the PerRoad software, which is open-source software meant for PP design and uses Monte Carlo simulations to account for the variability within an individual pavement section (Timm et al., 2014). The second tool is AASHTO PMED, which uses more traditional design methods. The third tool is FPS, a program that has been established and recommended for Texas PP (Walubita et al., 2010). All tools employ mechanistic-empirical procedures.

### *PerRoad*

As summarized by Timm et al. (2014), the Asphalt Pavement Alliance commissioned the development of the PerRoad computer application to assist in PP design. The tool enables the designer to add up to five pavement layers and mimic the seasonal impacts of each material, as well as the inherent variability of the building process. The designer must identify critical pavement responses (such as strain or deflection) within the pavement structure and the criteria for the program to work. PerRoad employs load spectra to characterize the expected vehicle loading and allows for entry of traffic volume and expected growth. The application uses a method known as Monte Carlo Simulation to mimic the real-world nature of the pavement. A stochastic approach is employed to predict the distributions of pavement response based on user-defined or default values for the coefficient of variation of pavement layer thicknesses and layer moduli. It considers up to five seasons which can be used to adjust pavement modulus. Construction and material variability are accounted for by utilizing layer thickness and layer moduli variability. Additionally, default values are included for asphalt concrete layers based on the binder's performance grade (PG).

PerRoad allows the user to define the criteria used for PP design. As noted previously, there are two critical locations for PP design, the bottom of the asphalt concrete layer and the top of the subgrade. However, PerRoad allows for the determination of pavement responses at the top, middle, or bottom of any layer except the lowest layer subgrade), for which pavement responses can be determined at the top of the layer. Regarding the criteria, PerRoad allows for a threshold of strain (horizontal, principal, or vertical), stress (horizontal, principal, or vertical), vertical deflection, or horizontal cumulative strain distribution. The latter option was recently included in the program based on the development and validation of the cumulative strain distribution for predicted strains in PerRoad by Tran et al. (2015). This allows the design to follow one of several approaches.

Designs can be based on a singular threshold (strain, stress, or deflection) for a given location within the structure. When a particular threshold is selected, the user can define the target percentile. For example, if the user is targeting 100% of the horizontal tensile strains be below 70 με, 100 percentile would be entered, or in the case of vertical strain at the top of the subgrade, 200 με at the 50th percentile has come to be the targeted threshold (Tran et al., 2015).

Rather than target a certain percentile, the user can use transfer functions to determine the damage ratio. This requires the user to enter the k1 and k2 coefficients values for a transfer function. Only pavement responses exceeding the threshold are included in determining the number of loads to failure when a transfer function is selected. For PP design, the damage ratio should be 0.10 or less.

When horizontal strain is used as a criterion to guard against bottom-up fatigue cracking, the user may define a cumulative strain distribution. The user also can use a default distribution developed by Tran et al. (2015) and as shown in Table 5. Alternatively, the user may enter a FEL to mitigate bottom-up fatigue cracking based on the concept of the fatigue ratio, defined by Willis et al. (2009) and refined for predicted strain distribution by Tran et al. (2015). When the FEL is entered, the program uses the maximum fatigue ratios recommended by Tran et al. (2015) and shown in Table 5 to determine a strain distribution by multiplying the FEL by the maximum fatigue ratio at a given percentile. The predicted strain distribution is then compared to the selected or calculated targeted distribution.

### *Mechanistic-Empirical Pavement Design Guide (MEPDG)*

The NCHRP 1-37A project developed the MEPDG and the AASHTOWare PMED software. Where the designers may enter layer material characteristics and traffic characteristics in three levels, the program forecasts specified pavement distresses and smoothness based on these input parameters. The MEPDG performance was calibrated using Long Term Pavement Performance (LTPP) field pavement performance data. The LTPP database collects data on design, material characteristics, climate, traffic, and performance from hundreds of flexible and rigid pavement projects across the country.

The PMED software is an iterative procedure where the designer adjusts the pavement thickness and/or pavement materials until predicted performance at the end of the design period meets the designers target performance thresholds. The software can be used for PP design in various ways.

First, the user has the option to enter a FEL. However, the user is cautioned the performance models were not calibrated in this manner. When this option is selected, only predicted strain values exceeding the FEL are considered in the calculation of damage and pavement performance. Next, the user may design based on a longer performance period. Perpetual pavements are often referred to as long-life pavements, as such, one option is to use a design life of 50 years, as opposed to the typical 20 year period for a conventional design.

Lastly, AASHTO has made the predicted tensile strain at the bottom of the asphalt layer, and the vertical strain at the top of the subgrade available as text files in the output files generated at the completion of a design. As part of their study, Islam et al. (2017) compared strain results from PerRoad with strain from AASHTOWare PMED software. They reported predicted tensile strain from PMED was much less than those predicted in PerRoad.

### *Flexible Pavement System (FPS) Software*

According to Walubita et al. (2010), the FPS (Version 21W) is a computer analysis program used in Texas to facilitate PP design. It is frequently used by the Texas Department of Transportation (TxDOT) to design an overlay or pavement thickness, compute pavement stress-strain response, and predict pavement life based on mechanistic-empirical methods for rutting and fatigue. The back-calculated FWD modulus of the subgrade layer is a vital material characterization input for this design technique, which relies on a linear-elastic analytic system. Table 3 shows recommended PP material property design values at 77F and uses the heaviest expected load as the design load. First, a trial pavement structure is developed using the given loading and material properties, and a thickness is designed. Second, design checks, including performance prediction, are performed. The FPS system includes a built-in performance feature. Based on maximum horizontal strains at the bottom of AC layers and maximum vertical compressive strains not exceeding 70 με and 200 με respectively (Walubita et al., 2010). a mechanistic design assessment is carried out to ensure that a project's mechanistic responses are adequate.

**Table 3 Proposed Future Texas PP Design Moduli Values at 77 °F. (Walubita et al., 2010).**

| Layer/Material TxDOT | 2004 Spec Item | Proposed Design Modulus Value (ksi) | Recommended Design Modulus Range (ksi) | Poisson's Ratio |
|---|---|---|---|---|
| PFC (optional) | Item 342 | 350 | 300 – 450 | 0.30 |
| SMA | Item 346 | 600 | 500 – 850 | 0.35 |
| RRL – ¾″ Superpave | Item 344 | 800 | 600 – 1200 | 0.35 |
| RRL – Type B | Item 341 | 800 | 700 – 1300 | 0.35 |
| RBL– Type C or ½″ Superpave | Item 341 | 500 | 400 – 650 | 0.35 |
| Base/foundation | Items 247, 260, 263, 275, & 276 | Min 35 | 35 – 150 | 0.30 – 0.35 |
| Subgrade | | Should be back-calculated from existing or adjacent structure | - | 0.40 – 0.45 |

## Highly Polymer Modified (HPM) Asphalt

Polymer-modified asphalt binders have been used to enhance the performance of asphalt mixtures for many years [Diefenderfer et al., 2018]. It is usual practice to add a polymer to the binder, such as styrene-butadiene-styrene (SBS) copolymer, which enhances the high-temperature binder performance grade (PG). Historically, polymer-modified binder dosages have seldom surpassed 3.5 percent polymer (by weight) to prevent production difficulties such as jammed binder pumps or decreased mixture workability. High polymer modified (HPM) asphalt mixes contain approximately 7.5% of styrene butadiene styrene (SBS) modifier. The first HPM mix, was developed by Kraton Corporation (Kraton™ D0243) and is referred to as highly modified asphalt (HiMA), other companies have since developed similar formulations with the

same or similar dosage rates of SBS to achieve HPM binders. HPM mix costs more than conventional AC but has been shown to significantly improve resistance to rutting, fatigue cracking, and moisture damage, thus leading to better pavement performance and longer pavement life (Timm et al., 2013; Sargand, et al., 2015; Chen et al., 2018; Habbouche et al., 2019).

NCAT Test Track Structural and Laboratory Evaluation of HiMATimm et al. [2012] noted that despite the optimistic findings of the laboratory and simulation work on the HiMA formulation, field testing was necessary to understand the in-situ characteristics of the formulation fully. It is vital to examine if HiMA behaves like a conventional material under truck loading and falling weight deflectometer (FWD) loading and whether it can be represented using existing methodologies (such as layer-based elasticity) inside mechanics-based design frameworks. In 2009, a full-scale experimental test section was funded by Kraton Performance Polymers, LLC and constructed at the National Center for Asphalt Technology (NCAT) Test Track to evaluate HiMA relative to a control section featuring conventional asphalt mixes. The NCAT Test Track is an accelerated pavement testing facility located in Opelika, AL. The 1.7 mile oval track is a closed facility and features 200-ft (61-m) long test sections in which full-scale construction and evaluation of pavement test sections can be evaluated under accelerated traffic loading. Traffic loads are applied over a two-year period (as part of a 3-year test cycle) via five triple trailer trucks traveling 45 mph (72 km/h). These trucks exceed the gross vehicle weight allowed on open roadways which accelerate traffic loads and thus, pavement damage by applying 10 million equivalent single axle loads (ESALs) in the two-year period.

Both the control test section, section S9, and the HiMA test section, N7 were constructed as a part of the 2009 NCAT Test Track cycle, as such, both were subjected to the same traffic loads. Comparisons were drawn between the two test sections in regards to in-situ resilient modulus, measured tensile strain at the bottom of the asphalt layer, measured pavement performance, laboratory determined material properties, and laboratory performance testing. The HiMA section was constructed at 5.75" (146 mm) thick, 1.25" (32 mm) thinner than the control section to determine if HiMA materials could deliver the same or better performance. Both sections were constructed over a 6-inch granular base on top of compacted natural subgrade. The cross-sections are provided in the Table below.

**Table 4 NCAT Test Track HiMA Study: Layer Thickness and Binder Grade by Test Section (*after* Timm et al., 2013)**

| Layer | N7: HiMA | S9: Control |
|---|---|---|
| Surface | 1.25 in (3.18 cm)<br>PG 88-22 | 1.25 in (3.18 cm)<br>PG 76-22 |
| Intermediate | 2.25 in (5.72 cm)<br>PG 88-22 | 2.75 in (6.99 cm)<br>PG 76-22 |
| Base | 2.25 in (5.72 cm)<br>PG 88-22 | 3.00 in (7.62 cm)<br>PG 67-22 |

Regarding laboratory testing, the Timm et al. (2013) reported the HiMA asphalt base layer showed greater fatigue resistance than the control base layer in terms of S-VECD and beam fatigue testing. The researchers reported Hamburg Wheel Tracking Test (HWTT) showed statistically similar rut depth results, with mixes in both sections resulting in values well below the commonly used threshold of 0.5 in (12.5 mm).

Falling weight deflectometer (FWD) testing was conducted three to four times per month, throughout the trafficking period. FWD data were backcalculated using EVERCALC 5.0 and surveyed layer thicknesses modeled in a three layer pavement system (AC over aggregate base over subgrade). The backcalculated AC moduli were corrected based on the measured mid-depth pavement temperature at the time of testing to a reference temperature of 50F (10C), 68F (20C), and 110F (43C) to enable a comparison between the two test sections, as shown in Figure 5 below. Although the mean backcalculated moduli appear to be similar at each temperature, statistical tests showed they were statistically different, with the control section having higher moduli at 50F (10C) and 68F (20C), and the HiMA section having a great modulus at 110F (43C) (Timm et al., 2013).

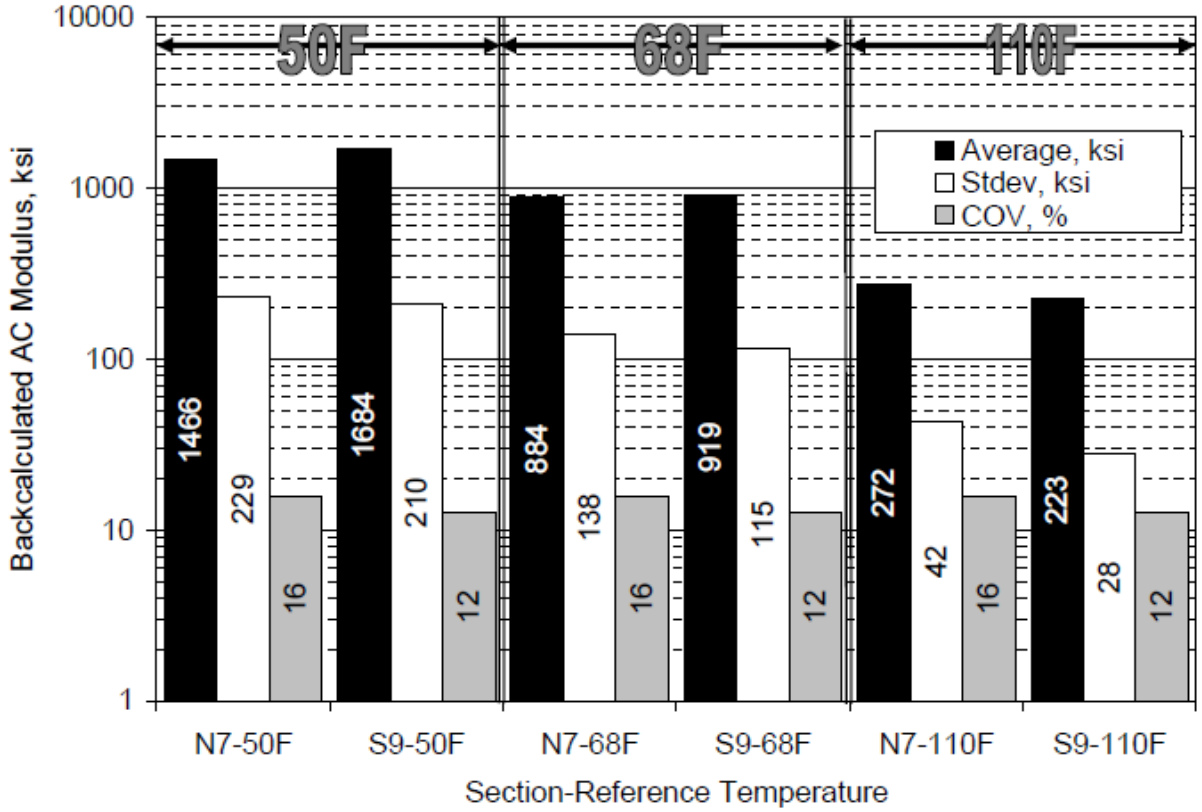


**Figure 5 NCAT Test Track HiMA Study: Backcalculated AC Modulus Corrected to Reference Temperatures (Timm et al., 2013)**

Pavement responses (tensile strain at the bottom of the asphalt layer in the longitudinal and transverse directions, pressure at the top of the aggregate base layer, and pressure at the top of the subgrade) were measured at the bottom in each section on a weekly basis, for three truck passes of each truck. Regression equations were developed for longitudinal strain as a function of mid-depth pavement temperature, from which tensile strain was then temperature corrected in a fashion similar to the backcalculated moduli, as shown in Figure 6. At 50F (10C) and 68F (20C) the HiMA section (N7) had statistically greater strain than the control section (S9), however there was no statistical difference at 110F (43C). Timm et al. 2013 concluded the increase in backcalculated AC modulus of the HiMA section over the control section at the high temperature was sufficient to overcome the 1.25-inch (3.18-cm) difference in thickness.

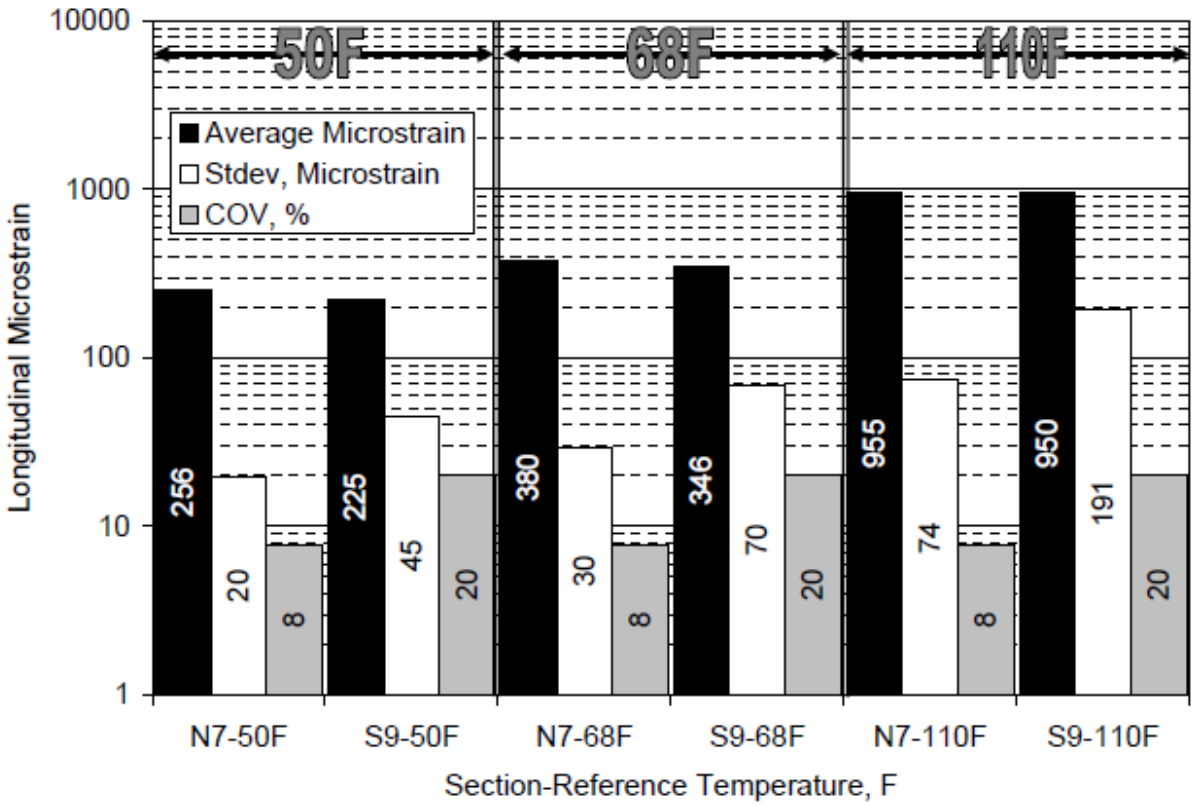


**Figure 6 NCAT Test Track HiMA Study: Longitudinal Tensile Strain Temperautre Corrected to Reference Temperatures (Timm et al., 2013).**

An earlier report by Timm et al. (2012) on the HiMA study developed a transfer function from laboratory test results for the HiMA and conventional asphalt base mixes. In the 2013 report, Timm et al. applied the average measured tensile strain at the 68F (20C) to the transfer functions to predict the number of cycles to failure by fatigue, as shown in Table 5. The researchers reported that despite the statistically higher strain value in the HiMA section, the HiMA section has improved fatigue characteristics which resulted in predicted fatigue life nearly 17 times greater section than the control section.

**Table 5: NCAT HiMA Study: Predicted Fatigue Life at 68F(20C) (Timm et al., 2013)**

| Test Section | Avg Measured Tensile Strain at 68F (20C) | Cycles to Failure at 68F (20C) Using Laboratory-Determined Transfer Function |
|---|---|---|
| N7 (HiMA) | 380 | 6,515,371 |
| S9 (Control) | 346 | 367,056 |

Pavement performance was measured in terms of international roughness index (IRI), rutting in each wheelpath and manual crack mapping. Timm et al. reported no cracking in either section at the end of the two-year test cycle. At the end of the trafficking period, Timm et al. reported 2.1 mm of rutting in the HiMA test section compared to 7.2 mm of rutting in the control section. IRI in the HiMA test section was found to be greater than the control test section, however Timm et al., noted the higher IRI values in the HiMA section were driven by the first 75 feet of the test section which are related to constructing the transition from one section to the next

and had IRI measurements between 170 and 220 in/mile at the end of the test cycle. The remainder of the HiMA test section had IRI values between 60 and 75 in/mile at the end of the two-year traffic cycle.

### *Structural Layer Coefficient of HPM Asphalt Mixtures*

The flexible pavement design procedure in the current ODOT Pavement Design Manual (ODOT PDM, 2022) is based on the 1993 AASHTO Guide for Design of Pavement Structures (AASHTO, 1993), which is a revised version of the 1962 (and subsequently revised 1972 and 1986) AASHO Pavement Design procedure. The AASHTO design method is an empirical procedure based on statistical analysis of the pavement performance at the original AASHO Road Test (1958-1960 at Ottawa, Illinois). The pavement structure required for a given design traffic loading, subgrade soil conditions and environment is expressed as a Structural Number (SN).

Structural Number (SN) can be converted to thickness of flexible pavement layers through a combination of structural layer coefficients related to the type of material being used in each layer of the pavement structure and thickness of each pavement layer.

$$SN = a_1D_1 + a_2D_2 + a_3D_3 + \ldots \quad (6)$$

where

$a_1, a_2, a_3, \ldots$ = structural coefficient related to the type of material being used in each layer the pavement structure; and

$D_1, D_2, D_3, \ldots$ = thickness of flexible pavement layers

Structural layer coefficient (or structural coefficient) is defined as “a measure of the relative ability of a material to function as a structural component of a flexible pavement structure and used to convert a design structural number to actual thickness” (ODOT PDM, 2022). Higher AC layer structural coefficient means a corresponding reduction of AC layer thickness, thus saving initial pavement construction cost.

Statistical analysis based on the performance of the AASHO Road Test showed that the structural layer coefficient ranged from 0.33 to 0.83 for the asphalt concrete (AC) layers in the original Road Test (Timm et al. 2014). AASHO recommended a structural coefficient of 0.44 for AC layers, but also recommended each state calibrate its own structural coefficients based on its regional soil, environment, and materials.

Subsequent research (Van Til, et al., 1972) used layered elastic theory to expand the applicability of the empirical design beyond the traffic, soil and environment at the original AASHO Road Test. Figure 7 shows a relationship derived using layered elastic theory to relate AC layer structural coefficient with its resilient (elastic) modulus.

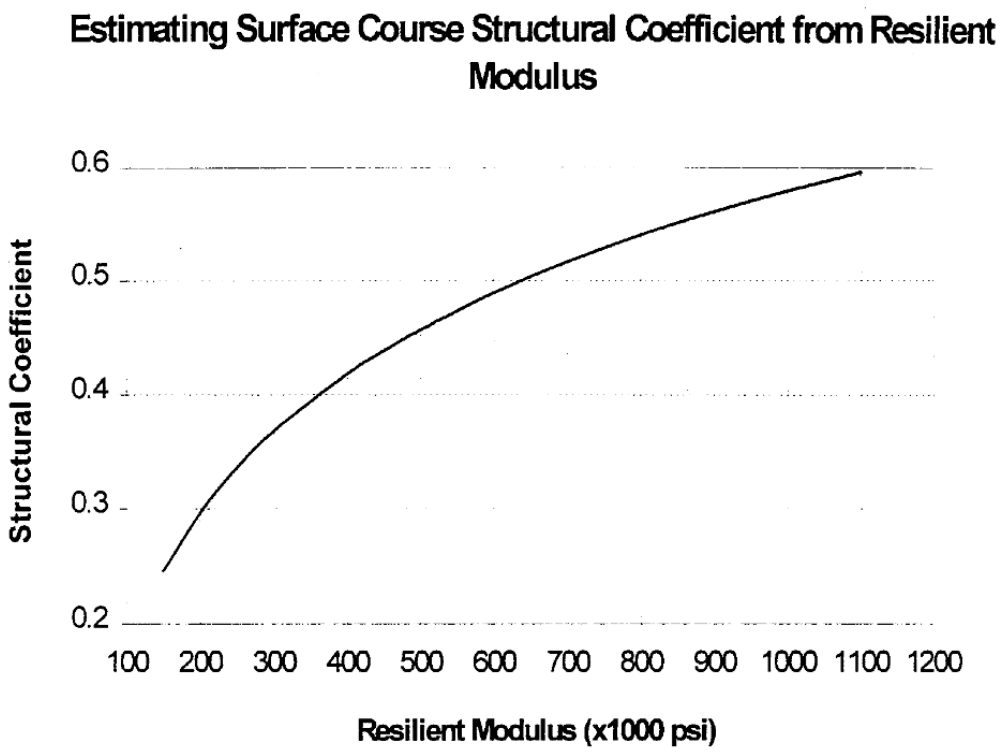


**Figure 7 Estimating AC Structural Coefficient from Resilient Modulus (source: Van Til, et al, 1972)**

Gomez & Thompson (1983) used ILLI-PAVE, a stress-dependent finite element method, to determine the structural layer coefficients of various paving materials, and concluded that a set of constant structural coefficients cannot be found because the values vary with respect to: 1) layer thickness, 2) material type, 3) material quality, 4) layer location (base, subbase), 5) traffic level, and 6) limiting criterion (stress, strain, deflection, etc.). They recommended that instead of calibrating structural layer coefficients, a mechanistic-based approach be used to develop flexible pavement design procedures.

Von Quintus & Killingsworth (1998) showed laboratory-measured resilient moduli differ significantly from moduli back-calculated from pavement deflections. Therefore, adjustment factors must be applied to the laboratory measured values for predicting the structural response of pavement structures to wheel loads.

Bahia et al. (2000) indicated most AC materials have similar resilient moduli values and deriving new layer coefficient from the resilient modulus test result is rather questionable, because the position of the material in the structure and the mode of distress could influence the relation between the layer coefficient and the resilient modulus. It was recommended that layer coefficients be derived based on a collection of adjustment factors including damage functions, stress and temperature variations that affect pavement performance. These factors will adjust the layer coefficient based on how a particular mixture performs in comparison to the reference material. (Bahia, 2000).

Many states initially chose to adopt an AC layer structural coefficient of less than 0.44. For example, prior to 1999, ODOT used a value of 0.35 for all AC materials. However, as AC material specifications and construction methods have seen significant improvements since the early

1960s, including but not limited to Superpave mix design, performance grade (PG) binder specifications, in-situ density QA/QC, …, etc., a number of states have calibrated state-specific structural coefficients (Alabama, Florida, New Hampshire, Ohio, Washington, Wisconsin, ...). Since ~2000, ODOT has adopted a structural layer coefficient of 0.43 for all AC surface and intermediate course (items 424, 441, 442, 443, 823, 826, 859, 880-top 3" (76 mm)), and 0.36 for AC base course (items 301, 302, and 880-below top 3" (76 mm)). This was based on a research study (Chou et al., 1998) that showed back-calculated resilient modulus from FWD and actual pavement performance in Ohio warranted higher AC layer structural coefficients. This increase in structural layer coefficient resulted in thinner pavements and significant construction cost savings.

As shown in Figure 8 not all states use the same AC layer structural coefficients. Only a handful of states have switched to Mechanistic-Empirical design methods and no longer use AC structural coefficient.

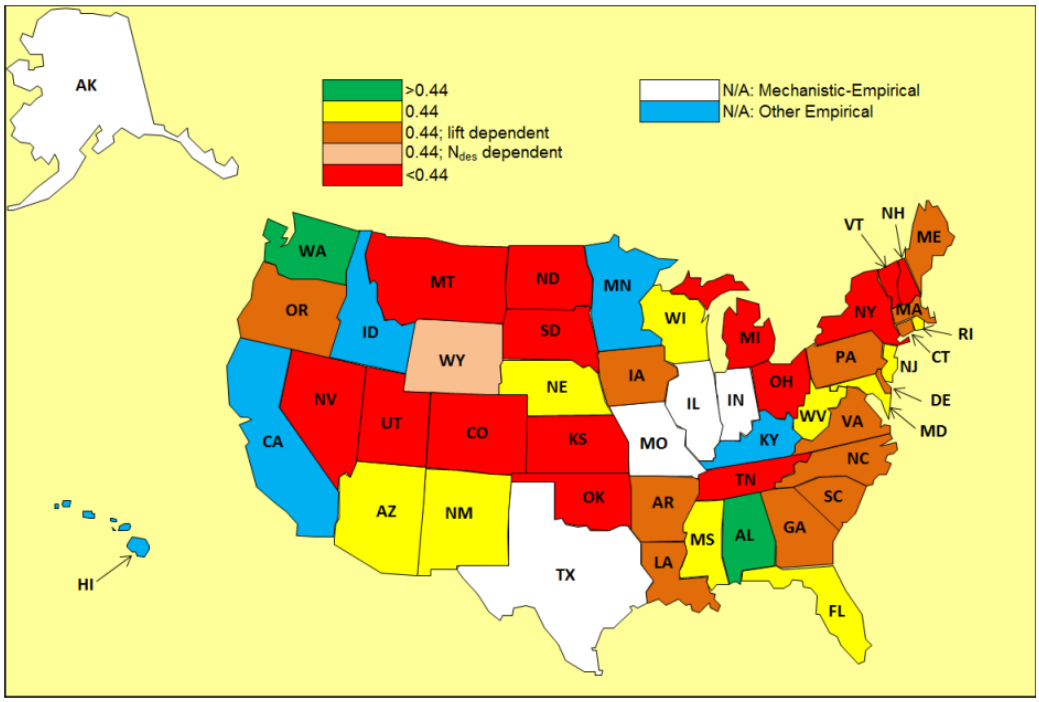


**Figure 8 AC Layer Structural Coefficient Used by Different States (source: Davis & Timm, 2011)**

Methodologies used to calibrate AC layer structural coefficients include deflection-based, pavement performance-based, laboratory characterization, and MEPDG-based (Rohde, 1994; Chou et al., 1999; Bahia et al., 2000; Pologruto, 2006; Peters-Davis & Timm, 2009; Li et al. 2011; Timm et al. 2014; Sargand et al., 2016; Habbouche et al., 2019; Nemati et al., 2021).

Recently, Habbouche et al. (2020) showed HPM mix and non-HPM mix have similar lab-measured dynamic modulus, but HPM mix has significantly better rutting and cracking performance both in the laboratory and in the field. Habbouche et al. (2020) recommended using $a_1$ = 0.54 for HPM mix layers in Florida. For context, Timm, et al. (2014) recommended $a_1$ = 0.54 for all AC layers in Alabama; and unpublished findings from NCAT suggest using $a_1$ = 0.77 for HPM asphalt layers.

References

Zeiada, W. A., B. S. Underwood & K. E. Kaloush (2017) Impact of asphalt concrete fatigue endurance limit definition on pavement performance prediction, International Journal of Pavement Engineering, 18:11, 945-956, DOI: 10.1080/10298436.2015.1127372

Carpenter S. H. K. Ghuzlan, and S. Shen, "Fatigue Endurance Limit for Highway and Airport Pavements," Transportation Research Record: Journal of the Transportation Research Board, No. 1832, TRB, National Research Council, Washington, DC, pp. 131-138, 2003

Nishizawa, T., Shimeno, S., and Sekiguchi, M. (1996). "Fatigue analysis of asphalt pavements with thick asphalt mixture layer." Proc., 8th Int. Conf. on Asphalt Pavements, Vol. 2, Univ. of Washington, Seattle, WA, 969–976.

Monismith, C. L. and D. B. McLean, "Technology of Thick Lift Construction: Structural Design Considerations" Proceedings, Association of Asphalt Paving Technologists, Vol. 41, pp. 258-304, 1972.

Prowell, B., E.R. Brown, R.M. Anderson, J.S. Daniel, A.K. Swamy, H. Von Quintus, S. Shen, S.H. Carpenter, S. Bhattacharjee, and S. Maghsoodloo, Validating the Fatigue Endurance Limit for Hot Mix Asphalt, NCHRP Report 646, NCHRP 9-38 Project, National 8 Cooperative Highway Research Program, Washington, DC, 2010.

Walubita, L.F., W. Liu, T. Scullion, and J. Leidy. "Modeling Perpetual Pavements Using the Flexible Pavement System (FPS) Software," Transportation Research Board 2008 Annual Meeting, CD-ROM.

Von Quintus, H.L. "Hot-Mix Asphalt Layer Thickness Designs for Longer-Life Bituminous Pavements," Transportation Research Circular, Number 503, 2001, pp 66-78.

Thompson, M., and S. Carpenter, "Considering Hot-Mix-Asphalt Fatigue Endurance Limit in Full-Depth Mechanistic-Empirical Pavement Design," International Conference on perpetual pavement, Ohio 2006.

Advanced Pavement Laboratory, National Cooperative Highway Research Program Project

NCHRP 9-44, Research Plan, Washington, DC, Nov. 2008.

Timm, D. H., Robbins, M. M., Willis, J. R., Tran, N., & Taylor, A. J. (2012). Field and laboratory study of high-polymer mixtures at the NCAT test track interim report. National Center for Asphalt Technology (NCAT) Report 12-08, Auburn, AL.

Thompson, M. R., & Carpenter, S. H. (2006, September). Considering hot-mix-asphalt fatigue endurance limit in full-depth mechanistic-empirical pavement design. In Proc., International Conference on Perpetual Pavement.

Willis, J. R., Timm, D. H. Field-Based Strain Thresholds for Flexible Perpetual Pavement Design. Report No. 09-09. National Center for Asphalt Technology, Auburn University, Auburn, AL, 2009.

Tran, N., Robbins, M. M., Timm, D. H., Willis, J. R., & Rodezno, C. (2015). Refined limiting strain criteria and approximate ranges of maximum thicknesses for designing long-life asphalt pavements.

Willis, J. R., Timm, D. H., Taylor, A. J., Tran, N. H., & Kvasnak, A. (2011). Correlating laboratory fatigue endurance limits to field-measured strains. Journal of the Association of Asphalt Paving Technologists, 80.

Wu, Z., Z. Q. Siddique, and A. J. Gisi. "Kansas Turnpike – An Example of Long Lasting

Asphalt Pavement". Proceedings International Symposium on Design and Construction of

Long Lasting Asphalt Pavements. National Center for Asphalt Technology, Auburn, Pp. 857-

876, AL 2004

Sun, L., & Hudson, W. R. (2005). Probabilistic approaches for pavement fatigue cracking prediction based on cumulative damage using Miner's law. Journal of engineering mechanics, 131(5), 546-549.

Ali, H. A., & Tayabji, S. D. (1998). Mechanistic Evaluation of Test Data From LTPP Flexible Pavement Test Sections, Vol. I (No. FHWA-RD-98-012). United States. Federal Highway Administration.

Miner, M.A. 1959. Estimation of Fatigue Life with Emphasis on Cumulative Damage. Metal Fatigue, edited by Sines and Wiseman, McGraw Hill, pp. 278-89.

Robbins, M. M., Nam Tran, P. E., & Rodezno, C. (2014). Flexible Pavement Design–State of the Practice NCAT Report 14-04.

Sargand, S., Khoury, I., Jordan, B., Scheer, M., & Cichocki, P. (2015). Implementation and thickness optimization of perpetual pavements in Ohio (No. FHWA/OH-2015/17). Ohio. Dept. of Transportation. Office of Statewide Planning and Research.

Islam, Shuvo; Sufian, Abu; Hossain, Mustaque; Miller, Richard; Leibrock, Christopher (2018). Mechanistic-Empirical design of perpetual pavement. Road Materials and Pavement Design, (), 1–14. doi:10.1080/14680629.2018.1546218

Johny Habbouche, Elie Y. Hajj, Peter E. Sebaaly & Murugaiyah Piratheepan (2020). A critical review of high polymer-modified asphalt binders and mixtures. International Journal of Pavement Engineering, 21:6, 686-702, DOI: 10.1080/10298436.2018.1503273

Diefenderfer, S. D., Diefenderfer, B. K., & Bowers, B. F. (2018). Evaluation of highly polymer-modified asphalt mixtures: Phase I (No. FHWA/VTRC 18-R14). Virginia Transportation Research Council.

Timm, D. H., Robbins, M. M., Willis, J. R., Tran, N., & Taylor, A. J. (2012). Field and laboratory study of high-polymer mixtures at the NCAT test track interim report. National Center for Asphalt Technology: Auburn, AL, USA.

Sargand, S., & Figueroa, J. L. (2010). Monitoring and modeling of pavement response and performance: task A, Ohio (No. FHWA/OH-2010/3A). Ohio Research Institute for Transportation and the Environment.

Retrepo-Velez, A. M. (2011). Long-term performance of asphalt concrete perpetual pavement WAY-30 project. (Unpublished MS thesis), Ohio University, Athens, OH.

Sargand, S., Figueroa, J. L., Edwards, W., & Al-Rawashdeh, A. S. (2009). Performance assessment of warm mix asphalt (WMA) pavements (No. FHWA/OH-2009/08). Ohio Research Institute for Transportation and the Environment.

Hernandez, J. A. (2010). Evaluation of the response of perpetual pavement at accelerated pavement loading facility: Finite element analysis and experimental investigation. (Unpublished MS thesis), Ohio University, Athens, OH.

Cichocki, P. F. (2015). Application of Highly Modified Asphalt (HiMA) Binders in Implementation and Thickness Optimization of Perpetual Pavements in Ohio (Doctoral dissertation, Ohio University).

Scheer, M. J. (2013). Impact of Pavement Thickness on Load Responses of Perpetual Pavement. (Unpublished MS thesis), Ohio University, Athens, OH.

Witczak, M., Mamlouk, M., Souliman, M., Zeiada, W. (2013). Laboratory Validation of an Endurance Limit for Asphalt Pavements. NCHRP Report 762, Transportation Research Board, Washington, D.C. (https://www.trb.org/Main/Blurbs/170034.aspx)

# APPENDIX B: DCP TESTING

Full-depth cores with diameter of 4 inches were removed by the contractor at the completion of all pavement layers in the structure at 5 locations within each test section. Dynamic cone penetrometer (DCP) testing was conducted by the ORITE research team through full depth core holes. Test locations are provided in Table 21. The section identification below is shown as the "section number.core number", i.e. section 1.2 is section 1, core number 2.

DCP raw data and filtered data is provided in terms of penetration rate (blows/depth) for the aggregate base, stabilized subgrade and unstabilized subgrade. The raw data was filtered as described in Wu and Sargand (2007).

Data collected 11/15/22

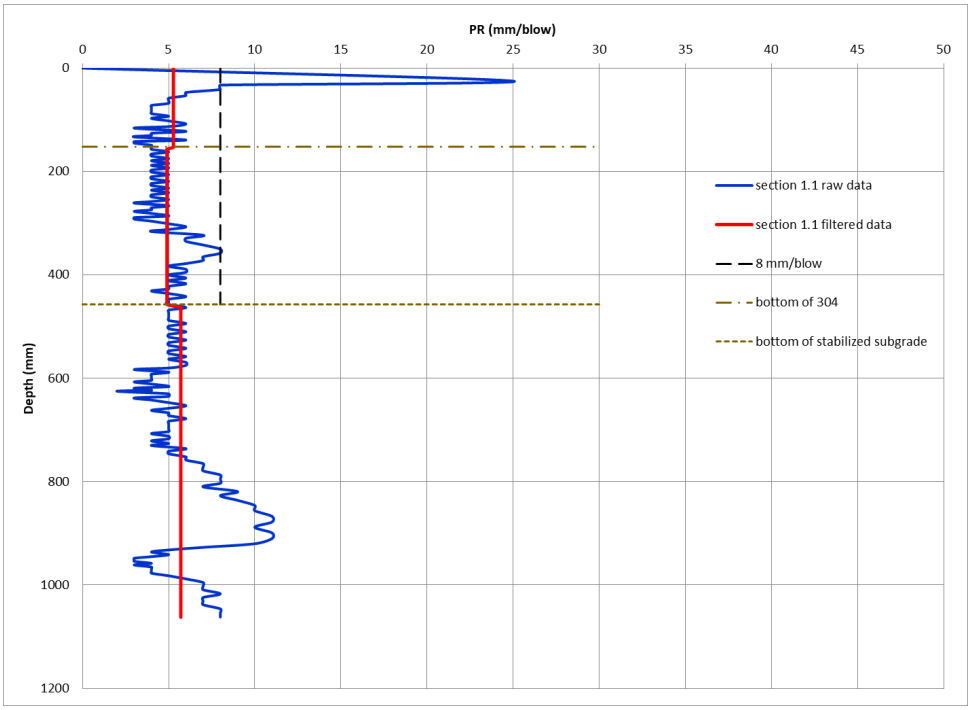

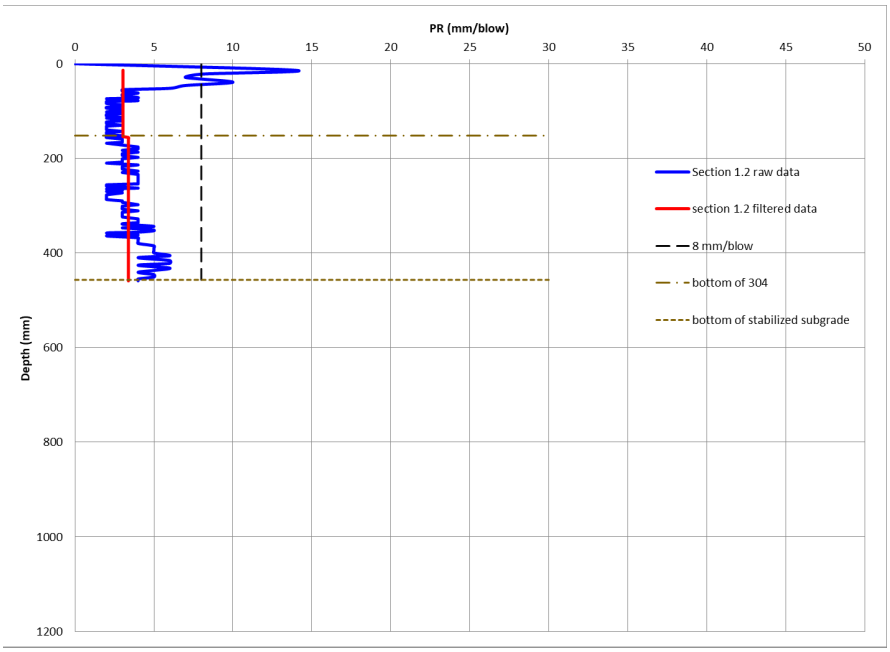
PR (mm/blow)
0
5
10
15
20
25
30
35
40
45
50
Depth (mm)
0
200
400
600
800
1000
1200
Section 1.2 raw data
section 1.2 filtered data
8 mm/blow
bottom of 304
bottom of stabilized subgrade

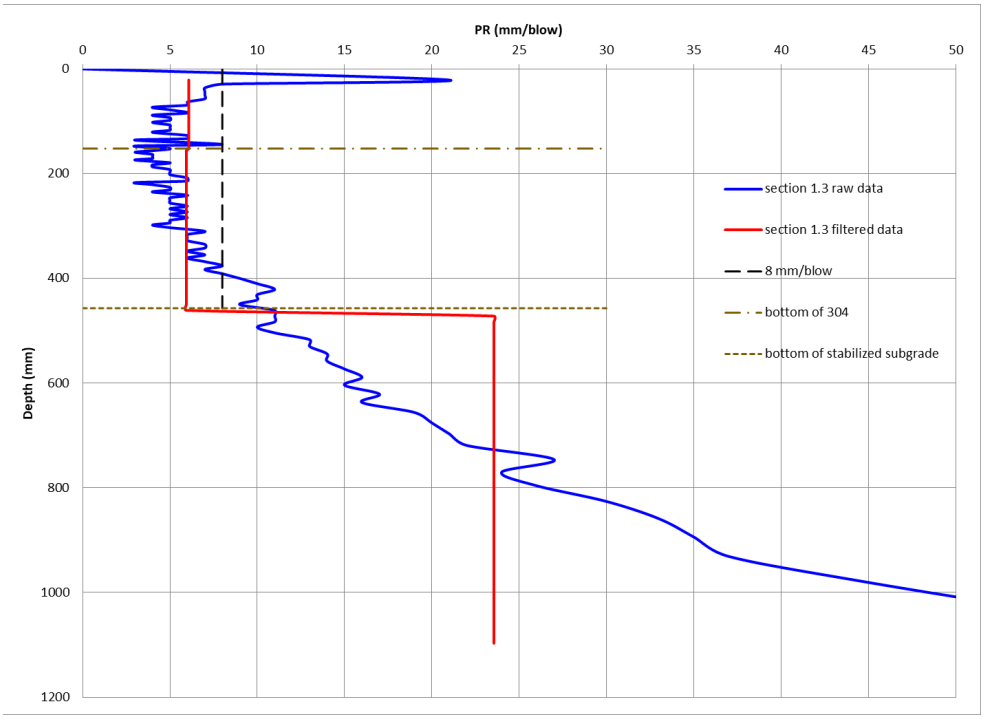
PR (mm/blow)
0
5
10
15
20
25
30
35
40
45
50
Depth (mm)
0
200
400
600
800
1000
1200
section 1.3 raw data
section 1.3 filtered data
8 mm/blow
bottom of 304
bottom of stabilized subgrade

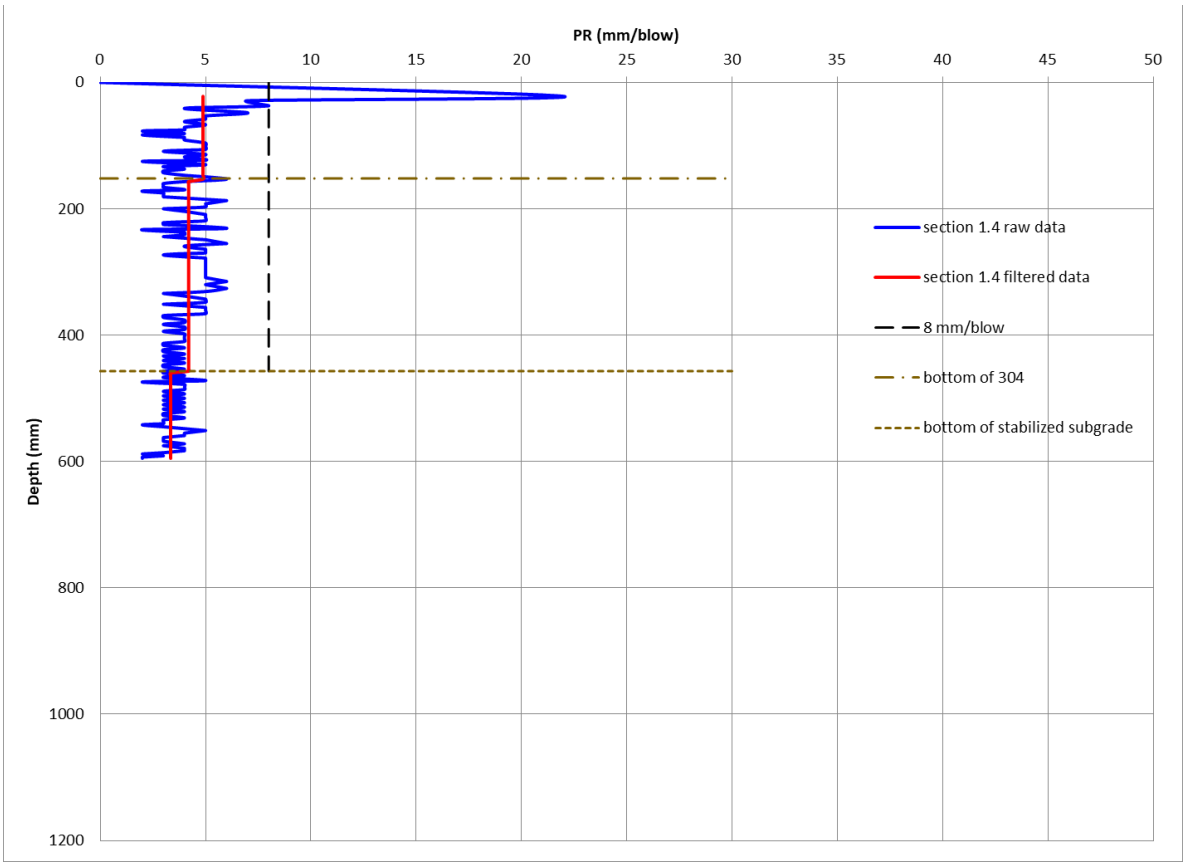
PR (mm/blow)
0
5
10
15
20
25
30
35
40
45
50
Depth (mm)
0
200
400
600
800
1000
1200
section 1.4 raw data
section 1.4 filtered data
8 mm/blow
bottom of 304
bottom of stabilized subgrade

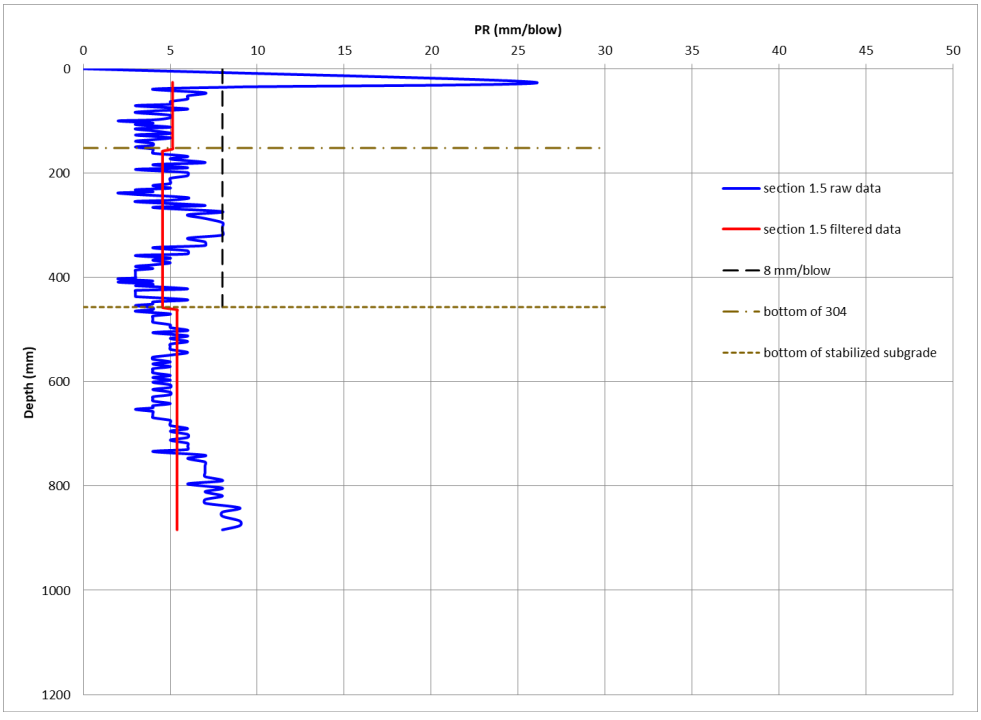
PR (mm/blow)
0
5
10
15
20
25
30
35
40
45
50
Depth (mm)
0
200
400
600
800
1000
1200
section 1.5 raw data
section 1.5 filtered data
8 mm/blow
bottom of 304
bottom of stabilized subgrade

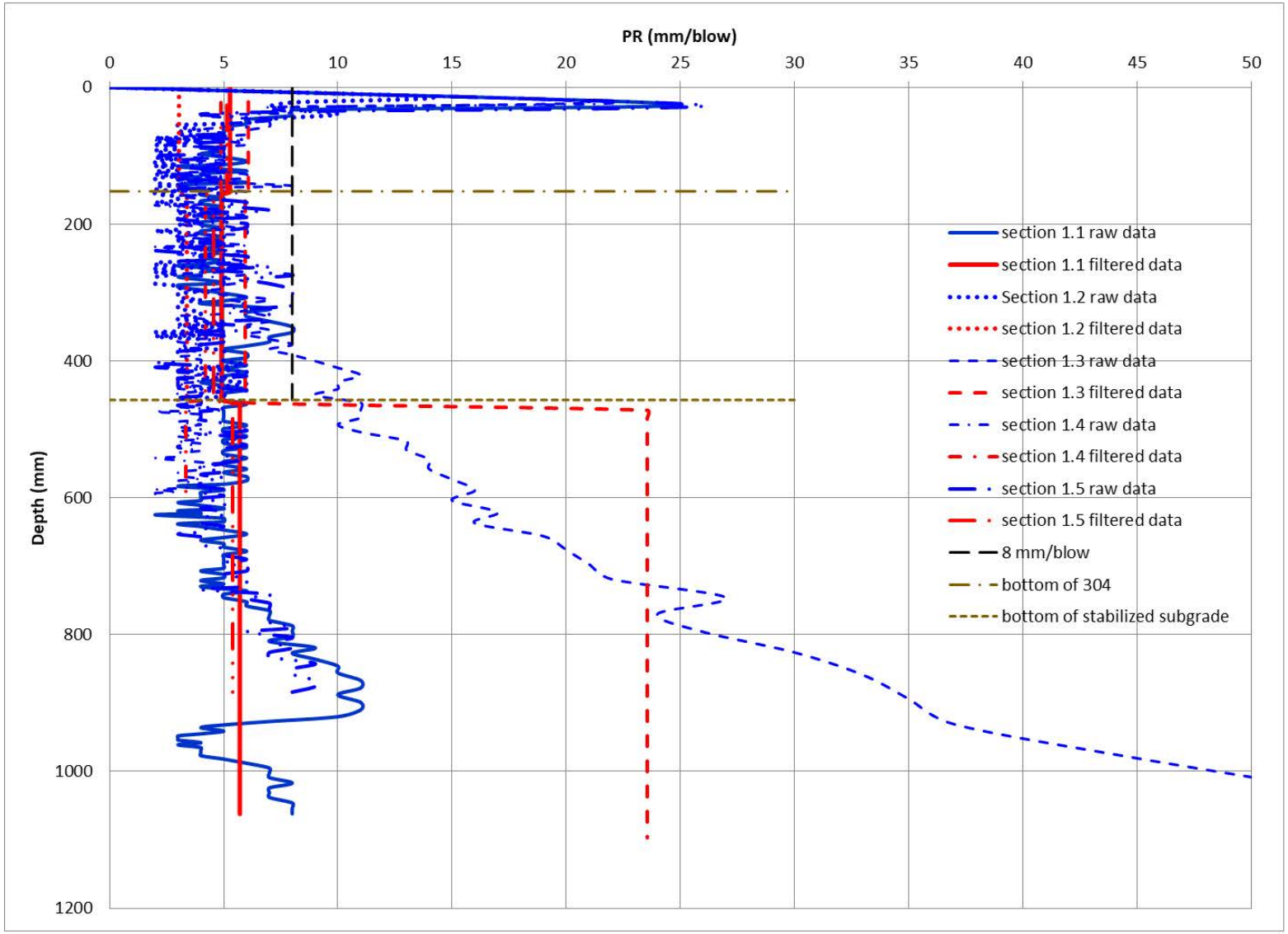
PR (mm/blow)
0
5
10
15
20
25
30
35
40
45
50
Depth (mm)
0
200
400
600
800
1000
1200
section 1.1 raw data
section 1.1 filtered data
Section 1.2 raw data
section 1.2 filtered data
section 1.3 raw data
section 1.3 filtered data
section 1.4 raw data
section 1.4 filtered data
section 1.5 raw data
section 1.5 filtered data
8 mm/blow
bottom of 304
bottom of stabilized subgrade

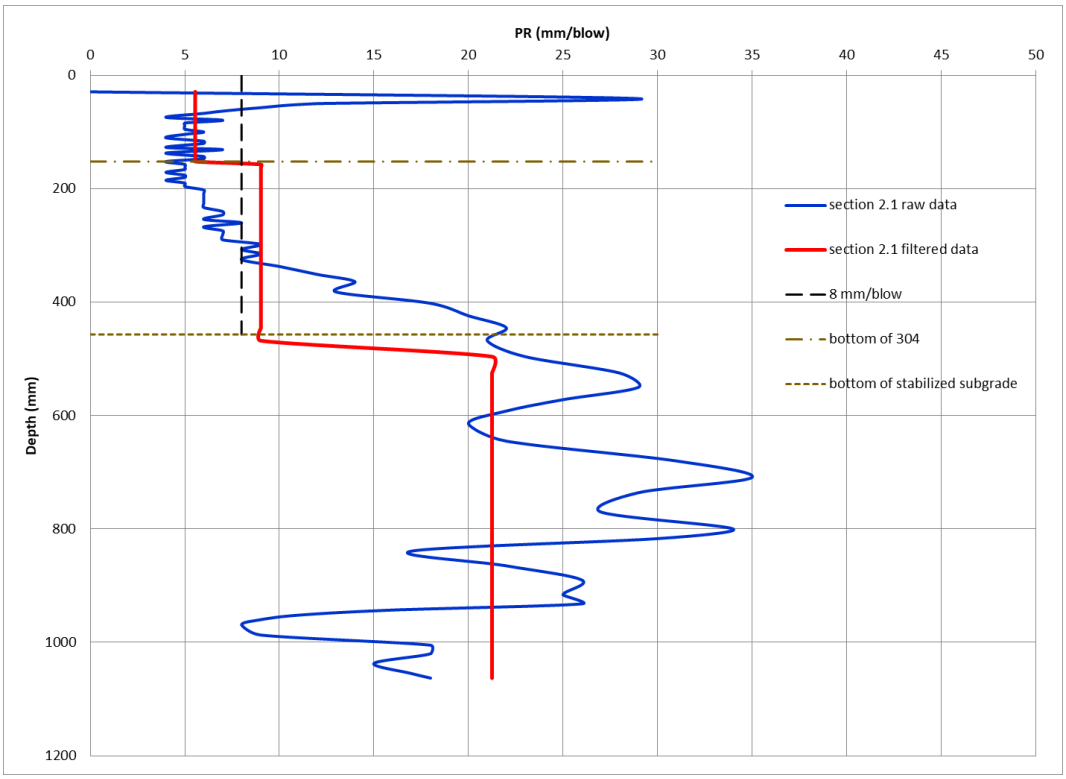
PR (mm/blow)
0
5
10
15
20
25
30
35
40
45
50
Depth (mm)
0
200
400
600
800
1000
1200
section 2.1 raw data
section 2.1 filtered data
8 mm/blow
bottom of 304
bottom of stabilized subgrade

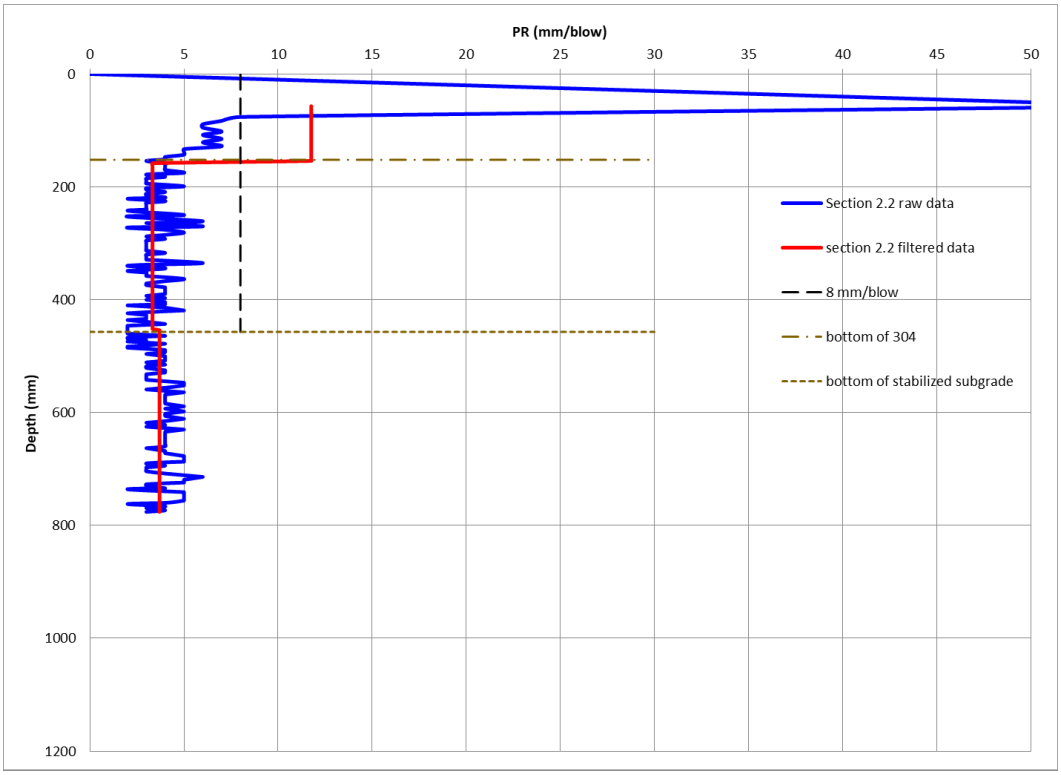
PR (mm/blow)
0
5
10
15
20
25
30
35
40
45
50
Depth (mm)
0
200
400
600
800
1000
1200
Section 2.2 raw data
section 2.2 filtered data
8 mm/blow
bottom of 304
bottom of stabilized subgrade

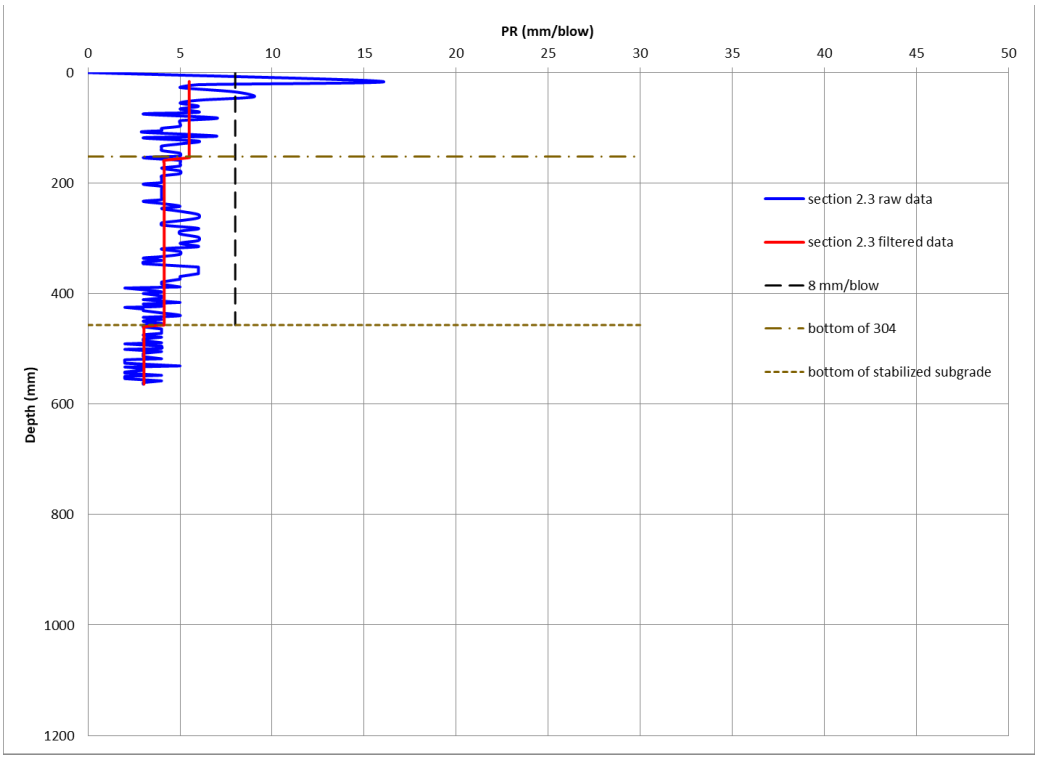
PR (mm/blow)
0
5
10
15
20
25
30
35
40
45
50
Depth (mm)
0
200
400
600
800
1000
1200
section 2.3 raw data
section 2.3 filtered data
8 mm/blow
bottom of 304
bottom of stabilized subgrade

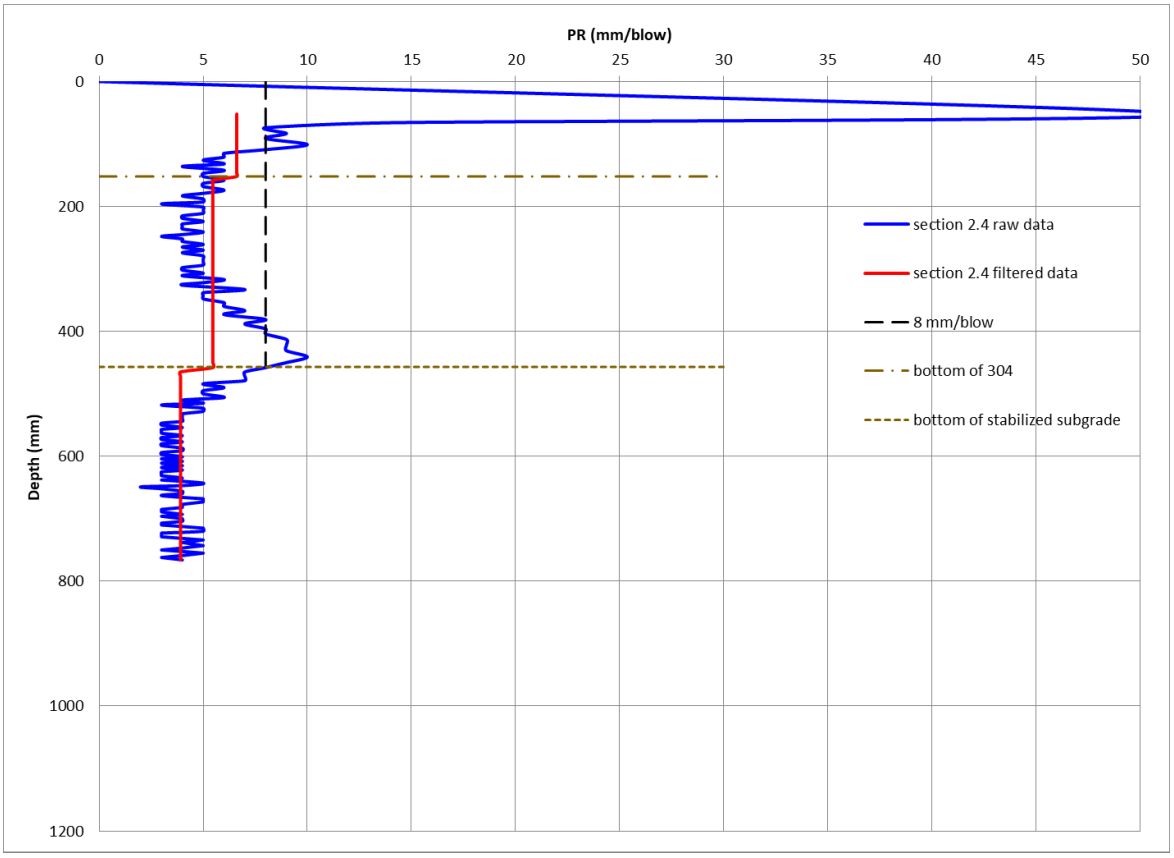
PR (mm/blow)
0
5
10
15
20
25
30
35
40
45
50
Depth (mm)
0
200
400
600
800
1000
1200
section 2.4 raw data
section 2.4 filtered data
8 mm/blow
bottom of 304
bottom of stabilized subgrade

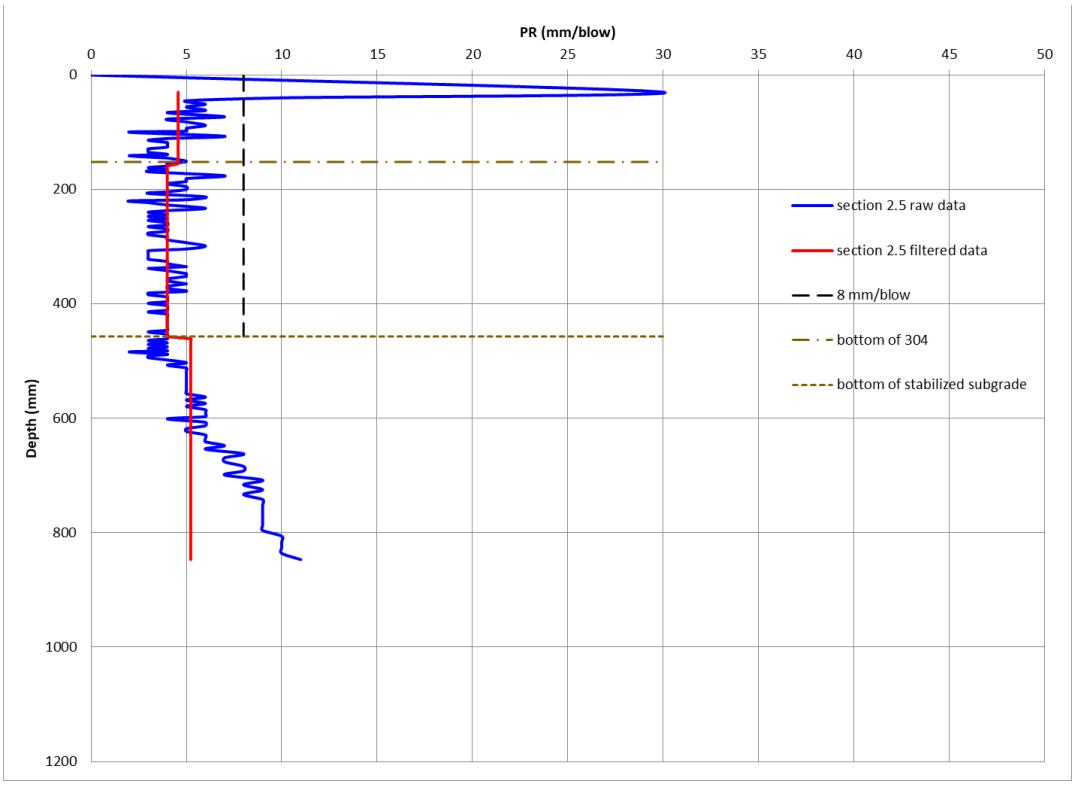
PR (mm/blow)
0
5
10
15
20
25
30
35
40
45
50
Depth (mm)
0
200
400
600
800
1000
1200
section 2.5 raw data
section 2.5 filtered data
8 mm/blow
bottom of 304
bottom of stabilized subgrade

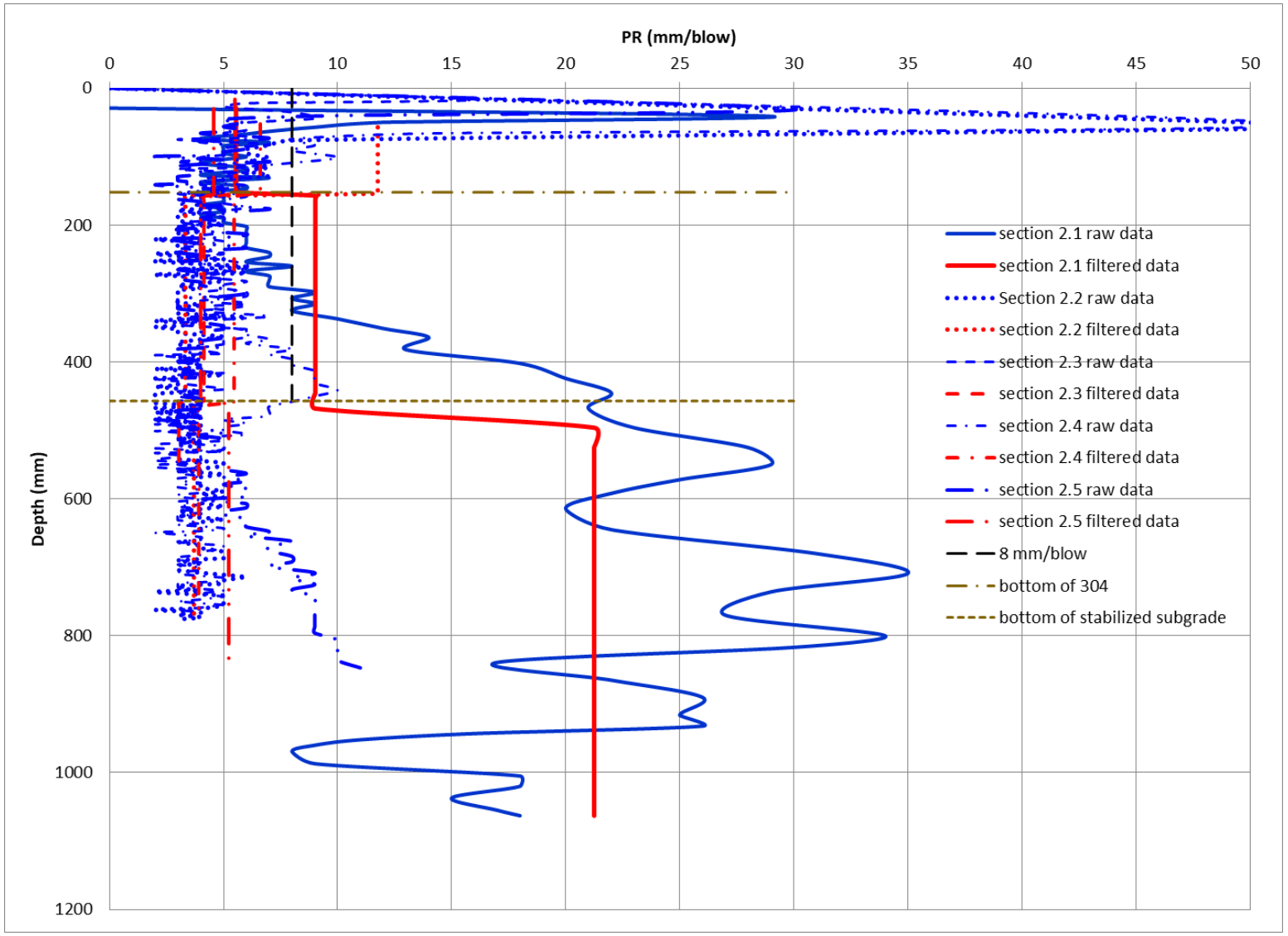
PR (mm/blow)
0
5
10
15
20
25
30
35
40
45
50
Depth (mm)
0
200
400
600
800
1000
1200
section 2.1 raw data
section 2.1 filtered data
Section 2.2 raw data
section 2.2 filtered data
section 2.3 raw data
section 2.3 filtered data
section 2.4 raw data
section 2.4 filtered data
section 2.5 raw data
section 2.5 filtered data
8 mm/blow
bottom of 304
bottom of stabilized subgrade

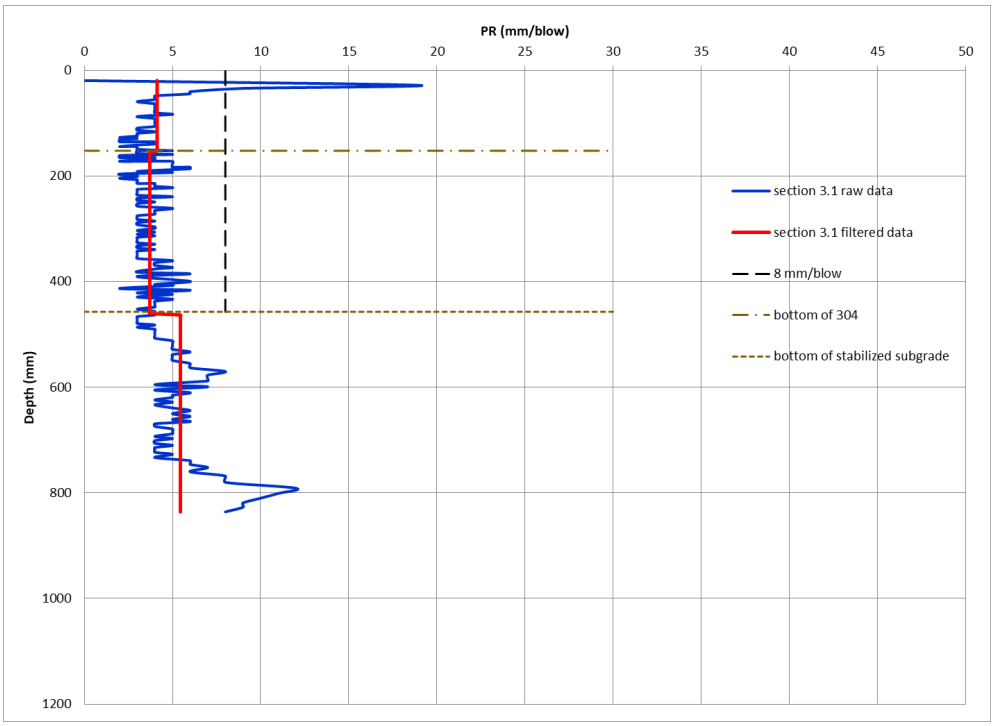
PR (mm/blow)
0
5
10
15
20
25
30
35
40
45
50
Depth (mm)
0
200
400
600
800
1000
1200
section 3.1 raw data
section 3.1 filtered data
8 mm/blow
bottom of 304
bottom of stabilized subgrade

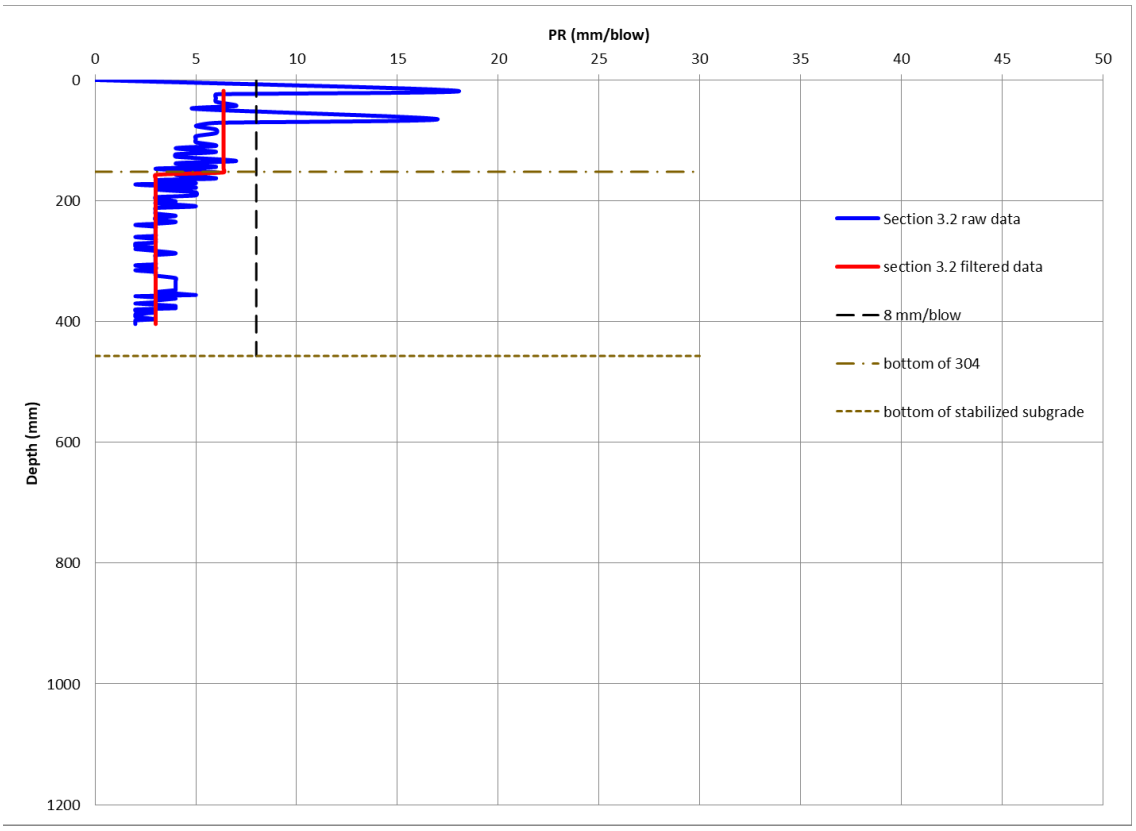
PR (mm/blow)
0
5
10
15
20
25
30
35
40
45
50
Depth (mm)
0
200
400
600
800
1000
1200
Section 3.2 raw data
section 3.2 filtered data
8 mm/blow
bottom of 304
bottom of stabilized subgrade

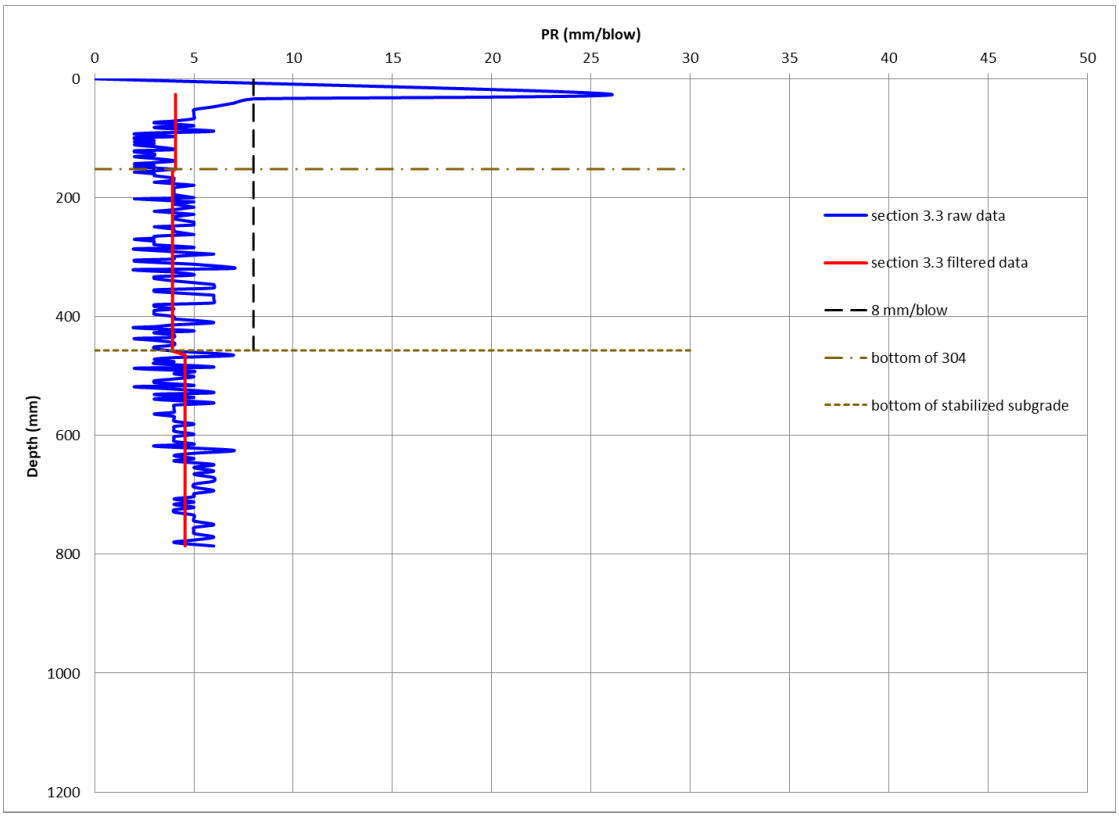
PR (mm/blow)
0
5
10
15
20
25
30
35
40
45
50
Depth (mm)
0
200
400
600
800
1000
1200
section 3.3 raw data
section 3.3 filtered data
8 mm/blow
bottom of 304
bottom of stabilized subgrade

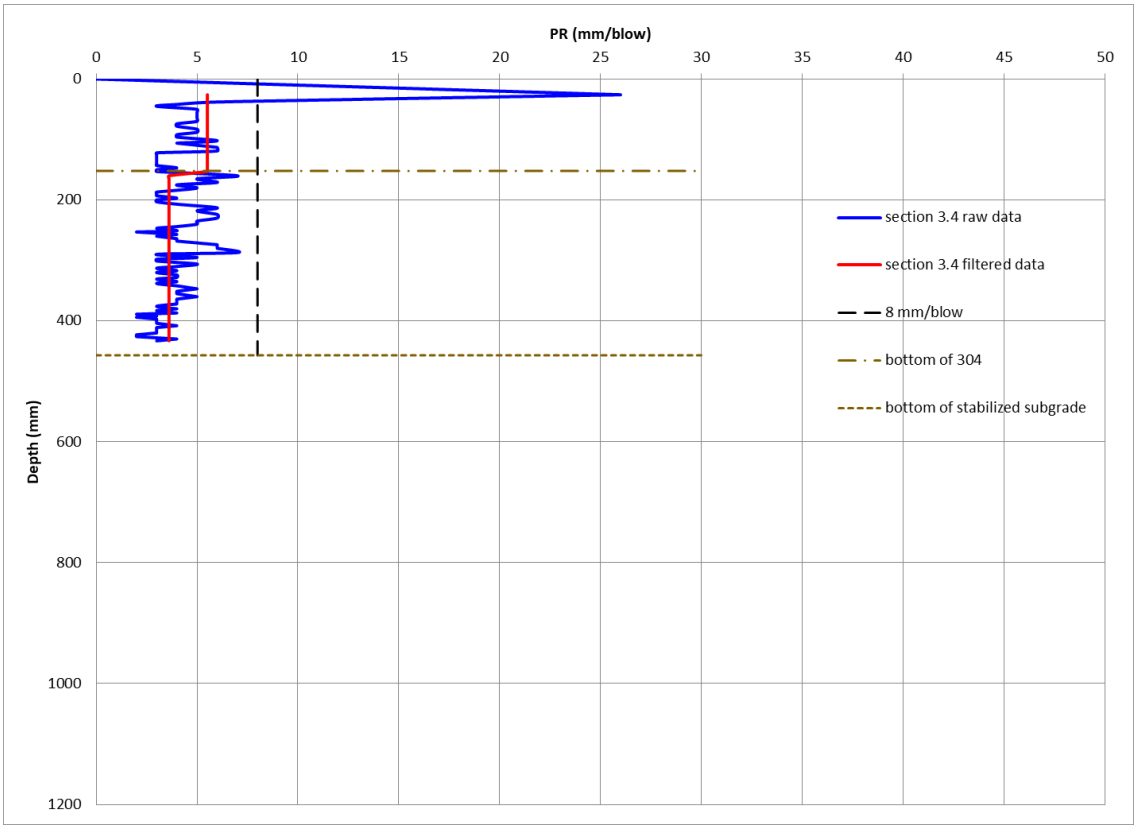
PR (mm/blow)
0
5
10
15
20
25
30
35
40
45
50
Depth (mm)
0
200
400
600
800
1000
1200
section 3.4 raw data
section 3.4 filtered data
8 mm/blow
bottom of 304
bottom of stabilized subgrade

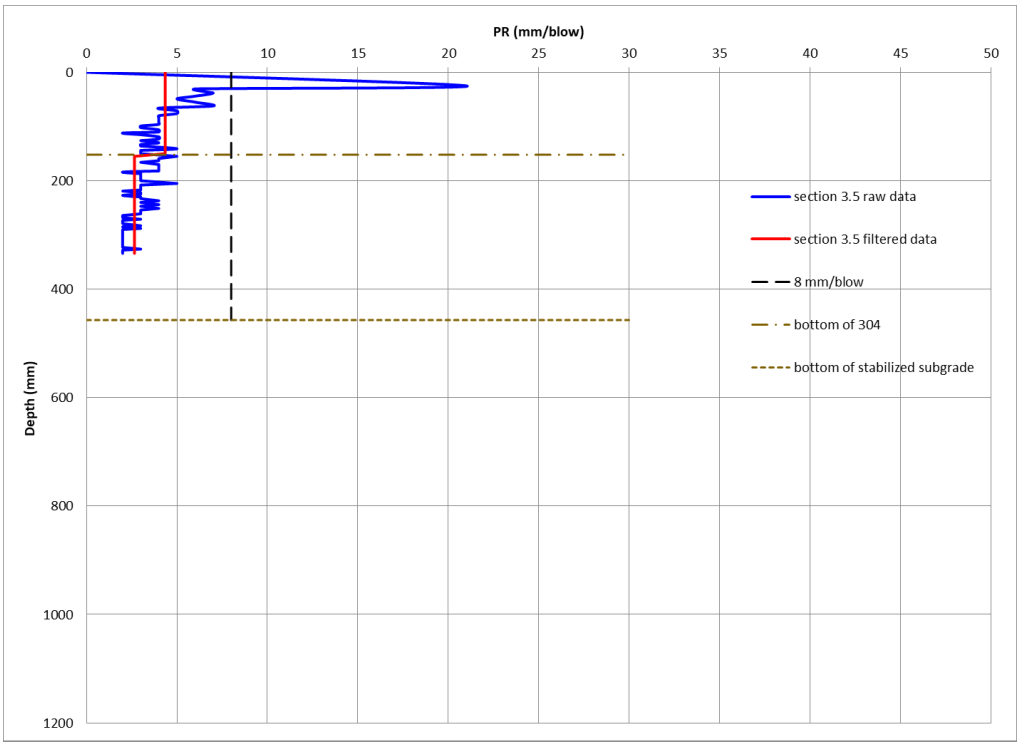
PR (mm/blow)
0
5
10
15
20
25
30
35
40
45
50
Depth (mm)
0
200
400
600
800
1000
1200
section 3.5 raw data
section 3.5 filtered data
8 mm/blow
bottom of 304
bottom of stabilized subgrade

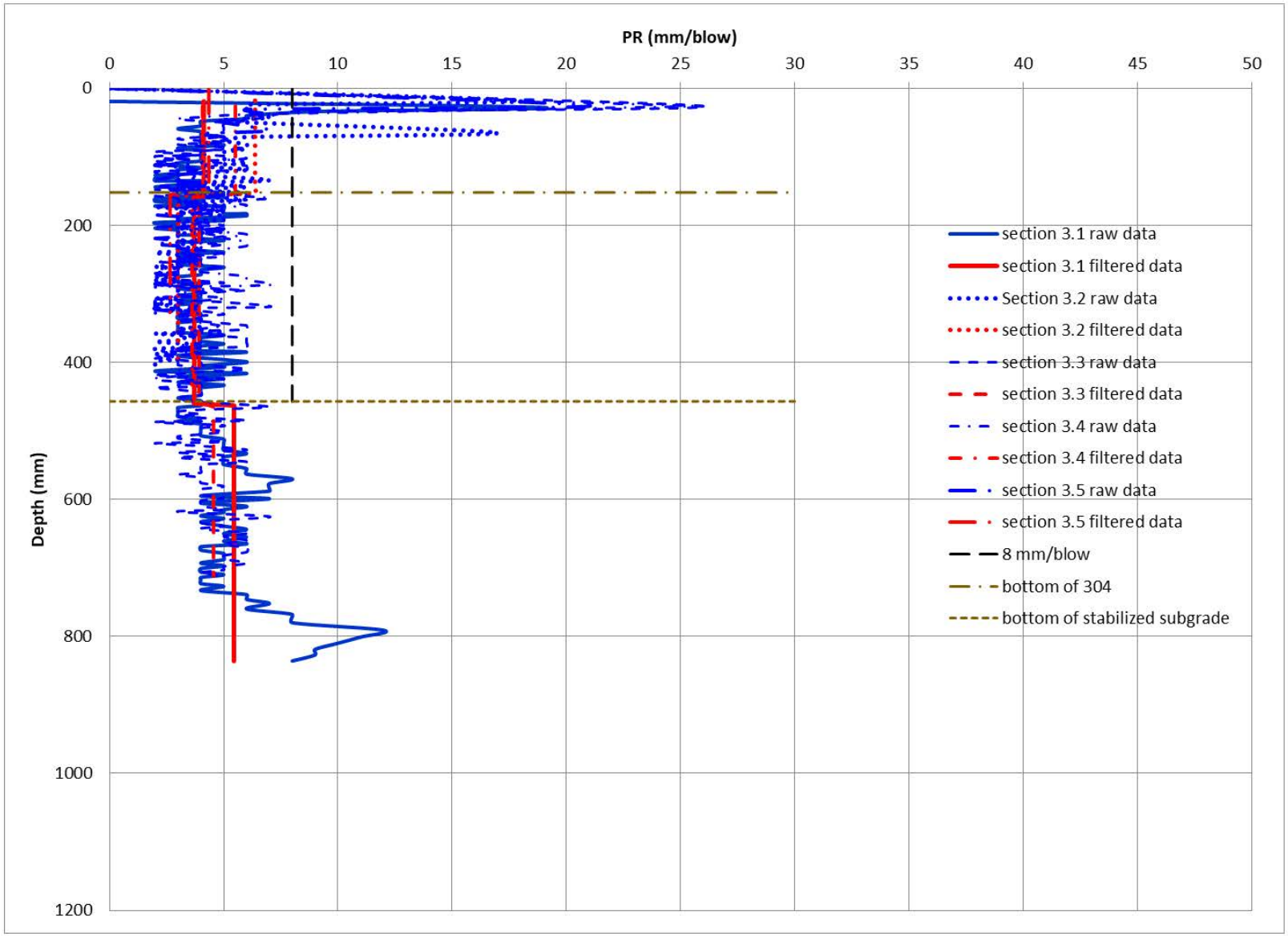
PR (mm/blow)
0
5
10
15
20
25
30
35
40
45
50
Depth (mm)
0
200
400
600
800
1000
1200
section 3.1 raw data
section 3.1 filtered data
Section 3.2 raw data
section 3.2 filtered data
section 3.3 raw data
section 3.3 filtered data
section 3.4 raw data
section 3.4 filtered data
section 3.5 raw data
section 3.5 filtered data
8 mm/blow
bottom of 304
bottom of stabilized subgrade

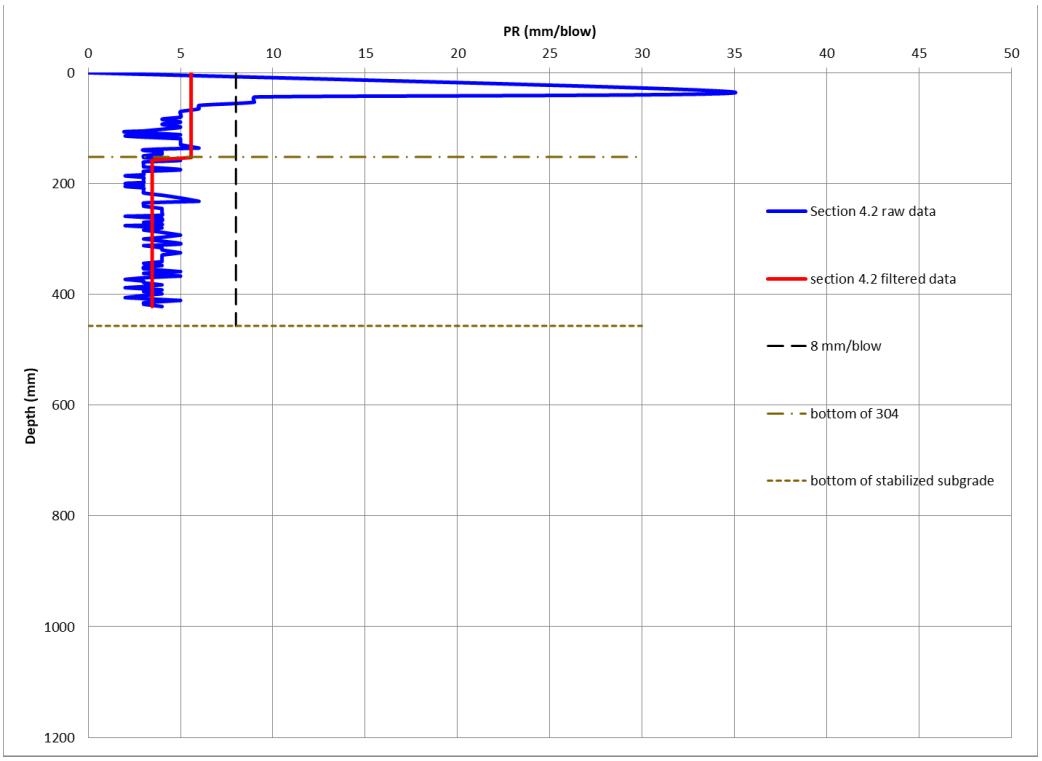
PR (mm/blow)
0
5
10
15
20
25
30
35
40
45
50
Depth (mm)
0
200
400
600
800
1000
1200
Section 4.2 raw data
section 4.2 filtered data
8 mm/blow
bottom of 304
bottom of stabilized subgrade

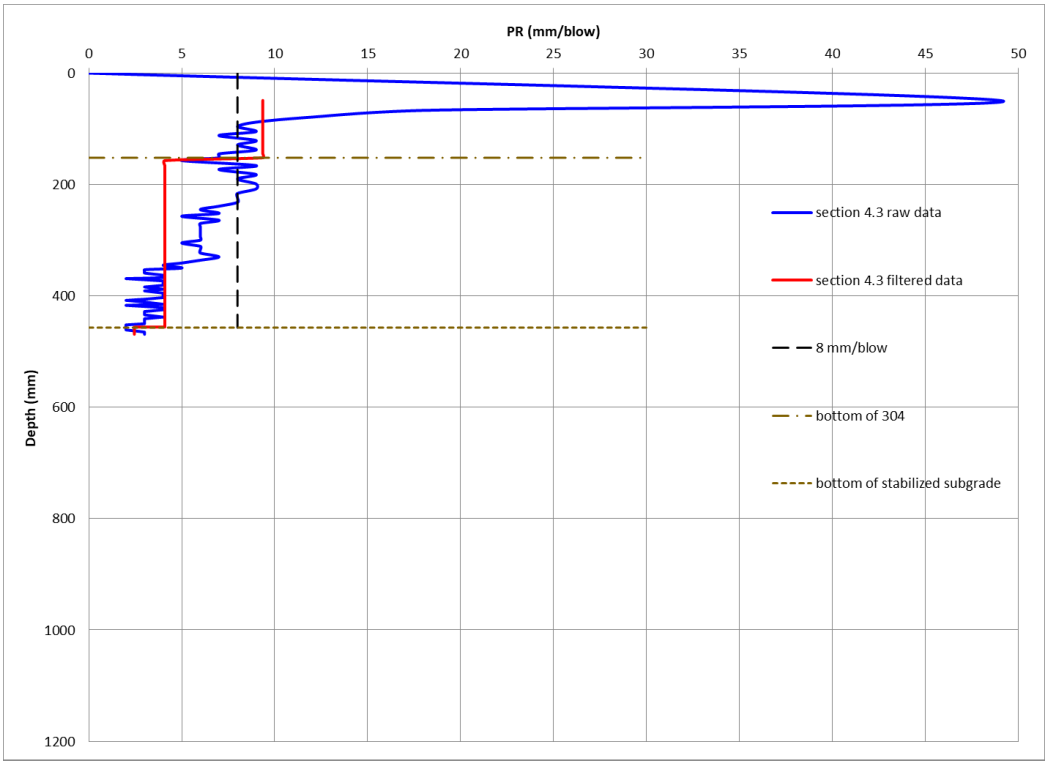
PR (mm/blow)
0
5
10
15
20
25
30
35
40
45
50
Depth (mm)
0
200
400
600
800
1000
1200
section 4.3 raw data
section 4.3 filtered data
8 mm/blow
bottom of 304
bottom of stabilized subgrade

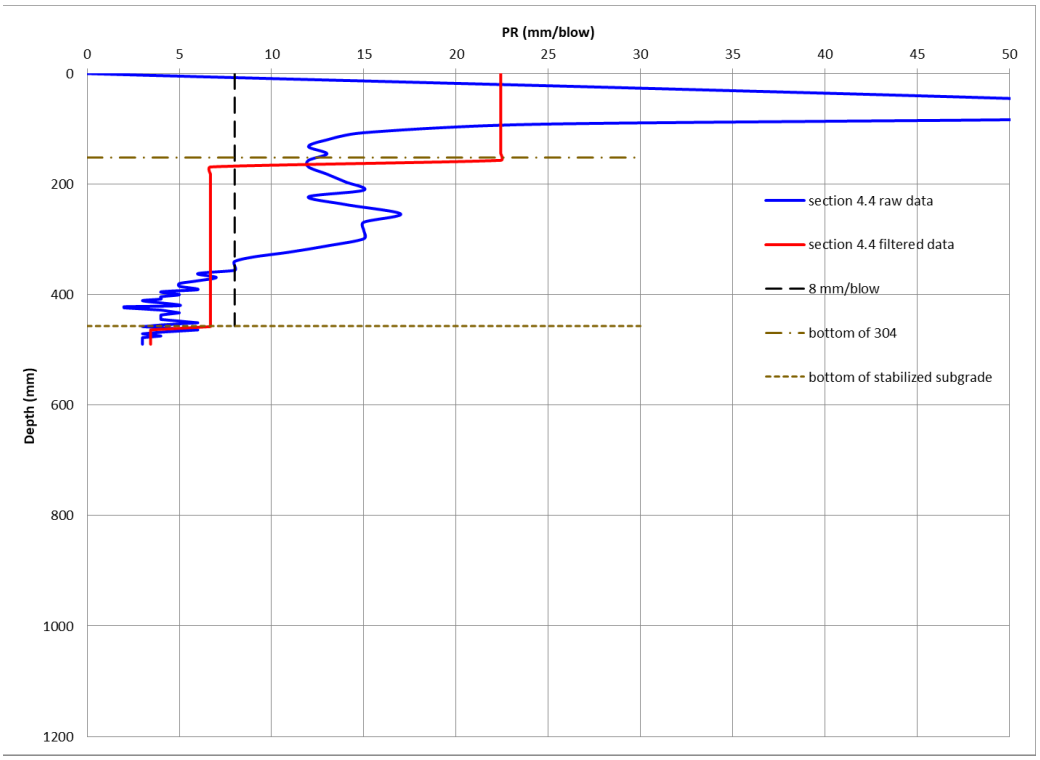
PR (mm/blow)
0
5
10
15
20
25
30
35
40
45
50
Depth (mm)
0
200
400
600
800
1000
1200
section 4.4 raw data
section 4.4 filtered data
8 mm/blow
bottom of 304
bottom of stabilized subgrade

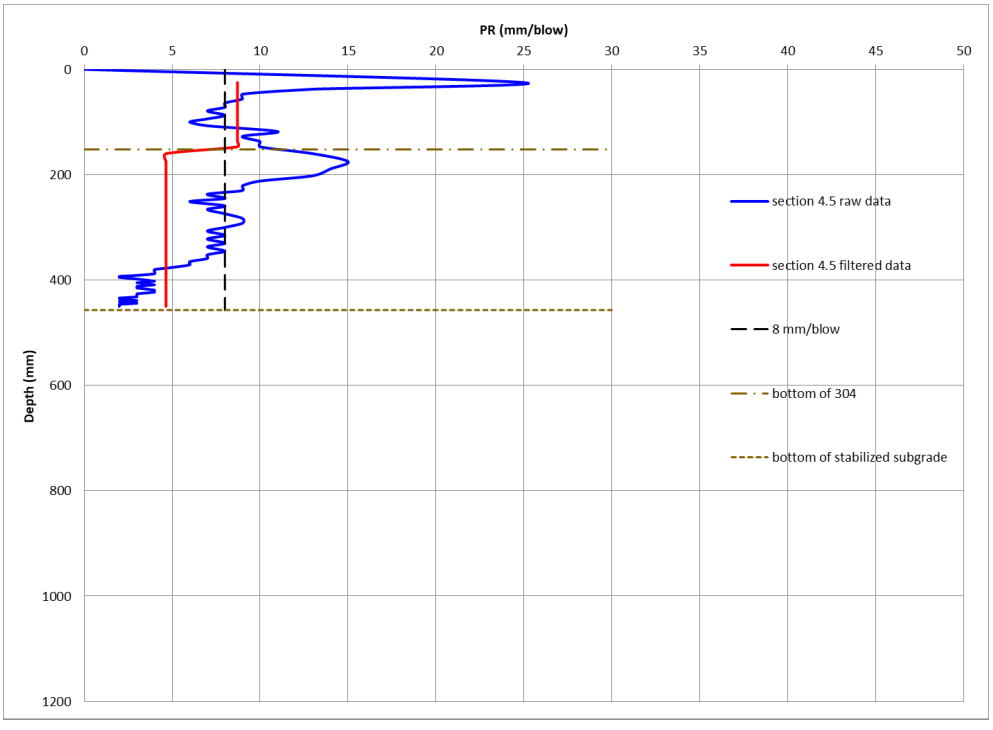
PR (mm/blow)
0
5
10
15
20
25
30
35
40
45
50
Depth (mm)
0
200
400
600
800
1000
1200
section 4.5 raw data
section 4.5 filtered data
8 mm/blow
bottom of 304
bottom of stabilized subgrade

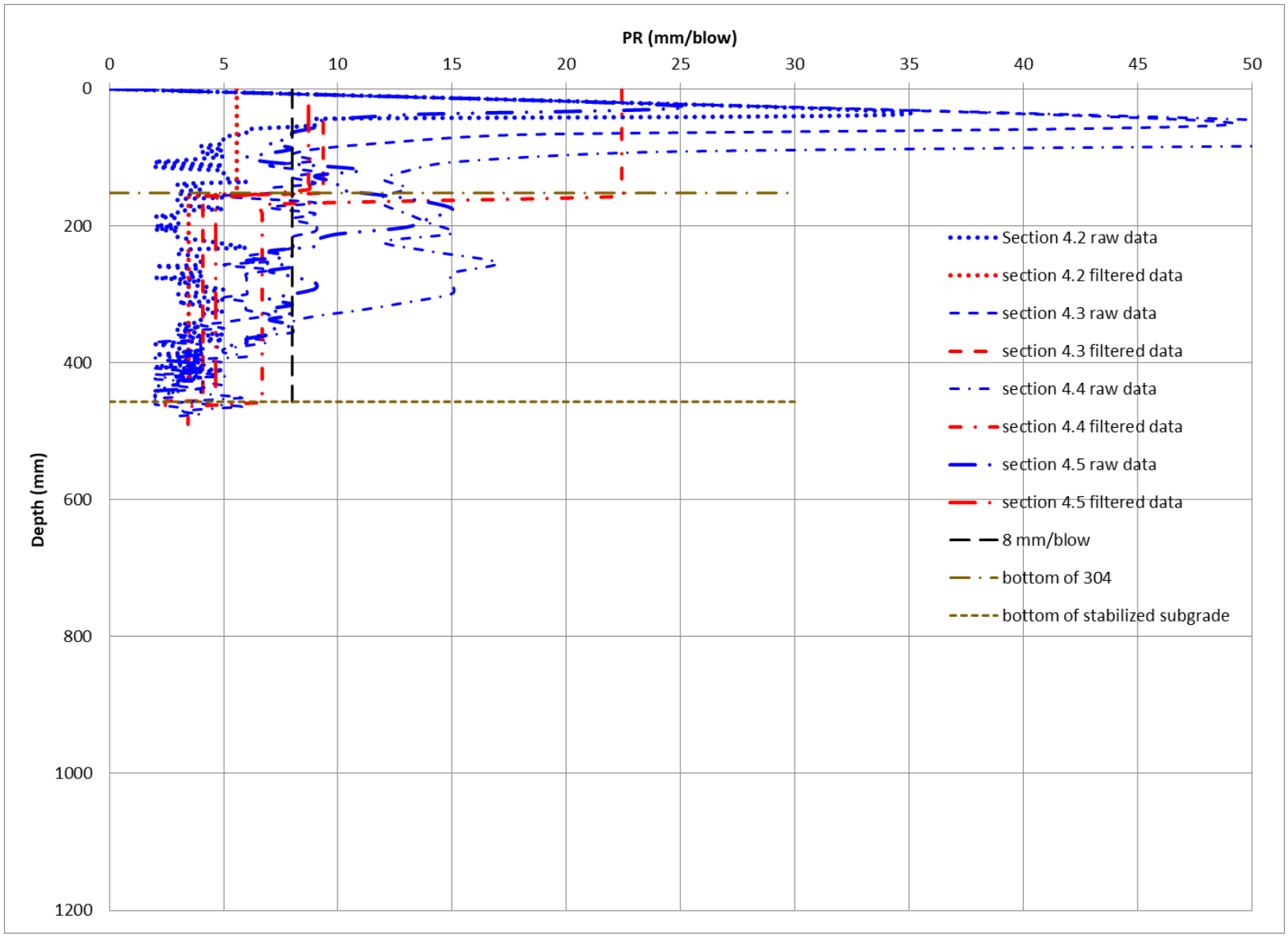
PR (mm/blow)
0
5
10
15
20
25
30
35
40
45
50
Depth (mm)
0
200
400
600
800
1000
1200
Section 4.2 raw data
section 4.2 filtered data
section 4.3 raw data
section 4.3 filtered data
section 4.4 raw data
section 4.4 filtered data
section 4.5 raw data
section 4.5 filtered data
8 mm/blow
bottom of 304
bottom of stabilized subgrade

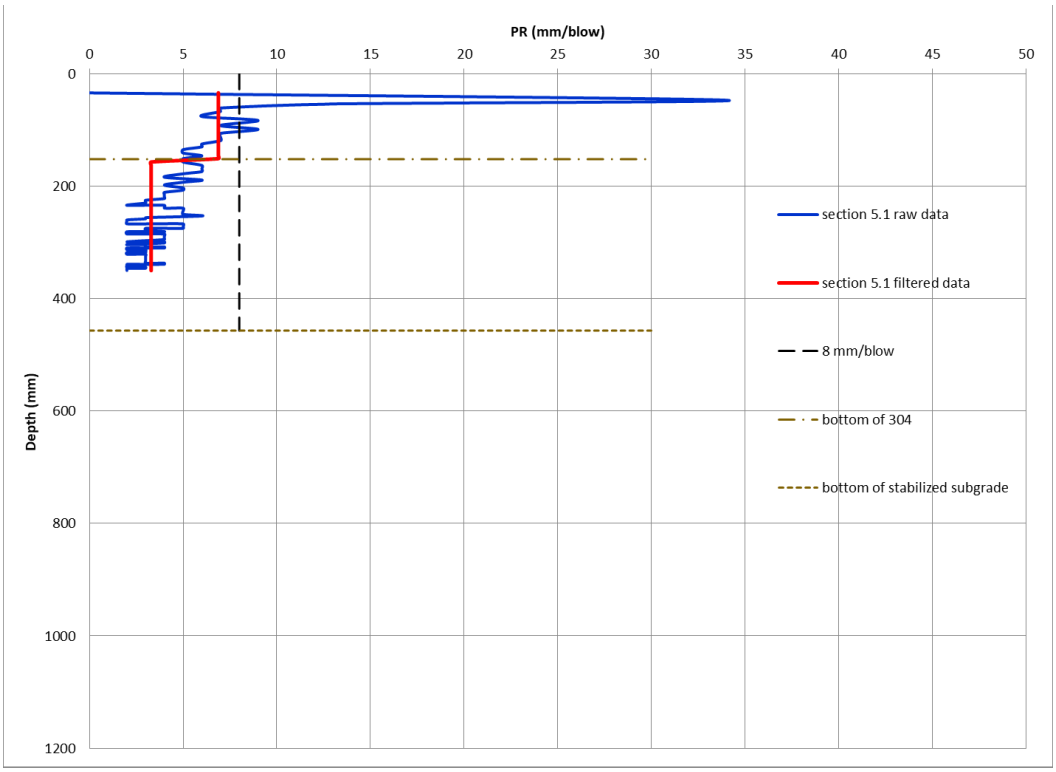
PR (mm/blow)
0
5
10
15
20
25
30
35
40
45
50
Depth (mm)
0
200
400
600
800
1000
1200
section 5.1 raw data
section 5.1 filtered data
8 mm/blow
bottom of 304
bottom of stabilized subgrade

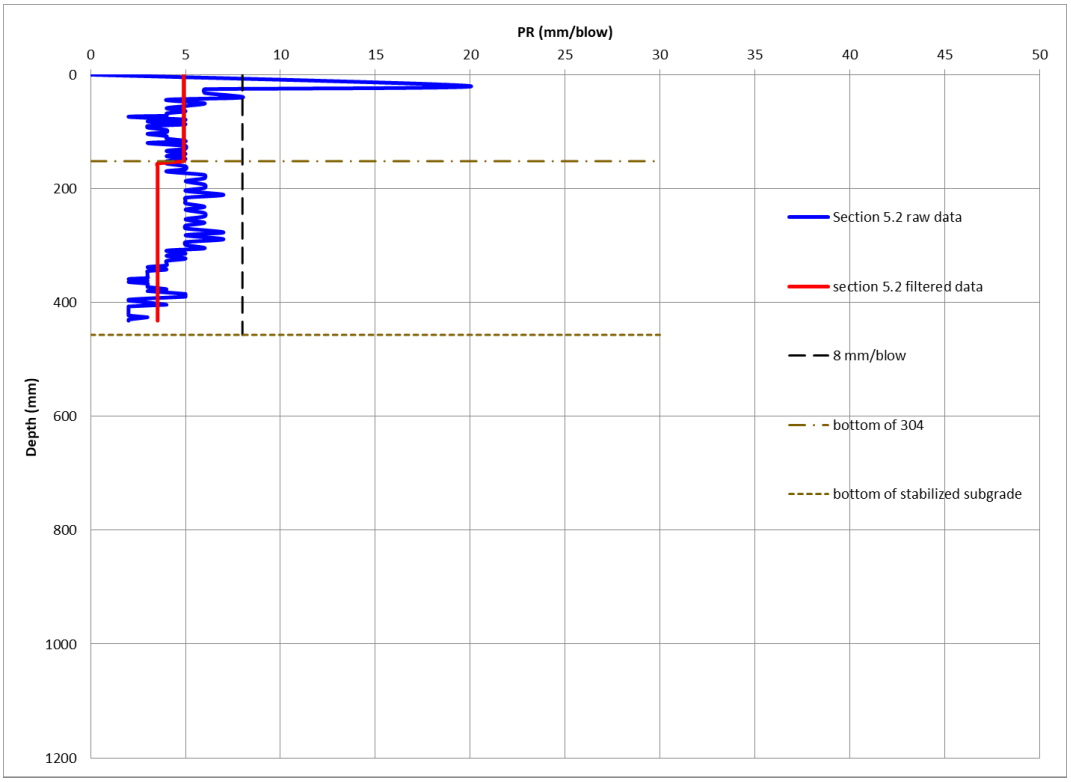
PR (mm/blow)
0
5
10
15
20
25
30
35
40
45
50
Depth (mm)
0
200
400
600
800
1000
1200
Section 5.2 raw data
section 5.2 filtered data
8 mm/blow
bottom of 304
bottom of stabilized subgrade

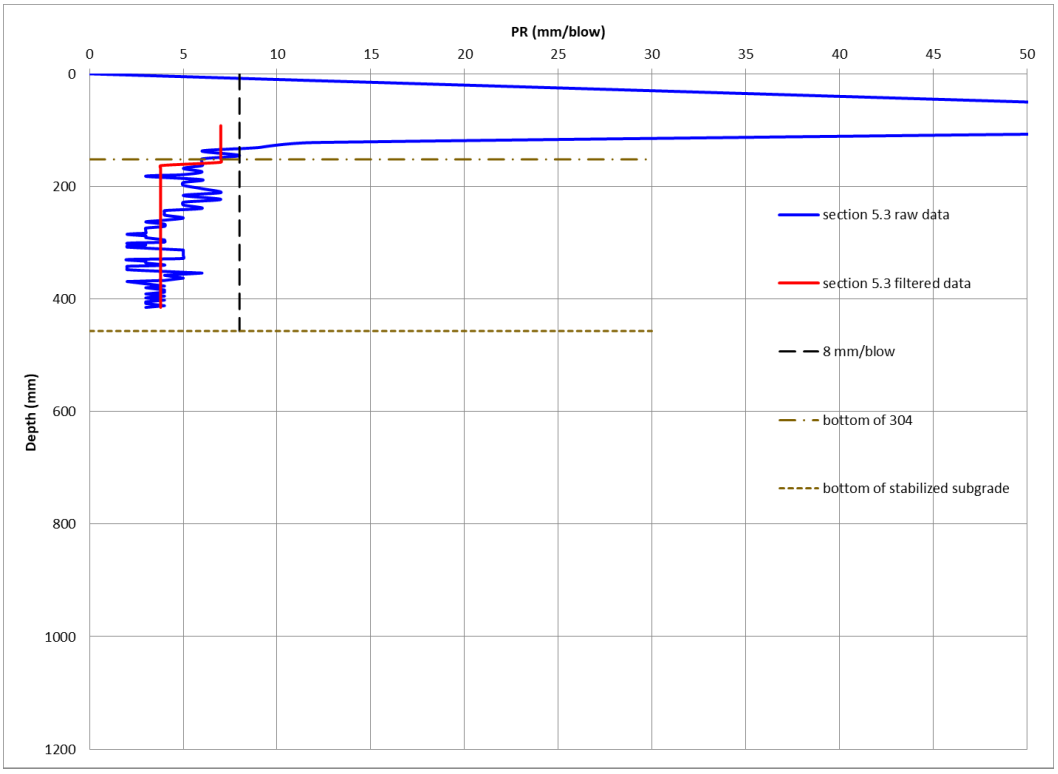
PR (mm/blow)
0
5
10
15
20
25
30
35
40
45
50
Depth (mm)
0
200
400
600
800
1000
1200
section 5.3 raw data
section 5.3 filtered data
8 mm/blow
bottom of 304
bottom of stabilized subgrade

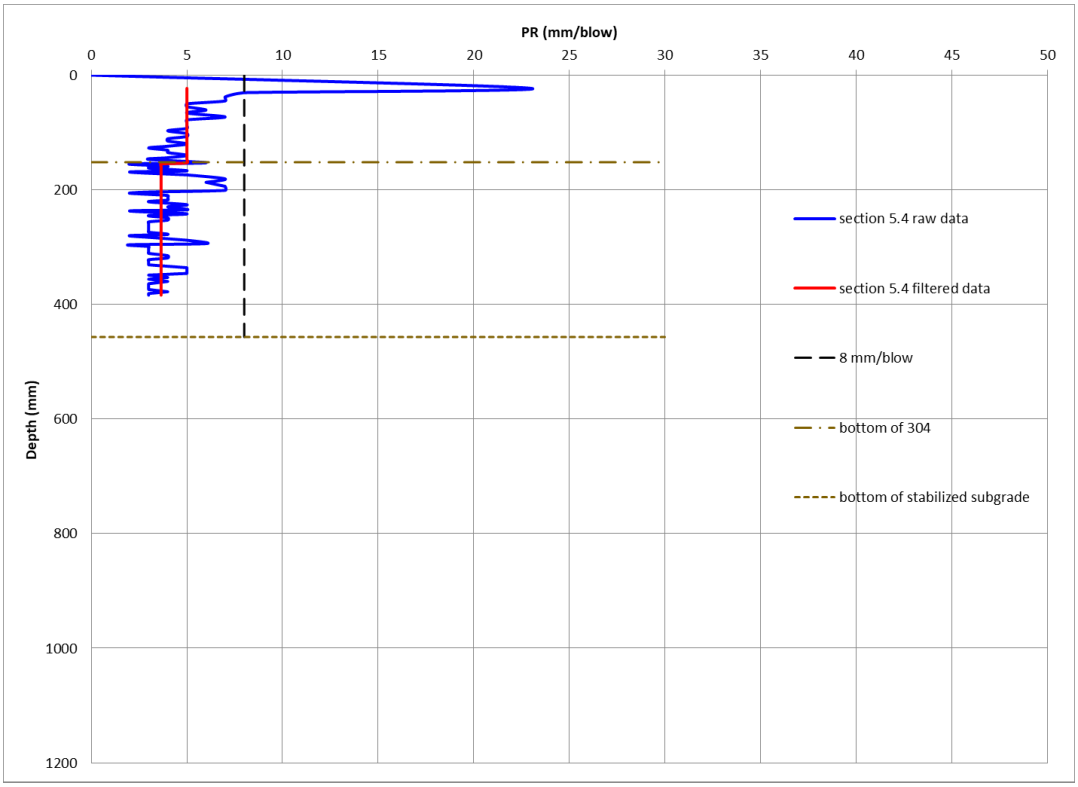
PR (mm/blow)
0
5
10
15
20
25
30
35
40
45
50
Depth (mm)
0
200
400
600
800
1000
1200
section 5.4 raw data
section 5.4 filtered data
8 mm/blow
bottom of 304
bottom of stabilized subgrade

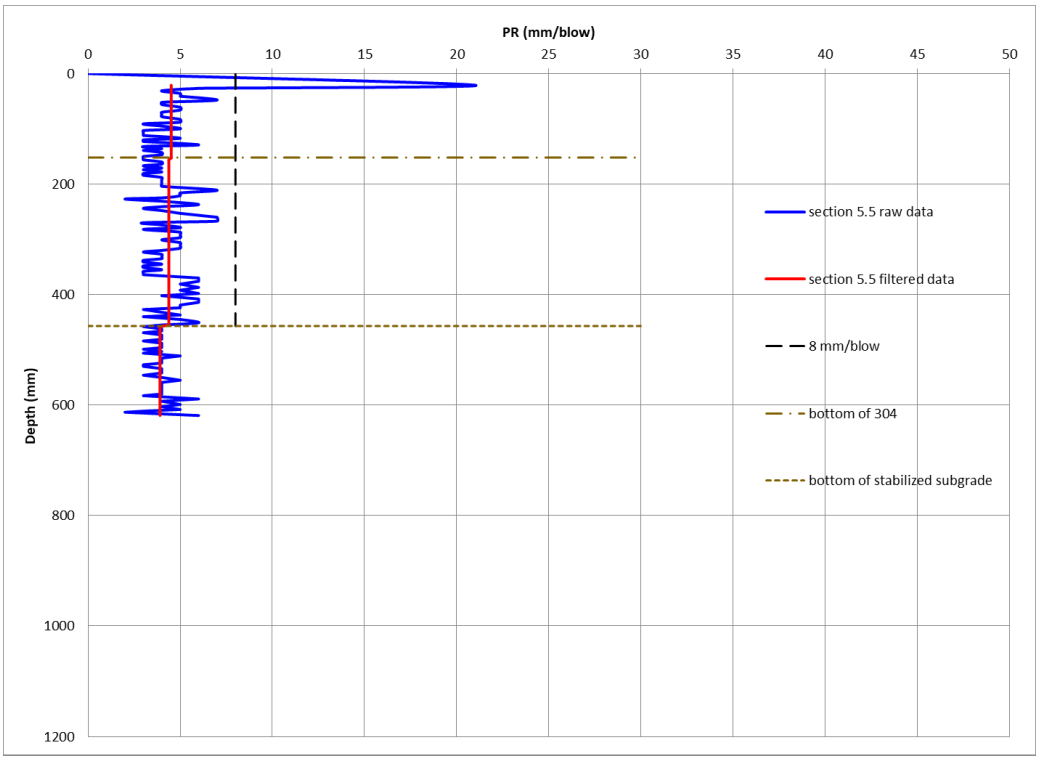
PR (mm/blow)
0
5
10
15
20
25
30
35
40
45
50
Depth (mm)
0
200
400
600
800
1000
1200
section 5.5 raw data
section 5.5 filtered data
8 mm/blow
bottom of 304
bottom of stabilized subgrade

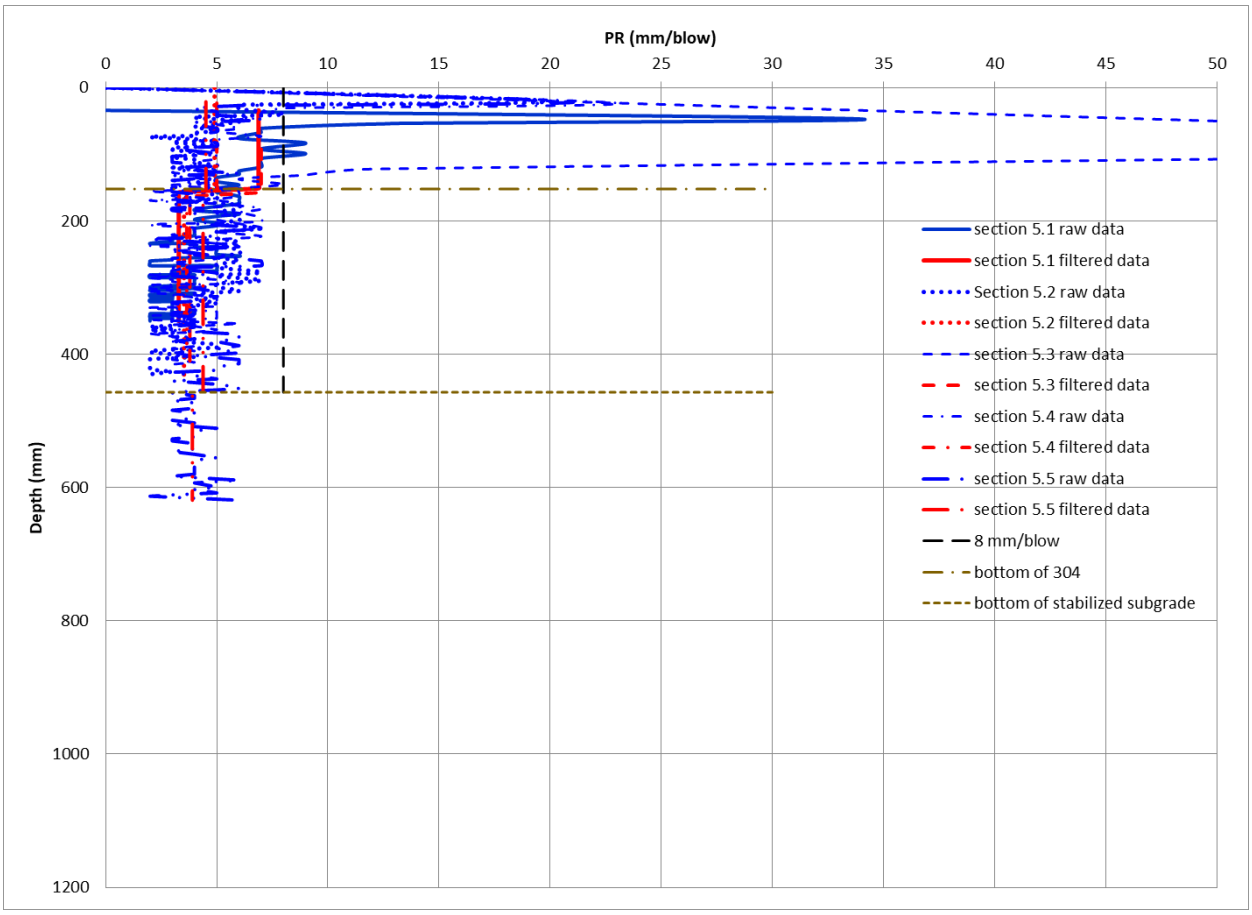
PR (mm/blow)
0
5
10
15
20
25
30
35
40
45
50
Depth (mm)
0
200
400
600
800
1000
1200
section 5.1 raw data
section 5.1 filtered data
Section 5.2 raw data
section 5.2 filtered data
section 5.3 raw data
section 5.3 filtered data
section 5.4 raw data
section 5.4 filtered data
section 5.5 raw data
section 5.5 filtered data
8 mm/blow
bottom of 304
bottom of stabilized subgrade

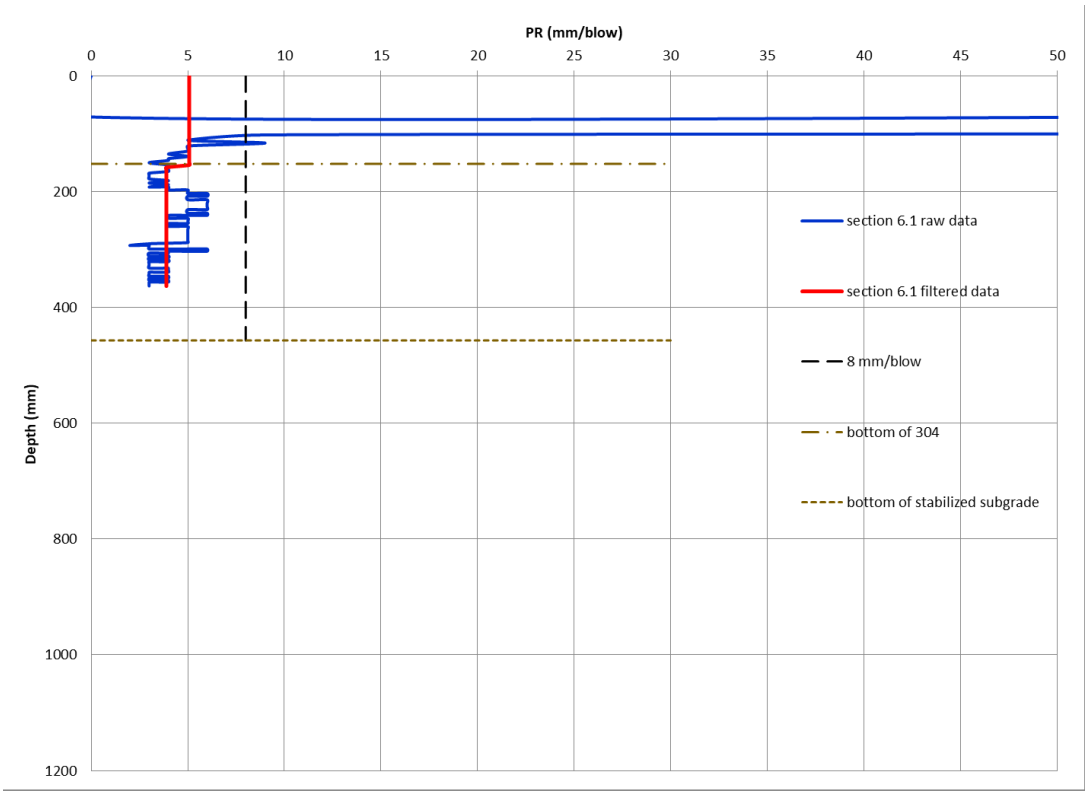
PR (mm/blow)
0
5
10
15
20
25
30
35
40
45
50
Depth (mm)
0
200
400
600
800
1000
1200
section 6.1 raw data
section 6.1 filtered data
8 mm/blow
bottom of 304
bottom of stabilized subgrade

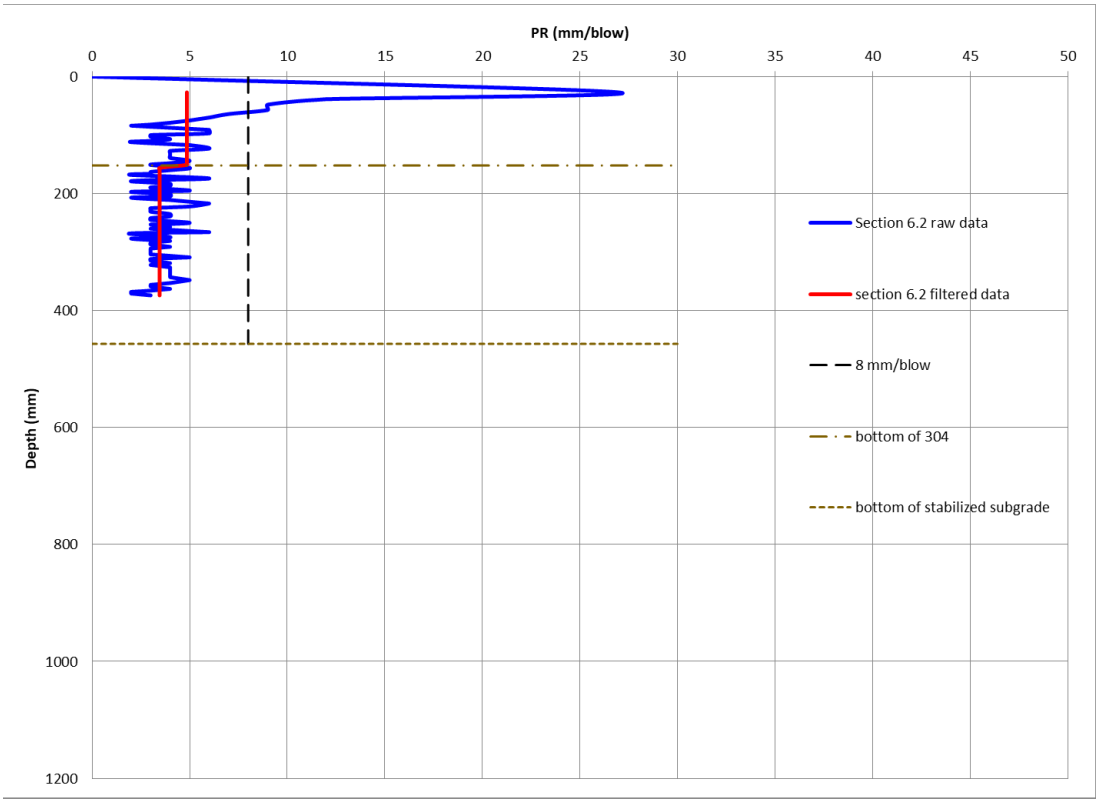
PR (mm/blow)
0
5
10
15
20
25
30
35
40
45
50
Depth (mm)
0
200
400
600
800
1000
1200
Section 6.2 raw data
section 6.2 filtered data
8 mm/blow
bottom of 304
bottom of stabilized subgrade

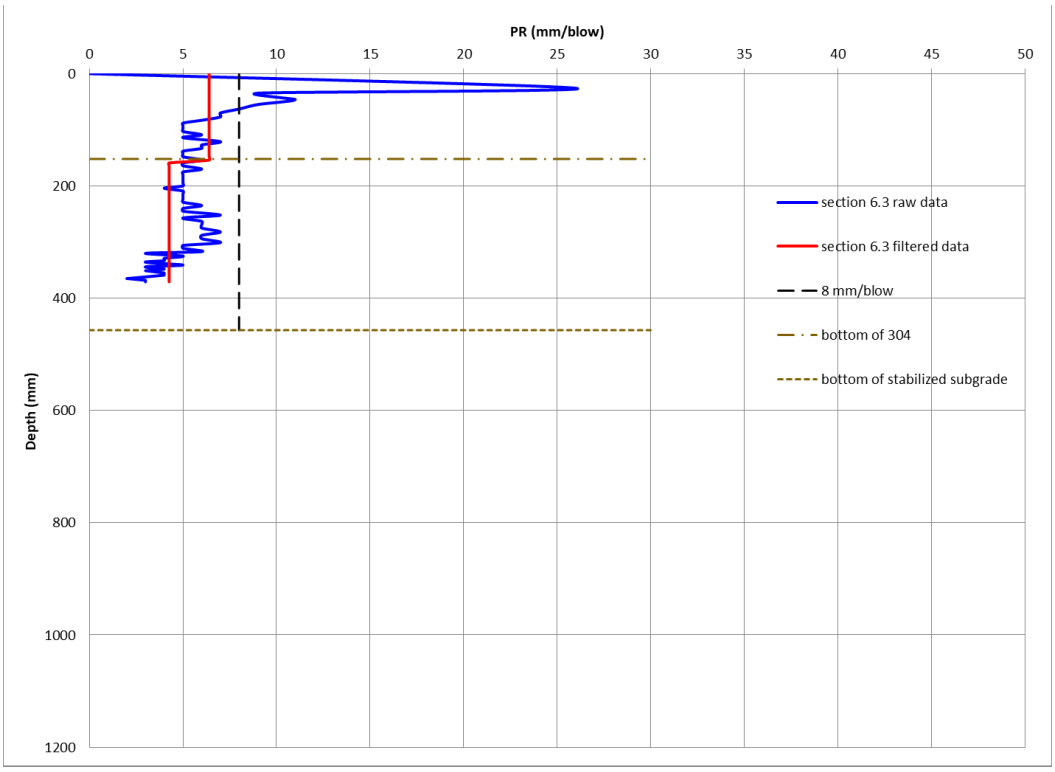
PR (mm/blow)
0
5
10
15
20
25
30
35
40
45
50
Depth (mm)
0
200
400
600
800
1000
1200
section 6.3 raw data
section 6.3 filtered data
8 mm/blow
bottom of 304
bottom of stabilized subgrade

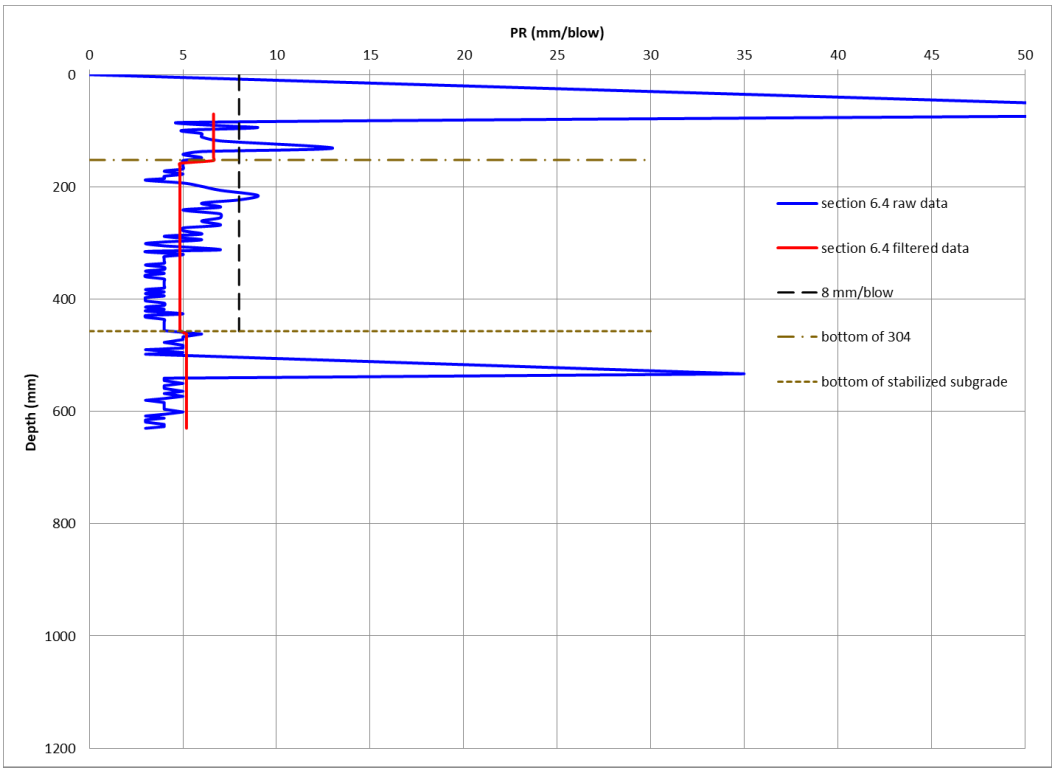
PR (mm/blow)
0
5
10
15
20
25
30
35
40
45
50
Depth (mm)
0
200
400
600
800
1000
1200
section 6.4 raw data
section 6.4 filtered data
8 mm/blow
bottom of 304
bottom of stabilized subgrade

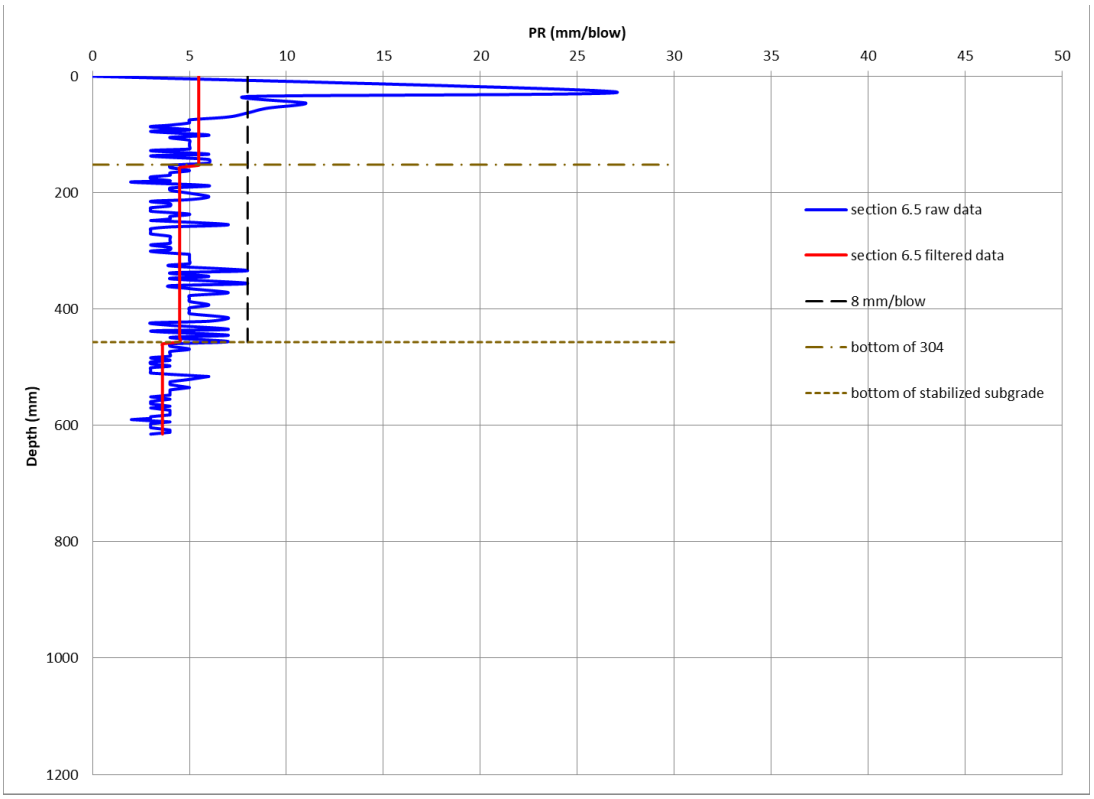
PR (mm/blow)
0
5
10
15
20
25
30
35
40
45
50
Depth (mm)
0
200
400
600
800
1000
1200
section 6.5 raw data
section 6.5 filtered data
8 mm/blow
bottom of 304
bottom of stabilized subgrade

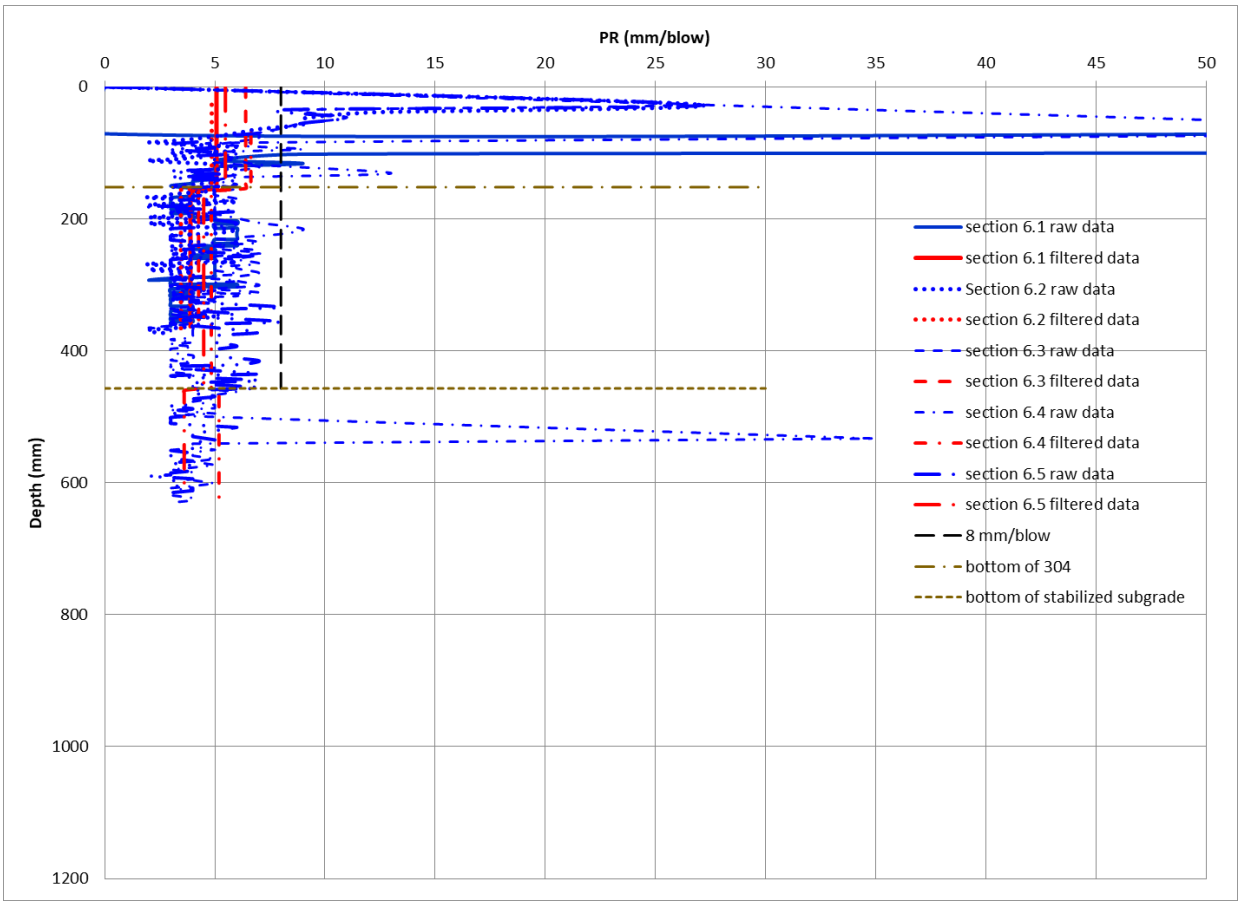
PR (mm/blow)
0
5
10
15
20
25
30
35
40
45
50
Depth (mm)
0
200
400
600
800
1000
1200
section 6.1 raw data
section 6.1 filtered data
Section 6.2 raw data
section 6.2 filtered data
section 6.3 raw data
section 6.3 filtered data
section 6.4 raw data
section 6.4 filtered data
section 6.5 raw data
section 6.5 filtered data
8 mm/blow
bottom of 304
bottom of stabilized subgrade

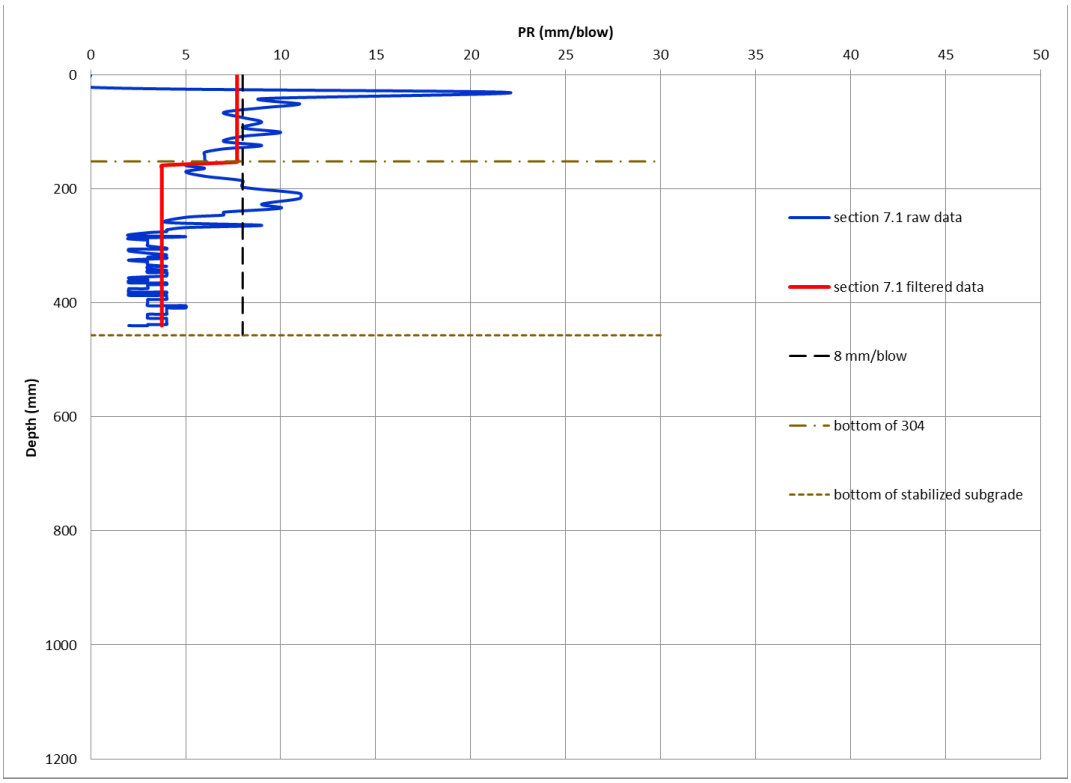
PR (mm/blow)
0
5
10
15
20
25
30
35
40
45
50
Depth (mm)
0
200
400
600
800
1000
1200
section 7.1 raw data
section 7.1 filtered data
8 mm/blow
bottom of 304
bottom of stabilized subgrade

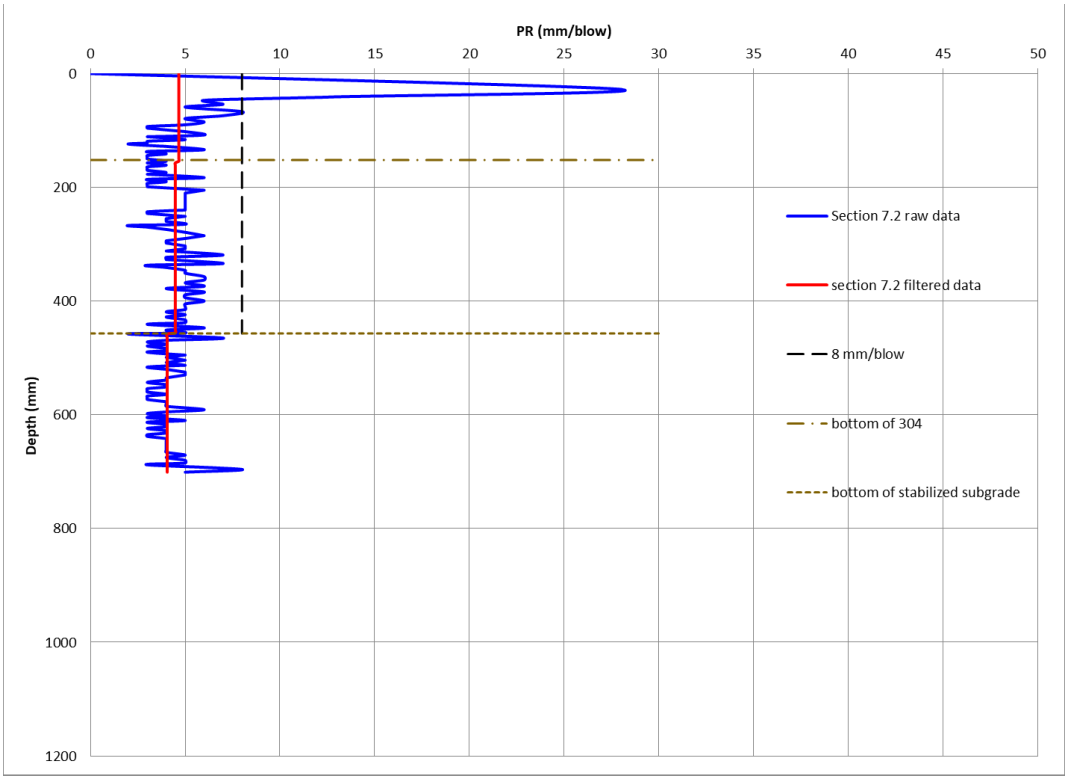
PR (mm/blow)
0
5
10
15
20
25
30
35
40
45
50
Depth (mm)
0
200
400
600
800
1000
1200
Section 7.2 raw data
section 7.2 filtered data
8 mm/blow
bottom of 304
bottom of stabilized subgrade

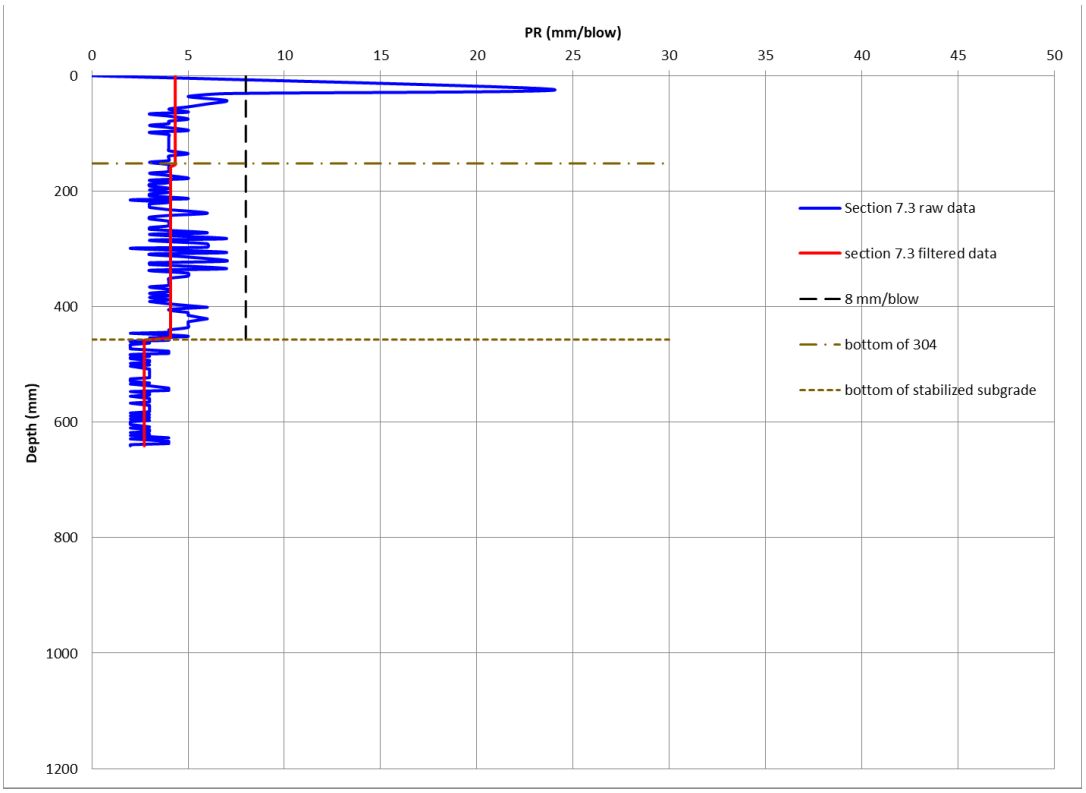
PR (mm/blow)
0
5
10
15
20
25
30
35
40
45
50
Depth (mm)
0
200
400
600
800
1000
1200
Section 7.3 raw data
section 7.3 filtered data
8 mm/blow
bottom of 304
bottom of stabilized subgrade

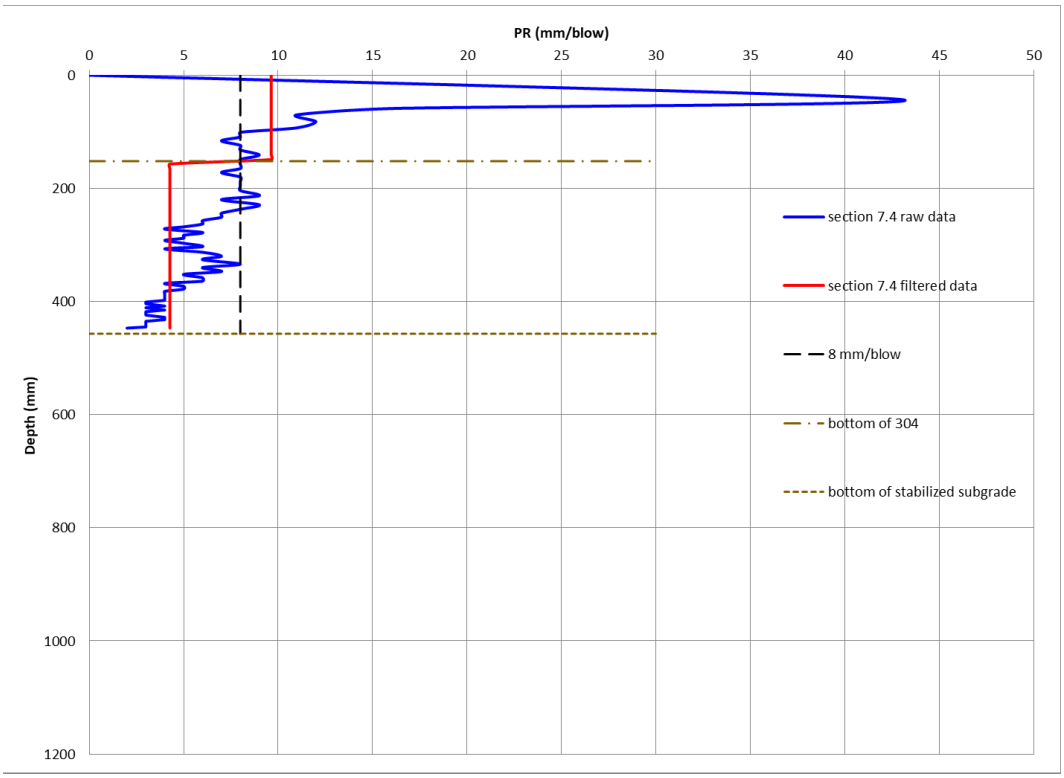
PR (mm/blow)
0
5
10
15
20
25
30
35
40
45
50
Depth (mm)
0
200
400
600
800
1000
1200
section 7.4 raw data
section 7.4 filtered data
8 mm/blow
bottom of 304
bottom of stabilized subgrade

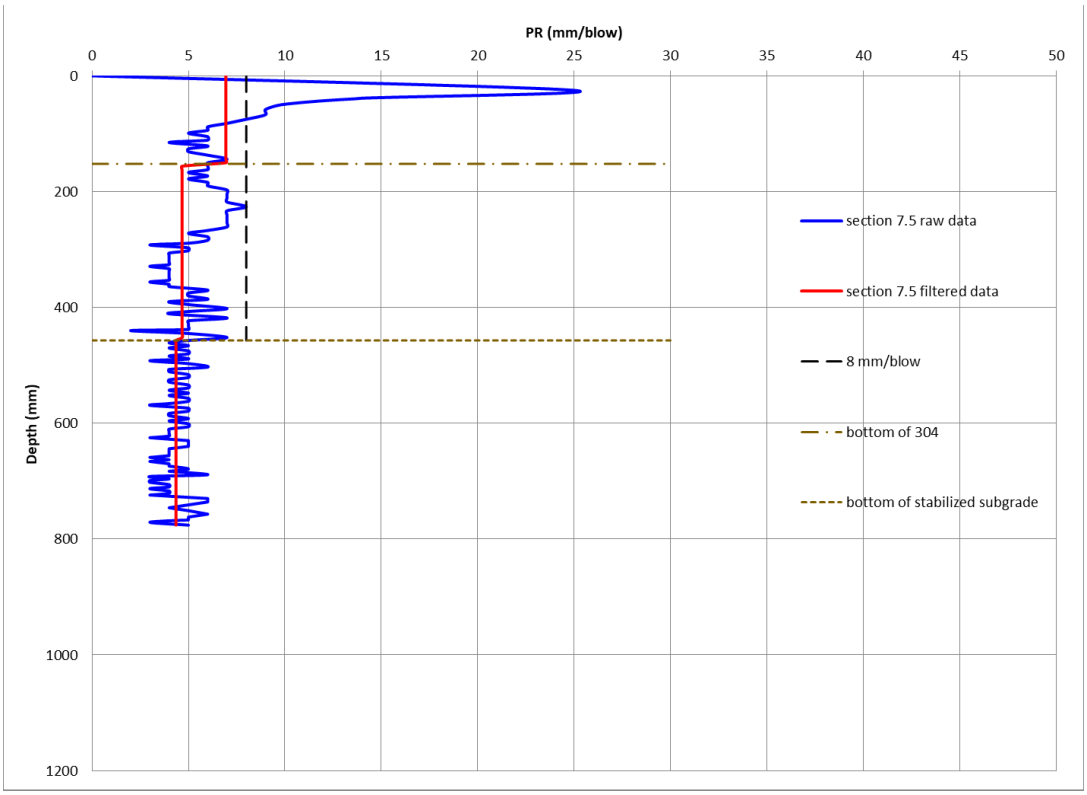
PR (mm/blow)
0
5
10
15
20
25
30
35
40
45
50
Depth (mm)
0
200
400
600
800
1000
1200
section 7.5 raw data
section 7.5 filtered data
8 mm/blow
bottom of 304
bottom of stabilized subgrade

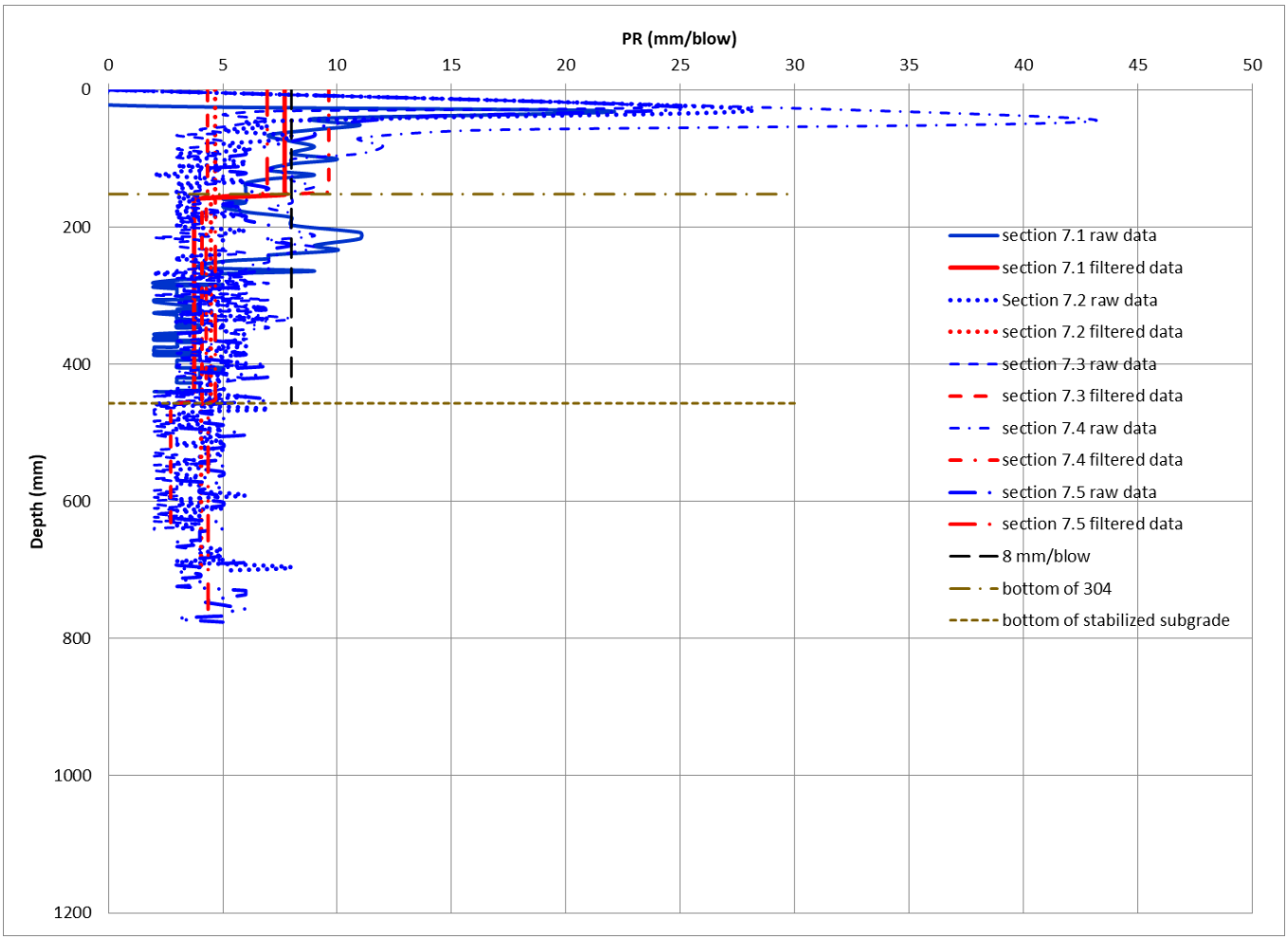
PR (mm/blow)
0
5
10
15
20
25
30
35
40
45
50
Depth (mm)
0
200
400
600
800
1000
1200
section 7.1 raw data
section 7.1 filtered data
Section 7.2 raw data
section 7.2 filtered data
section 7.3 raw data
section 7.3 filtered data
section 7.4 raw data
section 7.4 filtered data
section 7.5 raw data
section 7.5 filtered data
8 mm/blow
bottom of 304
bottom of stabilized subgrade

# APPENDIX C: PERROAD ANALYSIS OF CONSTRUCTED TEST SECTIONS

As described previously, the seven cross-sections were designed by modeling a 5-layer pavement system in PerRoad. For the three AC layers, seasonal dynamic modulus (|E*|) values were determined at a frequency of 12.57 Hz (or vehicle speed of approximately 55 mph) and temperatures from 2-year historical data from the Akron-Canton Airport in combination with laboratory measured E* data from previous studies (Sargand et al., 2015). The aggregate base resilient modulus was fixed for all seasons at 36,000 psi following the ODOT Pavement Design Manual (PDM) for aggregate base above stabilized subgrade. The stabilized subgrade resilient modulus was also fixed for all seasons at 16,320 psi, also based on the ODOT PDM in which the CBR (10 for the project) is multiplied by 1200 and 1.36 for stabilized subgrade. For the load spectra, 100% of the traffic was a single axle with 20-22 kip axle weight.

Several PerRoad analyses of the constructed test sections were completed. The first analysis utilized the same 5-layer cross-section as was done in the design of the cross-section, with 2 differences. The first difference was the AC layer moduli. In the evaluation of the as-constructed test sections, the AC layer moduli were determined from the laboratory measured E* data (presented elsewhere in this report) in conjunction with seasonal temperature data and a frequency of 12.57 Hz. The historical weather data was extended to include the 5 most recent years. The AC layer thicknesses reflect actual constructed thicknesses. The resilient moduli for aggregate base and stabilized subgrade reflected the design values of 36,000 psi and 16,320 psi, respectively. The load spectra remained at a 20-22 kip single axle load. This analysis enabled a comparison with the design cumulative distribution for tensile strain at the bottom of the AC layer and the vertical strain at the top of the subgrade.

Additional PerRoad Analyses were completed to compare predicted strain to field measured strain. For these analyses the actual load spectra were utilized as listed below. The aggregate base and stabilized subgrade moduli were varied, in which one analysis utilized backcalculated moduli and another analysis used DCP moduli as presented in Table 32. The AC layer thicknesses and moduli were consistent with the description above.

- 50% Single axles:
  - 76.25% at 26-28 kips
  - 23.75% at 30-32 kips
- 50% Tandem axles:
  - 76.25% at 40-42 kips
  - 23.75% at 46-48 kips

## PerRoad Analysis: Updating Cross-Section Designs to Reflect Actual AC Properties

In designing the cross-sections for the seven test sections designed AC layer thicknesses were used as well as dynamic moduli from previous studies. With laboratory measured E* data for the AC mixes placed on WAY-83 and known AC layer thicknesses the original designs should be updated, especially as these two parameters are known to influence tensile strain at the bottom of the AC layers. The same procedure to determine PerRoad inputs for the AC layers used to develop the target cumulative strain distribution was followed for this analysis as described below.

First, the historic weather data sourced from Weather Underground and collected at the Akron-Canton Regional Airport was expanded to include data from 2019 to 2023. From the

expanded dataset a cumulative average air temperature distribution was generated. The quintiles were then determined and used as the season average air temperature or MMAT for determining the MMPT or mean seasonal pavement temperature. The table below includes the season average air temperature and season duration.

**Table 1 Average Seasonal Air Temperature or MMAT**

| Season | Summer | Fall | Winter | Spring1 | Spring2 |
|---|---|---|---|---|---|
| Duration (weeks) | 11 | 10 | 11 | 10 | 10 |
| Temperature (F) | 75 | 67 | 30 | 41 | 54 |
| Temperature (C) | 23.9 | 19.4 | -1.1 | 5 | 12.2 |

Once known, the above MMAT values were used in the following equation to arrive at MMPT. For use in PerRoad, Z is the depth at the upper 1/3 of the given AC layer and MMAT and MMPT are the mean seasonal air temperature and mean seasonal pavement temperatures, respectively, in degrees Fahrenheit.

$$MMPT = MMAT\left[1 + \left(\frac{1}{Z+4}\right)\right] - \left[\frac{34}{Z+4}\right] + 6$$

As noted previously, E* master curves (reference temperature = 69.8F) were developed for each AC mix using the laboratory measured E* values. The computed MMPT values in combination with a frequency of 12.57 Hz (to represent a design speed of 55 mph) were used with the master curve equation to determine the seasonal AC moduli for each AC layer. These values, along with all other PerRoad Inputs are listed in Table 2 for each Test Section. The modulus for the aggregate base and stabilized subgrade remained at 36,000 psi and 16,320 psi, respectively. As noted above, in this analysis the load spectra were 100% single axles of 20-22 kips.

PerRoad output horizontal tensile strain at the bottom of the AC layer and vertical strain at the top of the subgrade. Consistent with the original designs, no vertical strain was predicted at the top of the subgrade, indicating these sections should be resistant to structural rutting. This is likely due to the high AC moduli values. Cumulative distributions of tensile strain at the bottom for the AC layer were developed for each test section. Strain distributions for the updated design, the original design, and the target cumulative strain threshold were plotted.

Plotted in Figure 1 are the resulting cumulative strain distribution curves for each test section using the updated AC moduli and AC layer thickness. Consistent with the original designs, Sections 6 and 7 were the only sections that did not meet the design distribution threshold. However, as noted previously during the evaluation of measured strain data an error was found in the design of the cross-sections which led to the use of a singular cumulative strain distribution, "HPM Base, Stabilized Subgrade." It was determined that two design distributions should have been used, as listed in Table 15 under "Evaluate Existing Perpetual Pavement Test Sections in Ohio," depending on whether conventional or HPM AC base mix was used. Sections 1 through 3 should be compared to the cumulative strain distribution for conventional AC base with a stabilized subgrade, while sections 4 through 7 should be compared to cumulative strain distribution for HPM AC base with stabilized subgrade. While section 2 is closest to meeting the conventional AC base with stabilized subgrade distribution, it does not meet at the extreme conditions ($85^{th}$ percentile and greater). Sections 1 and 3 fall to the right of this cumulative strain distribution. As expected, sections 4 and 5 fall to the left of the design distribution, while sections 6 and 7 fall to the right. Sections 4 through 7 include HPM AC mix in the base lift and were designed around the HPM base with stabilized subgrade cumulative strain distribution.

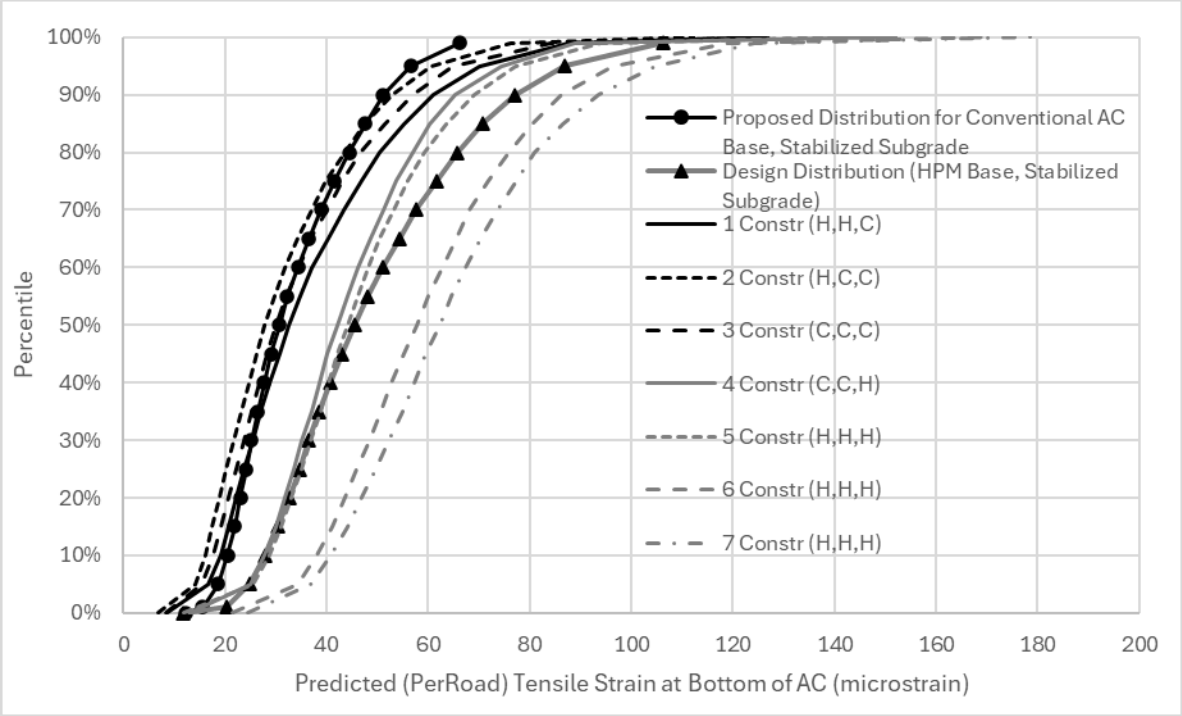


**Figure 102 Cumulative (Predicted) Strain Distribution of Updated Cross-Section Designs**

**Table 2 PerRoad Structural Inputs - Updated Cross-Section Design to Reflect Actual Thicknesses and Lab-Measured E***

| Section | Layer | PG | Poisson's Ratio | Layer thickness (in.) | Thickness Distribution Type | Thickness COV | Summer Modulus (psi) | Fall Modulus (psi) | Winter (psi) | Spring1 (psi) | Spring2 (psi) | Modulus Distribution Type | Modulus COV |
|---|---|---|---|---|---|---|---|---|---|---|---|---|---|
| 1 | AC Layer 1 - HPM | 70-22 | 0.35 | 1.5 | Default (Normal) | 0.05 | 471362 | 600102 | 1797874 | 1315302 | 893179 | Default (Lognormal) | Default (30%) |
| 1 | AC Layer 2 - HPM | 70-22 | 0.35 | 1.85 | Default (Normal) | 0.08 | 715747 | 919415 | 2404714 | 1893756 | 1349184 | Default (Lognormal) | Default (30%) |
| 1 | AC Layer 3 - Control | 70-22 | 0.35 | 9 | Default (Normal) | 0.15 | 1011726 | 1435937 | 3161310 | 2900291 | 2267280 | Default (Lognormal) | Default (30%) |
| 1 | Granular Base | | 0.4 | 6 | Default (Normal) | 0.2 | 36000 | 36000 | 36000 | 36000 | 36000 | Default (Lognormal) | 45% |
| 1 | Stabilized Subgrade | | 0.45 | Semi-infinite | | | 16320 | 16320 | 16320 | 16320 | 16320 | Default (Lognormal) | 50% |
| 2 | AC Layer 1 - HPM | 70-22 | 0.35 | 1.4 | Default (Normal) | 0.05 | 470217.7 | 598609 | 1797874 | 1315302 | 890955 | Default (Lognormal) | Default (30%) |
| 2 | AC Layer 2 - Control | 70-22 | 0.35 | 1.75 | Default (Normal) | 0.08 | 850366 | 1125766 | 2835846 | 2304883 | 1677998 | Default (Lognormal) | Default (30%) |
| 2 | AC Layer 3 - Control | 70-22 | 0.35 | 10.2 | Default (Normal) | 0.15 | 1015835 | 1441408 | 3161310 | 2900291 | 2267280 | Default (Lognormal) | Default (30%) |
| 2 | Granular Base | | 0.4 | 6 | Default (Normal) | 0.2 | 36000 | 36000 | 36000 | 36000 | 36000 | Default (Lognormal) | 45% |
| 2 | Stabilized Subgrade | | 0.45 | Semi-infinite | | | 16320 | 16320 | 16320 | 16320 | 16320 | Default (Lognormal) | 50% |
| 3 | AC Layer 1 - Control | 70-22 | 0.35 | 1.4 | Default (Normal) | 0.05 | 678864.5 | 903533 | 2289736 | 1875090 | 1360239 | Default (Lognormal) | Default (30%) |
| 3 | AC Layer 2 - Control | 70-22 | 0.35 | 1.8 | Default (Normal) | 0.08 | 853001.7 | 1125766 | 2835846 | 2304883 | 1677998 | Default (Lognormal) | Default (30%) |
| 3 | AC Layer 3 - Control | 70-22 | 0.35 | 9.4 | Default (Normal) | 0.15 | 1011726 | 1435937 | 3161310 | 2900291 | 2267280 | Default (Lognormal) | Default (30%) |
| 3 | Granular Base | | 0.4 | 6 | Default (Normal) | 0.2 | 36000 | 36000 | 36000 | 36000 | 36000 | Default (Lognormal) | 45% |

| Section | Layer | PG | Poisson's Ratio | Layer thickness (in.) | Thickness Distribution Type | Thickness COV | Summer Modulus (psi) | Fall Modulus (psi) | Winter (psi) | Spring1 (psi) | Spring2 (psi) | Modulus Distribution Type | Modulus COV |
|---|---|---|---|---|---|---|---|---|---|---|---|---|---|
| 3 | Stabilized Subgrade | | 0.45 | Semi-infinite | | | 16320 | 16320 | 16320 | 16320 | 16320 | Default (Lognormal) | 50% |
| 4 | AC Layer 1 - Control | 70-22 | 0.35 | 1.5 | Default (Normal) | 0.05 | 680911 | 906073 | 2289736 | 1875090 | 1363384 | Default (Lognormal) | Default (30%) |
| 4 | AC Layer 2 - Control | 70-22 | 0.35 | 1.83 | Default (Normal) | 0.08 | 855644 | 1128991 | 2835846 | 2309103 | 1677998 | Default (Lognormal) | Default (30%) |
| 4 | AC Layer 3 - HPM | 70-22 | 0.35 | 7.1 | Default (Normal) | 0.15 | 1360426 | 1614161 | 2552490 | 2355174 | 2020045 | Default (Lognormal) | Default (30%) |
| 4 | Granular Base | | 0.4 | 6 | Default (Normal) | 0.2 | 36000 | 36000 | 36000 | 36000 | 36000 | Default (Lognormal) | 45% |
| 4 | Stabilized Subgrade | | 0.45 | Semi-infinite | | | 16320 | 16320 | 16320 | 16320 | 16320 | Default (Lognormal) | 50% |
| 5 | AC Layer 1 - HPM | 70-22 | 0.35 | 1.4 | Default (Normal) | 0.05 | 470218 | 598609 | 1797874 | 1315302 | 890955 | Default (Lognormal) | Default (30%) |
| 5 | AC Layer 2 - HPM | 70-22 | 0.35 | 1.8 | Default (Normal) | 0.08 | 713800 | 916981 | 2404714 | 1889893 | 1349184 | Default (Lognormal) | Default (30%) |
| 5 | AC Layer 3 - HPM | 70-22 | 0.35 | 7.2 | Default (Normal) | 0.15 | 1357623 | 1614161 | 2552490 | 2355174 | 2020045 | Default (Lognormal) | Default (30%) |
| 5 | Granular Base | | 0.4 | 6 | Default (Normal) | 0.2 | 36000 | 36000 | 36000 | 36000 | 36000 | Default (Lognormal) | 45% |
| 5 | Stabilized Subgrade | | 0.45 | Semi-infinite | | | 16320 | 16320 | 16320 | 16320 | 16320 | Default (Lognormal) | 50% |
| 6 | AC Layer 1 - HPM | 70-22 | 0.35 | 1.5 | Default (Normal) | 0.05 | 471362 | 600102 | 1797874 | 1315302 | 893179 | Default (Lognormal) | Default (30%) |
| 6 | AC Layer 2 - HPM | 70-22 | 0.35 | 1.96 | Default (Normal) | 0.08 | 715741 | 919415 | 2404714 | 1893756 | 1349184 | Default (Lognormal) | Default (30%) |
| 6 | AC Layer 3 - HPM | 70-22 | 0.35 | 5.3 | Default (Normal) | 0.15 | 1354823 | 1608307 | 2552490 | 2353213 | 2017387 | Default (Lognormal) | Default (30%) |
| 6 | Granular Base | | 0.4 | 6 | Default (Normal) | 0.2 | 36000 | 36000 | 36000 | 36000 | 36000 | Default (Lognormal) | 45% |

| Section | Layer | PG | Poisson's Ratio | Layer thickness (in.) | Thickness Distribution Type | Thickness COV | Summer Modulus (psi) | Fall Modulus (psi) | Winter (psi) | Spring1 (psi) | Spring2 (psi) | Modulus Distribution Type | Modulus COV |
|---|---|---|---|---|---|---|---|---|---|---|---|---|---|
| 6 | Stabilized Subgrade | | 0.45 | Semi-infinite | | | 16320 | 16320 | 16320 | 16320 | 16320 | Default (Lognormal) | 50% |
| 7 | AC Layer 1 - HPM | 70-22 | 0.35 | 1.5 | Default (Normal) | 0.05 | 471362 | 600102 | 1797874 | 1315302 | 893179 | Default (Lognormal) | Default (30%) |
| 7 | AC Layer 2 - HPM | 70-22 | 0.35 | 1.8 | Default (Normal) | 0.08 | 715747 | 919415 | 2404714 | 1893756 | 1349184 | Default (Lognormal) | Default (30%) |
| 7 | AC Layer 3 - HPM | 70-22 | 0.35 | 5 | Default (Normal) | 0.15 | 1349230 | 1605381 | 2552490 | 2353213 | 2017387 | Default (Lognormal) | Default (30%) |
| 7 | Granular Base | | 0.4 | 6 | Default (Normal) | 0.2 | 36000 | 36000 | 36000 | 36000 | 36000 | Default (Lognormal) | 45% |
| 7 | Stabilized Subgrade | | 0.45 | Semi-infinite | | | 16320 | 16320 | 16320 | 16320 | 16320 | Default (Lognormal) | 50% |

# EVALUATION OF FIELD-MEASURED STRAIN RELATIVE TO PERPETUAL PAVEMENT CRITERIA

As noted previously, strain data were collected on four dates over a one-year period. The trucks used for the CVL testing varied from date to date, resulting in different single and tandem axle weights. Strain data were collected at three speeds: 5, 35 and 55 mph, except on 11/29/2023 the highest speed was only 50 mph. This amounted to 20 strain data measurements per section. Using the maximum measured tensile strain, regardless of orientation (longitudinal or transverse), cumulative strain distributions were generated for each test section and are presented in the plot below.

Overall, the measured strain values were very low (45 microstrain or less). Section 2 (HPM surface, control intermediate and base) had the lowest measured strain of all of the sections. This is likely due to the increased thickness as this section was designed at 12.5 inches of AC and was constructed with 13.35 inches. The control section, section 3, had the next lowest strain measurements. Sections 5 and 7, which featured HPM throughout with thicknesses of 10.4 and 8.3 inches, respectively, recorded the highest strain measurements. Previous studies have shown HPM mixes to be strain tolerant in the laboratory (Timm et al., 2012 and Bowers et al., 2018) and in the field (Timm et al., 2013). Given the thinner cross-sections and use of HPM which is strain tolerant and generally has lower E* data compared to the control mixes, higher strains were expected in the sections with HPM throughout.

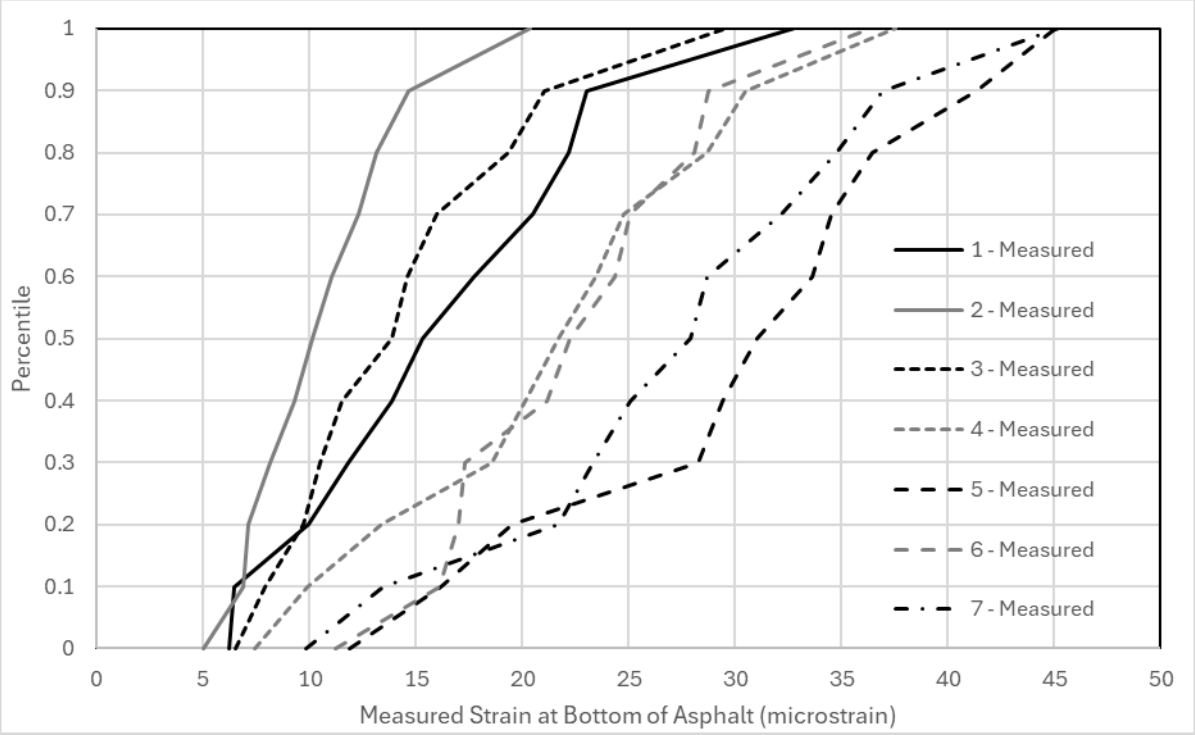


**Figure 2 Cumulative Distribution of Measured Strain for WAY-83, May 2023 – May 2024**

The maximum strain due to single axles are tabulated in the table below (bold font indicates maximum strain recorded in each section). The highest recorded strain of 45.19 microstrain occurred in section 7 at 5 mph on August 8, 2023. Temperatures were not recorded on the first date, however on the other three dates temperatures recorded in the AC did vary from section to section, with sections 6 and 7 having the largest difference. As noted previously, the single axle weights exceeded the value of 20-22 kips used in design, therefore it would be expected that the measured strain values would be a conservative estimate of strain under normal traffic conditions. Although the data represent only 4 test dates and therefore do not capture the whole range of temperatures to which the test sections may be exposed, the slow test speeds help to provide an understanding of the pavement response under extreme conditions. Interestingly, all strain values were much less than the traditional 70 microstrain threshold and much less than the predicted strain values.

**Table 3 Maximum Measured Strain under Single Axle**

| Date | Section | 5 mph | 35 mph | 50 mph | 55 mph | Temp (F) in AC Base |
|---|---|---|---|---|---|---|
| 5/10/2023 | 1 | 22.09 | | | | |
| 5/10/2023 | 2 | 13.98 | 10.98 | | 10.36 | |
| 5/10/2023 | 3 | 18.98 | 13.10 | | 13.55 | |
| 5/10/2023 | 4 | 28.52 | 24.72 | | 25.43 | |
| 5/10/2023 | 5 | **45.10** | 36.24 | | 36.79 | |
| 5/10/2023 | 6 | 28.57 | 24.61 | | 22.32 | |
| 5/10/2023 | 7 | 28.11 | 24.19 | | 23.36 | |
| 8/8/2023 | 1 | **32.77** | 21.20 | | 22.52 | 77 |
| 8/8/2023 | 2 | **20.40** | 14.48 | | 12.56 | 77 |
| 8/8/2023 | 3 | **29.58** | 21.00 | | 20.00 | 77 |
| 8/8/2023 | 4 | **37.53** | 29.60 | | 28.95 | 79.8 |
| 8/8/2023 | 5 | 43.98 | 41.54 | | 40.90 | 82 |
| 8/8/2023 | 6 | **36.42** | 28.50 | | 26.36 | 91.6 |
| 8/8/2023 | 7 | **45.19** | 33.26 | | 36.50 | 66.6 |
| 11/29/2023 | 1 | 10.04 | 9.50 | 10.16 | | 36.4 |
| 11/29/2023 | 2 | 8.90 | 7.10 | 6.80 | | 36.4 |
| 11/29/2023 | 3 | 10.30 | 8.70 | 9.30 | | 36.4 |
| 11/29/2023 | 4 | 13.36 | 13.43 | 11.70 | | 36.4 |
| 11/29/2023 | 5 | 20.20 | 18.55 | 18.33 | | 37.4 |
| 11/29/2023 | 6 | 16.99 | 16.10 | | | 32.4 |
| 11/29/2023 | 7 | 13.97 | 13.43 | | | 13.8 |
| 5/10/2024 | 1 | 22.90 | 16.80 | | 19.10 | 71.7 |
| 5/10/2024 | 2 | 14.70 | 11.90 | | 12.50 | 71.7 |
| 5/10/2024 | 3 | 21.10 | 16.00 | | 16.00 | 71.7 |
| 5/10/2024 | 4 | 30.90 | 24.70 | | 21.60 | 71.7 |
| 5/10/2024 | 5 | 31.80 | 34.40 | | 32.90 | 72.4 |
| 5/10/2024 | 6 | 24.90 | 28.80 | | 25.20 | 68.3 |
| 5/10/2024 | 7 | 33.10 | 27.70 | | 29.00 | 53.2 |

Axle weights varied from date to date, and due to the varying temperatures from section to section on a given date, comparisons between sections and against predicted strains are not appropriate without first normalizing the measured strain data. First, each strain value was divided by the axle weight under which strain was incurred. The strain/kip values at 5 mph were then plotted against the temperature recorded in the AC base layer. An exponential trendline ($\varepsilon$/kip = $a*e^{(bT)}$) was fitted to the data resulting in the coefficients and $R^2$ values listed in the following table. The curve parameters were then applied to three temperatures, 20F, 50F, and 90F, to represent the range of temperatures that may be seen in the field, although the extreme ends are extrapolations of the measured data. The resulting estimated strain/kip was then multiplied by 10.5 kips to represent a 20-22 kip single axle. This enables a more even comparison of sections and pavement response to temperature. The results are presented in the plot below.

**Table 4 Exponential Curve Parameters for Strain/kip at 5 mph**

| Section | a | b | $R^2$ |
|---|---|---|---|
| 1 | 0.3115 | 0.0223 | 0.5716 |

| | | | |
|---|---|---|---|
| 2 | 0.3287 | 0.0185 | 0.8584 |
| 3 | 0.309 | 0.0242 | 0.9109 |
| 4 | 0.4082 | 0.0241 | 0.9985 |
| 5 | 0.7822 | 0.0166 | 0.9153 |
| 6 | 0.7993 | 0.013 | 0.9772 |
| 7 | 0.7504 | 0.0225 | 0.9979 |

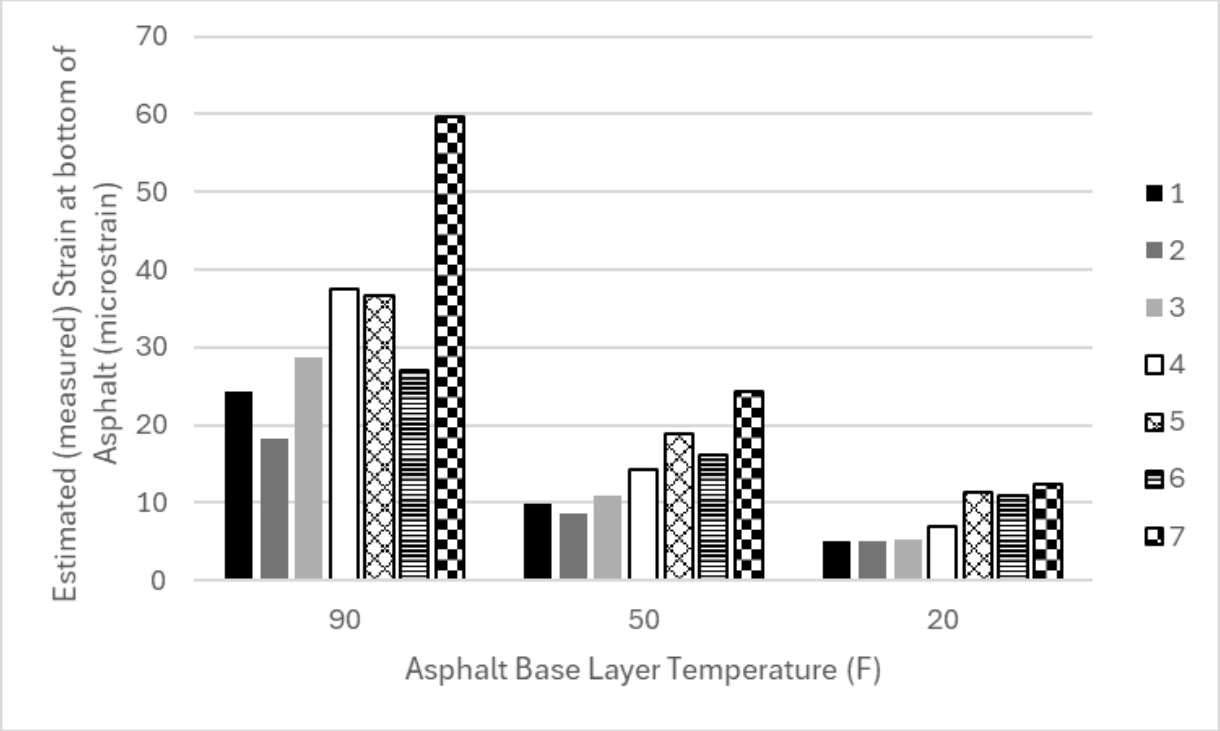


**Figure 3 Estimated Field Strain at 5 mph 20-22 kip Single Axle**

Consistent with the cumulative strain distribution of measured strain values, section 7 had the highest strain values for all three temperatures which is expected as it is the thinnest section. Similarly, the thickest section, section 2, resulted in the lowest strain values. The table below shows the ranking of the predicted strain and measured strain values by lowest to highest strain values. As shown in the following table, the only other section that had the same ranking between predicted strain and estimated field strain was section 5. Interestingly, section 6, the second thinnest test section, had lower estimated strain based on field measurements than Test Sections 3 - 5 at the high temperature. The 8.76-inch cross-section of HPM AC mix would be expected to have higher strains than sections 1 – 5 due to the thickness and use of the strain tolerant HPM AC mixes which had lower dynamic moduli than the control AC mixes.

**Table 5 Ranking of Test Sections by Lowest to Highest Strain Values**

| Predicted Strain | Estimated Field Strain (Normalized at 90F) |
|---|---|
| 2 | 2 |
| 3 | 1 |
| 1 | 6 |
| 4 | 3 |
| 5 | 5 |
| 6 | 4 |
| 7 | 7 |

To put the strain estimated from field-measured data into context, it is worth taking a look at past research. Robbins et al. (2015) refined the original cumulative strain distribution concept (Willis,

2009) by creating a limiting strain distribution for predicted strain to be used in design. As shown in the table below, even when section specific material properties from construction and FWD test results were applied, predicted and field strains do not perfectly line up. At the NCAT Test Track the field limiting strain was greater than the predicted limiting strain. While this is contrary to the observations made in this study, it should be noted cross-sections were generally thinner at the NCAT Test Track, with sections N3 and N4 which defined the limiting strain for both field and predicted strain, consisted of approximately nine inches of conventional AC on top of six inches of aggregate base, on top of a stiff unstabilized subgrade (backcalculated resilient modulus approximately 30 ksi) (Robbins et al., 2015). Additionally, air temperatures in Alabama tend to be hotter. Recorded mid-depth pavement temperatures used in the development of the NCAT Test Track limiting predicted strain distributions for the summer season for sections N3 and N4 were 87F and 96F, respectively (Robbins et al., 2015). These values are 10 to 20 degrees higher than summer temperatures used in the modeling of WAY-83 test sections. This combination of higher temperatures and thinner cross-sections on an unstabilized subgrade would lead to greater field measured strain at the NCAT Test Track relative to WAY-83. This helps to explain why the measured strains on WAY-83 are much less than the measured strains reported at the NCAT Test Track.

In terms of the predicted tensile strain, Robbins et al. utilized backcalculated moduli for the AC layers in developing the limiting predicted strain. Whereas, in this study, laboratory measured E* data were used in PerRoad to predict the tensile strain at the bottom of the AC layers. Given that E* values are greater than backcalculated moduli it would be expected that predicted strain would be less than strain predicted with backcalculated moduli. This helps to explain the difference between the limiting strain criteria for predicted strain at the NCAT test Track and the proposed limiting strain criteria for predicted strain calibrated to Ohio conditions (see table below), as developed in this study.

**Table 6 NCAT Field Limiting Strain and Limiting Predicted Strain Distributions (Robbins et al., 2015 [AAPT paper]) Compared with Proposed Cumulative Strain Distributions**

| Percentile | NCAT Field limiting strain | NCAT Limiting predicted strain | Proposed Conventional AC base with stabilized subgrade | Proposed HPM AC base with stabilized subgrade |
|---|---|---|---|---|
| 50 | 181 | 100 | 30.70 | 45.52 |
| 55 | 193 | 110 | 32.25 | 48.15 |
| 60 | 205 | 120 | 34.35 | 51.02 |
| 65 | 218 | 131 | 36.56 | 54.40 |
| 70 | 232 | 143 | 38.93 | 57.64 |
| 75 | 247 | 158 | 41.64 | 61.62 |
| 80 | 263 | 175 | 44.47 | 65.77 |
| 85 | 282 | 194 | 47.59 | 70.77 |
| 90 | 310 | 221 | 51.15 | 76.98 |
| 95 | 346 | 257 | 56.53 | 87.01 |
| 99 | 394 | 326 | 66.16 | 106.30 |

To provide context to strain measured in the WAY-83 test sections, they should be compared with field-measured strain from the perpetual pavement test sections which the proposed cumulative strain distributions were based. The proposed cumulative strain distribution for conventional AC base with a stabilized subgrade was based on the DEL-23 SB ramp test section. Strains were measured on DEL-23 in November and December of 2012 and in July of 2013. The controlled vehicle testing included a single axle wide based tire with tire pressure of 80, 110, and 125 psi. The axle load varied between winter and summer test dates. For comparisons with strain measured in tests sections 1 through 3 on WAY-83, strain measured under 5 mph and with a 110 psi tire pressure were utilized, as 110 psi is comparable to the tire pressure of the vehicles used for testing on WAY-83 (see Table 29 under Controlled Vehicle Load (CVL)

Tests). Strain of 32.2 microstrain was measured in the fall at pavement temperatures of 44.2F under a 29 kip axle load. In the summer, 77.1 microstrain was measured under a 21-kip axle load with a pavement temperature of 81.5F. To compare field measured strain for WAY-83 Sections 1 through 3 which had conventional AC in the base lift, these conditions were applied to the exponential curves developed for each test section and multiplied by one half of the axle load. Listed in Table 7 are the estimated strains for the two pavement temperatures. This provides a fair comparison between all three sections and the DEL-23 SB ramp test section. All three test sections have estimated field strain well below the strains measured on DEL-23 SB ramp under the same conditions. Section 3 on WAY-83 had an estimated strain of only 23 microstrain at 81.5F and 21-kip axle load, which amounts to only 30% of the strain measured on DEL-23 SB ramp under the same conditions. While the conditions under which the strain was measured on DEL-23 SB ramp were not considered extreme, the comparison does provide some insight into the expected performance of the WAY-83 test sections. DEL-23 SB ramp was able to handle higher strains with similar materials under the same conditions, without structural failures; therefore, there is a strong likelihood that the WAY-83 Test Sections 1 through 3 will perform as well or better than the DEL-23 SB ramp.

**Table 7 Estimated Strain at 5 mph, WAY-83 Test Sections 1 - 3**

| Section | T = 44.2F<br>Load = 14.5 kips | T = 81.5F<br>Load = 10.5 kips |
|---|---|---|
| 1 (H,H,C) | 12.10 | 20.14 |
| 2 (H,C,C) | 10.80 | 15.59 |
| 3 (C,C,C) | 13.06 | 23.32 |

For sections 4 through 7 which feature HPM AC in the base lift, comparisons should be drawn with Lane C of the APLF. Strain measurements in the APLF were made after the entire cross-section reached 70F, and 100F. Strain was measured under 3 axle loads: 6 kips, 9 kips, and 12 kips. The maximum strain value of 67 microstrain was measured under 12-kips at 100F and 51 microstrain at 70F under the same loading. In looking at the Table 6, that is approximately the 82$^{nd}$ percentile of the predicted strain. To compare the WAY-83 Test Sections against the maximum strain for Lane C in the APLF, the exponential curve parameters for 5 mph were applied for each test section at pavement temperatures of 70F and 100F. The results (in strain/kip) were then multiplied by 12 kips to enable a comparison with measurements made in the APLF. As shown in the table below, the only WAY-83 section to have strain exceeding the strain measured in APLF Lane C is section 7. The estimated strain for section 7 at 70F is less than the 51 microstrain measured in the APLF. However, at 100F the estimated strain in Section 7 is 85.4 microstrain, which is 27% greater than the maximum strain measured in APLF Lane C. Section 7 strain at T = 100F represents the 94$^{th}$ percentile of the target distribution, whereas the maximum strain at these conditions in the APLF crossed the target distribution at the 82$^{nd}$ percentile. Although these conditions are extreme and would occur in the field infrequently, it could be concluded that Section 7 is the only section that may not behave perpetually.

**Table 8 Estimated Strain at 12 kips and 5 mph WAY-83 Test Sections 4 - 7**

| Section | T = 70F | T = 100F | T = 100F,<br>Percentile of<br>Target Distribution |
|---|---|---|---|
| 4 (C,C,H) | 26.5 | 54.5 | 65$^{th}$ |
| 5 (H,H,H) | 30.0 | 49.4 | 57$^{th}$ |
| 6 (H,H,H | 23.8 | 35.2 | 26$^{th}$ |
| 7 (H,H,H) | 43.5 | **85.4** | **94$^{th}$** |

Based on field measurements and relative comparisons to previous perpetual pavement test sections in Ohio, Sections 1 through 5 are expected to behave perpetually. Section 6 was found to have surprisingly low measured strain values. Further investigation and field measurements should be made in

this section to confirm data are accurate and representative. The performance of Section 6 should be closely monitored.

## PerRoad Analysis: Comparison with Field Measured Strain

Pavement responses, both field-measured and estimated based on field-measured strain (see Tables 4 and 6 and Figure 10), deviate from the predicted strain, in terms of magnitude and in terms of ranking. Therefore, a further look at in-situ material properties is necessitated to understand why the large differences exist and why Section 6 has the potential to perform perpetually despite being designed to be non-perpetual. In modeling the pavement sections in PerRoad, the actual AC layer thicknesses were utilized as well as laboratory-measured E* data for the AC mixes. The aggregate base and stabilized subgrade utilized design values. Regarding the AC layers, the laboratory measured E* values are the best estimate of in-situ modulus, although mat density and consistency of the gradation (i.e. presence of segregation) could impact the in-place layer modulus. Additionally, there has long been a debate surrounding the translation from laboratory testing conditions, namely frequency, to field conditions (speed). While these differences are acknowledged, it is unlikely they alone are the source for the large deviations between predicted strain and field-measured strain.

Backcalculated moduli and estimated moduli from DCP testing for previous perpetual pavement sections (DEL-23 and APLF) were difficult to determine due to the stress hardening properties of these layers. Previous analyses of the in-situ moduli for the aggregate base and cement stabilized subgrade in the APLF resulted in very high values depending on the tool (DCP or FWD) used. The number of layers on the DEL-23 perpetual pavement NB and SB ramp sections in which the subgrade was modified with lime necessitated the combination of like layers. As such, the aggregate base and lime modified subgrade were combined and variable results noted. The research team could not draw a conclusion based on the limited data as to what design value should be used for cement stabilized subgrade and aggregate base on top of the stabilized subgrade. Therefore, PDM design values for the aggregate base and stabilized subgrade were used to model the previous perpetual pavement test sections.

In designing the cross-sections, PDM values were used for the aggregate base and stabilized subgrade, while E* values from similar mixes were used in conjunction with designed layer thicknesses. These designs were updated in Figures 7 through 13, in which the constructed cross-sections of the WAY-83 test sections were modeled in PerRoad using measured E* values and layer thicknesses and assumed moduli for aggregate base and stabilized subgrade based on the CBR for the project. While material properties for the AC layers were based on measured values (in design - from the APLF and DEL-23 test sections; and in Figures 7-13 – from measured E* values for WAY-83 mixes), the aggregate base and stabilized subgrade moduli were the only material properties that were not based on measured values. Rather, they were based on a resilient modulus-CBR correlation, and a correction factor. As such, they are a likely source for some of the deviations between predicted and measured strain values at the bottom of the AC layers and warrant further investigation.

As noted previously in this report, DCP testing was conducted on 11/15/2022. From those tests results the resilient modulus of the aggregate base and stabilized subgrade were estimated for each section, which are presented in the figure below along with the PDM design values used for WAY-83. As shown in the figure, all sections had aggregate base modulus which exceeded the PDM design value of 36 ksi. Section 4 had the lowest modulus, which was only slightly greater than the PDM value, at 38 ksi. DCP-derived modulus for the stabilized subgrade in each test section far exceeded the PDM value of 16.32 ksi. Section 1 had the lowest stabilized subgrade modulus derived from DCP measurements at 66 ksi, which is four times the PDM value. Overall, DCP derived aggregate base moduli and stabilized subgrade moduli vary spatially with no obvious trends, despite test sections being contiguous and in sequential order.

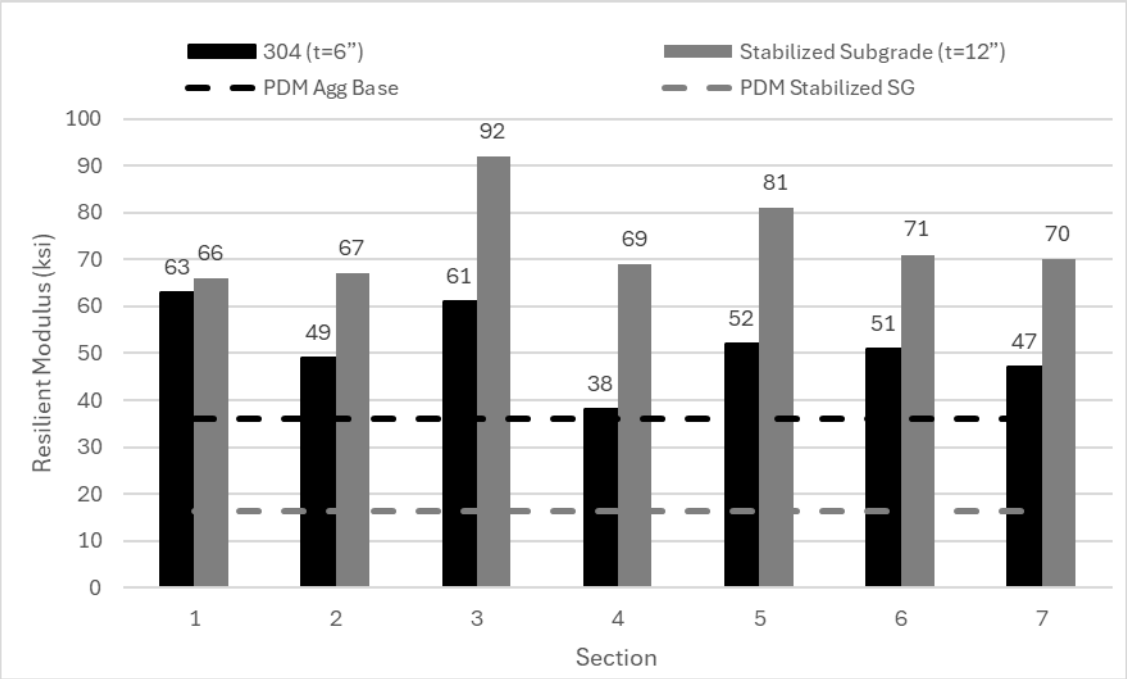


**Figure 4 DCP-Derived Moduli for Aggregate Base and Stabilized Subgrade, WAY-83 Test Sections (11/15/2022)**

FWD data were collected on five dates, from which layer moduli were backcalculated using BackFAA. Outliers were removed through a visual evaluation of the data. Based on the average air temperature on the date tested, each date was assigned to a season as listed below. The following tables and figures present the average seasonal backcalculated moduli for the aggregate base and stabilized subgrade for each section.

- 11/10/2022: Average Temperature = 58.9F, representing Fall
- 5/8/2023: Average Temperature = 60.3F, representing Spring 2
- 8/8/2023: Average Temperature = 68.2F, representing Summer
- 11/28/2023: Average Temperature = 21.1F, representing Winter
- 5/11/2024: Average Temperature = 50.3F, representing Spring 1

**Table 9 Aggregate Base Backcalculated Moduli (psi) by Season. WAY-83**

| Section | Summer 8/8/2023 | | Fall 11/10/2022 | | Winter 11/28/2023 | | Spring1 5/11/2024 | | Spring2 5/8/2023 | |
|---|---|---|---|---|---|---|---|---|---|---|
| | Modulus | CoV | Modulus | CoV | Modulus | CoV | Modulus | CoV | Modulus | CoV |
| 1 | 11,824 | 0.49 | 43,524 | 0.41 | 161,381 | **0.42** | 26,474 | 0.39 | 11,200 | **0.70** |
| 2 | 21,444 | **0.78** | 45,050 | 0.37 | 234,571 | 0.30 | 62,889 | **0.89** | 5,875 | 0.56 |
| 3 | 22,500 | 0.56 | 59,167 | 0.38 | 201,667 | 0.35 | 33,579 | 0.60 | 11,050 | 0.33 |
| 4 | 13,053 | 0.56 | 105,905 | **1.30** | 87,444 | 0.35 | 18,842 | 0.30 | 8,941 | 0.12 |
| 5 | 22,316 | 0.53 | 29,105 | 0,67 | 129,700 | 0.33 | 46,053 | 0.42 | 35,500 | 0.57 |
| 6 | 27,300 | 0.39 | 45,263 | 0.26 | 103,650 | 0.32 | 53,000 | 0.23 | 40,450 | 0.26 |
| 7 | 24,278 | 0.43 | 26,100 | 0.57 | 98,789 | 0.37 | 45,500 | 0.32 | 37,650 | 0.40 |
| Avg | 20,388 | | 50,588 | | 145,315 | | 40,905 | | 21,524 | |

**Table 10 Average Stabilized Subgrade Backcalculated Moduli (psi) by Season, WAY-83**

| Section | Summer | Fall | Winter | Spring1 | Spring2 |
|---|---|---|---|---|---|

| | 8/8/2023 | | 11/10/2022 | | 11/28/2023 | | 5/11/2024 | | 5/8/2023 | |
|---|---|---|---|---|---|---|---|---|---|---|
| | Modulus | CoV | Modulus | CoV | Modulus | CoV | Modulus | CoV | Modulus | CoV |
| 1 | 123,845 | 0.63 | 132,582 | 0.39 | 300,890 | 0.23 | 138,483 | 0.43 | 123,684 | 0.63 |
| 2 | 312,990 | 0.65 | 201,111 | 0.43 | 376,555 | 0.31 | 196,003 | 0.64 | 403,657 | 0.65 |
| 3 | 184,054 | 0.63 | 269,990 | 0.58 | 372,089 | 0.25 | 330,237 | 0.53 | 178,023 | 0.63 |
| 4 | 140,590 | **0.79** | 204,469 | **0.79** | 207,417 | **0.31** | 236,659 | **0.65** | 471,053 | **0.79** |
| 5 | 162,140 | 0.50 | 114,984 | 0.29 | 289,985 | 0.18 | 193,872 | 0.42 | 130,718 | 0.50 |
| 6 | 149,738 | 0.50 | 93,519 | 0.36 | 193,481 | 0.30 | 173,045 | 0.24 | 131,030 | 0.50 |
| 7 | 155,165 | 0.73 | 76,099 | 0.17 | 234,409 | 0.20 | 148,222 | 0.32 | 115,150 | 0.73 |
| Avg | 175,503 | | 156,108 | | 282,118 | | 202,360 | | 221,902 | |

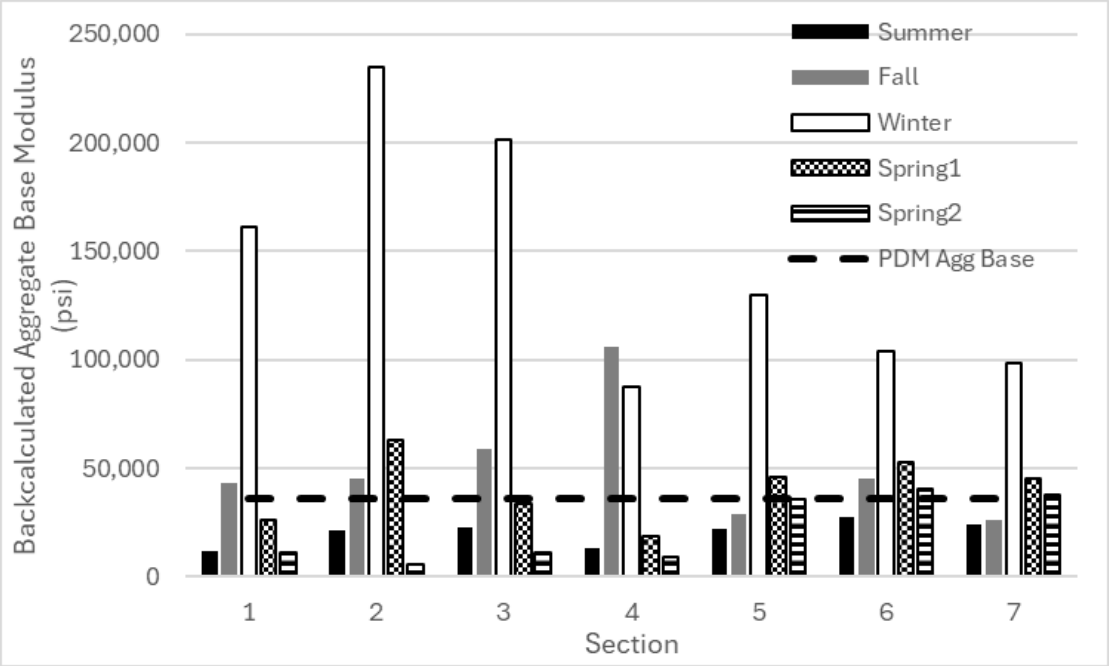


**Figure 5 Backcalculated Aggregate Base Modulus by Section and Season, WAY-83**

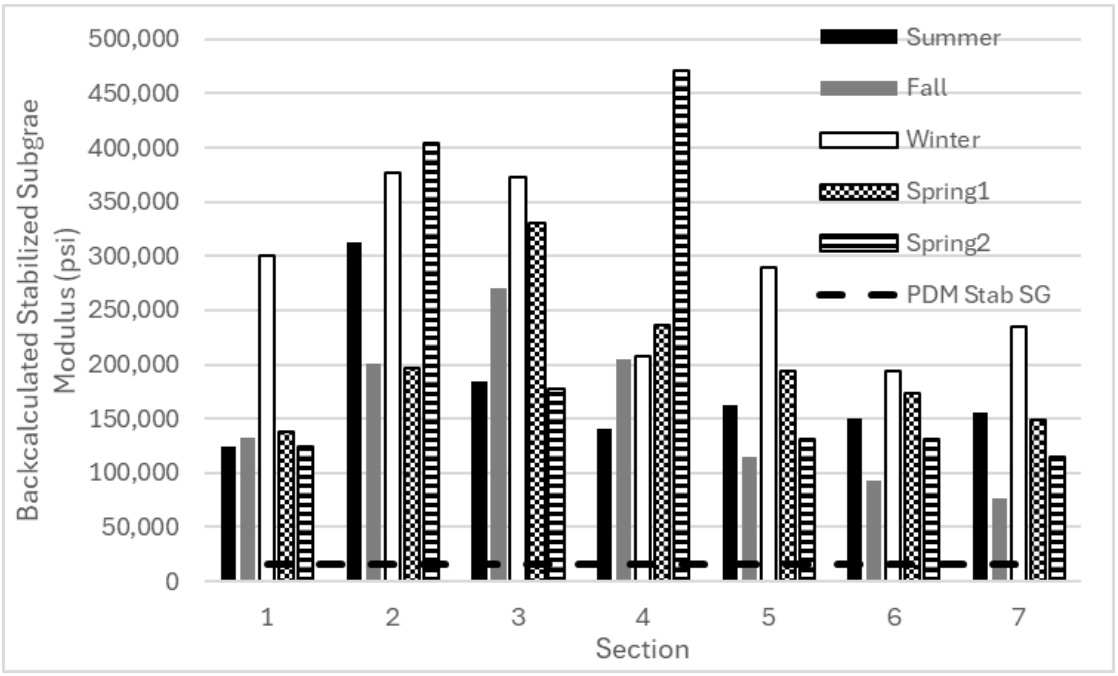


**Figure 6 Backcalculated Stabilized Subgrade Modulus by Section and Season, WAY-83**

The spatial (section to section) variation in both aggregate base and stabilized subgrade moduli for a given season, is more pronounced in the backcalculated moduli data than the DCP-derived moduli. This is especially true for the backcalculated moduli for the aggregate base in the fall and winter seasons. Backcalculated aggregate base moduli ranged from 26,100 psi to 105,905 psi in the fall season and from 87,444 psi to 234,571 psi in the winter season. Backcalculated moduli for the stabilized subgrade also varied by section for each season, with the largest variation occurring in Spring 2 with values ranging from 115,150 psi (Section 7) to 471,053 psi (Section 4).

In comparing the backcalculated moduli to the PDM values, it is evident the PDM values (16,320 psi), drastically underestimates the in-situ modulus of the stabilized subgrade for all seasons. For the aggregate base, the backcalculated moduli are greater than the PDM value (36,000 psi) for most sections in the fall and winter seasons, and for some sections in spring 1.

Overall, the DCP-derived modulus, backcalculated modulus, and PDM modulus generally do not agree with one another. Additional PerRoad simulations were run for each section to determine if DCP-derived aggregate base and stabilized subgrade moduli or backcalculated aggregate base and stabilized subgrade moduli were a better predictor of field measured strain. The intent of these simulations were to model the cross-sections under the actual field conditions to provide a fair comparison between the field measured and predicted strain. For these PerRoad simulations, the load spectra represented the actual CVL traffic, as follows, as opposed to 100% at the 20-22 kip single axle load level used in design. For the AC layers, the measured E* values for the WAY-83 mixes and measured layer thicknesses used in the previous PerRoad simulations were utilized (see values listed in Table 2 for the AC layers). For the DCP-derived moduli, the moduli shown in Figure 4 were used for all seasons, as DCP testing was only conducted once in the study period. For PerRoad simulations in which the backcalculated moduli were used for the aggregate base and stabilized subgrade, the seasonal values listed in Tables 9 and 10 were used. Although CoV values were calculated for the backcalculated moduli (see Tables 9 and 10), the values used previously and listed in Table 2 were used to model the variation of the aggregate base and subgrade moduli.

- CVL load spectra:
    - 50% Single axles:
        - 76.25% at 26-28 kips
        - 23.75% at 30-32 kips
    - 50% Tandem axles:

- 76.25% at 40-42 kips
- 23.75% at 46-48 kips

Lastly, PerRoad simulations were conducted for each section to provide a relative comparison, in which PDM values were used for the aggregate base and stabilized subgrade moduli and were held constant across all seasons (as was done previously, see Figure 1). However, rather than use the design load spectra, the CVL load spectra was used to provide a more fair comparison with the aforementioned simulations and measured strain values.

Results for all three PerRoad simulations ("Backcalculated E," "PDM E," and "DCP E") are presented for each section as well as the proposed strain distribution for use in design. To provide context to the field measured strain shown, the strain estimated from field measured strain at the same conditions as the DEL-23 SB ramp (T = 81.5F, speed of 5 mph, and load of 10.5 kips) are also plotted for sections 1 through 3. For sections 4 through 7, estimated strain at the same conditions as the maximum strain measurements in the APLF (T = 100F, speed of 5 mph, and load of 12 kips) are also plotted.

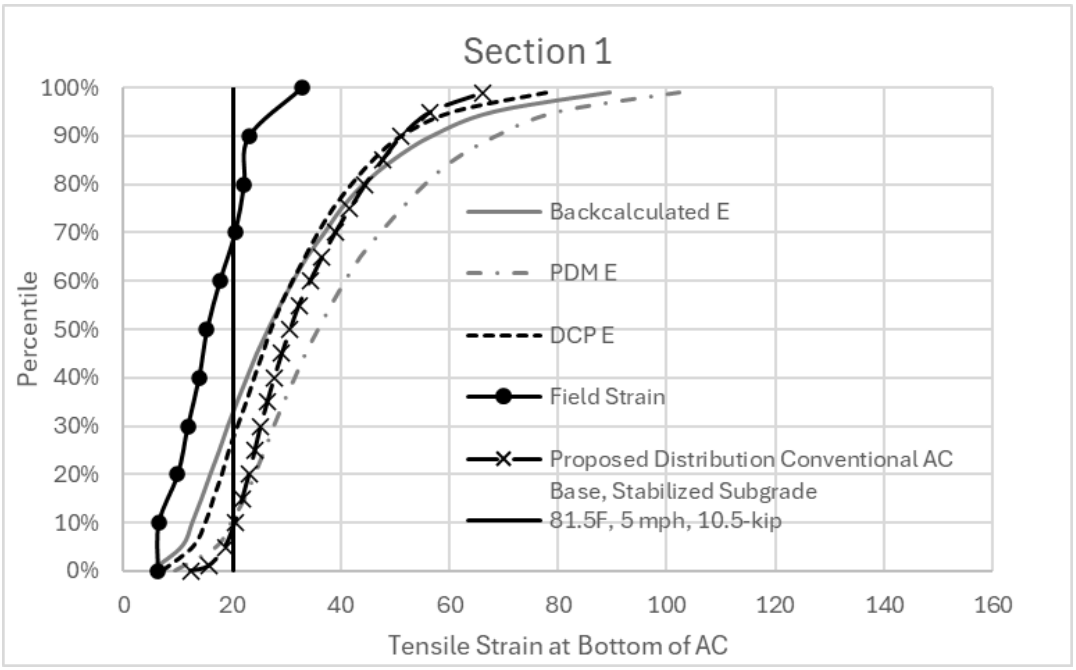


**Figure 7 Comparison of Tensile Strain under CVL Loading, Section 1 (H,H,C)**

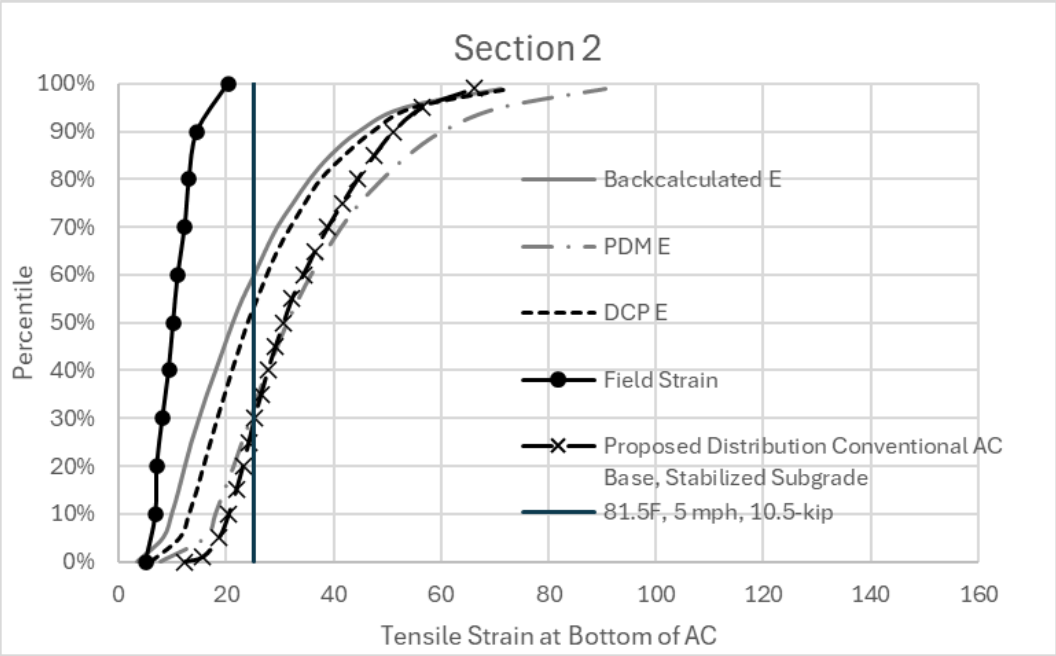


**Figure 8 Comparison of Tensile Strain under CVL Loading, Section 2 (H,C,C)**

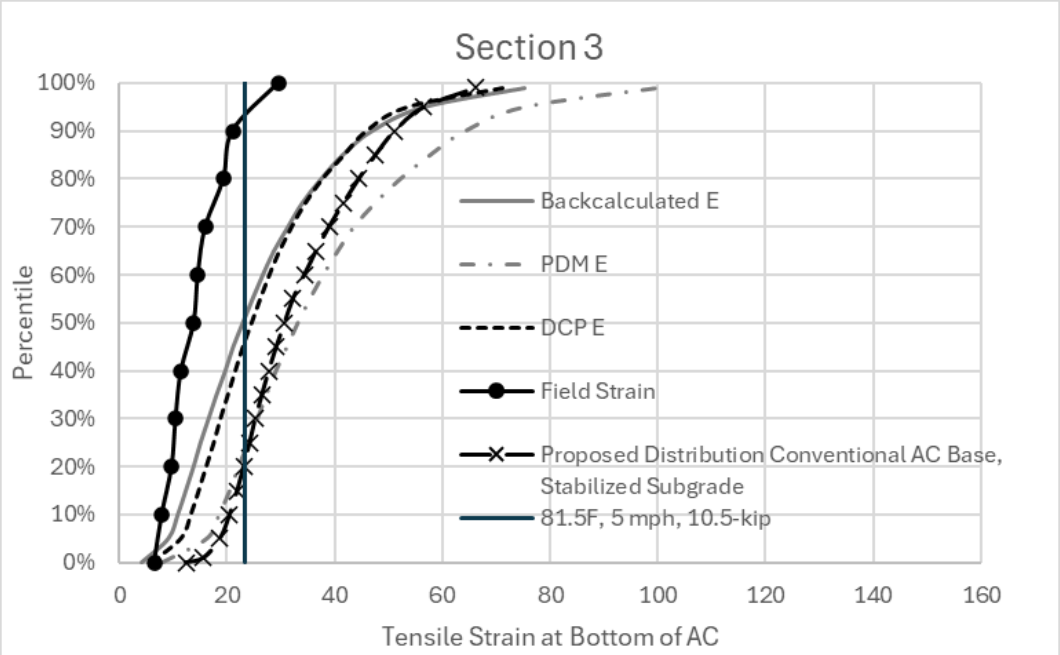


**Figure 9 Comparison of Tensile Strain under CVL Loading, Section 3 (C,C,C)**

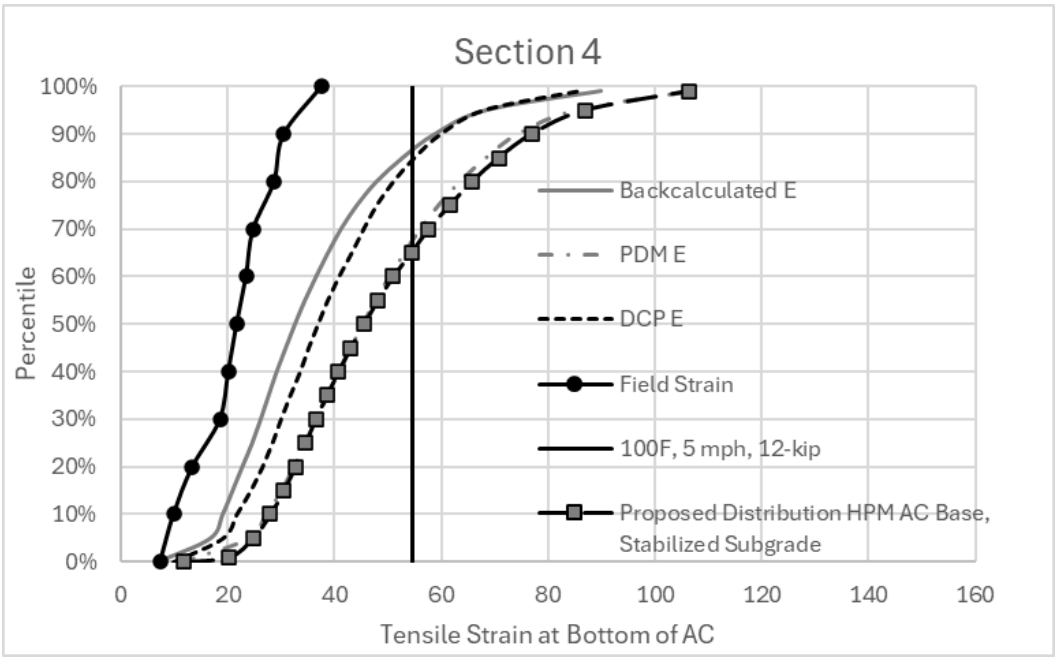


**Figure 10 Comparison of Tensile Strain under CVL Loading, Test Section 4 (C,C,H)**

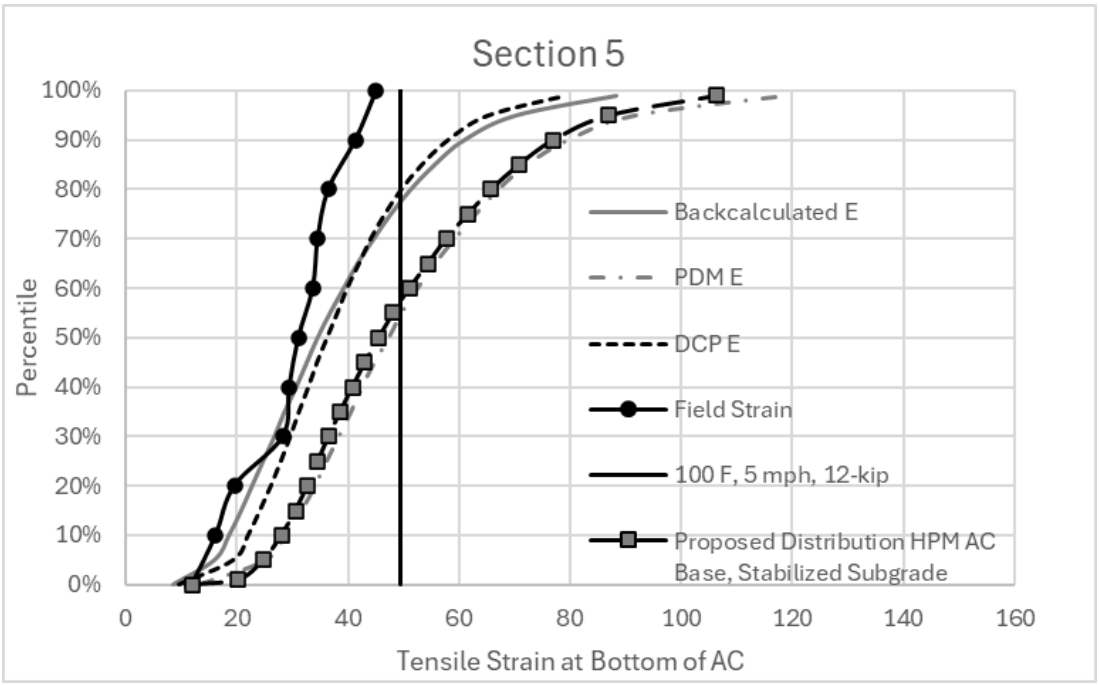


**Figure 11 Comparison of Tensile Strain under CVL Loading, Test Section 5 (H,H,H)**

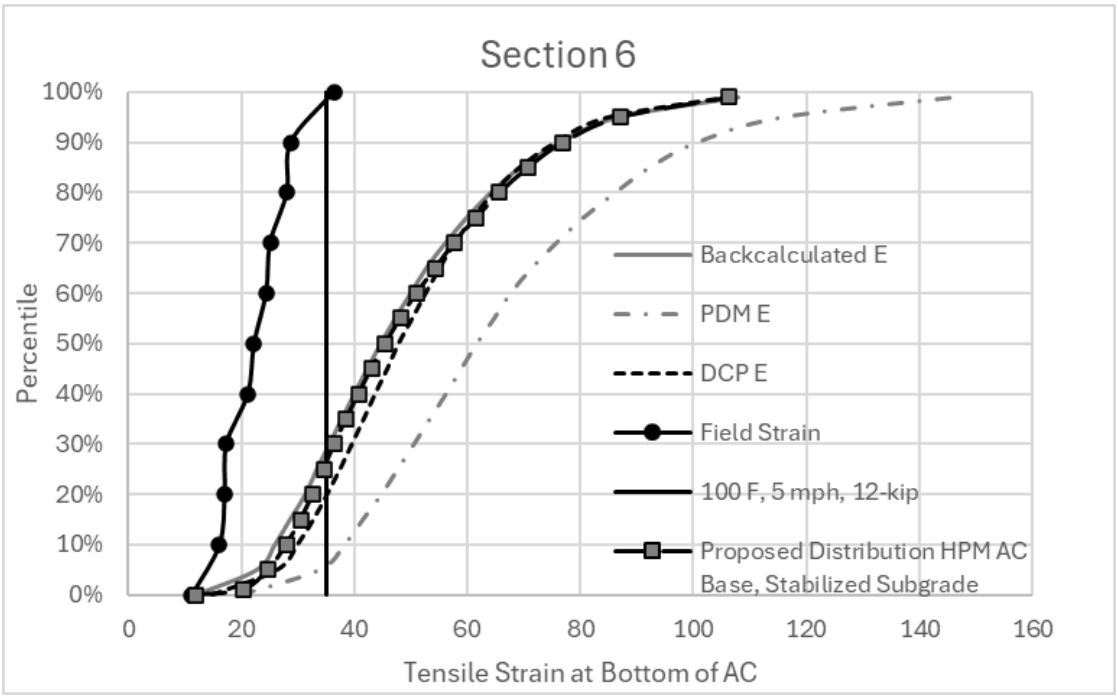


**Figure 12 Comparison of Tensile Strain under CVL Loading, Test Section 6 (H,H,H)**

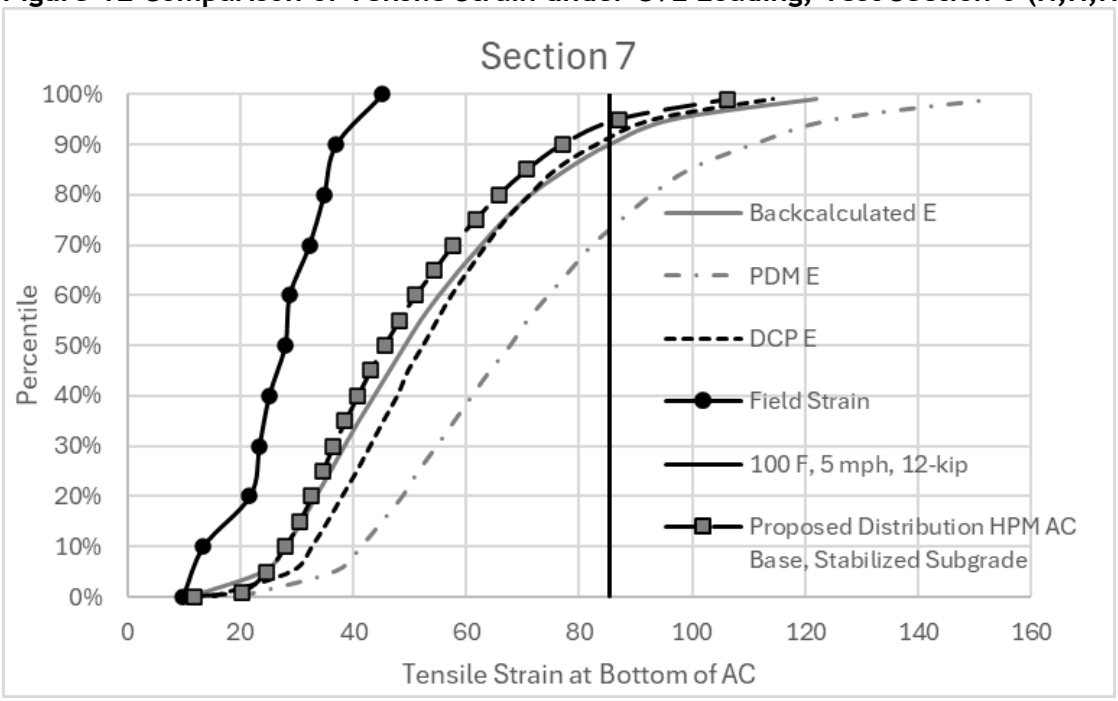


**Figure 13 Comparison of Tensile Strain under CVL Loading, Test Section 7 (H,H,H)**

It should be kept in mind that the field measured tensile strain distribution is somewhat limited in terms of pavement conditions, as data were only collected on four test dates. The temperatures for a given date varied from section to section, with large differences noted on the hottest test date (8/8/2023). As such, the field-measured cumulative strain distribution may not be a complete curve. The vertical line in Figures 7 – 9 represent strain estimated at a pavement temperature of 81.5F, vehicle speed of 5 mph and load of 10.5 kips (one half of a 21-kip axle). In a similar fashion strain estimated at a pavement temperature of 100F, vehicle speed of 5 mph and load of 12 kips (representing a 24 kip single axle load) were plotted as a vertical line in Figures 10 - 13. These conditions, reflect the conditions under which some of the highest strains were measured in past, relevant perpetual pavement test sections. The estimated strain (vertical line) in section 7 is much greater than the measured field strain, although the estimated strain for sections 5 and 6 either cross or nearly cross the field measured strain distribution.

Sections 5 and 6 recorded pavement temperatures 15F to 25F greater than Section 7 on the hottest test date which helps to explain the gap between the estimated strain (vertical line) and measured strain distribution in Section 7. This implies Sections 5 and 6 were exposed to more extreme conditions during CVL testing than section 7. For this reason, when comparing predicted strain to measured strain, it is best to compare to the singular strain value on each plot, as they are estimated at the same conditions across Figures 7-9, and Figures 10 - 13.

Putting these predicted strain curves and estimated/measured strain values in perspective requires a look back at the development of the design strain distribution. Lane C of the APLF was considered a perpetual pavement based on measured strain, the calculated stiffness ratio and early pavement performance. This section was modeled in PerRoad using laboratory-determined E* values to estimate AC moduli at the seasonal temperatures, actual AC layer thicknesses. For the underlying layers, the aggregate base and stabilized subgrade moduli were modeled following the ODOT PDM with values of 36,000 psi and 16,320 psi, respectively. For the aggregate base and stabilized subgrade, the moduli were held constant across all seasons. The load spectra consisted of 100% single axle loads of 20-22 kips. The resulting cumulative strain distribution then served as the design threshold. Cross-sections for test sections 1 – 5 were originally designed such that predicted strain distribution curves were less than the design curve (i.e. the curves fell to the left of the design threshold). However, as was noted previously, an error was made in the E* values during the evaluation of DEL-23 test sections and the error was carried over into design of WAY-83 Sections 1 through 3. After the error was discovered, the DEL-23 test sections were modeled again in PerRoad, with the correct E* values, which resulted in the proposed strain distribution for conventional AC base with stabilized subgrade shown in Figures 7 – 9 and reported in Table 15 of "Evaluate Existing Section with Various Perpetual Pavement Criteria." This explains why the proposed strain distribution for conventional AC base with stabilized subgrade is greater than the cumulative strain distribution when PDM values were used to model the aggregate base and stabilized subgrade in PerRoad. Despite being greater than the proposed design cumulative strain distribution for sections with conventional AC base mix on stabilized subgrade, measured strain values were very low for Sections 1 through 3. When compared to strain measured on DEL-23 SB ramp at 81.5F, 5 mph vehicle speed, and 10.5 kip load, estimated strains at the same conditions were much lower in these three test sections. Since DEL-23 SB ramp is believed to be perpetual, this is an indicator that Sections 1 through 3 are also likely to perform perpetually.

The thickness of Section 6 was selected to replicate Lane B of the APLF which was believed to have a lower probability of being perpetual when compared with Lane C. The design of section 6, showed predicted strains greater than the design threshold, indicating it was not expected to perform perpetually. The thickness of Section 7 matched the mainline cross-section and based on the design was not expected to perform perpetually.

As noted previously, maximum strain of 67 microstrain was measured in Lane C (HiMA throughout) of the APLF under pavement temperature of 100F, speed of 5 mph and load of 12 kips. This value corresponds to the 82$^{nd}$ percentile of the design strain distribution. Sections 4 and 5 which are expected to perform perpetually should have measured strain under those conditions which is less than 67 microstrain. Another way to look at that is the vertical line on the above plots should cross the design, or target, distribution at a percentile smaller than 82 for those that were designed to be perpetual. This holds true for Sections 4 through 6. Sections 6 and 7 were not expected to perform perpetually. Section 7 has estimated strain at the extreme conditions to be greater than 67 microstrain, thus, it is not expected to perform perpetually. Section 6, however, had an estimated strain of only 35 microstrain which is nearly half of the maximum strain (67 microstrain). PerRoad simulations for both DCP derived and backcaclulated aggregate base and stabilized subgrade moduli resulted in predicted strain slightly smaller than the target strain distribution for 65 percentile and above. Which would also imply Section 6 has the potential to be perpetual. However, the DCP moduli and backcalculated moduli for the aggregate base and stabilized subgrade in section 6 are in-line with section 7. Furthermore, just like section 7, section 6 was also constructed with HPM mixes throughout, albeit ½" thicker than section 7. This small increase in AC thickness is unlikely to result in the large decrease in strain relative to section 7. Therefore, section 6 should be closely monitored moving forward.

Although, the DCP-derived modulus, and backcalculated modulus generally do not agree with one another, when applied in PerRoad, the predicted strains do not result in large differences. They do, however, result in lower predicted strains than the PDM inputs. As the curves move to the left in the plot, they come closer to the measured tensile strain at the bottom of the AC layer. Neither the backcalculated moduli, nor the DCP-derived moduli result in predicted strains completely in-line with the measured strain, however they do drastically improve the predictions. As such, the difference between in-situ modulus (backcalculated and DCP-derived) and the PDM values help to explain the low strain values measured in the field. However, as shown in the plots (Figures 7 -13), the low strain values cannot be fully accounted for by the DCP-derived or the backcalculated moduli.

While the predicted strain values may be low where ODOT PDM moduli were used for the aggregate and stabilized subgrade layers, the same PDM moduli were used in the development of the proposed cumulative strain distributions for HPM AC and Conventional AC base. This means that as long as the underlying layers (aggregate base and stabilized subgrade) on WAY-83 are comparable, in terms of modulus, to DEL-23 SB ramp and the APLF Lane C underlying layers, the proposed cumulative strain distribution curves can be used for design. Due to the unexpectedly low measured strain values, it is postulated that the moduli of the underlying layers on WAY-83 were much greater than those in the APLF or DEL-23 SB ramp. This would explain why strain values measured in the WAY-83 test sections were much smaller than those measured in the APLF under the same conditions (12-kip load, T = 100F, and vehicle speed of 5 mph) (see Table 8).

To test this hypothesis, backcalculated moduli and DCP derived moduli for the stabilized subgrade in the APLF should be compared to WAY-83 and to other stabilized subgrades across the state. The average DCP derived stabilized subgrade modulus in the APLF was found to be 113.5 ksi when tested in 2021. Which is a 54% increase over the average DCP derived stabilized subgrade modulus of 73.7 ksi for the WAY-83 test sections. Challenges were encountered in backacalculating FWD deflections in the APLF, which led the research team to combine the aggregate base and stabilized subgrade layers. Therefore, the backcalculated modulus of the stabilized subgrade layer in the APLF is unknown. Chou et al. (2004) reported an increase in backcalculated stabilized subgrade modulus overtime. Therefore, comparing backcalculated moduli determined in the APLF from FWD testing conducted eight years after construction to WAY-83 backcalculated moduli determined from FWD testing immediately after and up to one year after construction may not be appropriate as it is unknown if moduli are expected to increase, level off or decrease beyond three years. Chou et al.'s study did not address the effect of age on DCP derived stabilized subgrade moduli, so it is also unclear what impact, if any the eight years between construction and DCP testing would have.

Chou et al.'s study does provide an opportunity for comparisons with other stabilized subgrades in the state. For context, the 1.36 multiplier used to adjust stabilized subgrade moduli in ODOT's PDM was established based on the report by Chou et al. (2004). In that study the authors conducted DCP testing on three in-service pavements which were constructed with stabilized subgrade, and three in-service pavements in which the subgrade was not stabilized. The authors reported the DCP-derived subgrade moduli generally decrease with depth, in which 6-inch intervals were evaluated. Chou et al. reported higher DCP derived moduli for the stabilized subgrade relative to the non-stabilized subgrade results. These results are summarized below:

- In-service pavements, average DCP derived stabilized subgrade moduli
    - 0 – 6" depth: 89.8 ksi
    - 6 – 12" depth: 74.6 ksi
    - 12 – 18" depth: 55.7 ksi
    - 18 – 24" depth: 51.3 ksi
    - Average (0 – 24" depth) = 67.9 ksi
- In-service pavements, average DCP derived non-stabilized subgrade moduli
    - 0 – 6" depth: 62.3 ksi
    - 6 – 12" depth: 42.6 ksi
    - 12 – 18" depth: 24.3 ksi
    - 18 – 24" depth: 20.5 ksi
    - Average (0 – 24" depth) = 37.4 ksi

The aforementioned study included four test sections, constructed on route SR 2 in Erie County, to evaluate the impact of lime-, cement-, and lime and cement-stabilization on the subgrade moduli relative to non-stabilized subgrade. DCP and FWD testing were also conducted on each test section from which moduli of the subgrade layer were determined. FWD testing was conducted annually over a three-year period, while DCP testing was conducted once. For the cement stabilized subgrade test section, Chou et al. reported an increase in backcalculated moduli from year to year. The resulting DCP-derived and backcalculated moduli for the cement-stabilized test section are summarized below (Chou et al., 2004).

- Erie – SR 2, average DCP derived stabilized subgrade moduli
  - 0 – 6" depth: 170.3 ksi
  - 6 – 12" depth: 123.7 ksi
  - 12 – 18" depth: 96.6 ksi
  - 18 – 24" depth: 75.4 ksi
  - Average (0 – 24" depth) = 120.3 ksi
- Erie – SR 2, average backcalculated stabilized subgrade moduli
  - Year 1: 29.5 ksi
  - Year 2: 31.1 ksi
  - Year 3: 37.0 ksi

Interestingly, the DCP derived and backcalculated moduli for the stabilized subgrade on Erie – SR 2 did not agree either. Further, the DCP derived stabilized subgrade moduli on WAY-83 were much less than those determined for the Erie – SR 2 test sections, but comparable to those measured at three in-service pavements with varying ages at the time of test. The backcalculated moduli for the stabilized subgrade layers on WAY-83 are significantly higher than those on Erie – SR 2. Despite having DCP-derived modulus less than Erie – SR 2, the average backcalculated stabilized subgrade modulus of 207.6 ksi for WAY-83 was nearly seven times greater than the average determined for Erie – SR 2.

As part of Sargand et al.'s (2015) report ten in-service pavements with excellent performance were revisited. FWD and DCP testing were conducted from which underlying layer moduli were estimated. Two of the ten sites with varying pavement ages were reported to have stabilized subgrades, HAM-126-11E and ROS-35-1W. Moduli derived from DCP results utilized 1500*CBR, rather than 1200*CBR prescribed in ODOT's PDM which was also utilized in Chou et al.'s (2004) report and for the estimation of moduli in the APLF. Therefore, results reported by Sargand et al. (2015) should be divided by 1.25 (1500/1200) to offer a fair comparison. The DCP derived moduli listed below reflect that adjustment. The backcalculated moduli for the stabilized subgrade pavements are also listed below (*after* Sargand et al. (2015)).

- HAM-126-11E, average DCP derived moduli
  - Aggregate Base: 56.8 ksi
  - Stabilized Subgrade: 29.6 ksi
- ROS-35-1W, average DCP derived moduli
  - Aggregate Base: 47.2 ksi
  - Stabilized Subgrade: 21.6 ksi
- HAM-126-11E, average backcalculated moduli
  - Aggregate Base: 81 ksi
  - Stabilized Subgrade: 76 ksi
- ROS-35-1W, average DCP derived moduli
  - Aggregate Base: 59 ksi
  - Stabilized Subgrade: 27 ksi

Both sections with stabilized subgrades evaluated by Sargand et al. (2015) had DCP derived stabilized subgrade moduli much smaller than the WAY-83 test sections (average moduli of 73.7 ksi). The backcalculated moduli reported for the stabilized subgrades on HAM-126-11E and ROS-35-1W were significantly smaller than the average backcalculated moduli of 207.6 ksi for the WAY-83 stabilized subgrade.

Based on the available information, it cannot be concluded that the assumption that the stabilized subgrade modulus in the APLF was representative of a typical stabilized subgrade was incorrect. Therefore, it is recommended that the proposed cumulative strain distributions for conventional AC base layers and for HPM AC base layers on stabilized subgrade developed in this study be used for the design of perpetual pavements in conjunction with the PDM inputs for the aggregate base and stabilized subgrade (based on CBR of the project site). It is also recommended future evaluations be conducted across the state to determine expected in-situ moduli of stabilized subgrade and the overlying aggregate base for initial construction values. Once completed, comparisons should be made with the stabilized subgrade and overlying aggregate base moduli reported herein for WAY-83 to determine if adjustments to the design threshold are necessitated.

Section 6 has the potential to perform perpetually based on the evaluation of the constructed cross-section in PerRoad and estimated and measured strain values. However, replicating that cross-section elsewhere may not provide the same results, as stabilized subgrade moduli vary from project to project and there is concern that the stabilized subgrade on WAY-83 may be greater than typical.

# APPENDIX D: Ohio Perpetual Pavement (PerRoad) Design Guide

Based on the findings of this study, an Excel Spreadsheet was developed as a step-by-step guide for design. There are 12 steps as listed below. A brief description/instruction is provided herein to supplement the Excel Spreadsheet and supporting documents provided to ODOT. Recommended values are also provided in the following subsections.

1. Collect weather history for project site (optional)
2. Determine the mean seasonal air temperatures for the project site (optional)
3. Identify an initial cross-section (layer type and thickness)
4. Develop E* Mastercurves for each AC mix type (optional)
5. Determine the mean seasonal pavement temperatures
6. Determine E* based on the mean seasonal pavement temperatures and fixed frequency
7. Setup PerRoad file
8. Enter structural parameters in PerRoad
9. Enter traffic information in PerRoad
10. Run PerRoad
11. Develop cumulative strain distribution curve
12. Adjust AC layer thicknesses until design criteria are met

## Weather History for Project Site (optional)

Test sections at the WAY-83 site were designed based on air temperatures from the Akron-Canton Regional Airport weather station (https://www.wunderground.com/history/monthly/us/oh/canton/KCAK/date/2019-1). The designs were than updated as reported in this chapter, using E* data specific to the AC mixes and measured layer thicknesses. At that point the temperature data were also updated to reflect a 5-year history of temperatures. The following mean monthly (seasonal) air temperatures (MMATs) were used for the updated designs on WAY-83. Since quintiles were used, each season should be of the same duration, however, PerRoad does not allow for a decimal in the duration input, therefore the balance of the weeks was applied to the summer and fall seasons.

**Table 1 Mean Monthly (Seasonal) Air Temperatures for WAY-83 Test Sections**

| Season | Summer | Fall | Winter | Spring1 | Spring2 |
|---|---|---|---|---|---|
| Duration (weeks) | 11 | 10 | 11 | 10 | 10 |
| Temperature (F) | 75 | 67 | 30 | 41 | 54 |
| Temperature © | 23.9 | 19.4 | -1.1 | 5 | 12.2 |

The above MMATs and durations can be utilized or the pavement designer may elect to utilize climatic data specific to the project site. It is recommended the data be compiled first and if the MMATs deviate significantly from the above, the site-specific MMATs be utilized. The provided Excel spreadsheet supports five years of historical data. By copying historical climatic data from weatherunderground.com into the provided spreadsheet, a cumulative mean air temperature distribution will be generated. Cells highlighted in green represent the midpoint of each quintile. With each quintile

representing a season, the mid-point temperature is used to represent each season. The table above will be generated in the provided spreadsheet.

## Identify an Initial Cross-Section

Once the seasonal air temperatures have been decided on, an initial cross-section should be identified. The minimum and maximum lift thicknesses listed in ODOT PDM should be followed.

## Develop E* Master Curves for AC Mix in the Cross-Section

E* master curves are necessary for each AC mix in the cross-section, as the master curve is used to estimate E* at the mean monthly (seasonal) pavement temperatures and a set frequency. These values are in turn used in PerRoad to predict tensile strain at the bottom of the AC layer. Master curves were generated for laboratory-determined E* data from the APLF and DEL-23 experiments. These values were utilized in the creation of the cumulative tensile strain distribution curves, and in the design of WAY-83 test sections. As part of the WAY-83 experiment, E* was determined in the laboratory for each unique mix. All mixes were tested at the same temperatures and frequencies. While no two mixes were identical, average E* values for a given test temperature and frequency were determined for like mixes (e.g., HPM surface mixes from the APLF, DEL-23 and WAY-83).

Recommended E* values are provided in the following tables. As part of the WAY-83 research study, E* master curve Excel Spreadsheets were provided to ODOT for each of the following mix types, which incorporates the recommended values. It is advised that to use the recommended E* values (or provided E* master curves) the AC mix type selected for design be comparable to those used in the APLF and DEL-23 experiments (Sargand et al., 2015) and the WAY-83 experiment.

- Control surface AC mix
- Control intermediate AC mix
- Control base AC mix
- HPM surface AC mix
- HPM intermediate AC mix
- HPM base AC mix

**Table 2 Recommended E* Values for Conventional Surface AC Mix**

| Test Temperature (F) | Test Frequency (Hz) | Average E* ($x10^6$ psi) |
|---|---|---|
| 40 | 25 | 2.091 |
| 40 | 10 | 1.935 |
| 40 | 5 | 1.766 |
| 40 | 1 | 1.459 |
| 40 | 0.5 | 1.315 |
| 40 | 0.1 | 1.032 |
| 70 | 25 | 1.741 |
| 70 | 10 | 1.38 |
| 70 | 5 | 1.193 |
| 70 | 1 | 0.864 |
| 70 | 0.5 | 0.727 |

| Test Temperature (F) | Test Frequency (Hz) | Average E* (x$10^6$ psi) |
|---|---|---|
| 70 | 0.1 | 0.461 |
| 100 | 25 | 0.566 |
| 100 | 10 | 0.421 |
| 100 | 5 | 0.324 |
| 100 | 1 | 0.194 |
| 100 | 0.5 | 0.165 |
| 100 | 0.1 | 0.116 |
| 130 | 25 | 0.266 |
| 130 | 10 | 0.219 |
| 130 | 5 | 0.175 |
| 130 | 1 | 0.086 |
| 130 | 0.5 | 0.052 |
| 130 | 0.1 | 0.036 |

**Table 3 Recommended E* Values for Control Intermediate AC Mix**

| Test Temperature (F) | Test Frequency (Hz) | Average E* (x$10^6$ psi) |
|---|---|---|
| 40 | 25 | 2.619 |
| 40 | 10 | 2.463 |
| 40 | 5 | 2.300 |
| 40 | 1 | 1.973 |
| 40 | 0.5 | 1.825 |
| 40 | 0.1 | 1.466 |
| 70 | 25 | 1.731 |
| 70 | 10 | 1.419 |
| 70 | 5 | 1.214 |
| 70 | 1 | 0.788 |
| 70 | 0.5 | 0.639 |
| 70 | 0.1 | 0.371 |
| 100 | 25 | 0.720 |
| 100 | 10 | 0.532 |
| 100 | 5 | 0.414 |
| 100 | 1 | 0.222 |
| 100 | 0.5 | 0.175 |
| 100 | 0.1 | 0.109 |
| 130 | 25 | 0.268 |
| 130 | 10 | 0.200 |
| 130 | 5 | 0.147 |
| 130 | 1 | 0.078 |
| 130 | 0.5 | 0.065 |
| 130 | 0.1 | 0.046 |

**Table 4 Recommended E* Values for Control Base AC Mix**

| Test Temperature (F) | Test Frequency (Hz) | Average E* ($x10^6$ psi) |
|---|---|---|
| 40 | 25 | 3.121 |
| 40 | 10 | 2.953 |
| 40 | 5 | 2.768 |
| 40 | 1 | 2.401 |
| 40 | 0.5 | 2.257 |
| 40 | 0.1 | 1.859 |
| 70 | 25 | 1.907 |
| 70 | 10 | 1.591 |
| 70 | 5 | 1.428 |
| 70 | 1 | 1.034 |
| 70 | 0.5 | 0.924 |
| 70 | 0.1 | 0.641 |
| 100 | 25 | 0.800 |
| 100 | 10 | 0.653 |
| 100 | 5 | 0.547 |
| 100 | 1 | 0.340 |
| 100 | 0.5 | 0.279 |
| 100 | 0.1 | 0.165 |
| 130 | 25 | 0.420 |
| 130 | 10 | 0.308 |
| 130 | 5 | 0.236 |
| 130 | 1 | 0.139 |
| 130 | 0.5 | 0.115 |
| 130 | 0.1 | 0.082 |

**Table 5 Recommended E* Values for HPM Surface AC Mix**

| Test Temperature (F) | Test Frequency (Hz) | Average E* ($x10^6$ psi) |
|---|---|---|
| 40 | 25 | 1.9615 |
| 40 | 10 | 1.761 |
| 40 | 5 | 1.613 |
| 40 | 1 | 1.3265 |
| 40 | 0.5 | 1.188 |
| 40 | 0.1 | 0.9355 |
| 70 | 25 | 1.027 |
| 70 | 10 | 0.822 |
| 70 | 5 | 0.7155 |
| 70 | 1 | 0.524 |
| 70 | 0.5 | 0.4605 |
| 70 | 0.1 | 0.3275 |
| 100 | 25 | 0.531 |

| Test Temperature (F) | Test Frequency (Hz) | Average E* (x$10^6$ psi) |
|---|---|---|
| 100 | 10 | 0.4195 |
| 100 | 5 | 0.34 |
| 100 | 1 | 0.221 |
| 100 | 0.5 | 0.192 |
| 100 | 0.1 | 0.1365 |
| 130 | 25 | 0.271 |
| 130 | 10 | 0.213 |
| 130 | 5 | 0.179 |
| 130 | 1 | 0.109 |
| 130 | 0.5 | 0.083 |
| 130 | 0.1 | 0.0635 |

**Table 6 Recommended E* Values for HPM Intermediate AC Mix**

| Test Temperature (F) | Test Frequency (Hz) | Average E* (x$10^6$ psi) |
|---|---|---|
| 40 | 25 | 2.376 |
| 40 | 10 | 2.0875 |
| 40 | 5 | 1.926 |
| 40 | 1 | 1.627 |
| 40 | 0.5 | 1.499 |
| 40 | 0.1 | 1.2125 |
| 70 | 25 | 1.336 |
| 70 | 10 | 1.1175 |
| 70 | 5 | 0.9615 |
| 70 | 1 | 0.715 |
| 70 | 0.5 | 0.6185 |
| 70 | 0.1 | 0.4305 |
| 100 | 25 | 0.6385 |
| 100 | 10 | 0.5245 |
| 100 | 5 | 0.4275 |
| 100 | 1 | 0.2785 |
| 100 | 0.5 | 0.238 |
| 100 | 0.1 | 0.164 |
| 130 | 25 | 0.27 |
| 130 | 10 | 0.217 |
| 130 | 5 | 0.1755 |
| 130 | 1 | 0.1095 |
| 130 | 0.5 | 0.0935 |
| 130 | 0.1 | 0.0695 |

**Table 7 Recommended E* Values for HPM Base AC Mix**

| Test Temperature (F) | Test Frequency (Hz) | Average E* (x$10^6$ psi) |
|---|---|---|
| 40 | 25 | 2.8645 |
| 40 | 10 | 2.644 |
| 40 | 5 | 2.492 |
| 40 | 1 | 2.1785 |
| 40 | 0.5 | 2.032 |
| 40 | 0.1 | 1.705 |
| 70 | 25 | 2.0275 |
| 70 | 10 | 1.6825 |
| 70 | 5 | 1.4275 |
| 70 | 1 | 1.0605 |
| 70 | 0.5 | 0.936 |
| 70 | 0.1 | 0.689 |
| 100 | 25 | 1.1545 |
| 100 | 10 | 0.796 |
| 100 | 5 | 0.652 |
| 100 | 1 | 0.4135 |
| 100 | 0.5 | 0.3525 |
| 100 | 0.1 | 0.241 |
| 130 | 25 | 0.546 |
| 130 | 10 | 0.3985 |
| 130 | 5 | 0.338 |
| 130 | 1 | 0.182 |
| 130 | 0.5 | 0.147 |
| 130 | 0.1 | 0.1095 |

## Determine the Mean Seasonal Pavement Temperatures

Once known, the MMAT values are used in the following equation to arrive at the mean monthly (seasonal) pavement temperatures (MMPTs).

$$MMPT = MMAT\left[1 + \left(\frac{1}{Z+4}\right)\right] - \left[\frac{34}{Z+4}\right] + 6$$

For use in PerRoad, Z is the depth at the upper 1/3 of the given AC layer and MMAT and MMPT are the mean seasonal air temperature and mean seasonal pavement temperatures, respectively, in degrees Fahrenheit.

Once determined, the E* master curves are used to determine the seasonal AC moduli for design given the MMPT and a fixed frequency of 12.57 Hz (to represent 55 mph). Using the provided E* master curve Excel spreadsheets, the MMPT and frequency of are entered as shown in the figure below. The designer will then copy the resulting predicted E* in $10^6$ psi to the "MMPT and E" tab in the PerRoad Design Guide spreadsheet.

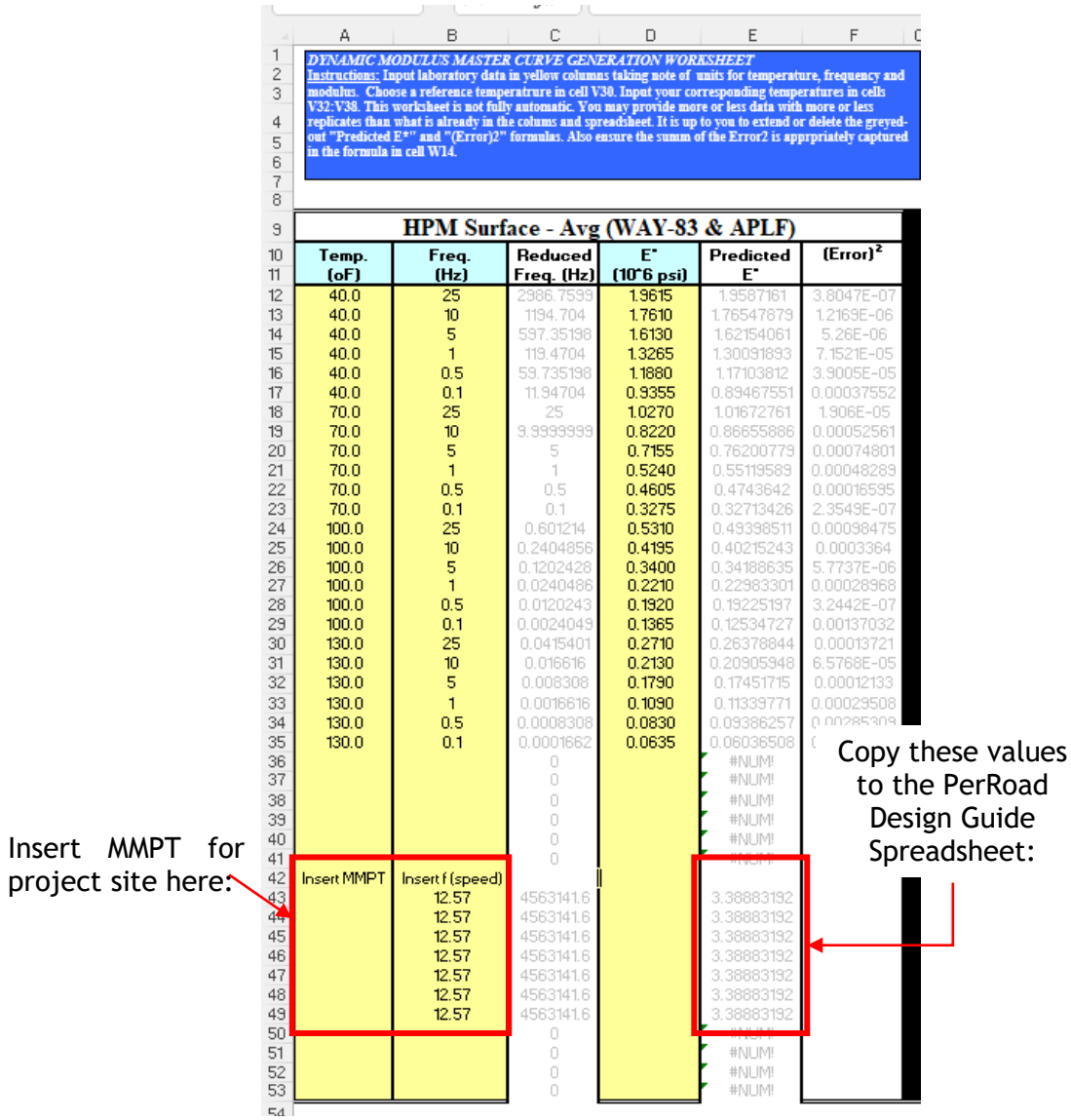


**Figure 1 E* Master Curve, MMPT Input and Predicted E* Output**

## Setup PerRoad File

A 5-layer pavement structure was utilized in the design of the perpetual pavement section son WAY-83. The layers consisted of

- AC Surface Layer
- AC Intermediate Layer
- AC Base Layer
- Aggregate Base
- Stabilized Subgrade

The designer will manually the seasonal temperatures and durations. This information can be used to correct moduli by temperature. However, seasonal AC moduli were determined in the previous step and the aggregate base modulus and stabilized subgrade modulus will remain constant across all seasons. Therefore, the

designer needs to ensure this box is unchecked as it will overwrite the moduli the designer input.

## Enter Structural Parameters in PerRoad

Step-by-step instructions are provided in the PerRoad Design Guide spreadsheet for each layer. Additionally, a separate spreadsheet was developed and provided to ODOT to help the designer tabulate each parameter for each trial and the result of each trial. Structural parameters and the recommended inputs are listed below.

- AC layers:
    - Material Type: AC
    - Performance Grade (PG) of the asphalt binder in the mix: PerRoad will provide default moduli values based on the PG selected. However, for the design process laid out herein, AC moduli are manually entered. Therefore, the designer is advice the PG of the binder as specified for the mix type should be entered for record keeping
    - Poisson's ratio: Use a value of 0.35
    - Layer thickness: Enter the thickness from the initial cross-section
    - Layer moduli: Enter the seasonal AC moduli previously determined, to do so, the designer must select the season from the drop-down menu at the top right of the screen. The designer is advised to enter properties for all layers for one season before selecting the next season.
    - Variability parameters:
        - Modulus variability, distribution type: unless known, use the default value, log-normal
        - Modulus variability, coefficient of variability (COV): unless known, use the default value, 30%
        - Thickness variability, distribution type: unless known, use the default value, normal
        - Modulus variability, coefficient of variability (COV): unless known, use the default value
            - Layer 1 = 5%
            - Layer 2 = 8%
            - Layer 3 = 15%
    - Performance Criteria (this is selected for the bottom AC layer (layer #3) only):
        - Position: Bottom
        - Criteria: From the drop-down menu, select "Horizontal Strain Distribution"
            - Percentile and microstrain: Ensure microstrain is entered as a negative value to represent tension.
            - For conventional AC Base layers on stabilized subgrade, use the following criteria:
                - 95th: -66.16
                - 85th: -47.59
                - 75th: -41.64
                - 65th: -36.56
                - 55th: -32.25
            - For HPM AC Base layers on stabilized subgrade, use the following criteria:
                - 95th: -87.01

        - 85th: -70.77
        - 75th: -61.62
        - 65th: -54.40
        - 55th: -48.15
    - For conventional AC Base layers on unstabilized subgrade, use the following criteria:
        - 95th: -45.15
        - 85th: -37.42
        - 75th: -32.54
        - 65th: -28.55
        - 55th: -25.38
- Granular Base Layer:
    - Material Type: Gran Base
    - Poisson's ratio: Use a value of 0.40
    - Layer thickness: Enter the thickness from the initial cross-section
    - Layer moduli: For stabilized subgrades, use 36,000 psi for all seasons. While an unstabilized subgrade could be entered, it is not advised as the research study evaluated test sections with stabilized subgrade only, therefore the cumulative strain distributions for conventional AC base on unstabilized subgrade has not be verified.
    - Variability parameters:
        - Modulus variability, distribution type: unless known, use the default value, log-normal
        - Modulus variability, COV: unless known, use the default value, 40%
        - Thickness variability, distribution type: unless known, use the default value, normal
        - Modulus variability, coefficient of variability COV: unless known, use the default value, 20%
- Stabilized Subgrade Layer:
    - Material Type: Soil
    - Poisson's ratio: Use a value of 0.45
    - Layer thickness: Since this is the last layer, it will not enable a thickness to be entered and it will be modeled as a semi-infinite layer
    - Layer moduli: For stabilized subgrades, use 1.36*1200*CBR. While an unstabilized subgrade could be entered, it is not advised as the cumulative strain distribution for unstabilized subgrade has not been verified.
    - Variability parameters:
        - Modulus variability, distribution type: unless known, use the default value, log-normal
        - Modulus variability, COV: unless known, use the default value, 50%
    - Performance Criteria:
        - Position: Top
        - Criteria: From the drop-down menu, select "Vertical Strain"
        - Threshold: 200
        - Target Percentile: 50

## Enter Traffic Information in PerRoad

To be conservative, the perpetual pavement test sections on WAY-83 were designed for 100% of the traffic load spectra consisting of 20-22 kip single axles. As such, this is the recommended load spectra for future perpetual pavement designs following the procedure laid out herein. Step-by-step instructions are provided in the PerRoad Design Guide Excel spreadsheet for entering this load spectra into the software.

## Run PerRoad

Once all design information has been entered into the software, the designer will need to initiate the analysis. PerRoad employs a stochastic layered analysis approach in which, by default, 5,000 Monte Carlo simulations are run. Step-by-step instructions are provided in the PerRoad Design Guide Excel spreadsheet to perform the analysis. Once complete, actual strain percentiles will be reported along with whether the designed passed or failed each criterion. Two Excel files will be generated, a raw output file, and a formatted output file.

## Develop Cumulative Strain Distribution Curve

From the raw output file, the designer can copy the strain values recorded for location 1 to the "Strain Distr" tab in the PerRoad Design Guide spreadsheet. These values will be negative, as they are tensile strain values predicted at the bottom of the AC Layer. From these values, a cumulative strain distribution will be generated and plotted. This step is considered optional as formatted output file will show whether the cross-section meets the perpetual pavement design criteria or not.

## Adjust Cross-Section until Design Criteria are Met

If the first cross-section did not meet the design criteria or if the designer would like to optimize the design, the designer should adjust AC layer thicknesses where appropriate. If small changes in layer thicknesses are made, the designer does not need to recalculate the MMPT as the changes will result in negligible changes to the seasonal moduli and predicted strain values.

The designer may also change the AC mix type as needed. If a different AC mix type is selected, the correct seasonal moduli will need to be determined and entered into the software.


23


Smithville
next right

ORITE • 231 Stocker Center • Athens, Ohio 45701-2979 • 740-593-1465
Fax: 740-593-0625 • orite@ohio.edu • http://www.ohio.edu/orite/